Enhancing RC Buildings' Structural and Sustainability Performance by Design Optimisations and a Novel Connection

Reza Keihani

A thesis submitted in partial fulfilment of the requirements of The University of West London for the degree of Doctor of Philosophy.

Supervisors and advisory team:

Professor Ali Bahadori-Jahromi – University of West London

Dr Katherine A. Cashell – Brunel University London

Mr Charles Goodchild & Ms Emily Bonner – The Concrete Centre

School of Computing and Engineering

The University of West London,

United Kingdom

November 2020

Abstract

In the UK, the use of shear walls has become an expansive technique in almost any reinforced concrete (RC) frame building, as indicated by The Concrete Centre, and the construction industry recently criticised the necessity for such vertical resisting elements in low-to-medium-rise RC buildings. In this regard, a moment-resisting system could be another solution for the construction of RC frame buildings with higher ductility in structural performance than shear walls, potentially leading to the collapse of lower columns and connections, problems of serviceability and even to overturning of the whole structure. In view of this, in this PhD research, the viability of eliminating shear walls in low-to-medium-rise RC frame buildings in different locations in the UK was evaluated. Furthermore, the effect of several factors on the design of RC moment-resisting frames in residential low-to-medium-rise buildings was explored in order to identify pitfalls of this approach in height using ETABS software. Thereafter, an innovative beam-column connection (Mini-Haunch) was designed, experimentally tested and analysed with various finite element simulations using Abaqus and ANSYS software, with a view of reducing construction costs and time as well as enhancing sustainability and performance of RC moment-resisting structures. This was followed by an experimental investigation on the feasibility of using polypropylene as a fine aggregate substitute as another step towards more sustainable construction. According to results, it was shown that low-to-medium-rise RC frame buildings in the UK could be constructed without shear walls while having sufficient serviceability and strength, in compliance with Eurocode 2 Part 1-1 guideline. In addition, the same design layout could be constructed at various locations in the UK, thus demonstrating acceptable serviceability and strength of Eurocode 2 Part 1-1. Furthermore, it was noted that by adjusting various parameters, i.e. concrete grade, column size, column section and slab thickness, the overall height of RC moment-resisting frames for typical buildings in the UK could be raised to up to 13 storeys. These findings and further investigations have led to a practical guideline for

UK structural engineers in RC moment-resisting frames in partnership with The Concrete Centre. Moreover, the Mini-Haunch connection demonstrated an advancement in the design and performance of RC moment-resisting frames, offering a considerable potential to increase structural performance of such buildings and promote the economy and environmental sustainability of construction by using less volume of concrete during construction. Eventually, it was found that polypropylene could be a feasible material to replace fine aggregates in the concrete mix design. The experimental testing showed satisfactory results with a low reduction in the concrete mix design and some of the specimens even exceeding the aimed ST5 standardised compressive strength of the concrete mix.

1 Table of Contents

List of Figures

List of Tables

List of notation:

In this list the symbols used in this PhD research are provided. The symbols that are not given here are defined in the manuscript.

a	Acceleration
A_p	Area
A_s	Area of reinforcement
$A_{sw,min}$	Minimum area of punching shear reinforcement
A_{sw}	Area of punching shear reinforcement
B	Background factor
b	Width of building
b	Slab width
b_e	Active breadth of a slab
B_{eff}	Effective beam width
c_1	Column's dimension in the direction of the applied lateral load
c_d	Dilatational wave speed
C_d	Dynamic factor
c_{prob}	Probability factor
C_s	Size factor
C_t	Coefficient for RC moment-resisting frames
d	Maximum displacement
d	Depth of building
d_ε	Concrete strain
E	Modulus of elasticity
E_{cd}	The design value of concrete's modulus of elasticity

E_d	The applied actions
E_{it}	Initial tangential modulus
f	Frequency
f_{ck}	Characteristic concrete compressive strength
F_d	The design value of an action
F_k	Characteristic value of an action
$F_{L.}$	Line load
F_p	Point load
$F_{V,Ed}$	Total vertical load
f_{yd}	Design yield of reinforcement
f_{yk}	Reinforcement characteristic yield strength
$f_{ywd,ef}$	Effective design strength for shear reinforcement
g	Gravitational acceleration
GF	Gauge factor
G_k	Characteristic value of a permanent action
H	Storey height
h	Slab thickness
i	Minimum radius of gyration of the uncracked section
I_c	The second moment of area
I_c	Moment of inertia of column
I_g	Gross moment of inertia
I_p	Moment of inertia
I_{s1}, I_{s2}	Moment of inertia of slab
K	Lateral stiffness

k_1, k_2	Relative stiffness at ends 1 and 2
L	Unstressed length of gauge wire
l_0	Effective length of the member calculate
l_1, l_2	Slab length
I_v	Turbulence intensity
L^e	Characteristic element length
M	Moment
M_{Ed}	Design applied bending moment
$M_R x$	Overturning moment in X axis
$M_R y$	Overturning moment in Y axis
$M_{t,max}$	Positive moment
n_1	Natural frequency
n_s	Number of storeys
p	Annual probability of exceedance
P_p	Uniformly distributed surface load
$Q_{k,1}$	Characteristic value of a leading variable action
$Q_{k,i}$	Characteristic value of an accompanying variable action
R	Gauge wire resistance
R	Return period
R_1, R_2, R_3, R_4	Resistor number 1-4
R_d	Resistance of the member
S	Scale factor
S_r	Radial spacing in shear reinforcement perimeters
S_t	Tangential spacing in shear reinforcement perimeters

T	Time length
T	The forces of tension in the reinforcement
u_1	Basic control perimeter
u_{out}	Perimeter at which punching shear links are no longer required
U_p	Linear displacement
V	Volume
V_b	Base shear
V_{col}	Shear forces from the columns
V_{Ed}	Punching shear stress (without reinforcement)
V_{EX}	The excitation voltage
V_{jh}	Average horizontal shear force
V_o	The output voltage of the bridge
V_P	Shear force
$V_{Rd,c}$	Design shear resistance (without reinforcement)
$V_{Rd,max}$	Concrete resistance capacity
x	Coefficient for RC moment-resisting frames
Z_s	Reference height
β_{cr}	Cracked stiffness factor
γ_F	Partial factor for actions
δ_{i-1}	Interstorey drift from the first-order analysis
ε_c	Strain of the concrete
ε_c'	Corresponding concrete strain
ε_u	Ultimate strain
σ_c	Concrete stress
σ_s	Stress in reinforcement

σ_{su}	ULS unmodified stress in reinforcement
$\psi_{O,1}$	Characteristic combination factor for 1st variable load
$\psi_{O,i}$	Characteristic combination factor for ith variable load
Δ	Horizontal displacement
ΔL	Full change in length
ΔR	The strain-induced resistance change
Δt	Stability limit
α	Effective width factor
β	Material parameter that depends on the shape of the stress-strain curve
β	Punching shear eccentricity factor
δ	Interstorey drift
δ_s	Logarithmic decrement of structural damping
σ_P	Stress
λ	Slenderness of column
ρ	Tension reinforcement required
ρ_p	Density
ψ	Factor defining representative values of variable actions
$\sum V_1$	First-order storey shear
$\sum V_i$	Modified storey shear at the ith cycle
$\sum P$	Sum of all Vertical loads acting on the floor

Acknowledgements

Writing this PhD thesis would not have been possible without the encouragement and support of the good people around me, to some of whom it is feasible to give special mention herein.

This research would not have been carried out without the significant help, guidance and dedication of my principal supervisor, Professor Ali Bahadori-Jahromi, not to mention his expertise and unsurpassed knowledge of structural design and analysis. The excellent advice, motivation and support of my second supervisor, Dr Katherine A. Cashell, has been crucial throughout my research, for which I am immensely thankful.

I would like to thank the Concrete Centre and, in particular, Mr Charles Goodchild and Ms Emily Bonner for their collaboration and invaluable technical expertise and support for this research.

I would also like to pay my respect to the Graduate School and its wonderful staff, Professor Stylianos Hatzipanagos, Professor Maddie Ohl, Professor Hafiz Khan, Dr Pauline Fox, Ms Kiran Johal, Ms Gigi Chang and dear Ms Maria Pennells, for their exceptional support and positive attitude toward me and the other PhD students not to feel lost during the journey.

It is not possible to thank everybody, but not to mention my family. My parents Asghar and Rouhangiz who have given me love, joy and happiness and always encouraged me to pursue my dreams. My wonderful and very kind sisters Maryam and Fatemeh have always been supportive and compassionate from far away. My kind brother in law Farzad, with his positive support to me, and my sweet younger brother Parsa, who has always looked up to me with his pure and precious heart.

And finally, Livia, who has always been there for me through difficult times from the very beginning and has shown me compassion, kindness and trust as a true friend, and now as my

love and partner in life. I have always valued her support and encouragement, and I consider myself very blessed to have her by my side in the upcoming journeys together.

List of Submitted Journal and Conference Papers

1. Keihani, R., Bahadori-Jahromi, A., Cashell, K. and Bonner, E., 2020. Evaluation of Mini-Haunch Connection in Moment-Resisting Frames. (In progress)
2. Keihani, R., Bahadori-Jahromi, A., Goodchild, C. and Bonner, E., 2020. How to Design Moment-Resisting Frames. London: The Concrete Centre. (Submitted)
3. Keihani, R., Bahadori-Jahromi, A., Goodchild, C. and Cashell, K., 2020. The Influence of Different Factors on Buildings' Height in the Absence of Shear Walls in Low Seismic Regions. Techno-Press, 76(1). https://doi.org/10.12989/sem.2020.76.1.001.
4. Keihani, R., Bahadori-Jahromi, A. and Clacy, T., 2019. Sustainable Development of Medium Strength Concrete Using Polypropylene as Aggregate Replacement. World Academy of Science, Engineering and Technology International Journal of Civil and Environmental Engineering, 13(9). https://doi.org/10.5281/zenodo.3462071
5. Keihani, R., Bahadori-Jahromi, A. and Goodchild, C., 2019. The Significance of Removing Shear Walls in Existing Low-Rise RC Frame Buildings – Sustainable approach. Techno-Press, 71(5). http://dx.doi.org/10.12989/sem.2019.71.5.563.

Abstract submission

1. Keihani, R. and Bahadori-Jahromi, A., 2020. Investigate the influence of Polypropylene as fine Aggregate Replacement on the mechanical and thermal properties of the concrete mix. EGU General Assembly 2020. https://doi.org/10.5194/egusphere-egu2020-21782

1 Introduction

1.1 Background

Braced and moment-resisting (unbraced) frames are two lateral resisting systems made of concrete, steel, composite and timber. There are two methods for the classification of braced frames: bracing and shear wall and both mechanisms have lateral stiffness and structural strength (McCormac and Csernak, 2012; Gardner, 2014). In the construction industry, a braced system can be used with all standard materials to provide higher robustness and ductility (Gardner 2014).

Furthermore, it is well established that shear walls are one of the most popular resisting elements to use against lateral forces in reinforced concrete frame structures, and the characteristics of shear walls control the performance of structure against applied loads (Cao, Xue and Zhang, 2003; Chandurkar and Pajgade, 2013). These structural components extend across the building's height to its base through load paths that serve as vertical stability systems. They are generally acknowledged as the primary structure with relative lateral stiffness against horizontal and vertical forces to pass loads to the foundation. Based on ultimate limit state design, shear walls can fail due to tension/compression, horizontal shear, vertical shear or buckling. These failure mechanisms contribute to overturning and sliding failure of equilibrium failure modes. The controlling failure depends on material properties, loading, geometry, construction and constraint (Gardner, 2015).

Various factors, including structural performance, construction method and sustainability, must be weighed to achieve the most suitable design for a building. As far as performance is concerned, capacity design recommends that a building should allow the frame to move in order to dissipate the absorbed energy using its maximum potential (Bisch et al., 2012). This concept is one of the key requirements for constructing a cost-effective building. On the other hand, the

presence of shear walls in a building tends to reduce the structural lateral displacement and prohibits the structure from dissipating the absorbed energies. This behaviour restricts the frame from taking part in lateral stiffness, which potentially affects the design and leads it to be conservative.

In the UK, shear walls have been commonly used, particularly in buildings with three up to six storeys known as low-rise (Emporis Codes, 2008 and 2009; Banks et al., 2014 and NFPA, 2016). As reported by The Concrete Centre, the use of shear walls has been criticized by the construction industry (The Concrete Centre, 2018). If such elements were being used, based on the design's need, they could provide sufficient stiffness to allow the structure to tolerate the applied lateral loads. On the other side, if shear walls were used, regardless of design criteria, they may negatively impact construction's economic and environmental sustainability and the requirement for design safety to evaluate and avoid risks. Thus, it is very desirable to remove them from some buildings without risking the inhabitants' safety.

On the other hand, moment-resisting system is another solution for the construction of RC frame buildings, as the frame is accounted for the resistance and transfer of the applied vertical and horizontal loads to the foundation. This construction technique has higher ductility (with a longer duration of oscillation) in the structural performance than shear walls; however, it is more vulnerable to higher heights due to its adverse effects on the exponential rise in the second-order (P-Δ) effect in buildings. This vulnerability of the moment-resisting frames can lead to the collapse of the lower columns and the connections, potential serviceability problems, such as cracking and perceptible motion, and even overturning the whole structure.

Therefore, moment-resisting frames require further attention as the building's structural behaviour and height can have a crucial effect on the design. Since moment-resisting frames are not ideal above a certain overall height, an advanced form of connection will be investigated as a potential solution to overcome this type of structure's deficiencies.

Furthermore, in recent years a crucial problem has been encountered in the construction industry, which is the strong demand for residential construction and workloads is rising while,

at the same time, there is a significant labour shortage in the construction industry. This concern can lead to a 20-25% decline in the workforce over the next decade. In addition, the labour workers are also ageing, and the number of newcomers joining the industry is smaller than the number that leaves the industry. This situation may be intensified by Brexit, as an eighth of the UK's construction workforce is from overseas. The proportion is also higher in London, where it is a third. (The Peasant, 2016).

Besides, the cost of imported materials, most of which come from the EU, has risen due to the weakening of the British Pound. Thus, on 5 July 2018, the Building Leadership Council and the UK Government released the Construction Industry Deal, which committed £420 m to fund the industry's transformation (Davies, 2018).

This transformation in the construction industry could take place in various applications, including sustainability in the environment. The incapability of the planet to withstand the harmful influence of human activity is increasingly recognised and given the unsustainable consumption level in industrial countries. This situation must improve before the exhaustible natural resources of the Planet run out. Enhancing construction practises to minimise these harmful environmental effects has also drawn the interest of building experts worldwide (Sev, 2009).

1.2 Identified Knowledge Gap

In the context of this research, a comprehensive literature review was undertaken to recognize the gaps in the literature, which are described in the following:

- No extensive studies have been performed on the significance of using shear walls in the UK construction industry.
- No research study was undertaken into the height limits of reinforced concrete frame structures constructed with shear walls and replaced with a moment-resisting system.

- No studies have been conducted to improve the structural performance of buildings that consider multiple factors, including the grade of concrete, the column's dimension, the shape of the column, and the slab's thickness.
- There is no comprehensive guideline in the UK RC moment-resisting frames with flat-slab to offer practical solutions to construction obstacles.
- There is no specially designed connection in moment-resisting frames in regions where the wind is the dominant design load.
- The low ratio of Polypropylene in the concrete mix is not thoroughly investigated in cubic samples.

1.3 Aim

This PhD research aims to address the issues outlined in the literature review in five stages. In the first stage, the possibility of eliminating shear walls in current residential building design will be explored using ETABS (Structural Analysis and Design Software) and Concept (Conceptual Structural Design Software). In the second stage, the ultimate overall height for a typical existing residential building, built initially with shear walls, will be determined by a moment-resisting method using ETABS software to perform various structural analyses. In the third stage, a design guide will be produced for the UK construction industry in partnership with the Concrete Centre for the Design of RC moment-resisting Frames in the UK which will offer realistic advice to resolve construction issues. Furthermore, a Mini-Haunch connection between beams and columns will be designed to enhance the RC moment-resisting frames' structural performance and sustainability in the economy and the environment. In this regard, the Mini-Haunch connection not only will provide the load path through the frame but also will increase the connection’s stiffness, participate the connection into the dissipation of the absorbed energy as well as, enhance the construction speed and reduce the cost. In this process, several experimental tests on scaled prototypes and various structural and finite element analyses using ANSYS and ABAQUS (Finite Element Analysis Software) will be performed to examine the

behaviour and interactions between the frames connections. Finally, the effect of using polypropylene as a fine aggregate substitute in the concrete mix process will be discussed in order to improve the sustainability of construction in the environment by reducing the extracted amount of natural resources for construction purposes.

1.4 Objectives

The research objectives are, therefore:

1. Identify the shortcomings in the literature for RC moment-resisting frames.
2. Demonstrate a comprehensive understanding of current structural constraints of reinforced concrete moment-resisting frames under the Ultimate Limit State (ULS) and Service Limit State (SLS) design.
3. Produce a design guide for the UK construction industry in partnership with the Concrete Centre.
4. Develop a Mini-Haunch connection in moment-resisting RC frames to improve their structural performance and sustainability in construction.
5. Conduct laboratory studies to examine the efficacy of the proposed connection.
6. Conduct finite element simulations to verify experimental findings under vertical loading and examine the proposed connection's effectiveness subjected to lateral loading.
7. Investigate the effect of polypropylene as a fine aggregate substitute in the construction of the concrete mixture.

1.5 Motivation and Research Questions

The primary motive behind the whole research is to improve existing knowledge of moment-resisting RC frames' performance. This, in turn, could improve the competitiveness of reinforced concrete frames as opposed to steel frames. Furthermore, the Mini-Haunch is an innovative connection for reinforced concrete moment-resisting frames that can significantly improve buildings' structural performance. Reducing the required concrete will be a key outcome of this

research, which can be converted into a decline in construction time, expense and negative environmental impact.

Meanwhile, as the Concrete Centre has funded this PhD research, collaborative work will be formed to produce a design guide for RC moment-resisting frames that could be used to the UK construction industry.

The research questions are as follows:

1. What are the economic advantages of eliminating shear walls in reinforced concrete frames?
2. What is the feasible height of the current RC moment-resisting frames, and what height guarantees safe structural performance?
3. How effectively can the Mini-Haunch connection perform under vertical and lateral loadings in RC moment-resisting frames?
4. What is the effect of polypropylene on the workability and compressive strength of the concrete mixing design?

1.6 Thesis outline and chapter layout

1. General Introduction

This chapter provides background knowledge of the research field of reinforced concrete (RC) frame structures, the use of shear walls and concrete frame connections. It further points out the aims and objectives of this research, the significance of the research, the identified knowledge gaps and the research questions.

2. Literature Review

This chapter provides a thorough review of the research, including the shortcomings in the literature on the performance of connections in RC moment-resisting frames when subjected to

wind loads. In addition, this chapter addresses the various types of concrete frame connections and their characteristics, as well as the height restriction of moment-resisting frames. Furthermore, current developments in structural engineering, including the use of numerous finite element simulation software and sensors for structural health monitoring and their applications, are discussed. Finally, this chapter explores the methods of sustainability in the construction industry and the use of aggregate substitution in the concrete mix design.

3. Methodology

The Methodology chapter outlines the research paradigm, research design and ethical concerns. Moreover, the techniques used for this research to conduct experimental testing at the laboratory and finite element simulations with ETABS, ANSYS and Abaqus software are discussed.

4. The Significance of Removing Shear Walls in Existing Low-Rise RC Frame Buildings

This chapter addresses the problem in two stages. In the first stage, the possibility of eliminating shear walls in existing residential building design was investigated where ETABS and Concept software were used to explore the structural performance and cost-effectiveness of removing shear walls, respectively. In the second stage, the same design layout was adopted in different locations across the UK in order to explore the environmental limitations of the proposed design.

5. The Influence of Different Factors on Buildings' Height in the Absence of Shear Walls in Low Seismic Regions

In this chapter, the effect of several variables (e.g. concrete grade, column size, column shape and slab thickness) on the structural performance of RC moment-resisting frame is investigated along with assessing the maximum overall height under wind actions in the UK through various finite element simulations with ETABS software.

6. Enhance the Practical Design of Reinforced Concrete Moment-Resisting Frames

This chapter aims to enhance the structural performance and economic and environmental sustainability of construction by developing the use of the moment-resisting system in low-to-medium-rise reinforced concrete frame buildings in the UK construction industry. Therefore, in this chapter, practical and technical design guidelines are provided for structural engineers, based on the current investigations in this research which has identified the limitations of moment-resisting RC frames in the UK.

7. Design a Mini-Haunch Connection

In this chapter, the concept of a mini-haunch connection as an innovative connection is introduced to improve the deficiencies of the traditional moment-resisting connections used in the construction industry. The structural performance of the mini-haunch connection is examined through laboratory tests and various finite element simulations using ANSYS and Abaqus software to verify the experimental findings under vertical loading and determine the efficacy of the proposed connection under lateral loading.

8. Sustainable Development of Medium Strength Concrete Using Polypropylene as Aggregate Replacement

As a further step towards achieving a more sustainable construction in the environment and reducing the volume of natural resources used in the construction industry, in this chapter, the influence of partial substitution of fine aggregates with polypropylene on the workability and compressive strength of concrete mixture designs is explored.

2 Literature Review

In the construction industry, there are various techniques to design RC frame buildings in order to provide lateral stiffness and structural strength. Each one of these methods has several advantages and drawbacks that require detailed technical considerations. In this PhD research, the previous studies regarding two of the most recognised construction methods in RC frame buildings and their characteristics are further explored. Moreover, the proficiency of current technologies in finite element simulations and sensors in structural health monitoring are discussed to be adopted in this research. Ultimately, the application of substituting fine aggregates with plastic polymers as one of the primary sustainable approaches in the construction industry to reduce the consumption of natural resources is investigated.

2.1 Shear Walls

It is well established that shear walls are among the most effective resistance components to use against lateral forces in reinforced concrete structures (Figure 2.1). The shear walls' characteristics control the performance of the building against the loads applied (Chandurkar and Pajgade, 2013). These structural components extend across the building's height to its foundation within the load paths, which serve as vertical support systems. They are usually assumed to be the primary structure and provide relative lateral stability to horizontal and vertical loads for transferring forces to the foundation (Gardner, 2015). The loads are transferred by an internal stress distribution and consist of axial, torsional, shear and flexural strains.

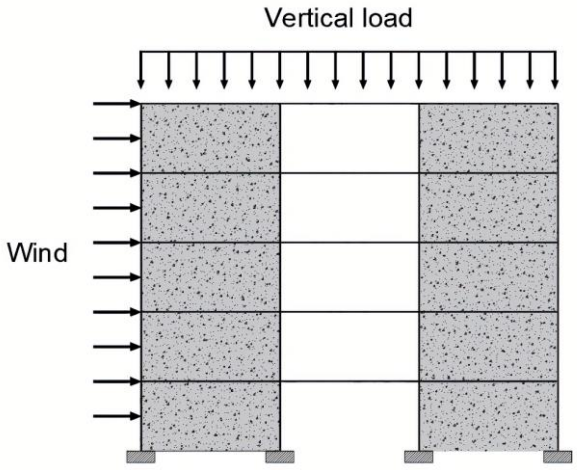

Figure 2.1: RC frame with shear walls

Based on the ultimate limit state design, shear walls can fail due to tension/compression, horizontal shear, vertical shear or buckling. These failure mechanisms are added to the overturning and sliding failures in the equilibrium failure modes. The governing failure depends on the material properties, loading, geometry, construction and restraint (Gardner, 2015).

Shear walls have a major effect on reducing structural lateral displacement due to their comparatively high in-plane lateral stiffness. However, the greater the stiffness of a structure, the higher the level of absorbed lateral forces, which may potentially lead to the building's failure (Cao, Xue and Zhang, 2003).

2.1.1 The Significance of Utilising Shear Walls in the UK

Typically, shear walls are necessary for the mid to high-rise buildings to withstand wind or earthquake actions. In this part, the importance of such applications is evaluated around the world and compared to UK practice.

Concerning the location of a building and its regional design loads (seismic and wind), the type of construction and the structural regulations applicable to the building could be diverse. According to Wu et al. (2018), shear walls are used to withstand lateral forces acting on buildings in active seismic regions due to their substantial lateral stiffness and strength.

Over the last two decades, natural disasters such as 1995 Kobe in Japan, 1999 Izmir in Turkey, 2003 Bam in Iran, 2010 in Chile and many more have resulted in large-scale loss of innocent lives and large-scale financial damage to infrastructure. In some cases, such as the 1995 earthquake in Kobe, as shown by Ghosh (1995), apart from all the destruction caused by the earthquake, there was a key factor in which reinforced concrete structures with load-bearing or shear walls did not experience any functional damage and were in a position to maintain their occupation instantly after the catastrophe.

However, in the case of the UK, as illustrated by Eurocode 8 Part 1 (BS EN 1998-1, 2013), except for certain unique types of structures due to very low seismic activity, there is no need to consider those forces. In addition, as shown by Musson and Sargeant (2007), the Peak Ground Acceleration (PGA) value with a 10% probability of exceeding 50 years (475 year return period) for most countries is less than 0.02-g, which confirms the scarcity of seismic activity in this area.

On the other hand, wind activities can create significant lateral loads on buildings due to the geographical situation of the UK region. Archer and Jacobson (2005) and Global Wind Atlas (2018) reported that Northern European countries, including the UK, have a large wind power capacity that can generate high lateral forces on buildings. In addition, the intensity of wind-induced loads on the structures can be influenced by the height of the buildings. Rajat Bongilwar et al. (2018) and Lu et al. (2016) reported that the use of concrete shear walls in high-rise buildings could improve their strength and stiffness.

Increasing the building's height influences different aspects that could result in the rise of the applied force. Murty et al. (2012) suggested that the density of a structure will increase proportionally to its height, but the total stiffness decreases, resulting in the natural period's growth and the lateral displacement of the structure. In another study, Manasa and Manjularani (2017) concluded that the interstorey drift was increasing with the building's height. Such height changes could increase the second-order (P-Δ) effect; as Dinar et al. (2013) stated, changing

the height of the structure will increase the displacement, the axial forces, and the moments accordingly.

Previous experiments have demonstrated that the building's height will directly influence the applied load, which makes this aspect important to the design. As pointed out at the beginning of this chapter, this research focuses on low to mid-rise buildings that face smaller lateral forces compared to high-rise buildings. As a result, it might be possible to develop low to mid-rise RC frame buildings without shear walls.

2.1.2 Structural Performance of Buildings with and Without Shear Walls

Over the last few decades, numerous experiments have been undertaken to examine reinforced concrete frame buildings' efficiency either with or without shear walls subjected to lateral forces. There are many types of research in this field on the effects of seismic behaviour, including several studies conducted by Chandurkar and Pajgade (2013), Thakur and Singh (2014) and Aainawala and Pajgade (2014), which conducted comparative analyses of multi-storey residential buildings with and without shear walls using STAAD and ETABS software. In their research, four types of structures were studied, three with separate shear wall positions and one without any shear walls. Based on the findings, the building with shear walls situated at the corner has the least lateral displacement relative to other structures. In the braced frames (with the shear wall), the shear forces and moments in the members were diminished instead of the simple moment-resisting frame. However, their research did not analyse buildings' global performance to explore the overall lateral displacement and the lateral deflection permissible based on the design codes. Also, Jayalekshmi and Chinmayi (2015) studied RC frames' behaviour with and without shear walls in multiple design codes (IS 1893 and IBC) to identify their distinctions without considering the lateral limitations of those codes.

In another study, Ghorpade and Swamy (2018) studied the efficiency of flat slab structures with and without shear walls using the SAP 2000 software. This research aimed to find an effective structural system for flat slab buildings using Pushover Analysis. The results of this study

showed that as the shear walls strengthen the structures' stiffness, the period of the structures decreases and the frequency of the structures increases accordingly. In addition, the inclusion of shear walls decreases the drift and displacement of the buildings significantly, and flat slab systems with shear walls are superior to RC frames with shear walls. It should be remembered that considering their higher drifts and lateral displacements, frames without shear walls are still within the safe range according to the serviceability limit state guidelines. However, they declined to carry out further studies on the economic component of the case study. Furthermore, another study was performed by Cismasiu et al. (2017), who used a pushover analysis to explore the applicability of this approach to model failure modes in RC shear walls. It was reported that the approach applied to the elements could yield results with fair precision.

Few studies test the efficiency of RC frame buildings subject to wind action that analyse arbitrary architectural plans, not real-world situations that ignore the constraints of lateral displacement in the design codes and their expense and time impact in the construction process. For instance, in research conducted by Rasikan and Rajendran (2013), RC frame buildings' performance with and without shear walls subjected to wind action was investigated using STAAD software. In this analysis, two structures of varying heights, with and without shear walls, were studied. The findings indicated that the overall displacement of buildings with shear walls, regardless of their height, was lower than that of a building without shear walls. As stated earlier, this research did not recognise the storey drifts' limitations and the second-order (P-Δ) effect in their analysis. Also, Hosseini et al. (2014) studied the effect of wind loads on shear walls' behaviour in concrete frame structures. It was apparent that the structure's torsional forces could be minimised by using shear walls within the frame.

In several other situations, the efficiency of shear wall systems was contrasted with other structural systems to determine the efficacy of such methods. Jayasundara et al. (2017), in their research, examined the use of a shear wall system to withstand wind loads using various design methods. The case studies in this publication involved two 60-storey towers, one with a diagrid

system and the other with a shear wall system. The study indicates that the diagrid framework could endure the same vertical and lateral forces while reducing the frame's weight by 35%. It can be inferred that considering their efficacy, shear walls suffer from the extra weight they bring to the structures. However, this analysis did not meet the parameters mentioned earlier.

2.2 Moment-Resisting Frames

Timber, steel and reinforced concrete are the most common construction materials used in moment-resisting frames. In the design for each type, the resistance against the combination of axial, flexural and shear forces can be provided and is important for the load transfer. Several factors can influence the selection of frame materials, including local environmental conditions, local construction priorities and material supply, along with regulated performance criteria. Site restrictions can also support or rule out choices. However, the use of reinforced concrete in moment-resisting frames is more desirable due to its monolithic design.

When a building's ductility increases in moment-resisting frames, more energy can also be dissipated by periodic displacements (Figure 2.2). The arrangement of the reinforcement is the key component in the behaviour of the frame. It is understood that moment-resisting frames are typically not as rigid as frames with shear walls and use identical designs that tie the application of such frames to low-to-medium-rise buildings. Such buildings have mild lateral shear forces, sway and global second-order (P-Δ) effects (Gardner, 2015).

In RC moment-resisting frames, the perception of movement is a vital aspect due to their ductile behaviour when subjected to lateral loading. There are numerous studies to determine this effect on the safety of the inhabitants. For example, Kwok, Hitchcock and Burton (2009) examined the perception of the vibration produced by wind action, considering its acceptability and its effect on occupant comfort in tall buildings. At the time, it was concluded that there were no generally agreed requirements for occupant comfort. However, in recent research, humans' sensitivity and perception to vibration building and movement have been studied, and different

values for comfort criteria have been established. The Concrete Centre (Banks et al., 2014) pointed out various values used in North America for a 10-year return cycle. Johann, Carlos and Ricardo (2015) have reviewed the comfort standards in the different construction codes and suggested that, in the future, inhabitants should be aware of the building movements and be prepared to deal with the situation.

Furthermore, in RC moment-resisting frames, connections are needed as intersection zones for beams and columns to enhance and sustain the ultimate capacity of adjacent members (Kaliluthin, Kothandaraman and Suhail Ahamed, 2014). Also, as defined by Wight, Richart and MacGregor (2012), intersections connect isolated members, such as beams and columns, to establish unity, and any disruption in the load transfer or structural failure could cause structural failure. Numerous natural seismic disasters in the past have demonstrated that the failure of reinforced concrete structures creates significant discomfort due to the presence of shear forces in the connections that can result in the destruction of the whole buildings (Uma and Jain, 2006). It is worth mentioning that resilience in disproportionate collapse cases is one of the characteristics of moment-resisting frames. This may be partially attributed to the battery configuration, which indicates that the stability of the entire system is divided between the number of subframes that can provide a variety of alternative load paths (Gardner, 2015).

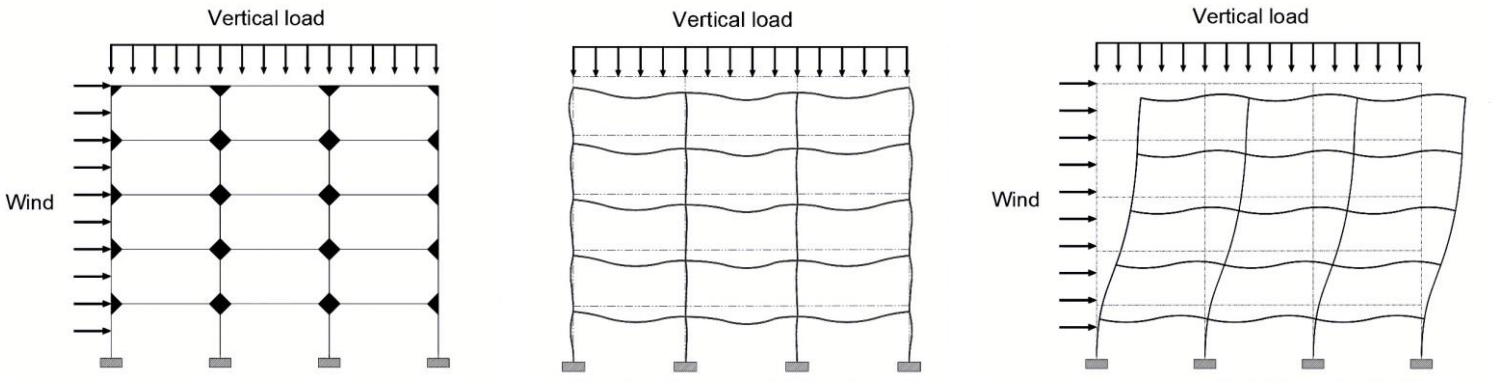

a) The applied loads b) Deflected shape (vertical loading) c) Deflected shape (a combination of axial and lateral loading)

Figure 2.2: Moment-resisting frames mechanism

Whenever it comes to the failure mechanism, the moment-resisting frames and their connections in each part are susceptible to numerous failure mechanisms. In such situations, the failure could be linked to ductility and strength at the ultimate limit state (ULS) or stiffness at the serviceability limit state (SLS). Besides, stiffness may influence the ultimate limit state in the form of second-order (P-Δ) effects (Gardner, 2015).

2.2.1 State of the Art in RC Moment-Resisting Connections

Concrete faces intense rivalry and multiple challenges as a conventional material in the construction industry, including technological developments, environmental problems and economic conditions, as well as the growing need for radical design. Therefore, there is always a constant and unavoidable pressure to enhance and modify structural performance (Dhir, Hewlett and Csetenyi, 2002).

The beam-to-column connection plays a significant role in moment-resisting frames, transferring forces between connecting components and thus, various methods have been implemented in the construction industry to enhance the behaviour of RC frame connections.

Many failures in moment-resisting frames occur in connections due to a lack of attention to details. As is technically crucial for the connection, the intersection zone between beams and columns is designed to allow members to progress and maintain their ultimate capacity (Darwin, Nilson and Dolan, 2016). In order to retain the internal loads generated by the members and transfer them to the adjacent supporting components, the connections should provide sufficient stiffness and strength (Lu et al., 2012). The forces that develop are diverse in the vicinity of the connections and, depending on the type of the lateral forces, are defined in stress and crack development (MayField, Kong and Bennison, 1971).

Also, the longitudinal rebars experience critical bond complications due to the strong internal forces propagated at the plastic hinges that pass through the connection, which exert severe shear stress on the middle of the connections. Also, the parameters for the bond between the

longitudinal rebars and the concrete in the RC beam-column connection have a more substantial effect on the shear resistance mechanism (Lu et al., 2012).

Stress changes in the internal connection from compression to tension, simultaneously around the region, generating a push-pull effect that shows a stronger need for bond strength. Moreover, Paulay and Scarpas (1981) clarified in more depth the behaviour of beam-column connections:

As the connections between beams and columns are subjected to applied loads, it is presumed that the inner forces are produced at the centre of the exterior connections as the plastic hinge progresses in the beam. As seen in Figure 2.3, the forces of compression and tension in the reinforcement are called Cs, Cs', Cs" and T, T' and T" respectively. At the connection's core, the three adjacent members generate the resultant compression stresses known as Cc, Cc' and Cc". V_{col}, V'_{col} and V_b also introduce shear forces from the columns and the beam at the boundaries of the connection's centre. The average horizontal shear force in the connection is shown in Equation 2.1:

$$V_{jh} = T - V_{col} \qquad \text{(Eq. 2.1)}$$

This is similar to the vertical shear forces in the connections, which usually result in severe tensile stresses and diagonal cracks in the core of the concrete (Figure 2.3a).

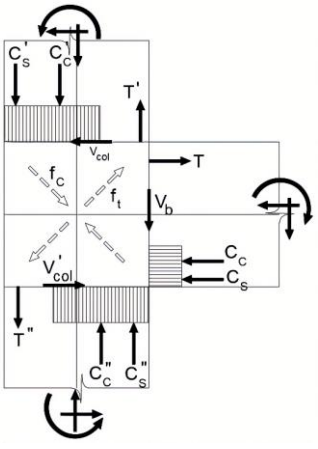

a) Force mechanism in the core of connection

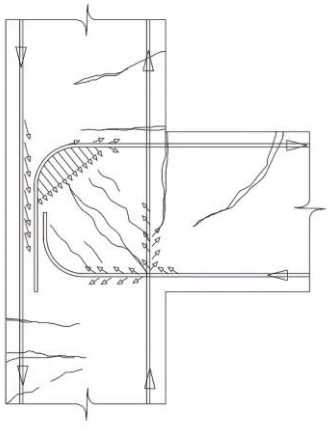

b) Crack development in the core of connection

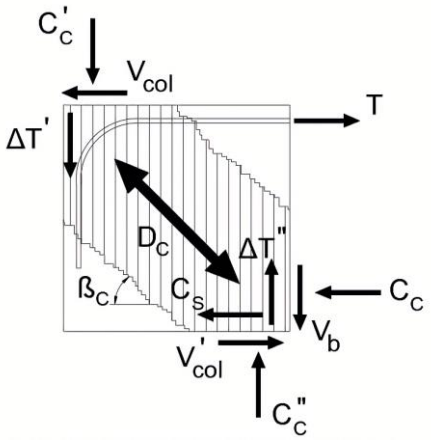

c) Concrete strut mechanism

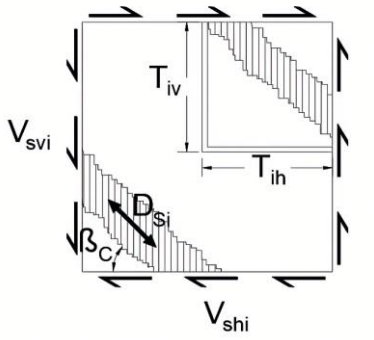

d) Truss mechanism

Figure 2.3: Force and reaction mechanism in connections (Asha and Sundararajan, 2011)

At the centre of the connection, diagonal cracks could transfer diagonal compression forces almost parallel to the cracks. Furthermore, the reinforcement forces in the beam and columns are transmitted to the centre of the concrete through the bearing stress arising from the bending of the top anchorage and the bond stress between the concrete and the reinforcement (Figure 2.3b). As seen in Figure 2.3c, the horizontal forces in concrete Cc at the bottom right corner of the connection, the column shear force Vcol' and most of the compression force in horizontal reinforcement Cs can be paired with the corresponding vertical forces to establish the diagonal strut force Dc. This method, called the strut mechanism, does not require the intervention of the horizontal/vertical shear reinforcement of the connection to be in equilibrium.

In addition, Figure 2.3d shows that the given shear force at the perimeter of the connection can be converted into a diagonal compressive element Dsi. This affects the horizontal or vertical tension element Ti and the strut, which the reinforcement must control, and this system is called the truss mechanism.

In regions of high earthquake activity or wind action, the design code (in the UK, EN 1992) controls the detailing of connections between beams and columns. This involves the details and position of the required transverse reinforcement in the connection region to withstand lateral

loads. However, as seismic events are not significant in the UK, the designs are primarily based on wind activities.

Various studies have been published on the effect of seismic activities on buildings' structural performance, including Kaung and Wong (2011). They performed an experimental analysis on the connection's shear strength and the influence of horizontal shear connections in the centre of connection. They, therefore, tested on six full-scale exterior beam-column connections under reversed cyclic loading constructed in compliance with BS 8110. It was concluded that by restricting the ratio of the shear connection by up to 0.4%, the horizontal shear link could increase the shear strength and behaviour of the connection when exposed to lateral loads. However, it was noted that, under the loads applied, the connection fails in shear while the beam is still under the service load (about 68% of the ultimate strength).

Besides, a wide variety of research studies have been conducted on cast-in-situ and innovative precast connections in RC moment-resisting frames subject to seismic activities, including research by Lu et al. (2012), who introduced diagonal rebars alongside columns with an overlap. When the results for this design were compared with the Standard design, it was found that the additional diagonal rebars had lower performance in terms of strength. When samples were put under the applied loads, shear cracks (angular direction) were initiated and formed into flexural cracks at higher loads. This action may be attributed to a lack of adequate length in the diagonal rebars. Providing enough length would result in the much-improved performance of the beam-column connections.

In the other design, additional diagonal rebars were added alongside the beams with overlap. The findings revealed crack propagation, beginning with shear cracks, but were concentrated at the beam and connection centre. Minor cracks were also detected at a distance from the connection's area, indicating that the external diagonal rebars, which hold the beam-column connection interface protected, offered adequate strength. This design has a high ductility as

the beam reaches the plastic region earlier than the column, complying with the strong column-weak beam principle.

In the other studies, Chen, Suswanto and Lin (2009) and Chen and Lin (2009) studied the behaviour and strength of a new method that provides a steel-reinforced concrete (SRC) beam-column connection with a single and two-sided force inputs.

Chen, Suswanto and Lin (2009) used an XH-shaped steel cross-section as a column and an H-shaped cross-section as a beam, along with longitudinal rebars and shear links with four anchorage beam rebars at the connection. The findings of five large-scale experiments demonstrate that the anchorage bars' position has a significant effect on the shear strength and the propagation of a crack in the connection, and higher shear resistance of the beam-column connection can be obtained by increasing the steel cross-section depth. Also, a combination of steel cross-sections and corner shear links can substitute closed hoops, providing adequate confinement to the concrete and provide sufficient lateral support to the longitudinal rebars.

Moreover, Chen and Lin (2009) used the same arrangement for two-sided force inputs. It was concluded that, compared to the standard RC connection, the steel-reinforced connection exhibited a milder pinching phenomenon, and the longitudinal H-shaped cross-section flanges had higher shear strength than expected. Besides, as previously suggested by Chen, Suswanto and Lin (2009), the combination of steel cross-sections and corner shear links can substitute the closed hoops, giving adequate confinement to the concrete without any negative impact.

Huang et al. (2017) focused on a new form of connection between beams and columns. In this connection, the CSTC beams are attached to the window style columns with openings at the storey level to support the beams temporarily, with a bolt connection pre-arranged at each end of the column to provide structural continuity. Then, for the monolithic assembly, a cast-in-

situ concrete grout is necessary. Based on the findings, the connection showed that the ductile behaviour and the lattice girders tend to work notably better than the more widely employed means of providing the beam's continuity, which consists of additional longitudinal reinforcement placed throughout the core connection.

Furthermore, Shufeng et al. (2018) presented another study on a new fabricated beam-to-column connection that uses end plates for precast concrete buildings. In this connection, the beams are welded to a steel plate and then attached to the columns using pre-stressed bolts. The experiment involves seven specimens subjected to pseudo-static loads to test the connections' energy dissipation and ductility. The new connection is compatible with a strong column-weak beam concept, which shows a plastic hinge in the beams based on the results obtained. Also, the connection indicates that there has been sufficient energy dissipation and ductility behaviour under the applied loads.

Similarly, Parastesh, Hajirasouliha and Ramezani (2014) have developed a new moment-resisting connection for precast concrete frames. In this research, a ductile connection in the beam-column link in precast elements was proposed. The connection consisted of a series of diagonal bars positioned at the connection and linked to the beam and columns. The area was cast in place by concrete for the appropriate integrity between the components. The results obtained using diagonal bars could delay the development of diagonal cracks. The proposed precast moment-resisting connection could have an acceptable strength, ductility and energy dissipation capacity for monolithic connections.

In some other studies, novel precast beam-column connections have been developed and compared with traditional cast-in-situ connections, e.g. Masi et al. (2013) studied the behaviour of reinforced concrete beam-column connections under various design loads (gravity and seismic loads). The experimental work consisted of four samples that were subjected to gravity and seismic forces. During the experiment, two main failure modes were detected. The first was a flexural failure involving only the beam, and the second was a combination in which both the

beam and the connection were affected. This showed the effect of various loads on the failure mode. Furthermore, the results were justified by numerical simulations using DIANA software.

Ghayeb, Razak and Sulong (2017) have also developed a new connection type between beam-column connections for precast concrete. The proposed connection consists of high-strength steel studs and steel plates placed in the connection between the beam and the columns. In this study, two precast and cast-in-situ RC connections were evaluated under cyclic load to determine the specimens' stiffness, ductility, and strength. The findings indicated that the drift and ductility in precast specimens were higher than in cast-in-situ specimens, and also, the resistance in the initial flexural crack in precast specimens was marginally higher (between 2.75-3.6) than in the other specimens. Additionally, the ratio of strength deterioration in precast connections was proven to be within an acceptable range.

Choi et al. (2013) developed a new connection between beams and columns composed of steel connectors and cement composites (ECCs). This form of connection is inside the column, connecting the columns to the beams with the bolts and is surrounded by ECC. In this experiment, five half-scale models, including one cast-in-situ and four precast beam-column connections, were tested under cyclic loading to determine their stiffness, strength, drift and energy dissipation. The results showed that the connection strength was 1.15 times greater than the standard cast-in-situ RC connection and, owing to the deformity characteristic of the ECC, the connection strength was ductile, thus reaching 3.5% of the drift capacity.

Breccolotti et al. (2016) performed another study comparing prefabricated solutions with cast-in-situ solutions in continuous RC frame structures. In this study, cast-in-situ and pre-cast solutions were compared, and a new reinforcement pattern using loop splices for pre-cast beam-column connections was introduced. The goal of this new connection was to achieve high strength and ductility and a simple construction for prefabricated elements and ease of operation on site. Two types of specimens, including cast-in-situ and precast, were tested under cyclic loads in this experiment. The findings indicated that the new connection would provide sufficient

structural efficiency in terms of ductility and strength. Therefore, numerous numerical analyses using Abaqus software were performed and validated with experimental findings.

Assaad, Chakar and Zéhil (2018) looked at wind-induced forces and explored the behaviour of tongue-and-groove connections in lightweight panels under wind actions. This study explained panel connectivity principles, including the transfer of force through steel dowels to the existing structure. The study indicated that connectivity is accomplished by shear forces between adjacent panels together with horizontal and vertical tongue-and-groove connections. However, the bending moment could not be transferred to the connection axes, even though the cement mortars bonded the panels.

Moreover, wind loads on buildings could directly affect the connections between the components inside the frame and cause damage to the buildings. As has been pointed out by Unanwa et al. (2000), which examined the development of wind damage bands for buildings, the damage caused by the wind regime could be heavily affected by the connections which, in the event of failure, could damage the connected components by a domino effect.

2.2.2 Height Limitation and the Influencing Parameters

The distinction between low and high-rise buildings is important in structural analyses since the structural performance can change with the overall height. For example, much of the discomfort and damage in buildings subjected to lateral loads is due to low-frequency dynamic vibrations, particularly in high-rise buildings, making them more vulnerable to wind action than earthquakes. On the other hand, in high-frequency dynamic vibrations, the low-rise buildings can become more vulnerable.

Over the last decades, both severe wind and catastrophic earthquakes have caused a great deal of destruction. Wind actions can be the dominant environmental design loading for high-rise buildings due to their unique load applying mechanism and the higher occurrence worldwide (Li et al., 2010; Aly and Abburu, 2015).

The height definition of a building is more of a dilemma since there is no universally agreed description of low and high-rise buildings, and it can differ depending on the design code and its application. According to Höweler (2003), the relationship between the height and the building's width can determine the classification of the building. Scott (1998) refers to a high-rise building as a building with very high facades, a small roof area and a smaller footprint, and the distinction between a low and a high-rise structure, due to its height, is unique to the required engineering systems.

Emporis Guidelines (2008 and 2009) categorise low-rise buildings as structures below 35 m and high-rise buildings as structures between 35 and 100 m. The National Fire Protection Association (NFPA, 2016) describes a high-rise building as a structure over 23 m in height. Furthermore, The Concrete Centre (Banks et al., 2014) classifies buildings as high-rise if the height ratio to the lowest lateral dimension is greater than 5:1.

This research follows the concept of The Concrete Centre criteria, where the classification of buildings height is based on the dimensions of individual buildings rather than a predefined value for height limitation.

In the following sections, the influencing parameters in the height of buildings are explained.

- **Second-Order (P-∆) Effect**

The second-order effect is one of the main factors that affect buildings' structural performance and limits the maximum overall height. This factor needs to be taken into account for buildings' design, particularly in slim and tall buildings.

The effect of second-order (P-∆) on most concrete frame buildings with shear walls is insignificant; nevertheless, according to BS EN 1992-1-1 (cl 5.8.3.3), the effect of second-order (P-∆) may also be neglected if Equation 2.2 is satisfied:

$$F_{V,Ed} \leq 0.31 \times \frac{n_s}{n_s+1.6} \times \frac{\sum E_{cd} I_c}{L^2} \qquad \text{(Eq. 2.2)}$$

where:

$F_{V,Ed}$: Total vertical load

n_s: Number of storeys

L: Overall height of a building

E_{cd}: The design value of concrete's modulus of elasticity

I_c: The second moment of area

A critical part of the second-order (P-Δ) effect, particularly in RC moment-resisting frames, is that when a building is subjected to lateral forces, it appears to distort in the form of large P-Δ and small P-δ (see Figure 2.4). With a rise in height, the deformation could become more extreme, resulting in a decrease in the structure's stiffness. In this case, the building is driven to its inelastic zone by cracking in concrete sections. In the meantime, the induced force at the bottom and the top of the columns due to P-Δ moments (P-Δ shear) creates an extra need for lateral shear resistance from the structural system, which significantly contributes to the shear loads applied.

On the other hand, the P-δ effect (P-small delta) induces localised deformation in the individual column members. In this case, the members would be under axial and horizontal forces, and then if the columns are slender or the displacements are exceedingly high, it could result in a buckling failure. Moreover, buckling failure in concrete columns seldom occurs with a single curvature. In many cases, particularly in multi-storey buildings, columns shift in a third-order displacement pattern (with x, y and z coordinates) with a double curvature pattern. As far as the building is constructed in compliance with the Eurocode slenderness criteria, it is desirable to remove the P-δ effect in the analyses as it can greatly increase the processing time without providing a noticeable advantage. An alternate approach to include this effect is the separation

of important components into smaller parts and the transition of their behaviour to the P-Δ effect (Kalny, 2017).

Figure 2.4 demonstrates the influence of P-Δ and P-δ effects on a structure.

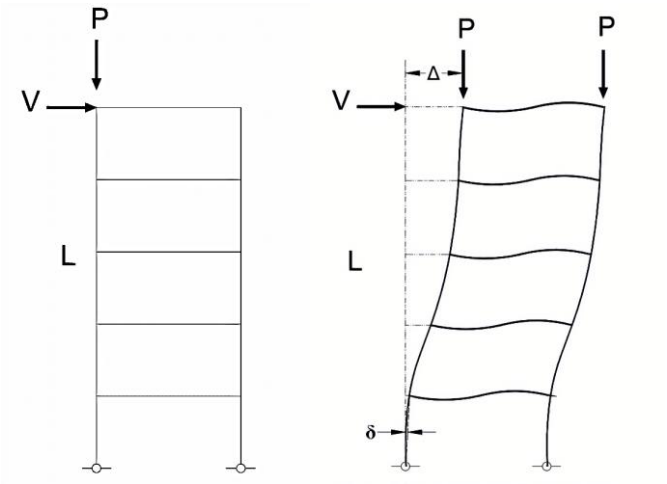

Figure 2.4: Second-order (P-Δ) effect

The second-order (P-Δ) effect can be affected by structures' dynamic response to lateral loadings, such as wind actions. In this respect, to assess the importance of the dynamic response of buildings, their natural frequency of vibration should then be quantified. In low-rise buildings, the dynamic reaction might be deemed negligible if it was based on the limit state strength and stiffness (Boggs and Dragovich, 2006).

Note: If the structure's natural frequency is less than 1 Hz, it tends to be dynamically sensitive and more vulnerable to second-order (P-Δ) effects under wind loading. In such instances, however, the second-order (P-Δ) effect is important and should be considered. (Buggs and Dragovich, 2006; Park and Yeo, 2018).

Furthermore, to explore the possibilities and limitations of the maximum overall height for buildings, many variables affect the building's structural performance and thus influence the maximum overall height. Some of the variables and their related studies are listed here:

- **Concrete Grade**

Several studies have been conducted on the impact of the concrete grade on the concrete components' ultimate capacity, including a study by Ibañez, Hernández-Figueirido and Piquer (2018) who investigated the effect of the concrete grades C30 and C90 on the CFST (concrete-filled steel tube) columns. The findings suggested that the concrete strength has a significant effect on the columns' ultimate capacity, which means that by raising the concrete grade from C30 to C90, the column sections could sustain higher loads.

- **Column Size**

As for the column size, there are not many studies on the impact of various parts of the concrete column on its load capacity or ultimate strength, e.g. Murty et al. (2012) stated that the size of the column had a direct effect on the density and strength of the building, in which the growth in the size of the column consequently increased its mass and stiffness. Also, Avşar, Bayhan, and Yakut (2012) established that variables such as axial load level, tension and compression reinforcement, concrete strength, and geometry directly influence the concrete beams and columns' rigidity. It can be inferred that larger columns can result in higher rigidity in the building's structural performance.

- **Column shape**

Furthermore, there is no thorough research on the effect of the shape of the concrete column on the building's structural performance and its impact on the punching shear. However, the moment of inertia, which reflects the mechanical characteristics of the material in response to applied stress due to the load, is an integral factor that can affect the strength of the element’s section (Singh, Nagar and Agrawal, 2016). This value for rectangle and square shapes can differ depending on the axis, while it is the same for circular shapes in both directions. That is why a rectangular shape that corresponds to a circular one with the same area will have a higher moment of inertia in one dimension and a lower value in the other.

Ibañez, Hernández-Figueirido and Piquer (2018) have studied the shape effect on the axial loading of high strength CFST stub columns. In this study, three distinct cross-section shapes of the same area were used: circle, rectangle and square. The findings revealed that the circular columns of the CFST were able to endure higher axial forces, shear forces and bending moments than the rectangular or square columns.

- **Slab Thickness**

Slab thickness is another factor that can affect the structural performance of the building in the lateral stiffness and punching shear, particularly in flat slabs. A big concern with such a factor is the concentration of bending and shear stress in the columns' surroundings, which could contribute to punching failure (Moreno and Sarmento, 2011; Lapi, Ramos and Orlando, 2019). Additionally, punching shear failures can occur in internal, edge or corner columns and its ratio in corner columns is more critical than the other two (Bond, 2011; Alkarani and Ravindra, 2013). On the other hand, adjusting the thickness of slabs can significantly affect the lateral vibration of the building. Islam Khan et al. (2013) examined the optimal slab thickness of reinforced concrete slabs to avoid the floor's excessive vibration. It has been reported that the frequency and stiffness are directly related, such that increasing the thickness of a slab increases the frequency and stiffness of the structure. Since the slab thickness variation can greatly affect the punching shear ratio ($V_{Ed}/V_{Rd,c}$) on flat slabs (Goodchild, 2009), two punching shear ratios, being 2 and 2.5, are recommended by the UK National Annex.

2.3 Finite Element Simulation

The finite Element Method (FEM) is a widely used numerical technique in the structural engineering community, as it is used to conduct finite element analyses of any specified physical phenomena. This method, due to its easier modelling, adaptability to individual specifications, accuracy, simulating time-dependent problems and the use of boundary conditions, can appeal to engineers (Ciarlet and Lions, 1991). Figure 2.5 illustrates the process of analysis in the finite element to achieve the desired results.

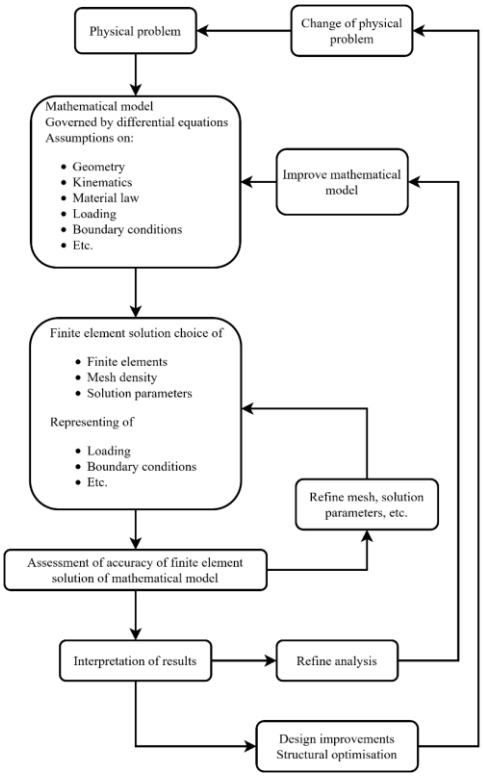

Figure 2.5: Finite element analysis procedure (Bathe, 2016)

There are various finite element software packages in the engineering filed such as ETABS, Abaqus ANSYS, Solid Work and many more, which depending on the nature of the investigated physical phenomena, can be used. In this research, ETABS, Abaqus and ANSYS were utilised to conduct various finite element simulations and achieve the desired results. In the following section, the application of ETABS, Abaqus and ANSYS in the literature is presented.

2.3.1 CSI ETABS

ETABS is an engineering software that is used for the design and analysis of buildings of any height. Some of this software's features are code-based load prescriptions, Modelling tools and templates, analysis methods and solution strategies, all combined with grid-like geometry along with simple and complex structures under static or dynamic loads. For an advanced analysis of seismic performance, direct time-history and modal analysis can be combined with large displacement and P-Delta effect. Intuitive and integrated designs allow implementing some complexity feasible to implement in ETABS (CSI Knowledge Base, 2013).

The use of ETABS has a wide range in the application of reinforced concrete frame buildings. For example, Nishanth et al. (2020) used ETABS to model a commercial building with various slab configurations, i.e. a conventional slab, a waffle slab, a flat slab with drop panels and a building with a load-bearing wall. The impact of seismic and wind forces on buildings with various slab configurations was studied. The analysis and modelling were carried out in compliance with IS 456-2000 regulations. In this analysis, multiple factors influencing the efficiency of the structure, such as the base shear, storey displacement and storey drift were examined for the response of a structure against the wind and the seismic forces. The results indicated that the storey displacement rose with the storey's height, and the building with the flat slab was stable and economical compared to the other slab arrangements used in the structural analysis with wind and seismic loads.

In some studies, the modification in the design of buildings was investigated, including the study conducted by Naveen E, Abraham and SD (2019) and Akhil Ahamad and Pratap (2020). They investigated reinforced concrete buildings' structural performance with different shear wall locations and different combinations of irregularities.

Naveen E, Abraham and S D (2019) explored the use of shear walls at various locations in a G+20 multi-storey residential structure, as well as the nature of the structure subjected to seismic activities, by implementing Response Spectrum Analysis. The multi-storey structure with G+20 was evaluated for base shear, storey drift, torsional irregularity and maximum allowable displacement. The modelling and analysis of the whole structure were carried out with ETABS 2015 in India's seismic regions as recommended by IS 1893. It was determined that the structure with the shear walls positioned symmetrically would show better performance compared to the structures without the shear walls and with shear walls at one end only.

Furthermore, Akhil Ahamad and Pratap (2020) evaluated the seismic response of reinforced concrete buildings with different combinations of irregularities. In this study, a nine-storey

regular structure was adjusted by integrating irregularities in different ways, both in plan and in elevation, into 54 irregular arrangements. Both frames were subjected to seismic loads, and the structural response was simulated with ETABS. It was reported that the irregularity has a significant impact on the seismic response. Also, out of the different forms of single irregularities examined, the stiffness irregularity was observed to have the maximum impact on the response.

The design optimisation was the focus of some other studies, including Huang et al. (2015), who focused on an advanced numerical modelling approach for the performance-based design of tall buildings exposed to different levels of wind excitation. Hence, a performance-based wind engineering method was designed by defining numerous performance targets associated with numerous levels of wind hazards. A non-linear static pushover analysis using ETABS was adopted to estimate the inelastic drift efficiency of an existing 40-storey residential building exposed to rather unusual intense wind incidents. Results showed that the design optimization approach offers an effective computer-aided design technique to solve the wind engineering design of high-rise buildings exposed to varying levels of wind excitations.

Moreover, there is a trend to enhance construction sustainability by investigating the impact of different construction materials on the structural performance of reinforced concrete buildings. In this regard, Gan et al. (2017) aimed to establish the relationship between various design criteria and the embodied carbon in tall buildings. In this analysis, various tall buildings were modelled using ETABS software with various construction materials, structural shapes, recycled contents and building heights. The findings revealed that tall buildings' embodied carbon varies significantly with the selection of building materials and structural shapes. Also, this study's finding can help make more environmentally friendly choices when constructing tall buildings to minimise the carbon emissions from the construction industry. In a similar study, Al-Tamimi, Ibrahim and Al-Sughaiyer (2014) performed an analysis of three different concrete mixtures with strengths of 100 MPa (High strength), 50 MPa (Normal) and 50 MPa (Lightweight) to measure their influence on sustainability and economics. A global analysis, including

structural, environmental and economic efficiency, was made using Life-365 software and ETABS to identify the most advantageous and sufficient material to use in sustainable structures. In this study, the only input parameters were the various mixtures of concrete but the other variables, including the dimensions of the buildings and the applied loadings, were the same. It was observed that the high strength concrete with micro silica was the most economical and sustainable substance to use in construction.

2.3.2 Abaqus Unified FEA

The Abaqus FEA software provides efficient and thorough solutions to common and advanced engineering challenges and addressing a wide variety of industrial applications. In the automotive sector, engineering workgroups can understand complete vehicle loads, dynamic vibration, multi-body structures, impact/crash, non-linear static, thermal and acoustic-structural couplings using standard model data structure and advanced solver technologies. Best in class, companies use Abaqus FEA to consolidate their systems and resources, lower costs and inefficiencies and achieve a strategic advantage (Abaqus Unified FEA - SIMULIA, 2007).

There are wide ranges of studies conducted with Abaqus on the application of reinforced concrete frames. For instance, Zhou et al. (2020) conducted an experiment to assess the progressive collapse performance of two half-scale RC and PC moment sub-structures under a sudden mid-column failure scenario. In the PC samples, the beam-column connection was completely assembled using the dowel bars implanted in the corbel, and the steel angle cleats were added to the connection between the upper surface of the beam-end and the column to transfer the flexural moment further. Horizontal hoops supported the beam-column connection and U-shaped bars. The experimental results revealed that the load-carrying capacity of the PC specimen was 76.9% of the RC specimen, while the ultimate deflection of the mid-column of the PC specimen was 106.1% of the RC specimen. Furthermore, finite element analysis with Abaqus was conducted, and the findings of the analysis were well correlated with the test results.

In many studies, individual reinforced concrete elements, e.g. reinforced concrete beams, were analysed, including Earij et al. (2017), who developed three-dimensional nonlinear finite element models with Abaqus to examine the loading-unloading and reloading behaviour of two reinforced concrete beams under four-point bending test. In this study, a perfect bond was considered between the steel rebars and the concrete section, in which the bond-slip behaviour and the damage induced by crack patterns were defined through concrete damage. Also, the effect of the shape of the tension softening principle on the numerical load-deflection response was evaluated considering bi-linear, exponential and linear post-failure stress-displacement and stress-strain relationships. In the post-yield process, differences were noticed when truss elements were being used for steel rebars, although a strong agreement was noticed when the bending stiffness of the rebars was being used with beam elements. This undiscovered finding might be necessary to remember when researching the progressive collapse of RC systems.

Also, Lee et al. (2020) studied the behaviour of post-tensioned concrete beams using Abaqus as a finite element method. This study aimed to investigate the concrete damage behaviour, using the concrete damaged plasticity (CDP) method in Abaqus, and the influence of the external post-tensioning (EPT) steel rod method. Since there is considerable complexity concerning the bond-slip relationship between concrete and steel, in this study, some assumptions for concrete beams were carried out, including the perfect bonding of steel and concrete and the CDP method for concrete properties. By comparing the analysis and the experimental findings, the simulated tensile deformations were close to the experiments' real crack patterns. The analytical responses, such as stress, strength and deflection of the exterior rods, were in good alignment with the measured responses.

Furthermore, Rahman et al. (2019) carried out an experimental study on a three-dimensional non-linear model, using the concrete damage plasticity method in Abaqus, with reinforced foamed concrete beams. This study aimed to use Agro-industrial wastes containing

supplementary cementitious materials (SCMs) since they are known to be sustainable measures to reduce the environmental impacts of residual agricultural by-products and manufacture cement. Therefore, this experimental study's concrete mix contained 20% Palm Oil Fuel Ash and 5 % and 10% Eggshell Powder as a partial cement substitute. As a result, the results showed that the suggested numerical simulation effectively predicted the damage behaviour of foamed concrete.

There are also various studies on the application of Abaqus in reinforced concrete columns. Dai et al. (2014) employed Abaqus to model the behaviour of slender concrete-filled steel tubular (CFST) columns with elliptical hollow parts under axial compression. The reliability of the FEM was confirmed by comparing the numerical estimation with the experiment results of eighteen elliptical CFST columns specifically chosen to reflect the standard sectional dimensions and the member slenderness. In addition, a parametric study was conducted out of different section sizes, lengths and concrete strengths to address a wider variety of member cross-sections and slenderness that are commonly used in practice. It was concluded that the design rules laid down in Eurocode 4 Part 1-1 (BS EN 1994-1-1, 2009) for circular and rectangular columns of the CFST might be implemented to measure the axial buckling load of the elliptical columns of the CFST. Although, the use of length /300 defined in Eurocode 4 Part 1-1 (BS EN 1994-1-1, 2009) for imperfections seems to be over-conservative for elliptical columns of the CFST with smaller non-dimensional slenderness.

Moreover, Elchalakani et al. (2018) conducted a parametric study with Abaqus to predict the response of glass fibre reinforced polymer (GFRP) and ordinary Portland concrete columns under concentric and eccentric axial load. The measured load-deflection reactions from actual laboratory data were compared with the predicted curves to verify the model. The experimental curves were found to be in near alignment with the expected load-displacement reactions. The predicted N-M strength interaction diagrams fitted the measured curves of the experiment,

especially for GFRP RC columns with a wide gap between the ligatures, as they showed a ductile failure that was well depicted by the numerical analysis.

Moreover, Cao, Wu and Li (2020) performed a finite element analysis with Abaqus to investigate the mechanical efficiency of steel-concrete columns under combined torsion and verify the outcome with experimental findings. In this study, the effect of seven parameters, including the axial load ratio, the concrete strength, the torsional bending ratio, the longitudinal reinforcement ratio, the steel ratio, the shear-span ratio and the stirrup ratio, on the torsional behaviour of the steel-concrete columns was extensively evaluated.

Some other studies on the application of shear capacity in reinforced concrete slabs, including the study done by Belletti, Walraven and Trapani (2015), who proposed a non-linear finite element approach with Abaqus software that adopts multi-layer shell simulation of RC slabs. In this study, post-processing of the non-linear finite element results using the Critical Shear Crack Theory (CSCT) was obtained to test the shell elements' shear resistance. The proposed numerical method's ability to calculate the punching shear resistance of the RC slabs was validated by comparing numerical results with experimental punching shear capacity obtained from circular slabs evaluated at the Stevin Laboratory of TU Delft. The same numerical technique was used for the Corick Bridge Deck in Northern Ireland, the United Kingdom, to test the effects of Compressive Membrane Action (CMA) on the punching shear resistance, which was subjected to concentrated loads. The analyses were compared with the experimental values produced by the British Code BD81/02 and showed a good correlation.

The beam-column and slab-column connections using Abaqus focused on some other studies, including the study conducted by Genikomsou and Polak (2015). They performed nonlinear finite element analyses of reinforced concrete slab-column connections under static and pseudo-dynamic loads using Abaqus to explore their failure modes in terms of ultimate loading and cracking patterns. The simulations of various slab-column connections without shear reinforcement illustrated the predictive capacity of the optimized model. The comparison

between experimental and numerical findings showed that the optimized model correctly estimates the slabs' punching shear response.

Additionally, Balineni, Jagarapu and Eluru (2020) intended to explore the behaviour of precast beam-column connections with two types of wet connections and two types of dry mechanical connections with Abaqus software. In this experiment, five prototypes comprising two wet connections, two dry mechanical connections and a monolithic connection were analysed with Abaqus software. The results showed that the wet connections showed a higher degree of fixity, which is required for the emulative method in precast design. In comparison, the dry connections worked less efficiently compared to wet and monolithic connections.

2.3.3 ANSYS

ANSYS structural analysis software can make the simulation simpler to tackle the most challenging structural engineering problems and make superior design choices more efficiently. ANSYS's finite element analysis (FEA) provides engineers with the ability to automate and configure simulations and parameterize them for various applications. ANSYS Structural Mechanics applications can be conveniently linked to other physical methods for even more accuracy, modelling even the most sophisticated projects' efficiency and behaviour. Engineers worldwide are optimising prototype designs using FEA from ANSYS (ANSYS FEA Software, 2016). ANSYS has been widely used in various studies to understand the characteristics of reinforced concrete frame buildings around the world, and here, some of the studies are mentioned.

In some studies, the influence of composite materials such as carbon fibre reinforced polymer (CFRP), glass fibre reinforced polymer (GFRP) bars and reinforced steel fibre concrete (SFRC) on reinforced concrete beams and columns were examined.

Sridhar and Prasad (2019) performed an experimental and numerical study on the static and dynamic characteristics of steel fibre reinforced concrete (SFRC) beams. The mechanical

properties were obtained by conducting the compression, split tensile and flexural strength of the SFRCs. Besides, the dynamic properties such as natural frequency, damping ratio and mode shape of SFRCs in free-to-free constraints were also determined by applying the addition of total fibre volume fraction as 0%, 0.5%, 0.75%, 1% and 1.25% of concrete. The static findings highlighted that the addition of steel fibre to concrete dramatically improves the efficiency of the mechanical properties. Dynamic test findings revealed that steel fibres' inclusion reduces the natural frequency and enhances the damping ratio. In addition, numerical modellings were developed with ANSYS for control and SFRC specimens to compare the experimental findings with computational model prediction.

In another study, Adam et al. (2015) provided an experimental, numerical and theoretical analysis of the flexural behaviour of reinforced concrete beams with locally manufactured glass fibre reinforced polymer (GFRP) bars. Ten beams were prepared and tested for failure under a four-point bending test. The key parameters were concrete compressive strength, reinforcement material type and reinforcement ratio. In this study, the crack width, mid-span deflection and GFRP reinforcement strains of the tested beams were measured and compared. A non-linear finite element analysis with ANSYS was also developed to model the flexural behaviour of the beams measured in terms of crack pattern and load-deflection behaviour. It was demonstrated that between experimental and numerical results, a strong agreement was achieved. In addition, modifications to the ACI 440.1R-06 equation were introduced to approximate the effective moment of inertia in FRP-reinforced concrete beams, using a regression analysis of experimental findings by adding empirical variables that efficiently minimise the moment of inertia at a high load level. It can be seen that the proposed variables provide a reasonable approximation of the effective moment of inertia in FRP reinforced concrete beams at a high load rate.

Furthermore, Al-Rousan (2020) adopted ANSYS three-dimensional finite element simulations to model the response of reinforced concrete columns with circular cross-sections confined with

different CFRP composite arrangements. According to the individual characteristics of each element, the nonlinear properties of the material were specified. The FEA findings were in terms of stress-stain distribution, axial load-axial strain and circumferential responses, and axial load-axial displacement response. It was concluded that the rise in the number of CFRP sheet layers leads to a significant rise in the ultimate axial strength and a slight increase in the ultimate displacement of the columns.

Many studies focused on the structural performance of reinforced concrete elements. For example, the study conducted by Kazaz, Yakut and Gülkan (2006) utilised ANSYS to perform numerical simulations of a 1/3 scaled, five-storey reinforced concrete load-bearing shear walls under seismic excitation in the form of the IAEA benchmark shaking table experiment performed in CEA laboratories in France. Several non-linear time-history analyses were done to model the damage experienced and the measured response quantities for the examined specimen on the shaking table. The simulation response was evaluated at the micro and macro levels, and the findings were compared with the calculated values to verify the precision of the numerical simulation. The comparison of numerical and experimental findings resulted in a strong agreement.

Hassan, Sherif and Zamarawy (2017) examined the problem of transverse openings to fit service ducts and pipes in reinforced concrete beams. In this study, fifty-seven beams were tested using the finite element ANSYS subjected to static load and the results of the study were validated with the results of fifteen experimental beams. The analysed beams were reinforced with six different fibre-reinforced polymers (FRP) system. The findings revealed that the enhancement of beams using FRP sheets would significantly increase its overall stiffness and recover a part of its lost stiffness due to the beam's opening. It was also found that the failure loads were primarily caused by the strengthening system and were partially influenced by the spacing when one sheet of GFRP laminates was used.

2.4 The Use of Sensors in Structural Health Monitoring

The lack of appropriate sensing technology has traditionally constrained studies in the area of RC to monitor the complete behaviour of these sophisticated composite structures. Discrete sensors, including displacement transducers and resistance strain gauges, provide localised measures of extremely nonlinear material behaviour, and failure mechanisms could be observed in depth with conventional sensors. The ability to detect, monitor, or anticipate such mechanisms could be crucial in designing or evaluating such systems (Broth and Hoult, 2020).

As a part of this PhD research, the current techniques of monitoring the performance of reinforcement in concrete sections will be explored to obtain a more detailed assessment of the failure of steel reinforcement under applied loads. Therefore, in this section, the mechanism and application of strain gauges as one of the most convenient techniques in structural health monitoring sensors will be discussed.

Although there are many ways of measuring strain changes, the most frequent technique is a strain gauge as an instrument whose electrical resistance changes with the amount of strain in the specimen. For instance, the piezoresistive strain gauge is considered as a semiconductor system whose resistance changes non-linearly with the strain. Though, the most commonly used gauge is the metallically bonded strain gauge. The metallic strain gauge contains a thin wire or, more generally, metal foil set in a grid pattern. The grid layout aims to maximise the total amount of metal wire or foil being strained in parallel (Figure 2.6). The cross-sectional area of the grid is reduced to mitigate the influence of shear strain and Poisson strain. The grid is connected to a thin frame, called the carrier, directly attached to the test specimen. The strain encountered by the test specimen is then passed directly to the strain gauge, which reacts with a linear change in resistance. Strain gauges are commercially available with nominal resistance values ranging from 30 to 3000, and 120, 350 and 1000 are the most common values.

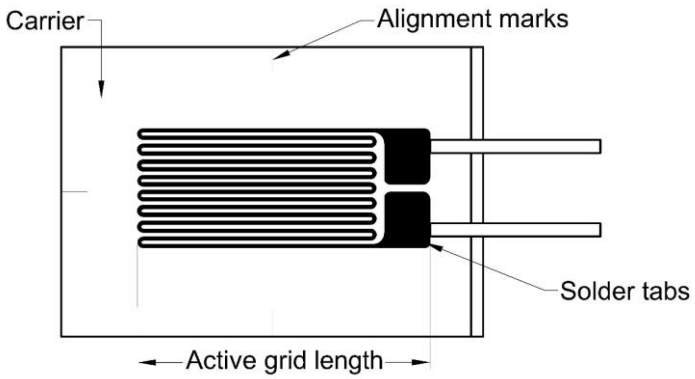

Figure 2.6: Metallic strain gauge

The strain gauge's primary parameter is its sensitivity to strain, defined quantitatively as the gauge factor (GF). As shown in Equation 2.3, the Gauge Factor is expressed as the ratio of the fractional alteration in electrical resistance to the fractional change in length (strain).

$$GF = \frac{\Delta R/R}{\Delta L/L} = \frac{\Delta R/R}{\varepsilon} \quad \text{(Eq. 2.3)}$$

where ΔR, ΔL, R and L are the strain-induced resistance change, full change in length, gauge wire resistance and unstressed length of gauge wire, respectively. Also, the gauge factor for the metallic strain gauges is generally taken as 2.

Theoretically, the strain gauge resistance should change only in response to the applied strain. However, the strain gauge material, as well as the specimen material to which the sensor is applied, will also react to temperature changes. Strain gauge producers are looking to reduce temperature sensitivity by treating the gauge material to account for the thermal expansion of the sample material for which the gauge is aimed. In fact, strain measurements seldom require quantities greater than a few millistrains ($\varepsilon \times 10^{-3}$); Hence, measuring the strain requires precise measurement of minor resistance changes.

In order to calculate certain minor variations in resistance and to account for the temperature sensitivity mentioned earlier, strain gauges are almost exclusively used in bridge setups with a source of voltage or current excitation. As seen in Figure 2.7, a commonly used Wheatstone

bridge consists of four sensitive arms with an excitation voltage, V_{EX}, which is applied through the bridge. The bridge can be designed in either quarter, half, diagonal or full arrangements.

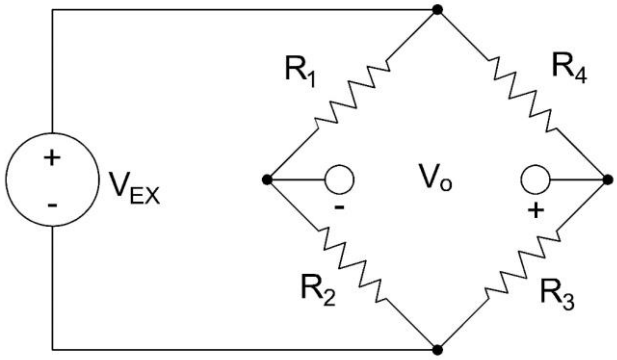

Figure 2.7: Wheatstone bridge

The output voltage of the bridge, V_0, is presented in Equation 2.4:

$$V_o = \left[\frac{R_3}{R_3+R_4} - \frac{R_2}{R_1+R_2}\right] \times V_{EX} \qquad \text{(Eq. 2.4)}$$

It is obvious from this equation that when $R_1/R_2 = R_3/R_4$, the voltage output of Vo is zero. The bridge is assumed to be balanced under these conditions. Any changes in the resistance of a bridge arm can lead to a non-zero output voltage. Thus, if the R4 in Figure 2.8 is substituted by an active strain gauge, any variations in the resistance of the strain gauge will unbalance the bridge and create a non-zero output voltage. If the nominal resistance of the strain gauge is regarded as R_G, the strain-induced resistance change, ΔR, can be expressed as $\Delta R = R_G \times GF \times \varepsilon$. Presuming $R_1=R_2$ and $R_3=R_G$, the bridge equation can be modified to represent V_O/V_{EX} as a function of strain (see Equation 2.5 and Figure 2.8).

$$\frac{V_o}{V_{EX}} = -\frac{GF\times\varepsilon}{4}\left(\frac{1}{1+GF\times\frac{\varepsilon}{2}}\right) \qquad \text{(Eq. 2.5)}$$

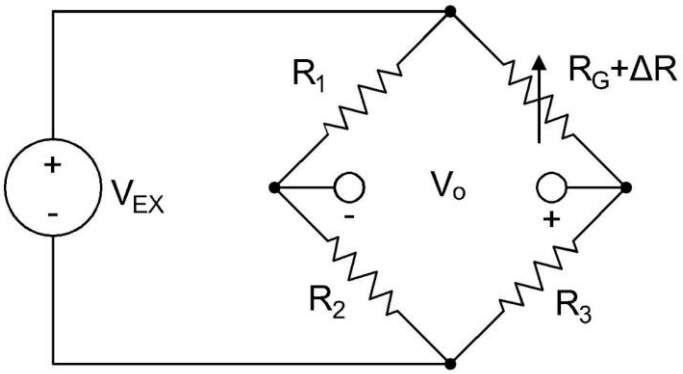

Figure 2.8: Quarter-bridge circuit

In order to obtain a more comprehensive behaviour of reinforced concrete frames, especially in terms of the stress-strain relationship for the concrete and reinforcement interactions, many strain gauges have been used in reinforced concrete beam or column components. In the following section, some of the previous studies in this regard are mentioned:

Depending on the study's purpose, strain gauges can be mounted on different positions to measure the strain. For example, Monserrat López et al. (2020) used strain gauges attached to the reinforcement along with displacement transducers and Digital Image Correlation to monitor the shear strength in continuous beams with and without shear links. The results showed that the shear strength given by concrete decreased as the bending rotation increased in both the elastic and plastic rotation ranges formed in continuous beams. The formulation of the code given by ACI 318-19, Eurocode 2 Part 1-1 (BS EN 1992-1-1, 2014) and Model Code 2010 was tested against experimental findings. It was shown that the iterative formulation of the M-V relationship greatly enhanced shear strength predictions by simple formulations.

In another study, Dok et al. (2020) investigated the residual flexural capacity of high-strength reinforced concrete beams using strain gauges attached to the shear reinforcement and displacement transducers. In this study, the experimental analysis is performed into the dynamic response of high-strength, full-scale reinforced concrete beams subject to various impact energies. The rectangular cross-section measurements of the RC beams were 250 mm × 400 mm. The impact experiments were carried out by dropping weights of 240, 360 and 480 kg from

a height of 3 m. The results found that the flexural stiffness of the specimens was remarkably decreased by the magnitude of the impact experienced.

In addition, Jirawattanasomkul et al. (2020) explored the use of natural jute reinforced polymer (JFRP) composite sheets as external RC beam material strengthening. In this study, strain gauges attached to the shear links and NFRP sheets and linear variable displacement transducers (LVDTs) were used to monitor the beam specimens' behaviour. Pre-damaged RC beam specimens were prepared to represent seismic damage. Test results have shown that JFRP can significantly increase the shear strength of the beams.

In some other studies, the researchers used strain gauges both embedded and on the specimens' surface, including Nie et al. (2020), who investigated the shear performance of reinforced concrete beams with GFRP needles. Therefore, it was proposed to cut FRP residue into randomly distributed, short-length reinforcement bars as a replacement for part of the coarse aggregate in concrete. In this study, to monitor the behaviour of the specimens, five LVDTs and strain gauges were placed on the top surface of the sample and attached to the longitudinal reinforcement. The increased load-carrying capability of 8–10% was observed in beams with spirally wrapped needles. The presence of GFRP needles raised the overall energy absorbed by the RC beams by approximately 33–40%. The research looked at 10 RC beams without steel stirrups in the critical half of the four-point bending and found that the needles had improved ductility.

Furthermore, Huang et al. (2019) examined the fatigue performance of reinforced concrete beams reinforced by a strain-hardening fibre-reinforced cement composite using LVDTs and strain gauges installed on the top surface of the concrete beam and attached to the longitudinal reinforcement. In this experiment, two series of strengthened beam specimens were prepared with various thicknesses of the enhancement layer, and three fatigue stress levels were tested to investigate the fatigue life, mid-span deflection, and crack mode of the tested

specimens. Several approaches are proposed further to improve the fatigue strength of reinforced concrete beams.

Moreover, Xingyu, Yiqing and Jiwang (2020) examined the flexural behaviour of steel-GFRP hybrid-reinforced concrete beams due to the fragility of GFRP and its poor bonding efficiency with concrete. To assess the influence of bonding performance on the flexural behaviour of GFRP-and hybrid reinforced concrete beams, LVDTs and strain gauges on the top, bottom and sides of the beam and attached to the shear links and GFRP inside the concrete were used. In this study, both forms of beams were made and tested with four-point bending tests. The flexural capacities of experimental findings were then correlated with theoretical results. Based on the FE simulation effects, it was shown that the theoretical method overstates the flexural capacity by 9%.

In a similar study, Zaki and Rasheed (2020) used six RC beams to determine the effects of new flexural anchorage devices on enhancing the performance of reinforced concrete beams in flexure. In this experimental study, LVDTs and strain gauges installed on the concrete beams' top surface and attached to the longitudinal reinforcement were used to monitor the compressive strain of concrete. T-beams anchored with GFRP sidebars demonstrated an improvement of 74% and 58% in strength over unanchored specimens, respectively. It was concluded that both anchorage sheets were used with CFRP devices greatly improved the flexural capacity beyond that of without anchoring and U-wrap of anchored specimens. It is worth mentioning during the test that it was noted that the results from the embedded strain gauges were suddenly lost and not recorded.

2.5 Sustainability in Construction

According to the United Nations' World Environment and Development Committee, sustainability means addressing current concerns without compromising future generations' capability to fulfil their necessities (Peake, 2004). Based on various scientific facts mentioned in

the previous studies (Uher and Lawson, 1998; Our Common Future, 2008; Building a low-carbon economy, 2008; Ortiz, Castells and Sonnemann, 2009; Yılmaz and Bakış, 2015), the planet's capacity to support life in the manner that has been done for thousands of years has hit an alarming limit, resulting in irreversible disruption to the planet and its resources, its inhabitants and the ecosystem. This situation has become more extreme, particularly after the Second World War, as rapid economic developments in construction occurred due to overpopulation and increasing demand in urban areas, which have been significantly harmful by over-excavation of natural resources, such as fossil fuels, minerals, forests and lands (Uher and Lawson, 1998; Yılmaz and Bakış, 2015). Recently, radical changes have been required to address global problems such as natural resource consumption, air pollution, climate change, waste production and environmental degradation in major cities. The planet must now decrease emissions up to about 50 % by 2050 since significant environmental problems such as global warming and climate change have been caused by carbon dioxide (CO_2) emissions and other greenhouse gases that are already affecting human lives (Building a low-carbon economy, 2008).

Additionally, as a strategically important sector in many countries, the construction industry provides the infrastructure and buildings needed for the rest of society and the economy. This sector is expanding intensively worldwide, producing about 9% of gross domestic product (GDP) throughout the EU and creating 18 million work openings (European Commission, 2016). However, this industry is responsible for a large amount of CO_2 pollution, including the production of Portland Cement, as an important part of the concrete, and other greenhouse gases (GHGs) added to the environment, including material production, construction process, renovation and demolition waste (González and García Navarro, 2006; Malhotra, 2010).

Besides, this sector is liable for the responsibility of other environmental concerns, such as industrial waste creation, internal and external emissions, water consumption and natural resource extraction, including 25% biomass, 40% gross and fine aggregate and 16% water

extraction (Green Building Home, 2018). Therefore, the sustainability of concrete in the construction industry is a vital factor for improving the quality of life, knowing that the environmental issues linked to CO_2 will have a key role in the sustainable development of concrete in the construction industry over the coming decades.

2.5.1 Sustainable Design in Reinforced Concrete Frame Buildings

Given the unsustainable level of consumption in industrial countries and the planet's inability to withstand the harmful influence of human activity, this situation must be changed before the exhaustible natural resources of the planet run out. Enhancing construction practises to minimise these harmful environmental effects has also drawn the interest of building experts worldwide (Sev, 2009).

As an appropriate response to the situation, in the UK, the Building Leadership Council and the UK Government released the Construction Industry deal in July 2018, which committed £420 m to fund the transformation of the industry (Davies, 2018). This transformation in the construction industry could occur in several fields, especially regarding sustainability in the design of reinforced concrete frame buildings to consume a lower level of concrete in the construction process.

Reducing the amount of concrete in the construction of RC frames may be a feasible option that would significantly affect the reduction of CO_2 emissions from the industry. As mentioned earlier in the literature (Chandurkar and Pajgade, 2013; Rasikan and Rajendran, 2013; Thakur and Singh, 2014; Aainawala and Pajgade, 2014; Jayalekshmi and Chinmayi, 2015; Ghorpade and Swamy, 2018), this reduction can be accomplished by removing the redundant components such as shear walls in the design of RC buildings that are considered to have negligible structural impacts while consuming a considerable amount of time and expense during the construction period.

Furthermore, innovative designs for RC buildings could be another potential option for improving the construction industry's sustainability. As investigated earlier in the literature Chen, Suswanto and Lin, 2009; Chen and Lin, 2009; Kaung and Wong, 2011; Lu et al., 2012; Masi et al., 2013; Parastesh, Hajirasouliha and Ramezani, 2014; Huang et al., 2017; Shufeng et al., 2018), such developments could be associated with different aspects of the design, such as in the connections between beams and columns, which could help to reduce the consumption of concrete in the construction process while ensuring safe and efficient structural performance in compliance with the Eurocodes.

2.5.2 Sustainable Development (SD)

Sustainable development (SD) is a comprehensive paradigm accepted by the international community to protect natural resources. In this approach, the natural resources should be consumed in a balanced approach that does not cause irreversible damage to unrenewable resources for future generations (Our Common Future, 2008). Moreover, this development is becoming a perception that applies to various fields, ranging from planning of production to architectural design (Hoúkara, 2007 cited in Yılmaz and Bakış 2015). Sustainable development seeks to increase the quality of our lives by helping our community to provide a healthier world with improved environmental, economic and social conditions (Ortiz, Castells and Sonnemann, 2009).

One of the most researched branches of sustainable development methods in the construction industry is the substitution of fine aggregates with waste materials in concrete mix design (Saxena et al., 2018; Sosoi et al., 2018; Smarzewski, 2018; Poonyakan et al., 2018; Ejiogu et al., 2018; Babafemi et al., 2018; Zaleska et al., 2018a and Rubio-de Hita, 2018). The substitute material varies depending on the size and use of the concrete mixture.

Four of the leading mixed plastic materials used as fine aggregate substitutes are:

- **Polythene Terephthalate (PET)**

In some of the studies, PET was used as a fine aggregate; for example, Saxena et al. (2018) conducted an experimental study of concrete properties under impact loading when the fine aggregate in the concrete mix was replaced by recycled plastic waste. Waste PET containers and cans have been recycled and shredded into fine and coarse aggregates, with fine plastic aggregate (FA) substitute noted to vary in particle size from 0 to 4.75 mm, substituting sand with a rise of 5% from 0 to 20%. The control mixture and four FA-replacement mixtures were cast into three 100 mm3 cube samples and 100 × 75 mm cylinders, with the average compressive strength of the concrete cubes measured at 7 28 and 90 days. The results showed a normal general decrease in compressive strength as the amount of plastic in the concrete mixture increased. Seven-day compressive strength was provided as 17.8 N/mm^2 for the control mixture and 3.6 N/mm^2 for 20 % plastic substitution, a 14.2 N/mm^2 drop from control. Readings at 28 and 90-day curing also indicated a reduction in compressive strength as the plastic was added. It was noticed that the smooth surface of the plastic aggregate used in the sample was an issue for the poor cohesion of the bond between the plastic aggregate and the cementitious material.

In comparison, Sosoi et al. (2018) used a significantly higher gradual aggregate replacement amount of 25% to determine the impact of two recycled material sources as a partial and complete replacement of the fine aggregate in the concrete mix. Chopped PET bottles and sawdust were used separately as sand substitutes in aggregate sizes of 0 to 4 mm, indicating that the workability of plastic-containing concrete mixtures improved as the plastic content increased. Following the control mix casting, the mixtures using the replacement aggregate consisted of partial 25, 50, 75% and 100% replacement, with the mixed coding representing PETPC1 as the 25% to PETPC4 as the 100% replacement. The concrete mixtures' variety of fresh and mechanical properties was investigated, including the compressive strength on 70 mm^3 cube samples cured for 14 days.

The control mixture achieved a compressive strength of 47.90 N/mm^2, whilst, considering a substantial improvement in compressive strength achieved for PETPC2 (containing 50% PET) given as 54.32 N/mm^2 (a 13.4% increase compared to control) and a small increase in PETPC3 (containing 75% PET) given as 48.73 N/mm^2 (a 1.7% increase compared to control). It was noticed that as PET increased in the concrete mix, the compressive strength reduced in a general pattern.

- **PET, Polyethylene (PE) and Polypropylene (PP)**

In some other experiments, PET, PE and PP were being used as fine aggregates. Thorneycroft et al. (2018) conducted a controlled experiment using five varieties of recycled plastic as a fine aggregate substitute for both granular and fibre morphologies. The efficiency of the concrete mix design was measured with recycled plastic comprising of a specified 10% partial sand replacement rate as calculated by the experimental mixtures before the study. PET, High-Density Polypropylene (HDPP), High-Density Polyethylene (HDPE), Polypropylene Multifilament Fibres (PPF), Polypropylene Strips (PPS) were substances tested in the experiment, using three 100 mm^3 cubes and 100 mm diameter cylinders as control and ten plastic-infused concrete mixtures. After 14 days of curing, the compressive strength test was carried out with a control mixture of 53.8 N/mm^2.

The results obtained that the first three PET mixtures (PET1, PET2, PET3) displayed average compressive strength of higher than 51.5 N/mm^2 where, in fact, PET1 with plastic particles showed a compressive strength rating of 54.4 N/mm^2 and a rise of 1.2% (or 0.6 N/mm^2) relative to the control mixture. However, HDPP1 and HDPE1 declined to 47.0 N/mm^2 and 45.6 N/mm^2, respectively, relative to the control mixture, where PPF1 produced a substantial reduction of 37.7% in compressive strength relative to the control mixture. Also, PPF2 was subsequently developed to resolve the poor workability of PPF1 using a 0.64% plastic replacement rate to attain the workability expected, offering a compressive strength value of 54.5 N/mm^2. Furthermore, PPS1 was designed to compensate for the workability of PPF2 and the

compressive strength of PPF1. PPS1 showed a compressive strength output of 52.2 N/mm^2. Finally, it was concluded that it is possible to manufacture structural grade concrete mixtures with 10% sand substitution.

- **PET and PE**

Most of the previous experimental studies primarily focused on PET and PE as aggregate substitutes in the concrete mix (Zaleska et al., 2018a). Polypropylene (PP), as the most desired plastics in the world (Plastics Europe, 2017), needs not only constant creativity in the application of recycled materials but also consistent markets for diverse PP quality content (Croke, B., 2017). As a result, there has been a recent growth in literature discussing concrete as a consideration for the re-use of recycled PP applications. According to Thorneycroft et al. (2018), plastic fibre as a fine aggregate substitute, especially smaller in size and a different form of plastic, is a concept deeper explored by other researchers. Smarzewski (2018) researched the flexural toughness of high-performance concrete using PP fibres (P) and Basalt (B), both in combination and independently, as partial substitutes for sand in a concrete mix design. Basalt and PP fibres were included in 11 concrete mixtures, including the control mix, where PP was used individually in mixtures P1 and P2 at 1% and 2% replacement ratios. Also, a 20 L/m^3 superplasticizer was used as a way of maintaining the great workability of fresh concrete when plastic fibres were applied to the concrete mix, limiting segregation and flow, effectively rising viscosity and reducing concrete slumps (Smarzewski, 2018).

Several mechanical tests, including compressive strength tests, were carried out on 66 of 100 mm^3 cube samples required to be cured for 28 days. Throughout all stages of sand substitution, regardless of the form of material, the concrete mixture's compressive strength reduces. However, when testing mixtures containing PP fibres, there is a noticeably positive association between raising the compressive strength and increasing the content of these fibres up to a 1% replacement rate. Thus, Smarzewski (2018) results indicate that a decrease in compressive

strength of less than 10% can be accomplished by replacing fine aggregates with PP fibres in a concrete mixture of up to 1%.

- **PP, PE, Polystyrene (PS) and Polyvinyl Chloride (PVC)**

Jacob-Vaillancourt and Sorelli (2018) investigated the feasibility of using plastic aggregates as a partial substitute for sand in environmentally friendly concrete production. In this study, the impact of the percentage of substitution, plastic-type, the timeline diversification of plastic processing and the degree of impurity on the fundamental properties of concrete was investigated. A detailed mix was designed for the experiments, where the mixes were sorted through infrared optical filtering and classified as five variations: PP, PE, PS, PVC and 'others'. A control mix was developed with all five varieties of plastic aggregates and was used individually in their mixing designs, recombined to a mixed sample (MIX) to contain between 56% and 62% PP and a sample mixing both PS and PVC (PS-PVC).

After 28 days of curing, the specimens of the concrete cylinders were tested under the compression machine to acquire their compressive strength. It was noted that the rise in the plastic aggregate content of the concrete mixture decreases the compressive strength, with a 20% substitution ratio demonstrating the most drastic decrease in the compressive strength of 46.9% relative to the control mix determined by the weakened interfaces between the plastic aggregate and the cement, in addition to the volume content. Concrete mixtures which separated the form of plastic were used as a coarse aggregate at a 20% sand substitution stage, in which it was observed that the differences in the type of plastic used in the mixture have a major effect on the compressive strength of the concrete mixture, providing some reductions in comparison to the control mix of 13 to 38%.

2.6 Summary

In this chapter, the previous work on the significance of using shear walls in high wind activity regions was discussed. It was shown that no comprehensive investigation had been undertaken

into the assessment of RC moment-resisting frames with and without shear walls that have been located in regions where the wind actions are deemed high. This is especially important in the UK, considering the widespread use of shear walls in low-medium rise reinforced concrete frame buildings and their detrimental effect on the sustainability of construction in the environment and the economy. In addition, it was noted that there is no extensive research in obtaining the maximum overall height of RC moment-resisting frames by optimising different variables, such as concrete grade, column size, column shape and slab thickness. It was also acknowledged that there was no thorough exploration of punching shear failure in flat slabs to determine the extent of its effect as a leading factor limiting the height of buildings.

It was established that the key focus of the previous research was on the performance of connections in seismic regions. This review highlights the literature's limitations when it comes to identifying the performance of connections in moment-resisting frames subjected to high wind actions. This point is extremely important for the UK, as the dominant lateral forces in the area are wind activities.

Furthermore, some of the current technologies used in structural engineering, including the finite element simulation software and the use of sensors in structural health monitoring, were explored. In this regard, some of the most well-known finite element software were introduced, and their efficiency in analysing reinforced concrete frame buildings was discussed. The previous studies demonstrated that ETABS, Abaqus, and ANSYS software have a wide range of applications for reinforced concrete elements and hence, could be used in this PhD research to simulate the structural performance of reinforced concrete frame buildings. Based on the previous research in structural health monitoring techniques, it was shown that the strain gauge, as one of the leading techniques in this criterion, is a viable option to use for monitoring the performance of reinforcement in concrete sections.

Furthermore, it can be inferred from the previously mentioned studies that with plastic aggregates being used as a fine aggregate substitute (usually for sand) in the concrete mix

design, there has been a decrease in compressive strength, which has been a prevailing pattern. Usually, increasing the level of plastic in a concrete mix makes it weaker. However, where PP is used individually and PS and PVC are used in combination, they give the lowest reductions.

In this PhD research, several steps will be undertaken to enhance the sustainability of construction in RC frame buildings, including the possibility of removing shear walls in low-to-medium-rise buildings, which can directly influence the consumption of aggregates (as natural resources) in concrete and speed up the construction process. Also, the Mini-Haunch connection design can improve the sustainability of construction by relying on the moment-resisting system (as the primary method of construction) with lower consumption of concrete and quicker construction process rather than using shear walls. Ultimately, the application of using Polypropylene as a partial replacement for fine aggregate can potentially reduce the volume of fine aggregate used in the concrete mix design and provide a more sustainable construction process.

3 Methodology

3.1 Research Paradigm

Examining the universe to discover reality has always been one of the human needs and has been accomplished by logic, knowledge and study (Moley, 1978; cited in Cohen, Manion and Morrison, 2009). The research consisted of a combined approach towards reasoning and experience, particularly in the natural sciences (Borg, 1963; cited in Cohen, Manion and Morrison, 2009). Research explores a phenomenon through analytical and systemic methods that answer an issue and respond to a particular question to improve established knowledge (Sekaran, 1992). As this is an engineering PhD based on the essence of engineering research, this thesis will use the positivist research paradigm as it is the most suitable choice to fulfil the research standards. This approach is related to various schools of thought, including naturalism, scientism, behaviouralism, determinism and empiricism. It also "reflects a deterministic theory in which the causes decide the consequences or outcomes" (Creswell, 2003, p. 7).

This PhD adopts a quantitative approach, which is a mathematically oriented approach since the goal is to investigate the structural performance of reinforced concrete frame buildings, and the data used are provided as numerical values, e.g. displacement, deflection, interstorey drift and acceleration. Punch (2005) points out that predefined targets, predefined research questions, analytical data and procedures are commonly used in a quantitative study. Compared to qualitative research, quantitative analysis uses statistical data from computer models that save time and money (Bryman, 2012). The quantitative research method is thus used in this research to evaluate structural simulations with ETABS, Abaqus and ANSYS software in order to examine the feasibility of eliminating shear walls in the UK in the construction and design a Mini-Haunch connection for RC moment-resisting frames.

3.2 Research Design

Research design is an overall method that logically and coherently combines various research sections to ensure that the research issue is properly addressed. It sets out a blueprint for the compilation, calculation and analysis of data. The crucial thing is that the research problem governs the form of design, not the other way around (Vaus, 2001).

In this PhD research, the research design assesses the potential for removing shear walls and their effect on residential buildings for low-to-medium-rise concrete frames. In this regard, it is important to explore the structural influence of the use of shear walls in RC moment-resisting frames and to identify key factors that can affect their performance. This process will help determine the feasibility of eliminating shear walls in low-to medium-rise RC moment-resisting frames and examine the maximum overall height for RC frame buildings.

This research also assesses RC moment-resisting frames' limitations, such as those related to overall height limits. Therefore, this part considers several factors such as concrete grade, column size, column shape and slab thickness to achieve the maximum overall height with the optimal combination of the factors.

The outcome of these investigations and further studies lead to produce a design guide for RC moment-resisting frames entitled 'How To Design Moment-Resisting Frames' as one of the Concrete Centre 'How-To' publications. This guideline promotes improvement within the UK construction industry and provides guidance for structural engineers. The guide will provide essential details, such as specifications, design and detailing of RC moment-resisting frames compliant with Eurocode 2 Part 1-1 (BS EN 1992-1-1, 2014).

The next step is to design the Mini-Haunch connection between beams and columns in RC moment-resisting frames. This goal can be accomplished by conducting comprehensive simulations, thorough analyses and experimental works aimed at reducing construction time and expense, as well as improving the sustainability of construction. In this innovative

connection, apart from the participation in the load path for the transfer of the applied forces, the interaction between the beams and the columns would increase the strength of the buildings, which is important, particularly in the mid to high-rise RC moment-resisting frame buildings.

Ultimately, the application of partially replacing fine aggregate with Polypropylene will be investigated through experimental studies. This part investigates the influence of Polypropylene on the compressive strength of the samples while improving the sustainability of construction by reducing the consumption of natural resources in the construction industry.

In this research, four pieces of software will be used to improve the precision and reliability of the results:

1. ETABS, a programme designed to analyse and design multi-storey buildings (Wiki.csiamerica.com, 2018). This programme can perform linear, non-linear, static and dynamic analysis. Over the past two decades, ETABS has been used in a range of large-scale projects that have achieved market recognition and become the industry standard (Ceanet.com.au, 2018).

2. Abaqus is a finite element simulation programme that provides efficient and detailed solutions to common and complex engineering challenges, covering a wide range of industrial applications. Engineering work teams can understand full vehicle loads, dynamic vibration, multi-body structures, impact/crash and non-linear static using standard model data structure and integrated solver technology. Best-in-class companies use Abaqus FEA to optimise their processes and resources, reduce costs and inefficiencies and achieve a competitive edge (Abaqus Unified FEA - SIMULIA, 2007).

3. ANSYS, a finite element simulation software that makes it simpler to tackle the most challenging structural engineering problems and make superior design choices more efficiently. ANSYS provides engineers with the ability to automate and configure simulations and also parameterize them for various applications. ANSYS Structural Mechanics applications can be

conveniently linked to other physical methods for even more accuracy, modelling the efficiency and behaviour of even the most sophisticated projects. Engineers worldwide are optimising prototype designs using FEA from ANSYS (ANSYS FEA Software, 2016).

4. Concept is a specialised programme used for the conceptual design of RC frames and calculates the optimal structural solution along with the cost of construction and time estimation. This programme selects frame choice, member sizes and reinforcement calculations by following a logical process (ConcreteCentre.com, 2018).

3.3 Research Ethical Considerations

In terms of ethical considerations, the software that is going to be used in this research study is a licensed ETABS copy provided by the university, a student licensed Abaqus and ANSYS and a licensed Concept software provided by The Concrete Centre. The structural and finite element analyses have been conducted for engineering purposes and hence entail considerations of codes of ethics in engineering. Therefore, the following issues will be avoided throughout the entire research:

- Falsification
- Plagiarism
- Fabrication
- Moreover, any elements associated with misconduct

All data collected and utilised during this research will be protected according to the Data Protection Act 2018.

4 Data Collection

4.1 The Significance of Removing Shear Walls in Existing Low-Rise RC Frame Buildings

In this section, the procedure is divided into two parts and explained in details to assess the significance of removing shear walls in the UK typical RC frame buildings.

4.1.1 First Stage

In the first part, a broad comparative analysis is carried out to determine the effect of removing shear walls on the performance of RC buildings and the sustainability of construction in the expenses. The comparative analysis is based on an architectural plan for an established retirement community-based in Home Counties (Figures. 4.1 and 4.2) in the UK, provided by Couch Consulting Engineers. This design was chosen as a specific case study, not an imaginary architectural plan that could reflect a traditional multi-storey structure in the UK. The building is a five-storey reinforced concrete structure with flat slab floors.

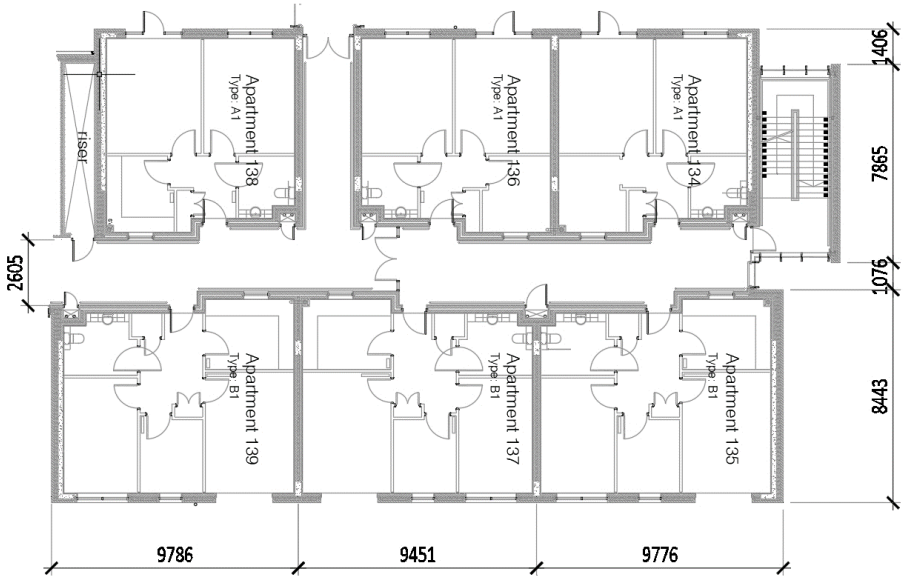

Figure 4.1: Case study architectural plan

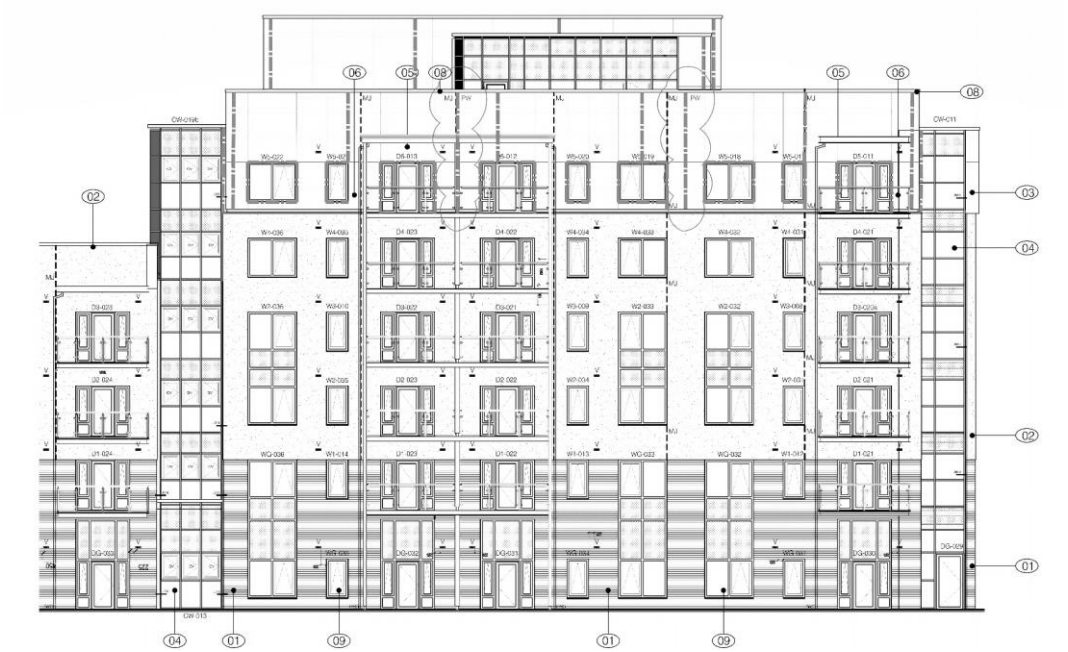

Figure 4.2: Case study elevation view

In order to carry out the analysis, two different systems of building frames were chosen based on the current architectural plan. The systems involved a moment-resisting frame with shear walls that was also the existing structure (Figure 4.3) and another moment-resisting frame without shear walls (Figure 4.4). In the second system, shear walls had been replaced by columns (of the same alignment of shear walls in the X direction). Such orientations could lead to a much stiffer frame in the direction of the Y and a less stiff frame in the direction of the X, which could result in an interstorey drift failure. These replaced columns were of the same size as the current columns on each floor.

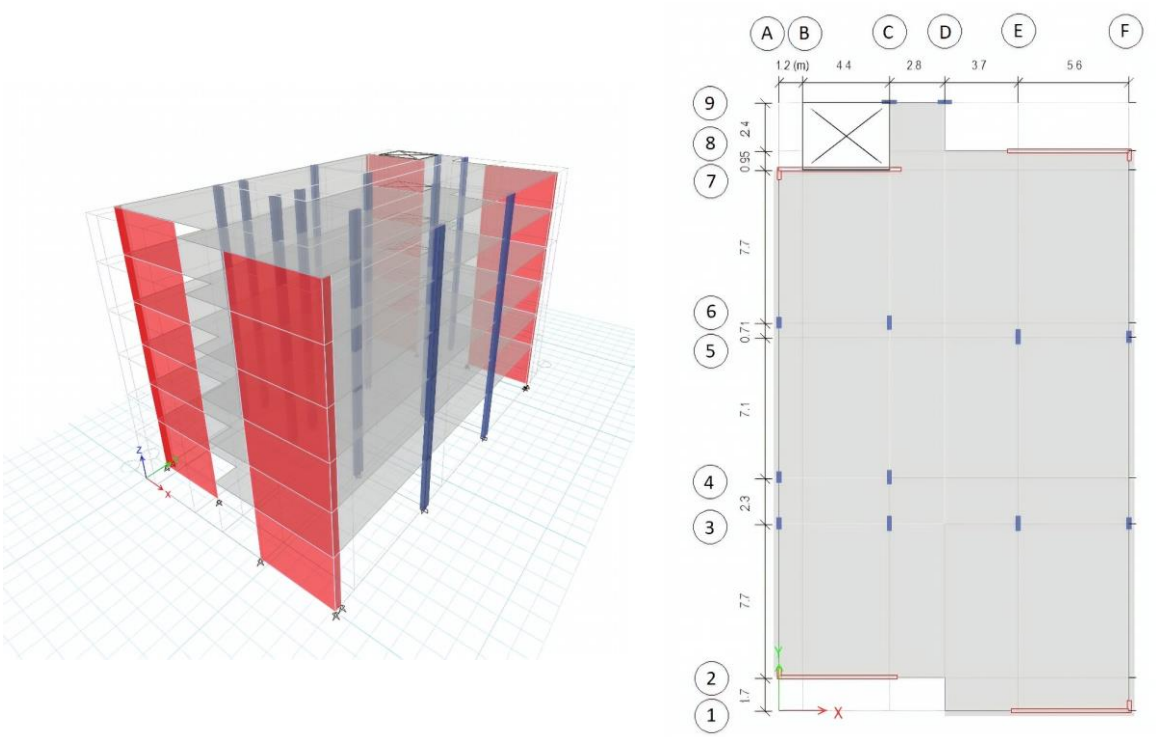

a) Three-dimensional view b) Plan view

Figure 4.3: Moment-resisting frame with shear walls (Case 1)

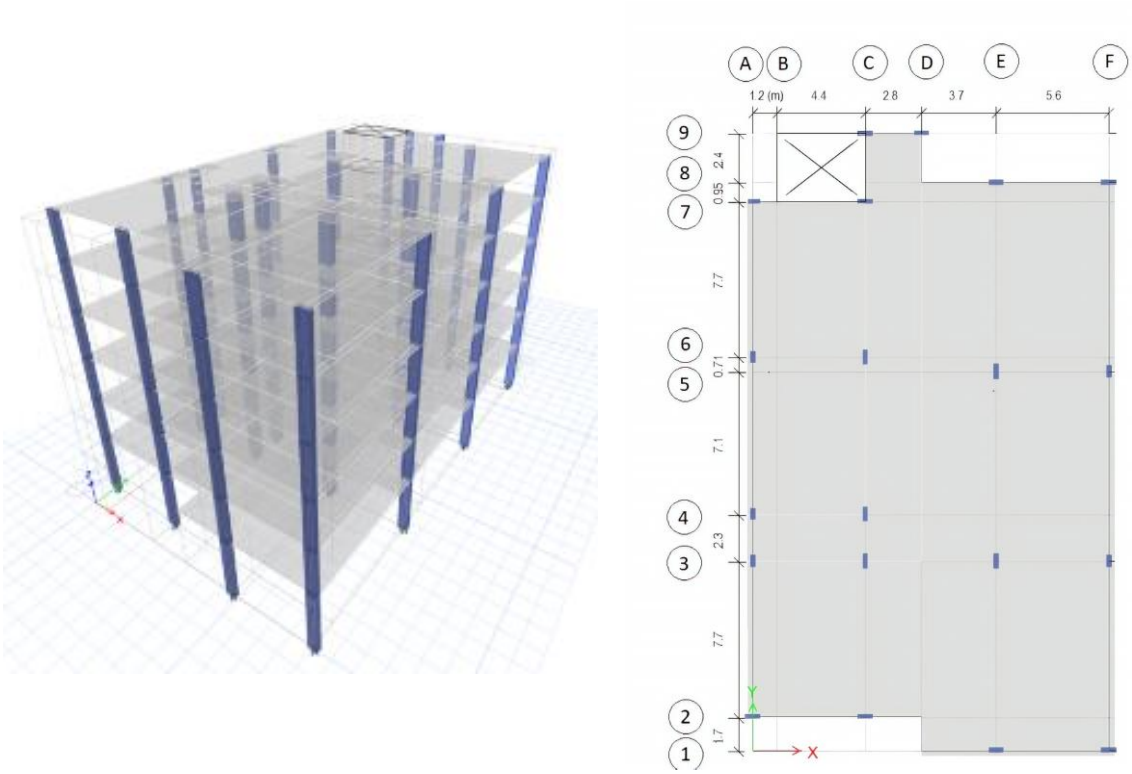

a) Three-dimensional view b) Plan view

Figure 4.4: Moment-resisting frame without shear walls (Case 2)

The specifications of the structure, including its dimensions, the properties of the concrete and steel materials and the gravity loads, are described in Table 4.1.

Table 4.1: Building specifications

Specification		**Value**	**Concrete**		**Steel rebar**
Height		19.46 m	-	-	-
Number of Storeys		6	-	-	-
Typical Floor Height		3.075 m	-	-	-
Ground Floor Height		4.125 m	-	-	-
Overall dimensions		17.7 × 27.3 m	-	-	-
Floor		Flat Slab 275 and 325 mm	-	-	-
Column		600 × 275 mm	-	-	-
		750 × 250 mm	-	-	-
Shear wall		Shell Thin 250 mm	-	-	-
Grade		-	C30/37	C 40/50	-
f_c'		-	30 N/mm^2	40 N/mm^2	-
Weight per unit volume		-	25 kN/m^3	25 kN/m^3	-
E (Modulus of Elasticity)		-	33000 N/mm^2	35000 N/mm^2	-
Poisson's Ratio		-	0.2	0.2	-
G (Shear Modulus)		-	13750 N/mm^2	14580 N/mm^2	-
Grade		-	-	-	B500B
R_e		-	-	-	500 N/mm^2
R_m/R_e		-	-	-	1.08
A_{gt}		-	-	-	5
Roof loads	Permanent (kN/m^2)	8.125	-	-	-
	Imposed (kN/m^2)	1.5	-	-	-
Floor loads	Permanent (kN/m^2)	6.875	-	-	-
	Imposed (kN/m^2)	2.5	-	-	-
Stairs loads	Permanent (kN/m^2)	4.3	-	-	-
	Imposed (kN/m^2)	4	-	-	-

Also, for the outer walls, the edge load is 5.4 kN/m in all directions.

Wind velocity could be seen as a mean value plus a variable component. According to the Eurocodes definition, wind actions are categorised as variable, fixed and direct actions. The method for measuring the static structural design load (3-second load once in 50 years) could be found in EN 1991.1.4, and it can be seen in Table 4.2 for Home Counties:

Table 4.2: Static structural design load (Home Counties)

Specification	**Value**	**Reference (EN 1991-1-4:2005)**
Terrain Category	III (Town)	Cl 4.3.2
Reference Height	11.67 m	Cl 6.3
Directional Factor	1 (Recommended)	Cl 4.2
Season Factor	1 (Recommended)	Cl 4.2
Fundamental Wind Velocity	21.5 m/s	Fig NA.1
Basic Wind Velocity	21.5 m/s	Cl 4.2-Exp (4.1)
Terrain factor	0.21	Cl 4.3-Exp (4.5)
Roughness Factor	0.77	Cl 4.3-Exp (4.4)
Terrain Orography Factor	1 (Recommended)	Cl 4.3
Mean Wind Velocity	16.5 m/s	Cl 4.3-Exp (4.3)
Turbulence Intensity	0.27	Cl 4.4-Exp (4.7)
Basic Velocity Pressure	0.17 kN/m^2	Cl 4.5-Exp (4.10)
Peak Velocity Pressure	0.49 kN/m^2	Fig NA.1
Structural Factor	1 (Recommended)	Cl 6.2
Wind Pressure	0.64 kN/m^2	Cl 4.2-Exp (4.1)
External Pressure Coefficient *	1.3	Cl 5.2-Exp (5.1)
Wind Force (X)	346 kN	Cl 5.3
Wind Force (Y)	201 kN	Cl 5.3

* The external pressure coefficient for the wider face (X direction) is selected.

Since the outcome of the analysis depends directly on the method of analysis, it is important to choose the appropriate method. In this chapter, due to the low height of the structure (19,46 m) as well as the magnitude of the loads applied, a non-linear dynamic analysis was the optimal choice.

It is worth mentioning that the determined wind-induced forces were constant values due to the low height of the building compared to its dimensions.

4.1.2 Second Stage

In the next section of this analysis, the probability of designing the same structure without shear walls was explored through the use of the same structural properties in different locations in the UK. As wind pressure activities rise towards the north (Table 4.3), many major cities in England, Scotland and Northern Ireland (not Wales, as their latitude and wind pressure were not substantially different from the area of England) with differing latitudes and wind pressure values were chosen within the UK from Birmingham, Belfast, Edinburgh and Shetland (as the worst possible). This selection could determine the effect of various climates in the UK on the structural performance of buildings.

Table 4.3: Static structural design load (3-second load once in 50 years)

Specification	**Birmingham (Case 3)**	**Edinburgh (Case 4)**	**Belfast (Case 5)**	**Shetland (Case 6)**
Terrain Category	IV (Town)	IV (Town)	IV (Town)	I (Country)
Wind Pressure (W_e)	0.45 kN/m^2	0.59 kN/m^2	0.63 kN/m^2	2.10 kN/m^2
External Pressure Coefficient (C_{pe})	1.3	1.3	1.3	1.3

4.2 The Influence of Different Factors on Buildings' Height in the Absence of Shear Walls in Low Seismic Regions

In this section, the procedure to assess the influence of different factors on the maximum overall height in RC moment-resisting frames using ETABS software is explained.

4.2.1 Case Study

The reference architectural plan used in this analysis was taken from a five-storey residential RC building in the UK (as seen in Figures. 4.5 and 4.6), provided by COUCH Consulting

Engineers. Belfast was chosen for the current analysis to be the most onerous of the different locations in the UK (excluding Shetland Island) in terms of wind loading.

Figure 4.5: The village overview (the reference building is highlighted in yellow)

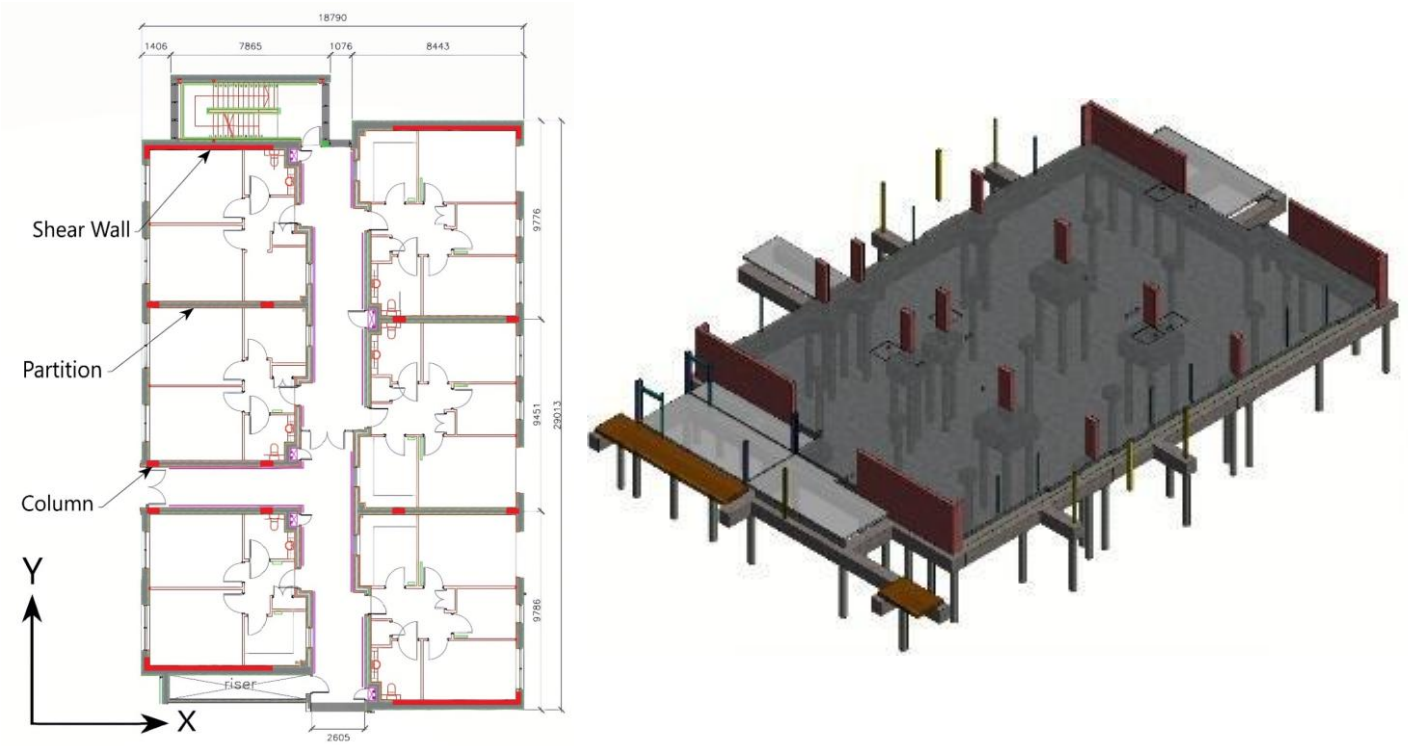

a) Architectural plan (values in mm)

b) Columns and shear walls location

Figure 4.6: Reference building with shear walls

For this analysis, additional columns from the same section size substituted the shear walls: see Figure 4.7.

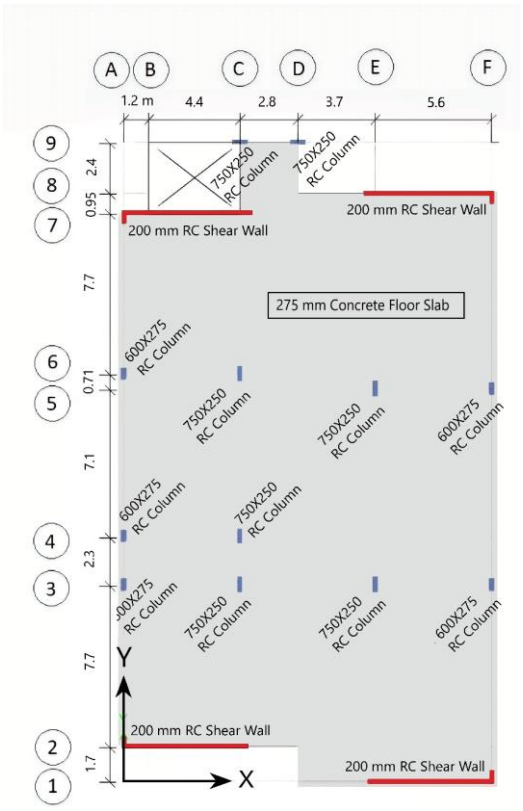

a) Reference plan design

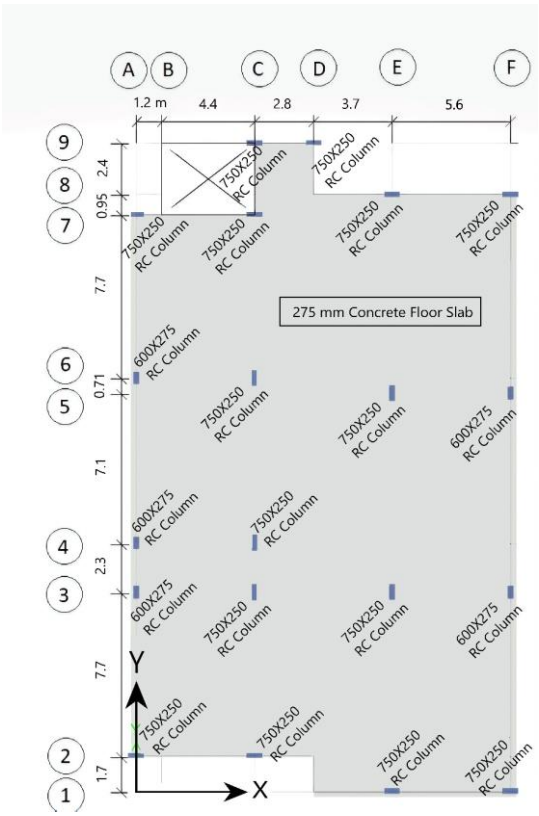

b) Modified plan design

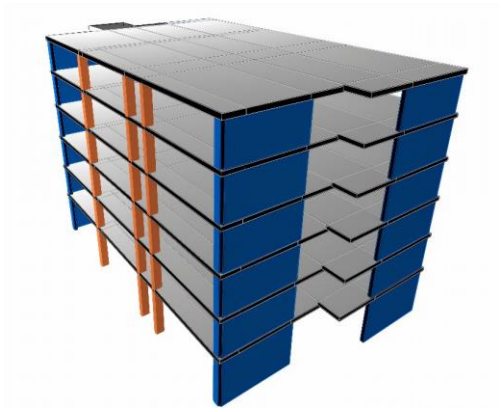

c) Isometric of the reference building

d) Isometric of modified building

Figure 4.7: Structural arrangement of reference and modified structures (values in m)

The characteristics of the structure, including its dimensions, the properties of the concrete and steel components as well as the applied vertical loads, are described in Table 4.4.

Table 4.4: Reference building (with shear walls) specifications

Parameter		**Value**		**Units**
Height		19.46		m
Number of Storeys		5		-
Typical Floor Height		3.075		m
Roof Height		2.96		m
Ground Floor Height		4.125		m
Overall dimensions		18.8 × 29		m
Floor		Flat Slab 275*	Flat Slab 300*	mm
Column		600 × 275	750 × 250	mm
Shear wall		250		mm
Concrete				
Grade		C 30/37	C 40/50	-
f'_c		30	40	N/mm^2
Weight per unit volume		25	25	kN/m^3
E (Modulus of Elasticity)		33000	35000	N/mm^2
Poisson's Ratio		0.2	0.2	-
G (Shear Modulus)		13750	13750	N/mm^2
Steel (Rebar)				
Grade		B500B		-
f_y		500		N/mm^2
f_{yd}		435		N/mm^2
R_m/R_e		1.08		-
Roof loads	**Permanent**	6.875-7.5*		kN/m^2
	Imposed	1.5		kN/m^2
Floor loads	**Permanent**	6.875-7.5*		kN/m^2
	Imposed	2.5		kN/m^2
Stairs loads	**Permanent**	4.3		kN/m^2
	Imposed	4		kN/m^2
Exterior walls	**Permanent**	5.4		kN/m

* Depending on the thickness of the slab, the permanent load ranges between 6.875 and 7.5 kN/m^2.

The next steps in the analysis were first to calculate the wind loading, then to develop the numerical simulations and finally to validate the design. Throughout the following subsections, all of these steps are explained in more details.

4.2.2 Design Wind Load

Wind is the dominant design load in high-rise buildings composed of static and dynamic elements. In high-rise buildings, extremely localised variable loads with large aerodynamic forces are applied to the facade and the structural system. Under the effect of such loads, the building oscillates, and the amplitude of oscillation is related to the dynamic properties of the structure and the aerodynamic design of the applied loads. If the vortex-shedding frequency and the natural frequency of the building co-occur, it can result in a large-scale movement in the response of the building, named the critical velocity effect (Mendis et al., 2007; Li, Zhang and Li, 2014; Zhi, Chen and Fang, 2015).

Wind gusts, as a rapid surge in wind speed, depend on the velocity at the moment, which is the worst-case scenario due to its force and high velocity that typically occurs for just a few seconds (Ambrose & Vergun, 1995 which Schueller, 1977). Owing to the fluctuating wind or gust elements, it is difficult to quantify the pressure, and it depends on several variables, including the nature of the wind, the local terrain and shape, the size and dynamic characteristics of the structure.

For the design of wind loads, the European standards Eurocode 1 Part 1-1 (BS EN 1991-1-1, 2009) offer a method for the determination of wind design loads for various locations in Europe. The input values for the simulations and the wind flow are shown in Table 4.5 and Figure 4.8 for the wind loads in Belfast.

Table 4.5: Static structural design load (Belfast)

Specification	**Value**	**Reference (EN 1991-1-4:2005)**
Terrain Category	IV (Town)	Cl 4.3.2
Reference Height	31.8 m	Cl 6.3
Directional Factor	1 (Recommended)	Cl 4.2
Season Factor	1 (Recommended)	Cl 4.2
Fundamental Wind Velocity	25.6 m/s	Figure NA.1
Basic Wind Velocity (3-second gust)	25.6 m/s	Cl 4.2-Exp (4.1)
Terrain factor	0.23	Cl 4.3-Exp (4.5)
Roughness Factor	0.79	Cl 4.3-Exp (4.4)
Terrain Orography Factor	1 (Recommended)	Cl 4.3
Mean Wind Velocity	20.48 m/s	Cl 4.3-Exp (4.3)
Turbulence Intensity	0.29	Cl 4.4-Exp (4.7)
Basic Velocity Pressure	0.26 kN/m^2	Cl 4.5-Exp (4.10)
Peak Velocity Pressure	0.78 kN/m^2	Figure NA.1
Structural Factor	1 (Recommended)	Cl 6.2
Wind Pressure	1.01 kN/m^2	Cl 4.2-Exp (4.1)
External Pressure Coefficient *	1.3	Cl 5.2-Exp (5.1)
Wind Force (X)	540 kN	Cl 5.3
Wind Force (Y)	324 kN	Cl 5.3

*External pressure coefficient is selected for the wider face (X direction).

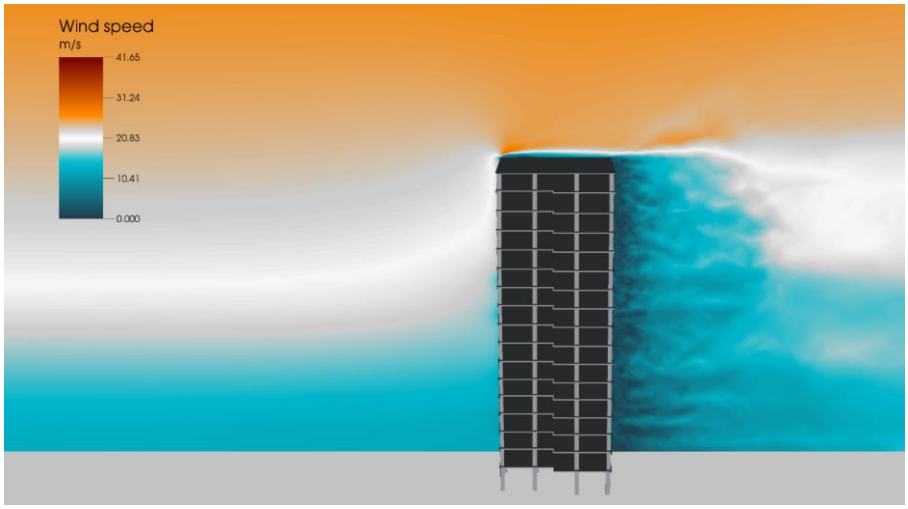

Figure 4.8: Wind flow (velocity) on the building

Figure 4.8 demonstrates the simulation of wind loads and their effect on the building using the Ingrid Cloud Simulator (Ingrid Cloud, 2018).

4.2.3 Simulation Procedure

The overall design process for the finite element simulations is shown in Figure 4.9.

- **Material Properties**

The design of RC buildings in Eurocode 2 Part 1-1 (BS EN 1992-1-1, 2014) is according to the characteristic cylinder strength rather than the cube strength and should comply with BS 8500: Concrete – Complementary British Standard to BS EN 206. Eurocode 2 Part 1-1 (BS EN 1992-1-1, 2014) could be used for the design of concrete classes up to C90/105, while additional modifications and rules may be added for classes beyond C50/60.

Moreover, Eurocode 2 Part 1-1 (BS EN 1992-1-1, 2014) could be used for reinforcement with the characteristic strength varying from 400 to 600 N/mm^2, and the relevant reinforcement characteristics for the UK could be observed in BS 4449 (2005), wherein the characteristic strength of 500 N/mm^2 is implemented in the UK construction industry.

The material properties for concrete were defined in accordance with Eurocode 2 Part 1-1 (BS EN 1992-1-1, 2014) and EN 206-1, for various concrete strength classes ranging between C40/50 to C80/95 using the Mander stress-strain curve (Mander, Priestley and Park, 1988). Also, for steel material properties, S355 was selected in compliance with EN 1993-1-1 according to EN 10025-2 mainly due to its variety of applications in the UK construction industry.

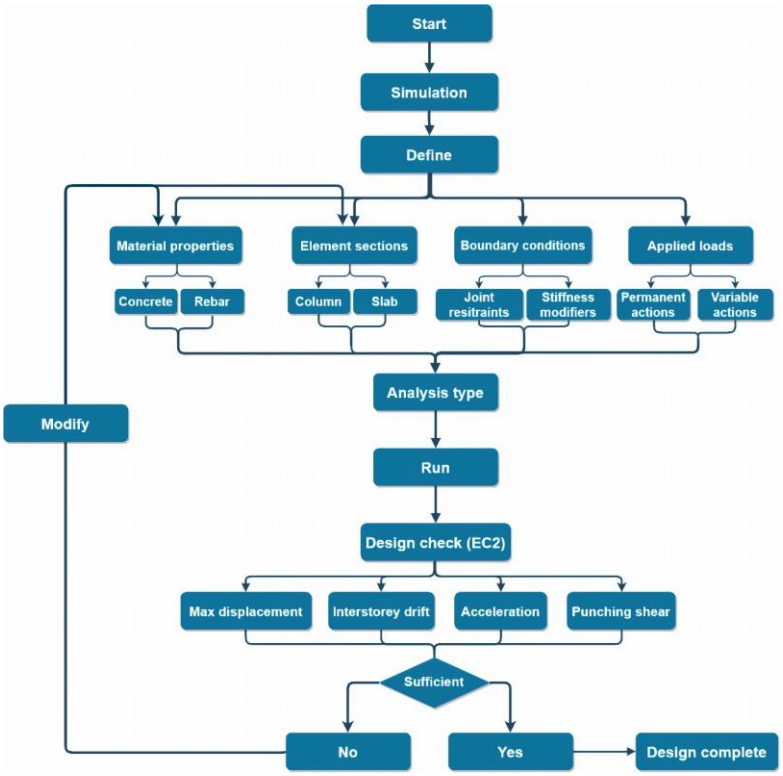

Figure 4.9: Overall design procedure

The properties of the column and slab sections were specified according to the various variables mentioned in this analysis (Table 4.6).

- **Element Section**

The cross-sectional shape of columns (either rectangle, square, circle or special shape) was established as the first step. This was accompanied by choice of the concrete grade, the size of the columns and the reinforcement details, including the rebar material, the clear confinement rebar cover, the number of longitudinal rebars in the X and Y axes, the longitudinal and corner rebar sizes and the size of the confinement rebars. Also, the elastic stiffness of the bilinear force-deformation relationship in reinforced concrete components had to be modified as per the Eurocodes in order to account for the cracking behaviour of the concrete. In this situation, the property modifiers for the X and Y axes were set to 0.5 for the moment of inertia.

In the slabs, first, the material was described as concrete (C30/37), and the model type could be used as shell-thin in order to accurately represent the behaviour of the flat slab in the

analysis. Also, to compensate for the crack behaviour of the slab, the property modifiers of the X and Y axes were set to 0.5 for the moment of inertia. In this analysis, the flat slab was perceived to be in accordance with the UK construction practice.

- **Boundary Conditions**

The boundary conditions rely on the design assumptions and could be diverse from one structure to another. In RC moment-resisting frames, connections between columns and other components (beams and slabs) and base columns to the foundation were assumed to be fixed for the transfer of stress distribution.

- **Applied Loads**

In a load case, the design value of an action (F_d) is in Equation 4.1:

$$F_d = \gamma_F \psi F_k \quad \text{(Eq. 4.1)}$$

Where

γ_F = Partial factor for actions

ψ = Factor defining representative values of variable actions

F_k = Characteristic value of an action

Ultimate limit state (ULS)

The designer can choose between expression 6.10, 6.10a or 6.10b (shown here as Equations 4.2 to 4.4) that are defined by Eurocodes for the design value according to the ultimate limit state.

$$1.35\ G_k + 1.5Q_{k,1} + \sum(\psi_{O,i}\ 1.5Q_{k,i}) \quad \text{(Eq. 4.2)}$$

Alternatively, the worst case of:

$$1.35\ G_k + \psi_{O,1}1.5Q_{k,1} + \sum(\psi_{O,i}\ 1.5Q_{k,i}) \quad \text{(Eq. 4.3)}$$

$$1.25\ G_k + 1.5Q_{k,1} + \sum(\psi_{O,i}\ 1.5Q_{k,i}) \quad \text{(Eq. 4.4)}$$

Where

G_k = Characteristic value of a permanent action

$Q_{k,1}$ = Characteristic value of a leading variable action

$Q_{k,i}$ = Characteristic value of an accompanying variable action

$\psi_{0,1}$ = Characteristic combination factor for 1st variable load

$\psi_{0,i}$ = Characteristic combination factor for ith variable load

Expression (6.10) appears to use γ_F= γ_G=1.35 regarding permanent actions and γ_F= γ_Q=1.5 regarding variable actions and is always assumed to be equal to or more conservative than the less favourable of (6.10a) and (6.10b) expressions.

Unless permanent actions are more than 4.5 times variable actions, or there are concrete structures supporting storage loads, expression (6.10b) will apply to most concrete structures.

Serviceability limit state (SLS)

There are three load combinations for SLS, which are shown in Table A1.4 of Eurocode 0 (BS EN 1990, 2010). According to the chosen limit state, the load combinations could be used.
In this analysis, the applied permanent and imposed loads were determined based on Eurocode 0 (BS EN 1990, 2010) and shown in Table 4.1. In addition, the load combinations for the finite element simulations were specified according to the ULS and SLS load combinations.

- **Analysis type**

Nowadays, in advanced structural engineering for the analysis and design of structures, finite element techniques have been widely employed in the construction industry to obtain more precise structural performance of buildings.

A crucial aspect of the analysis was to simulate the correct behaviour of the structure, especially in a high-rise RC frame building, because when a high-rise building is subjected to lateral forces,

it tends to distort, which can involve consideration of the second-order (P-Δ) effect. Also, the P-Δ shear (the force produced at the bottom and the top of the columns owing to P-Δ moments) creates an additional requirement for the lateral shear resistance of the structural system (Figure 4.10). This extra requirement is added to the demands of the applied shear, which could be crucial.

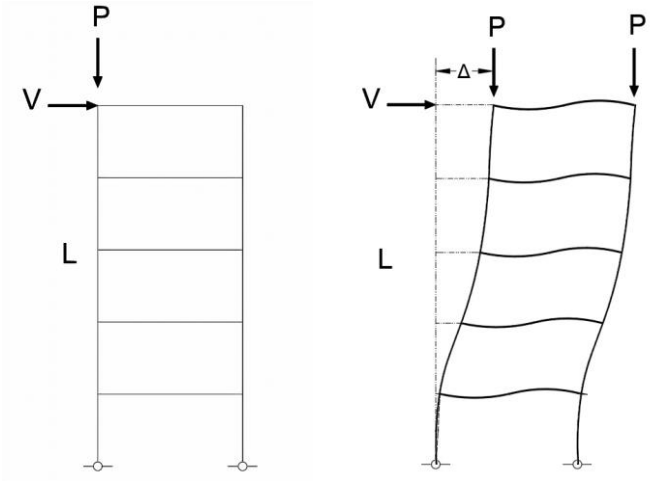

Figure 4.10: Second-order (P-Δ) effect

In Figure 4.10, P, V, L and Δ represented vertical loads, horizontal loads, building heights and second-order (P-Δ) effect, respectively.

Based on the geometry, material properties, support requirements, and structural loads on the building, the type of analysis could be selected. For high-rise buildings, due to the complication of the structure and non-linearity of the materials, a non-linear dynamic analysis offers more realistic results that could be used for both the ultimate limit state (ULS) and the serviceability limit state (SLS) criteria. This type of analysis refers to a nonlinear interaction between forces and displacements, which could occur from the nonlinearity of the material, geometric nonlinearity and restriction and nonlinearity of contact. These considerations result in a stiffness matrix that varies with the applied loads and can be used with both the ultimate (ULS) and serviceability (SLS) limit states.

In this analysis, various numerical analyses were conducted using ETABS software v16.2.1 to conduct accurate wind analysis, concrete elements design and punching shear ratio based on Eurocode 2 Part 1-1 (BS EN 1992-1-1, 2014). (Saisaran, Prasad and Venkat Das, 2016; Jolly and Vijayan, 2016; Tsay, 2019).

In order to carry out the analysis, first, the frame with a column size of 750 × 250 mm and flat slab thickness of 275 mm was developed in ETABS (Figure 4.7b), and the vertical and lateral loads were added according to Eurocode 1 Part 1-1 (BS EN 1991-1-1, 2009) (Table 4.1 and 4.2). A combination of values was then introduced for the chosen variables (Table 4.6), and the number of storeys was increased. For each simulation, the design limitations for the overall displacement, interstorey drift, horizontal acceleration and punching shear ratio (V_{Ed} /$V_{Rd,c}$) according to Eurocode 2 Part 1-1 (BS EN 1992-1-1, 2014) were verified to investigate the safety of the buildings and to monitor the ductile behaviour of the moment-resisting frames with flat slabs.

If the building's design values were smaller than the threshold, the number of storeys would have been raised, and if the design values were nearly equal to the threshold, the simulation would have been ended. This process was repeated until the maximum number of storeys with punching shear ratios of 2 and 2.5 were obtained.

The effect of four predefined factors (Table 4.6) on the structural performance of the building was explored. The four variables examined were as follows:

- Concrete grade
- Column size
- Column shape
- Slab thickness

In the first step, various grades of concrete, ranging from C40/50 to C80/95, were used and an optimised concrete design was developed, with a higher strength in the lower storeys and a

lower strength in the upper storeys for the columns, in order to determine their effect on the structural performance of the building. The rationale for such a selection was based on the advice of the Concrete Centre experts, given the range of strengths that would generally be accessible in the UK. At this point, the minimum values for column size and slab thickness (750 × 250 mm and 275 mm, respectively) were introduced in order only to observe the effect of the concrete grade.

The impact of different sizes of the column was then studied. As one axis was already 750 mm, the column sizes for the other axis were tested in increments of 50 mm, from 250 mm to 500 mm, using grade C40/50 concrete and slab thickness of 275 mm. The next step was to determine the effect of the shape of the column on the structural performance of the building, such as the punching shear. These shapes were circle, square and rectangular of the same cross-sectional area (approximately 0.375 m^2). One of the main motivations behind such a selection was to observe the influence of their shape on the punching shear. For the other factors, the concrete grade C40/50 and the slab thickness of 275 mm were selected. The influence of slab thickness was also explored in the structural performance of the building. In this part, just slab thicknesses of 275 mm and 300 mm were used for the concrete grade C40/50 and column thicknesses of 750 × 250 mm.

Table 4.6 indicates various adopted factors for the structural analysis, comprising eight concrete grades for columns, one concrete grade for flat slabs, six different column dimensions, three-column shapes and two slab thicknesses. The practicality and economic considerations of the building have been taken into account throughout this selection. For instance, eight different grades of concrete were chosen for columns, while only one grade of concrete was chosen for flat slabs, as the volume of concrete used for flat slabs was almost ten times higher than those used for columns. As a consequence, increasing the strength in flat slabs would dramatically increase the cost of construction and potentially cement requirement for a significant portion of the structure; thus, only one grade of concrete was preferred for flat slabs.

Table 4.6: Investigated variables

Specification	Variabl1	Variable2	Variable3	Variable4	Variable5	Variable6	Variable7	Variable8
Concrete grade (column)	C40/50	C45/55	C50/60	C55/67	C60/75	C70/85	C80/95	Optimised*
Concrete grade (slab)	C30/37	-	-	-	-	-	-	-
Column size	750×250	750×300	750×350	750×400	750×450	750×500	-	-
Column shape	Square	Rectangle	Circle	-	-	-	-	-
Slab thickness	275 mm	300 mm	-	-	-	-	-	-

* The optimised concrete was an improved mix of the grades of concrete, starting with a higher strength of concrete on the lower floors and a reduction in strength over the height.

4.2.4 Design Check

Increasing the height of the building could result in severe lateral movement, interstorey drift, punching shear failure and excessive acceleration, which, if the constraints were not taken into consideration, could lead to a collapse of the structure. The numerical analyses in this part of the research were therefore consistent with the regulations of Eurocode 2 Part 1-1 (BS EN 1992-1-1, 2014) as well as Eurocode 0 (BS EN 1990, 2017), that are as follows:

- Horizontal acceleration can have major impacts on the comfort of inhabitants if they contribute to rapid acceleration. Human reaction to building movements requires multiple psychological processes, typically determined by acceleration The Concrete Centre (Banks et al., 2014). NBCC: Section 4 (National Building Code of Canada, 2010) and Melbourne and Palmer (1992) describe the limits for residential and office occupancy in order to assess the permissible acceleration of the building in which occupants are deemed to be comfortable.

  There is currently no specified constraint within the Eurocodes for occupant comfort. According to The Concrete Centre (Banks et al., 2014), the standard values for a 10-year return period of wind activity are as follows:

- 10 to 15 milli-g (an acceleration unit equivalent to 1 cm/s^2) for residential occupancy;
- 20 to 30 milli-g for office use.

Acceleration can be determined using Equation 4.5:

$$a = \frac{2\pi^2 \times f^2 \times d}{g} \quad \text{(Eq.4.5)}$$

In which a, d, f and g indicate acceleration (m/s^2), maximum displacement (m), frequency (Hz) and gravitational acceleration (m/s^2).

The Melbourne criteria are currently the most widely used guidelines for the design and assessment of wind-generated horizontal acceleration in UK buildings (Breeze, 2011). In Equation 4.6, the value for horizontal (unweighted) peak acceleration can be seen as follows:

$$a = \sqrt{2\,ln\,nT}\left(0.68 + \frac{ln\,R}{5}\right) exp(-3.65 - 0.41\,ln\,n) \quad \text{(Eq. 4.6)}$$

In which a, R, n and T reflect acceleration (m/s^2), return period (year), natural frequency (Hz) and time length (seconds), taking into account the nature of the wind motion. In nations such as the United States, T is believed to be 10 minutes (600 seconds) due to prevailing storm activities. On the other hand, in the UK, provided that the storms have happened over a longer period, T is predicted to be 60 minutes (3600 seconds).

The horizontal peak acceleration used in Figure 4.11 was obtained from Equation 4.6.

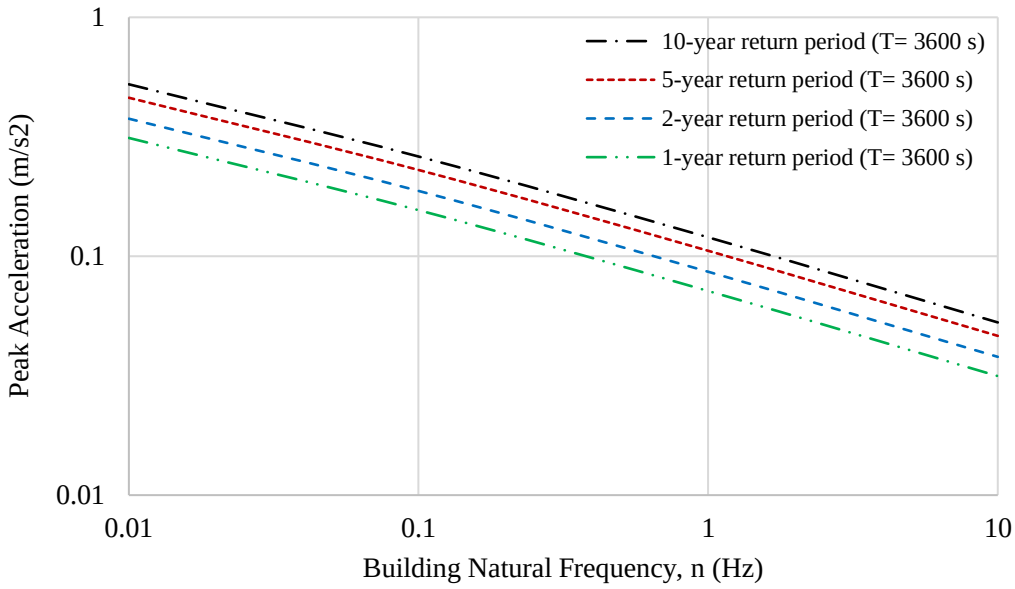

Figure 4.11: Limits for horizontal peak acceleration based on Breeze (2011)

- Lateral loads may cause horizontal displacement in a building and, based on the level of the displacement, can result in significant damage to buildings and their facades. It is also important to monitor these displacements for non-structural components, such as the interactions between the blocks and the partition walls. In order to manage the overall horizontal displacements and interstorey drifts, British Standards 8110:2 establish the constraint of H/500, where H is the overall/storey height, to mitigate lateral movements (EN 1990:2017).
- Flat slabs, despite their economic benefits, need design checks for punching shear.

4.3 Design a Mini-Haunch Connection

In this section, the undertaken approaches to design and investigate the performance of the Mini-Haunch connection through experimental tests and finite element simulations are explained.

4.3.1 Similitude Method

In laboratory experiments, full-scale projects are costly in terms of both expense and time (and often difficult to implement) and in some situations, the efficacy of the results cannot justify the

initiative. It is, therefore, desirable to build a reliably scaled-down version of the original prototype that can be tested at incredibly low prices, time and challenges (Simitses, Starnes and Rezaeepazhand, 2000).

Moreover, the complexity of engineering processes in a variety of practical applications makes analytical and numerical analyses inadequate to determine whether the efficiency of the system satisfies the design criteria. The strong demand for experimental research has resulted in a significant rise in the use of alternative approaches due to the limitations of full-scale experiments (Coutinho, Baptista and Rodrigues, 2016).

The similitude Concept is a segment of engineering science that attempts to establish the conditions of resemblance between two or more structures. This theory predicts the structural reaction of the prototype (full-scale system) from either the scaled-down or up (model) data. In order to achieve accurate performance, the model should meet the similitude requirements to have the same response as its prototype.

Similitudes based on the selected criteria can be defined as:

- Geometric Similitude: where the geometric parameters are measured equally.
- Kinematic similarity: when the same particles sit at the corresponding points at the corresponding times.
- Functional similarity: where corresponding components of the system are directed to the corresponding net forces.

There are many similitude approaches in the literature that could be used to rescale a prototype, such as DA (Dimensional Analysis), EM (Energy Methods), STAGE (Similitude Theory Applied to Governing Equations), SAMSARA (Similitude and Asymptotic Models for Structural-Acoustic Research Applications), SA (Sensitivity Analysis) and ESM (Empirical Similarity Method). Of these techniques, DA and STAGE are the most commonly used in the literature (Casaburo et al., 2019).

In this part of the research, DA (Dimensional Analysis) was proposed on the basis of its use in civil engineering applications (Sato, Vecchio and Andre, 1989; Kim, Kwak and Chang, 2004; Kim, Lee and Chang, 2009). This approach is considered a collection of dimensionless parameters that control the phenomena being studied. It depends on the principle of dimensional homogeneity; for example, an equation that defines a physical entity should have sides with the same dimensions. All of these principles are outlined in Buckingham's ∏ Theorem. According to this concept, K is the number of fundamental dimensions needed for the definition of physical variables, and P_1, P_2 ... P_N are N physical variables. These parameters are connected via the functional relation:

$$f_1 (P_1, P_2, \ldots, P_N) = 0 \qquad \text{(Eq. 4.7)}$$

Equation 4.7 can be interpreted in terms of (N – K) non-dimensional substances referred to as '∏ products,' as (Equation 4.8):

$$f_2 (\prod_1, \prod_2, \ldots, \prod_{N-K}) = 0 \qquad \text{(Eq. 4.8)}$$

Each ∏ is a non - dimensional product of K+1 physical variables (Equation 4.9):

$$\begin{cases} \prod_1 = f_3(P_1, P_2, \ldots, P_K, P_{K+1}) \\ \prod_2 = f_4(P_1, P_2, \ldots, P_K, P_{K+2}) \\ \ldots \\ \prod_{N-K} = f_5(P_1, P_2, \ldots, P_K, P_N) \end{cases} \qquad \text{(Eq. 4.9)}$$

Scale-modeling with dimensional analysis demands that all non - dimensional ∏ products be scaled to the same degree for both the model and the prototype, i.e.:

$$\prod_j^{(m)} = \prod_j^{(p)} \qquad \text{(Eq. 4.10)}$$

For j = 1, 2, ..., (N – K).

Whenever Equation 4.10 is satisfied for each value of j, the full similitude is obtained.

Table 4.7: Similitude relations (Ramu, Prabhu Raja and Thyla, 2013)

Parameters	**Scale factor**
Dimension	S
Area (A_p)	S^2
Volume (V_p)	S^3
Linear Displacement (U_p)	S
Moment of inertia (I_p)	S^4
Frequency (*f*)	$S^{-1/2}$
Density (ρ_p)	S_E/S
Point Load (F_p)	$S_E.S^2$
Line Load ($F_{.L.}$)	$S_E.S$
Uniformly Distributed Surface Load (P_p)	S_E
Shear Force ($V_{.P.}$)	$S_E.S^2$
Moment (M)	$S_E.S^2$
Stress (σ_P)	$S_{.E.}$

In this part of the research, the laboratory specimens were selected from a three-storey RC frame building, as seen in Figure 4.12. This specimen was chosen since its dimensions were appropriate to conduct experimental work at the UWL concrete laboratory with a lower scale factor than the other bays and consecutively to obtain the results with lower influence of size effect due to scaling. Besides, it was decided to select the specimen from the ground storey, as the elements on the ground storey are more critical and resist higher vertical and lateral loads compared to the other storeys, and this arrangement could result in sagging bending moments applied to the selected span.

The prototype dimensions were 3.2 × 3.2 m for both the width and height of the structure and 400 × 400 mm for the cross-sections of the beams and columns with 32 mm and 8 mm longitudinal reinforcement and shear links. Owing to laboratory constraints, a ratio of 1:4 (using the scale factor for dimensions in Table 4.7) was introduced, resulting in scaled models of 800 × 800 mm (width and height) frame lengths, 100 × 100 mm cross-section of beams and columns

and 8 mm and 10 mm rebar sizes as shear links and longitudinal reinforcement (Figures. 4.12 and 4.13).

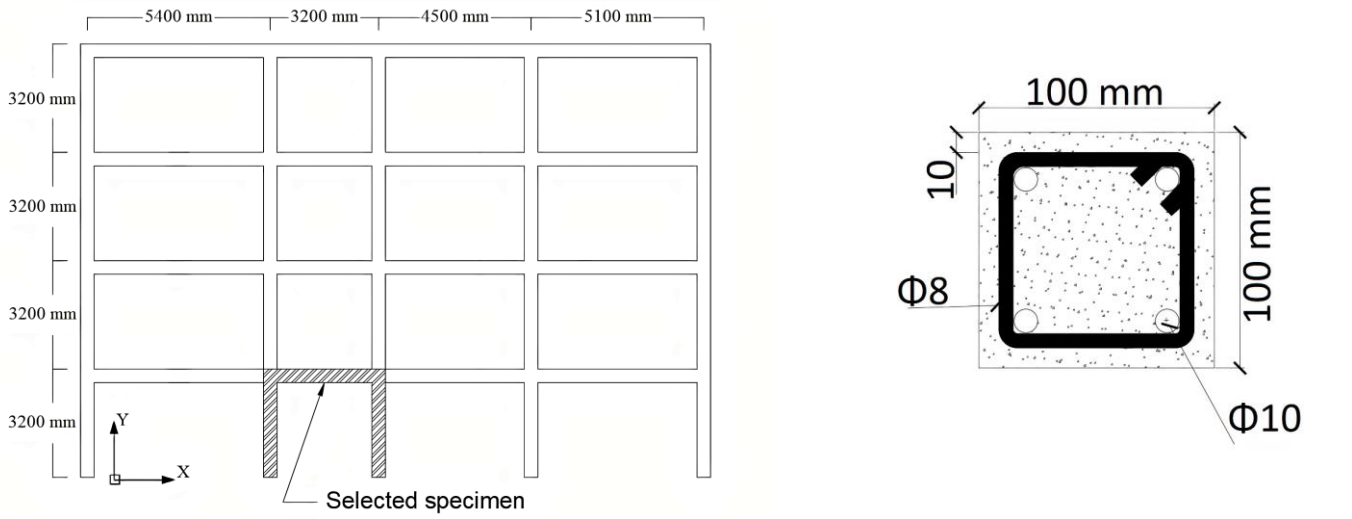

a) Prototype building b) Beam and column cross-section

Figure 4.12: Prototype building

4.3.2 Experimental Procedure

There were two different connections designed and examined in the test programme. The first was a standard connection (S), as shown in Figure 4.13a, with longitudinal reinforcement and shear links (varying from 50 mm to 130 mm throughout the beam and columns) designed per the detailing guidelines in Eurocode 2 Part 1-1 (BS EN 1992-1-1, 2014). Three repeat tests were conducted of this arrangement (labelled S1, S2 and S3 in this chapter). The second was the Mini-Haunch connection (MH) with a novel design in terms of the rebar arrangement and efficient for the practical considerations, as shown in Fig 3.13b, in which additional reinforcement was provided at the connections between the beam and columns to enhance the strength and ductility of the frame. Two repeats of this arrangement were included in the programme, namely MH1 and MH2. In this connection, new lap/anchorage lengths and also a hunched angle was included, in accordance with the requirements prescribed in Eurocode 2 Part 1-1 (BS EN 1992-1-1, 2014). The distance between shear links varied between 50 to 70 mm in the beam and 50

to 130 mm in the columns in order to prevent shear failure and to follow the minimum design requirement in Eurocode 2 Part 1-1 (BS EN 1992-1-1, 2014).

Furthermore, at each connection, four additional bent reinforcement bars were included with a bending angle of 135°. Two of these were 210 × 160 × 210 mm in size, whilst the remaining two were 160 × 160 × 160 mm, and all had a diameter of 10 mm. These reinforcement bars were attached to the longitudinal reinforcement and fixed with diagonal shear links.

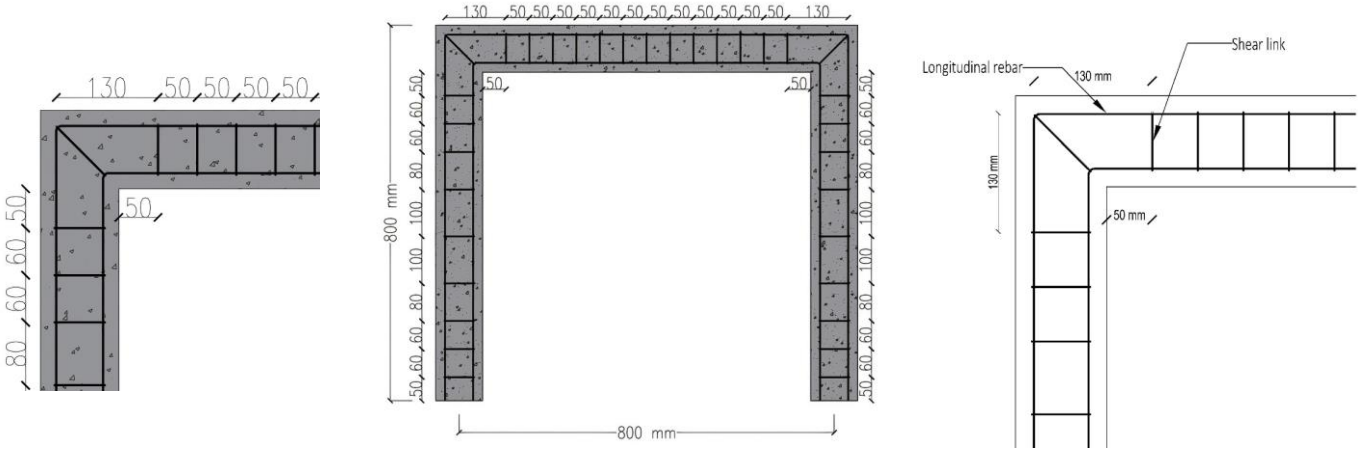

a) The standard connection

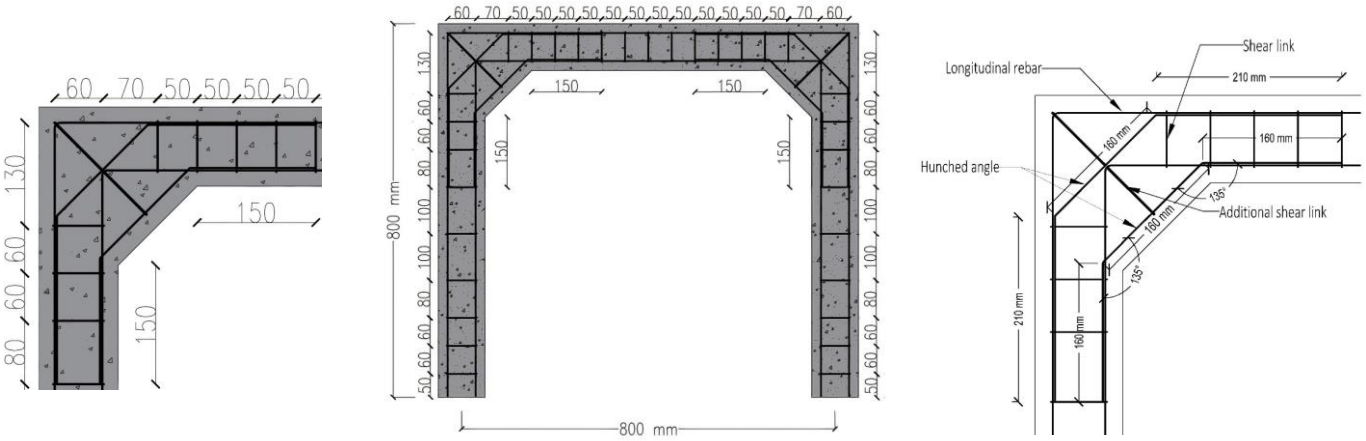

b) The Mini-Haunch connection

Figure 4.13: Design of the connections

In order to make the scaled frames with the proposed connections, the following procedure in Fig 3.14 was utilised:

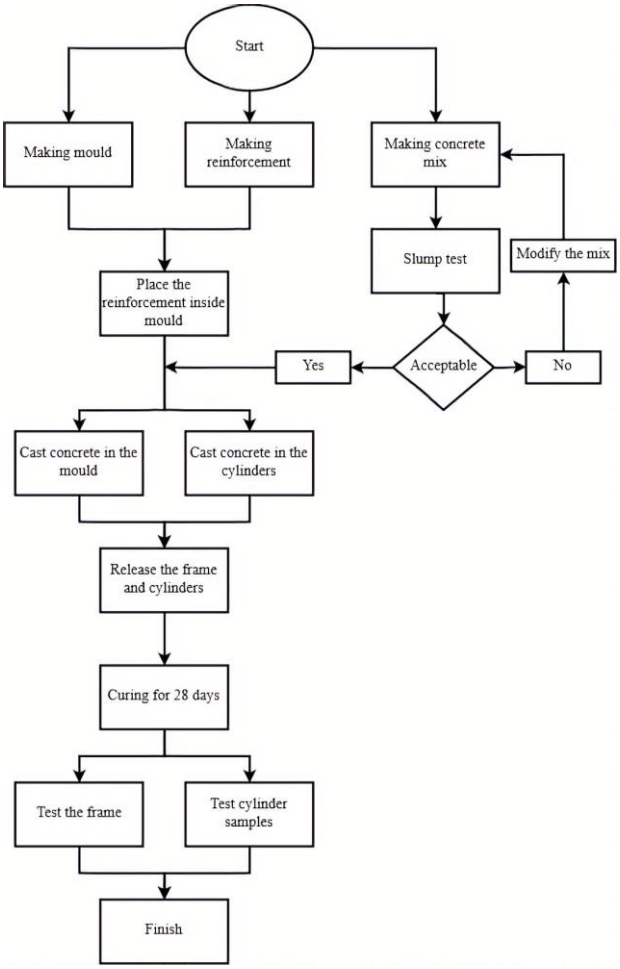

Figure 4.14: The experiment procedure flowchart

- **Wooden Mould**

The first step involved the use of marine plywood with a thickness of 12 mm, nails, wood glue and duct tape (Figure 4.15) for the development of wooden moulds for Standard and Mini-Haunch connections (Figure 4.17).

a) Marine plywood b) Nails c) Wood glue d) Waterproof tape

Figure 4.15: Required materials to make a mould

In order to make the mould for the two connections, the plywood sheet was cut into smaller pieces (Table 4.8) and then the parts were assembled one by one (the process is seen step by step in Figure 4.16) using wood glue, which is adhesive and water-resistant, and nails to ensure that the pieces were properly connected. After that, the dust was washed from the interior of the mould using a moisturised cloth, and waterproof duct tape was added to ensure that the interior side of the mould was protected with a smooth finish.

Table 4.8: Plywood piece size

Size	**Quantity**	**Unit**
1000 × 124 × 12	2	mm
1000 × 112 × 12	4	mm
900 × 112 × 12	2	mm
876 × 124 × 12	1	mm
124 × 112 × 12	2	mm

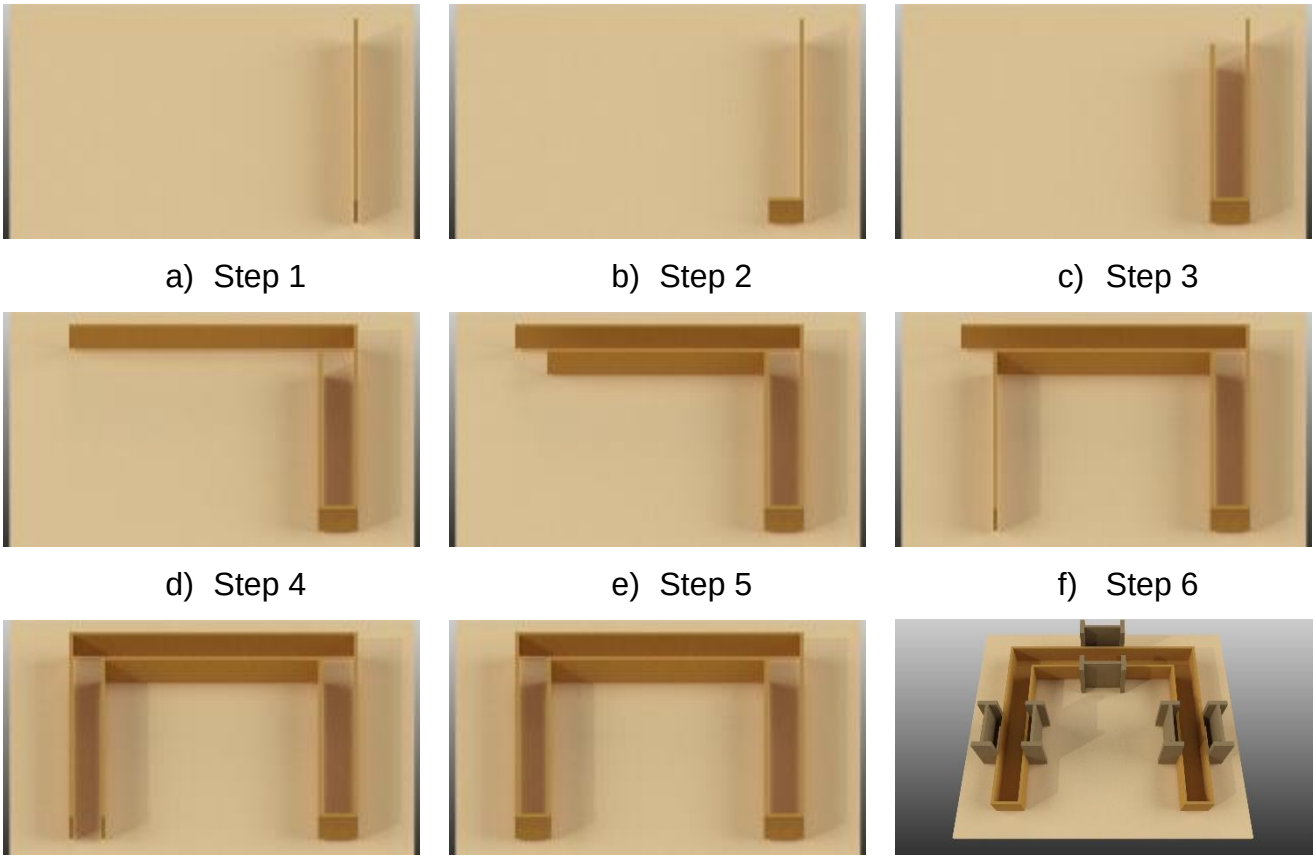

a) Step 1 b) Step 2 c) Step 3

d) Step 4 e) Step 5 f) Step 6

g) Step 7 h) Step 8 i) Step 9

Figure 4.16: Mould assembly procedure

a) Standard design b) Mini-Haunch connection

Figure 4.17: Wooden moulds

In this part, after evaluating the smoothness of the attached tape, the engineering judgement was made to discard the use of the release agent and to depend only on the smooth surface of the duct tape for release (Figure 4.18). This part was different from the cubic and cylindrical mould experiments of which the release agent substance (The Concrete Culture, 2016) must be added to the inside of the moulds, providing a safe and fast release. The mould was then attached to a plywood sheet with a scale of 1.4×1.4×0.025 m using sliced timber beams. The slices were made from 3 m timber beams to hold the mould in place. Fixing the mould to the plywood sheet was important for the concrete and vibration process.

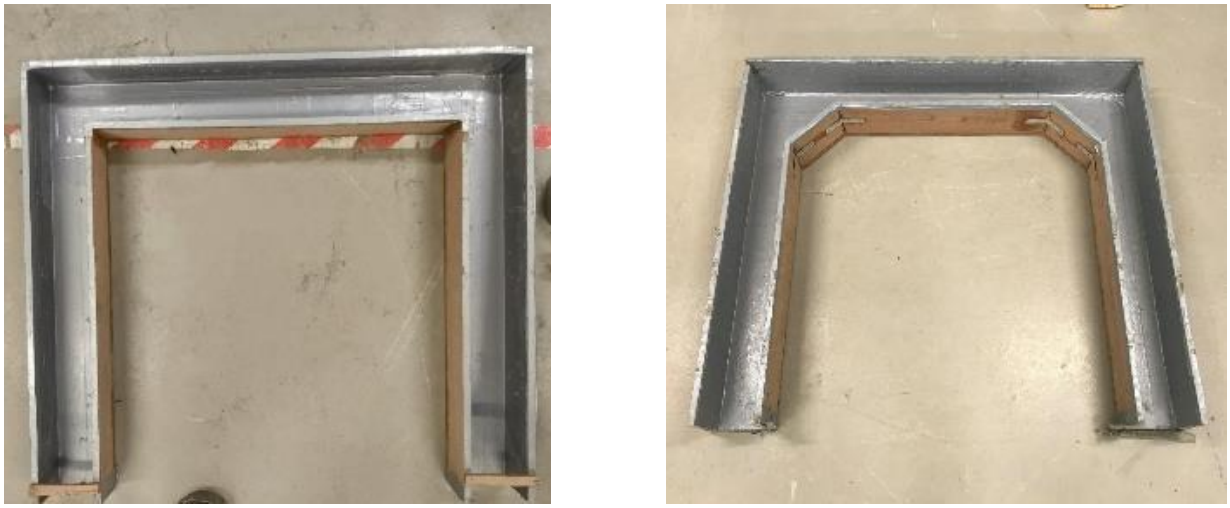

a) Standard design with duct tape b) Mini-Haunch design with duct tape

Figure 4.18: Mould and the placed reinforcement

The next step was the arrangement of the shear links and the longitudinal reinforcement, using the information given in Table 4.9. Owing to practical limitations in the construction industry, the longitudinal reinforcement was designed and detailed with laps and anchorages to maintain consistency across the members (Cresswell Riol, 2007).

Also, four additional bent reinforcing bars with a bending angle of 135 ° were included in the Mini-Haunch connection. Two of which were 210 × 160 × 210 mm in length, while the other two were 160 × 160 × 160 mm, and both are 10 mm in diameter.

Table 4.9: Reinforcement specifications

Parameter	Value	Dimension	Units	Number
Size	8 (Shear link)	72 × 72	mm	31
		72 × 115 *		2
	10 (Longitudinal)	860 × 780	mm	2
		740 × 720	mm	2
Grade	B500B	-	-	-
f_y	435	-	N/mm^2	-
f_u	550	-	N/mm^2	-
R_m/R_e	1.08	-	-	-

* The shear links with 80 × 115 mm dimensions were only used in the corners.

For all the shear links, the Roughneck Rebar Cutter (Figure 4.19a) was used to cut 3 m-long rebars with an 8 mm diameter into smaller parts (each 350 mm long) and bent with the Manual Stirrup Bender 12 mm DM-12 (Figure 4.19b) 4 times with 90-degree angles, a 16 mm radius and 25 mm end projections to form a shear link, as seen in BS 8666 (2005) and the practicality of the use of rebars as seen in Figure 4.20. After the reinforcement was prepared, the shear links were fitted in the longitudinal rebars using a reinforcement wire (with a diameter of 1 mm) with the distances defined according to Figure 4.21.

a) Roughneck Rebar Cutter 950mm

b) Manual Stirrup Bender 12mm DM-12

Figure 4.19: Reinforcement tools

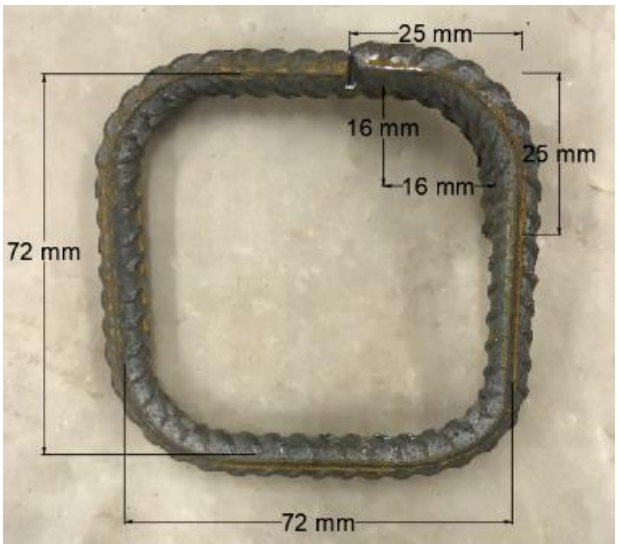

a) Shear link dimensions

b) Shear links

Figure 4.20: Shear links with dimensions

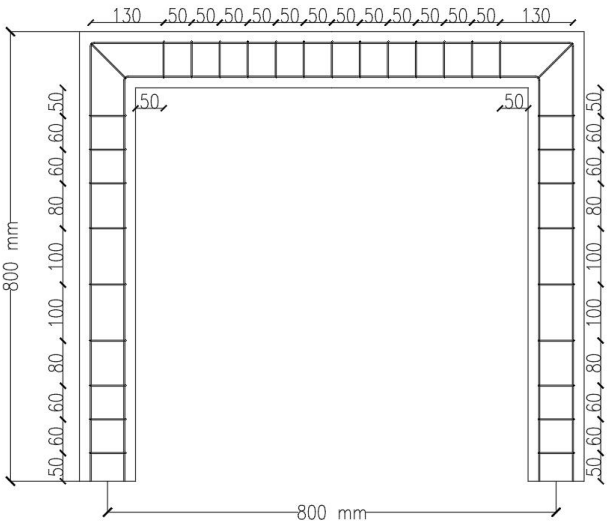

a) Standard design detailing

b) Standard design reinforcement cage

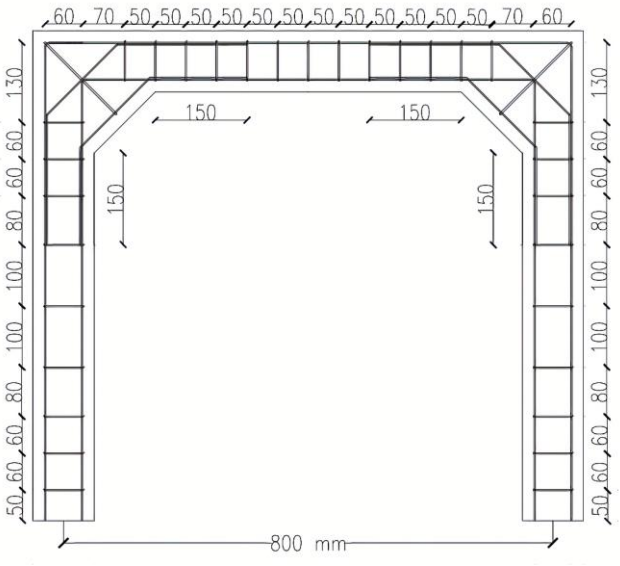

c) Mini-Haunch design detailing d) Mini-Haunch design reinforcement cage

Figure 4.21: Reinforcement arrangement

- **Strain Gauge**

Since it is visually possible to inspect the crack propagation and failure mechanism in the concrete parts, in this section, it was decided to investigate the performance of the reinforcement within the concrete when the concrete section is under the applied load to obtain a clearer understanding of the reinforcement. It was then planned to monitor longitudinal reinforcement behaviour in several positions as a side aim using structural health monitoring systems.

As mentioned earlier in the literature review, different techniques could be used to monitor the output of reinforced concrete components, including strain gauges, linear variable displacement transducers (LVDTs) and Digital Image Correlations. In this research, due to the validity and versatility of the strain gauge (Huang et al., 2019; Dok et al., 2020; Xingyu, Yiqing and Jiwang, 2020; Zaki and Rasheed, 2020), it was determined to use it to obtain the stress-strain behaviour of the longitudinal reinforcement.

Therefore, for each scaled frame, four RS Pro Wire Lead Strain Gauges (Figure 4.22) with a length of 13 mm, a width of 4 mm and a gauge length of 8 mm were used. This strain gauge provides a temperature compensation with 120 Ω and a gauge factor of 2.

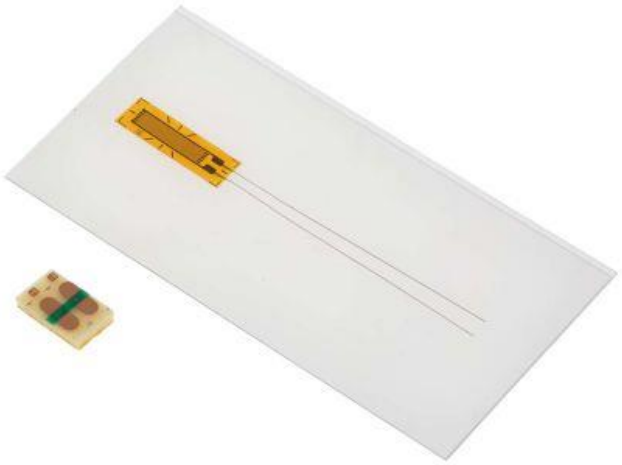

Figure 4.22: Strain gauge

A strain gauge should be used in a bridge circuit to determine the strain of a sample. In this research, due to practical considerations, for each strain gauge, a quarter-bridge circuit was used to indicate the measured strain with the degree of imbalance, which uses a precision voltmeter in the centre of the bridge to provide accurate measurement of the imbalance. Therefore, four quarter-bridge circuits were designed proportionally to the number of strain gauges that could receive the voltage from 1.5V AA Batteries, the strain data from the strain gauges (RS Pro Wire Lead) and transmit the data to a data logger (PicoLog 1012). In order to obtain the required results from each scaled frame, four different positions on the top and bottom sides of the longitudinal reinforcement, as shown in Figure 4.23, were selected (namely SG1, SG2, SG3 and SG4).

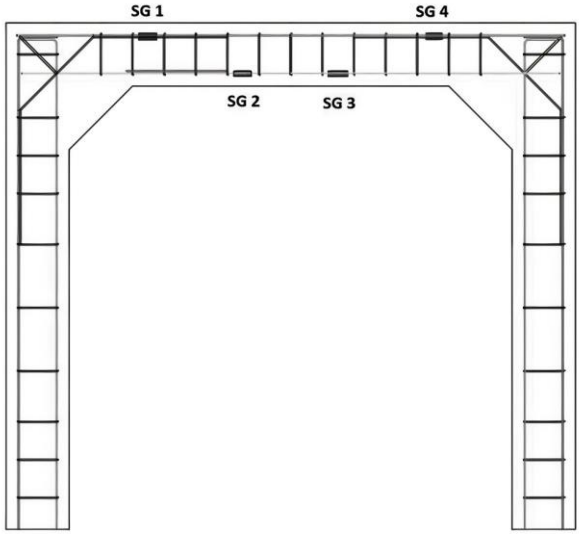

Figure 4.23: Strain gauge locations

An experimental check was then carried out using a strain gauge mounted on the centre of a 3 m timber beam to determine the efficiency of the circuit. However, it was noted during the test that the circuit created some noise before applying any force to the timber beam. The appearance of noise suggested that the bridge was unbalanced from the beginning, and the findings would not be correct. It was then agreed to insert a variable resistor with a capacity of 200 Ω and modify the resistance value to balance out the noise (Figure 4.24). It is crucial to use a sufficient capacity for the variable resistor, as the use of a larger resistor decreases the accuracy of the results, and a smaller resistor does not fully remove the noise from the circuit.

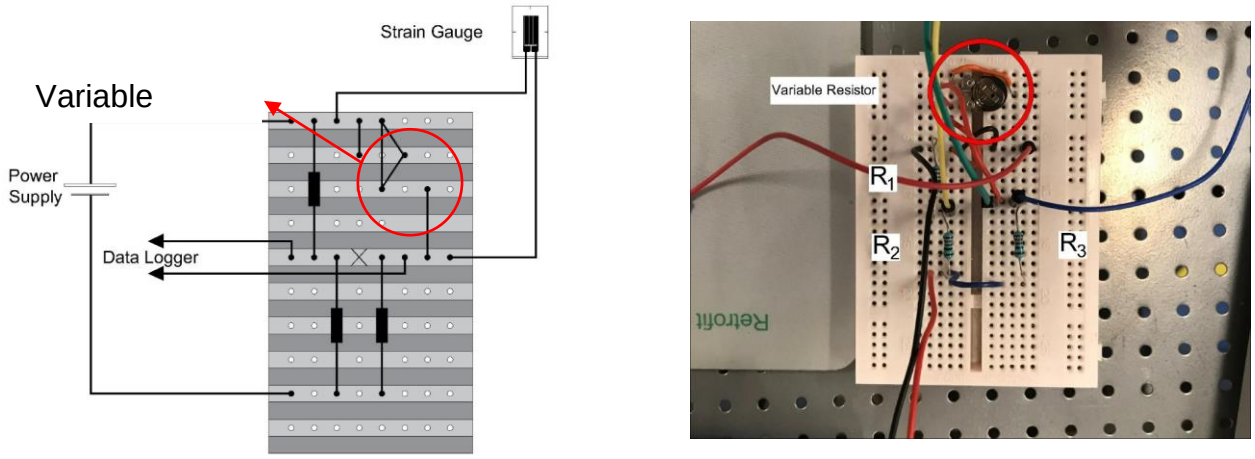

a) Schematic circuit b) Prototype circuit

Figure 4.24: Quarter-bridge circuit

Furthermore, the strength of the bond between a strain gauge and reinforcement is critical for the accurate transfer of the strain from the reinforcement to the foil (of strain gauge) through the adhesive and the strain gauge. Hence, to bind the strain gauge to the longitudinal reinforcement, the texture of the reinforcement was flattened using a file tool and sandpaper. After smoothing the surface (Figure 4.25a), it was then cleared of dust and grease using a surface cleaning agent and a clean piece of washcloth or cotton swab several times to ensure that the surface was prepared for bonding (Figure 4.25b).

a) Flattened reinforcement surface

b) Cleaning agent and a cotton swab

Figure 4.25: Smoothing process

Additionally, a thin layer of superglue was added on top of the treated surface to form a bond between the reinforcement and the strain gauge and then the strain gauge was carefully attached to it. The strain gauge was then gently pressured on the surface for one minute to ensure that the bond was solid (Figure 4.26a). In an attempt to protect the strain gauge from humidity, a thin coat of waterproof adhesive was added to the top surface of the strain gauge (Figure 4.26b). The integrated circuits of each strain gauge were then soldered to a 0.2 m silicone wire of 22AWG to connect the strain gauge to the circuit (Figure 4.26c).

a) Attach the strain gauge with super glue

b) Apply waterproof adhesive

c) Soldering the strain gauge to wire

Figure 4.26: Strain gauge installation

In this research, PicoLog 1012 data logger with an expandable multichannel data acquisition system was used for logging the reinforcement strain changes and for transferring it to the PicoLog 6 software connected to the data logger. The process of using strain gauges was adopted on two of the scaled frames to assess the efficiency of this approach in investigating the behaviour of reinforcement within the concrete sections under the applied loads. During each test, four strain gauges were connected to the frames (Figure 4.27a) and were logging the strain data simultaneously while the frames were tested under the applied loads (Figure 4.27b).

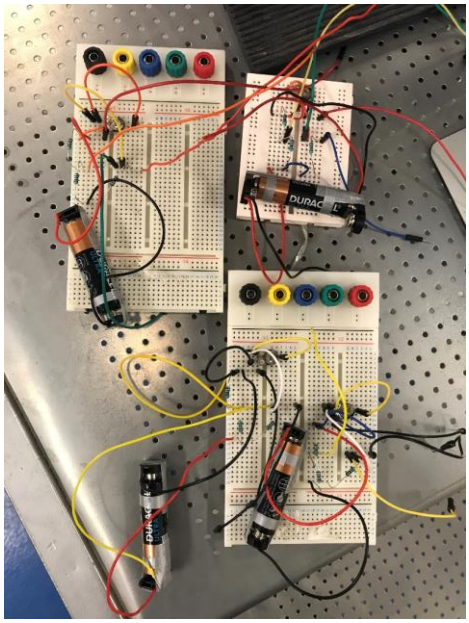

a) Four quarter-bridge circuits

b) Strain gauges connected to the circuits

Figure 4.27: Strain gauge configuration

Note: To ensure that the circuit is balanced before the beginning of each test, the wires connecting to the data logger were connected to a digital multimeter to determine whether the output voltage is zero. If the output voltage were zero, the circuit would be ready to start the test; otherwise, there could be some noise in the circuit that needed to be removed, either by changing the value of the variable resistor or by inspecting the wires connecting to the circuit and the data logger.

After the completion of the reinforcement cage, it was positioned within the mould with a coverage gap of 10 mm on either side of the mould, and the support wire was keeping the

concrete cover in the exact spot (Figure 4.28). Also, the height of the mould was purposely 10 mm higher than its width in order to give more space to the top of the frame throughout the concreting process and, consequently, to prevent bursts of concrete during the vibration process.

a) The reinforcement in place with wire

b) Fixate the mould with timber pieces

Figure 4.28: Fixating the reinforcement with reinforcing wire

- **Casting Concrete**

The next step was to produce concrete using cement (blue circle general purpose), coarse aggregate (10 mm gravel), fine aggregate (sharp sand) and water, as seen in Figure 4.29. Also, the configuration of the mixture is seen in Table 4.10, which indicated the quantity of each material needed in the mixture to achieve a compressive strength of 30 N/mm^2.

a) Cement

b) Coarse aggregate

c) Fine aggregate

d) Water

Figure 4.29: Materials to make concrete

As seen in Table 4.10, the ingredients were added to the ELE Concrete Mixer 34-3540 (Figure 4.30) and mixed to form a homogeneous concrete mixture. Besides, since the gap between the longitudinal rebars and the shear links in the Mini-Haunch was short, it was determined to ease the process of casting concrete by increasing the workability of the mixture. Therefore, one specific concrete mix was designed for the standard connection (Mix number 1) and another for the Mini-Haunch connection (Mix number 2). After the concrete was made, a slump test was carried out to determine the workability of fresh concrete mixtures in compliance with BS EN 206.

Table 4.10: Concrete mix design

Mix No.	W/C	Total weight	Water		Cement		Coarse Aggregate		Fine Aggregate	
	Ratio	kg	% of Mix	L	% of Mix	kg	% of Mix	kg	% of Mix	kg
1	0.33	105.5	8.05	7.00	19.90	21.00	49.76	52.50	27.09	23.69
2	0.40	106.9	7.85	8.40	19.64	21.00	49.11	52.50	27.23	23.39

a) Concrete mixer b) Mixing the materials c) Fresh concrete

Figure 4.30: Making concrete

- **Slump Test**

The slump test was carried out using the 'ELE International Slump Test Kit BS and ASTM 34-0192' seen in Figure 4.31a, in which the hollow cone was first positioned on a flat surface that

was kept in place by standing on the two handles of the cone. The cone was then filled with fresh concrete in three roughly identical layers, compacted 25 times, by using the compacting rod in each layer. The strokes had to be equally spread over the cross-section of the cone. At the end of the third layer, the remaining concrete had to be cleaned out of the top surface and levelled with a trowel at the top part of the cone. The cone was then removed vertically, which lasted about 2 to 5 seconds, and the length of the fresh concrete sample was determined (Figure 4.31). The calculated height was then deduced from 300 mm (height of the cone).

a) ELE slump test kit b) Filled cone c) Slump result

Figure 4.31: Slump test

Note: It is important to mention that if the sample had failed in the shear or collapsed, the water/cement ratio would have had to be changed in order to create a more consistent slump class.

- **Placing the Concrete**

After the slump test, the plywood mould was placed on a shaking table to ease the concreting process and then filled with fresh concrete using a concrete scoop in the mould. This process was achieved in two identical layers of 50 mm (100 mm in total) to minimise the quantity of undesired voids in the mould. It was important to pour the concrete cautiously not to dislocate the reinforcement within the mould. Two pieces of wood (100 × 40 × 1000 mm) were then used to help stabilise the mould on the shaking table (Figure 4.32). Also, for the scaled frames with strain gauges, the same procedure was followed, and the concrete with the same slump was poured into the moulds.

a) Standard design mould

b) Pouring concrete

c) Filled mould and cylinders

d) Mini-Haunch design mould

e) Pouring concrete

f) Filled mould and cylinders

Figure 4.32: Casting concrete

The shaking table was then turned on to vibrate the concrete within the mould to remove the trapped air. This process continued as long as the air emerged from the surface, although it was necessary not to over-vibrate, as this could lead to a loss of entrained air (BS EN 12390-2:2019). At the end of the process, the top surface of the mould was levelled with a trowel and cleaned out, eliminating the splashed concrete.

Three-cylinder samples (150 × 300 mm) were also prepared by cleaning the inside with a clean cloth and then using the release agent. After that, the cylinders were filled with the same fresh concrete mixture of the scaled frames to test the compressive strength of the mixture after 28 days. In each cylinder sample, the concrete was filled into three equal layers, compacted 25 times using the stroke rod for each layer, and then vibrated with the shaking table to remove the air.

The concrete frame and cylinder samples stayed in their moulds for 24 hours, secured from corrosion, vibration and shock. After 24 hours, the mould was removed easily (the engineering judgment not to use a release agent for the wooden mould was correct), as seen in Figure 4.33, using a rubber hammer and a screwdriver.

a) Standard design frame

b) Three samples of the Standard design

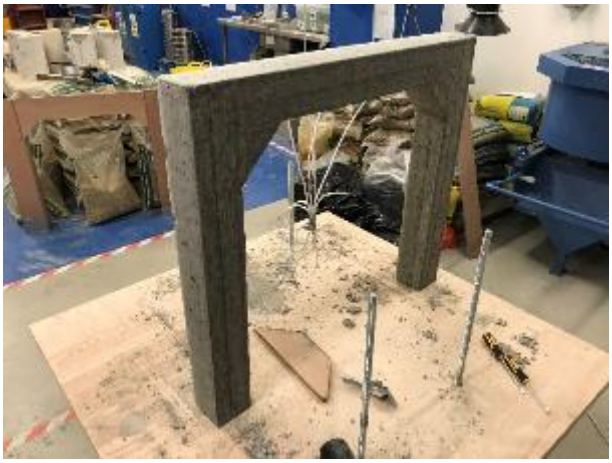

c) Mini-Haunch design frame

d) Three samples of the Mini-Haunch design

Figure 4.33: Frames and cylinder samples after releasing

- **Curing**

The frame and samples were placed inside a curing tank (1000 × 1000 × 500 mm) for 28 days and held at a temperature of (20 ± 2) ° C and cured until any further testing, as shown in Fig 3.34.

a) Standard design frame in the tank b) Mini-Haunch design frame in the tank

Figure 4.34: Curing of the frames and cylinder samples

- **Compression Test**

After 28 days of curing, the concrete frames and cylinder samples were removed from the tank. In order to determine the compressive strength of the concrete mixture, the density of the three-cylinder samples was first calculated by weighing the samples in water and air using the specific Gravity Apparatus, BS: 1881-114. The buoyancy balance is shown in Figure 4.35a and 4.35b, respectively.

The compressive strength of the samples was then assessed using the ELE ADR-Auto V2.0 2000 standard (Figure 4.35c). The compression machine measured the three samples at a speed of 10.6 m/s (Figure 4.35d).

a) Specific Gravity Apparatus

b) Weight in water to calculate the density

c) ELE ADR-Auto V2.0 2000 Standard

d) Compressive strength test

Figure 4.35: Cylinder sample testing apparatus

Moreover, the scaled frames were placed at the centre of the hydraulic actuator (with 500 kN compression capacity, which was able to apply a vertical load at the centre of the beam, on the top surface) and the base of the columns was placed on roller supports (Figures 4.36 and 4.37). It is important to point out that the hydraulic actuator was capable of either stopping the test

based on the applied loads (load-control) or the deflections (position-control). At the time of performing the tests, it was decided to set the limitation based on the deflection since it was safer and more convenient to control during the tests. Therefore, the machine was set to stop at 30 mm deflection in the middle of the beams where the frames could fail under the applied loads, and it was feasible from the health and safety point of view.

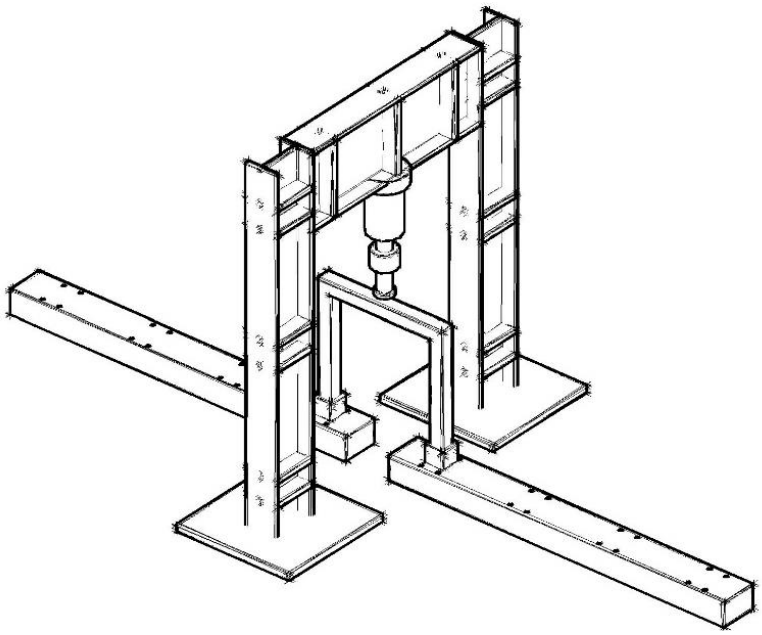

Figure 4.36: Schematic of the experimental test under the hydraulic actuator

To obtain the load-deflection curve, the hydraulic actuator was capable of applying the desired ramp load and measure the corresponding deflection at the centre of the beam using a built-in AEP TC4 transducer while recording the results in a LabVIEW based software connected to the actuator., as seen in Figures. 4.38 and 4.39.

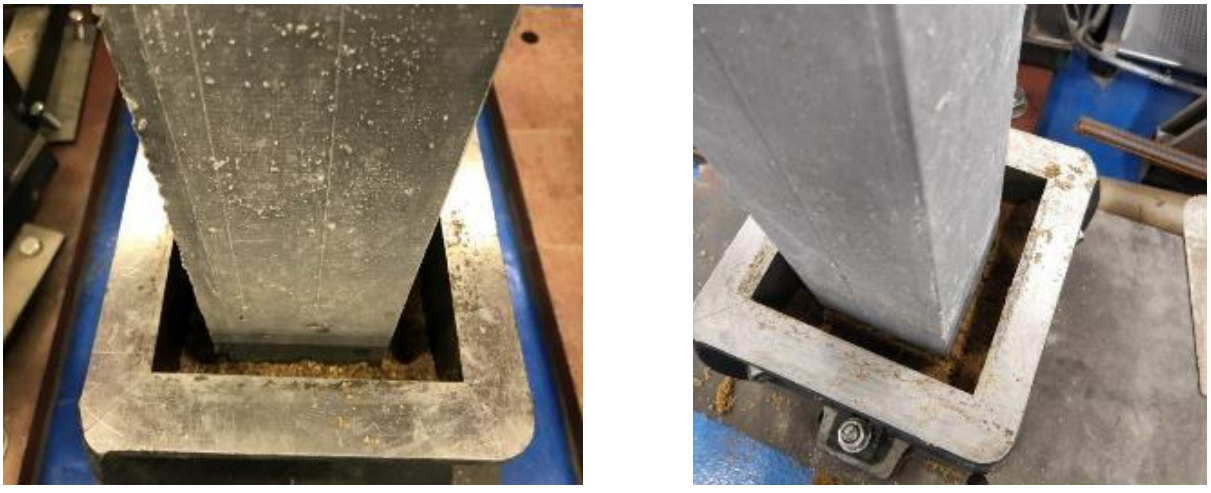

Figure 4.37: Roller supports

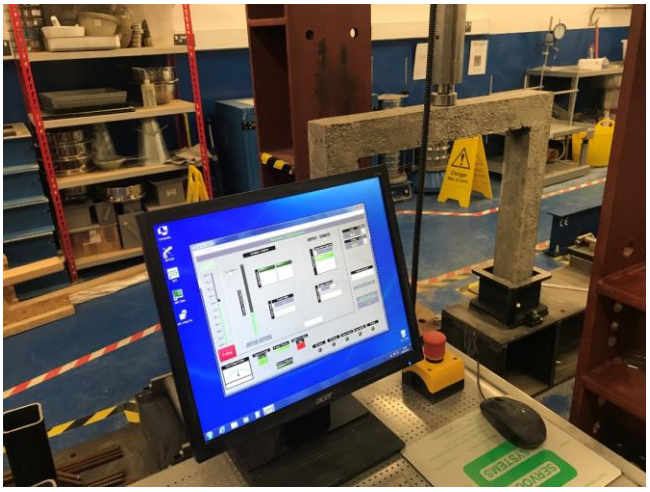

a) Standard design frame

b) Mini-Haunch design frame

Figure 4.38: Compression test under hydraulic actuator

a) Hydraulic actuator (500 kN)

b) Piston rod location

Figure 4.39: Placing the hydraulic piston in the middle of the beam

4.3.1 Finite Element Simulation with ANSYS

In this part of the research, various finite element simulations with ANSYS were conducted on the standard connection to investigate the efficiency and accuracy of this software in simulating the behaviour of the scaled frame with a standard connection.

- **Material properties and element type**

ANSYS uses a broad range of material properties that are available in the Engineering Data section and can be modified depending on the type of materials. The material for the scaled concrete frame was modelled by eight solid node elements (SOLID65) with three degrees of freedom at every point and the translation at x, y and z (Figure 4.41a). This element also provides plastic deformability, cracking in the direction of x, y, and z, until the crushed concrete (Adheem, 2013). In this model, the concept of Multilinear Kinematic hardening using compression stress-strain curves of unconfined concrete (Table 4.11) and tensile stress of ft = 0.7.√fc', which are proposed by Kent and Park (1971), were used.

Steel reinforcement was modelled as an axial rod element, using the Spar Link Element (LINK8), which has two points of three degrees of freedom at every point in x, y, and z (Figure 4.41b) and is capable of deforming plastically (Vasudevan and Kothandaraman, 2013). The reinforcement was expected to be able to transfer only axial forces. The Bilinear Isotropic Hardening type was used for the model of steel stress-strain relationship shown in Figure 4.40 and Table 4.11.

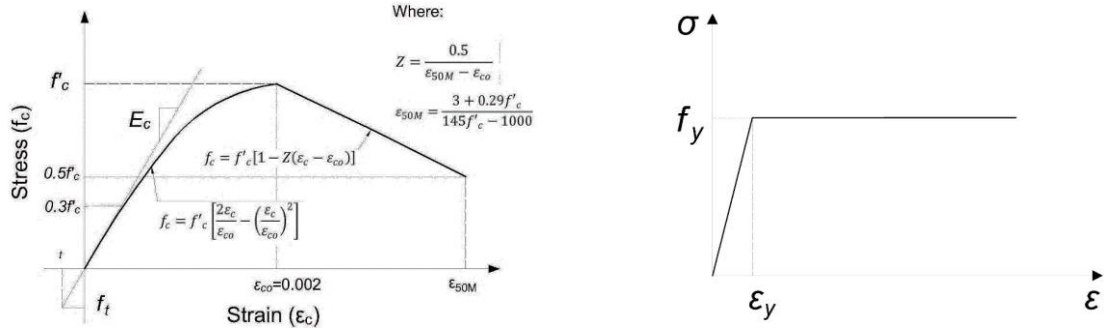

a) Concrete stress-strain relationship b) Steel stress-strain relationship

Figure 4.40: Concrete and steel behaviour

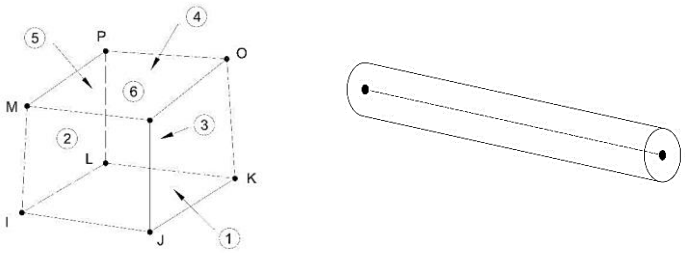

a) SOLID65 b) LINK8

Figure 4.41: Concrete and reinforcement elements

Table 4.11: Material properties

Concrete			**Nonlinear-Inelastic-Non-metal Plasticity- (Solid 65)**	
Compressive strength (N/mm^2)	30.6		Uniaxial crushing stress (N/mm^2)	30.6
Tensile strength (N/mm^2)	3.87		Uniaxial cracking stress (N/mm^2)	3.87
Modulus of Elasticity (kN/mm^2)	33		Tensile crack factor	0.6
Poisson's ratio	0.2		Open shear transfer coefficient	0.3
Density (kg/m^3)	2500		Closed shear transfer coefficient	1.0
Reinforcement	Ø8	Ø10		
Area (mm^2)	50.2	78.5		
Modulus of Elasticity (kN/mm^2)	205	205		
Yield strength (N/mm^2)	540	540		
Poisson's ratio	0.3	0.3		
Density (kg/m^3)	7850	7850		

- **Boundary conditions and loading**

In the experimental test with the standard connection, the frames were subjected to axial vertical loading generated from the hydraulic actuator at the middle of the beams. However, in the simulations, the forces were defined as vertical displacement (U_1=0 and U_2= 30 mm) to achieve the best results. Also, the boundary conditions in this analysis are illustrated in Figure 4.42, in

which roller supports were used at the bottom of columns in order to restrain the displacement in one degree of freedom (U_2=0).

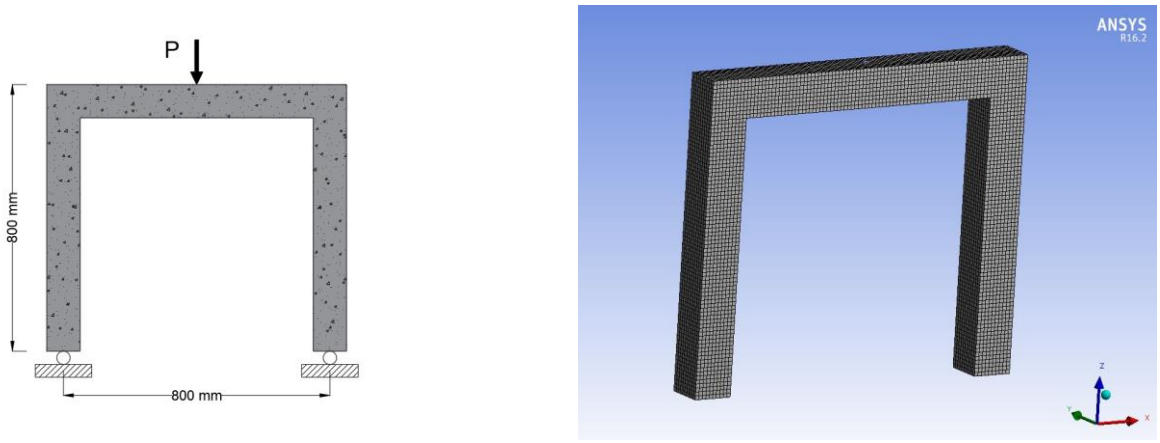

Figure 4.42: FE model arrangement including Boundary conditions and loading

- **Analysis type**

In this part of the simulation, due to the static nature of the experimental study and the ramp applied load on the scaled frames, it was decided to use static structural analysis.

4.3.2 Finite Element Simulation with Abaqus

This section describes the finite element (FE) analysis model, which was developed using the ABAQUS software (Dassault Systèmes, 2018) to investigate and further analyse the behaviour of RC frames with Standard and Mini-Haunch connections. The aim was to understand and quantify the influence of various parameters to develop focused design guidance. The tests described previously are employed for validation of the FE model.

- **Material properties**

Abaqus includes many different methods for simulating the behaviour of concrete in structural applications, including the smeared crack (SC) and concrete damaged plasticity (CDP) approaches. The SC method is suitable for all types of concrete structures, including trusses, shells and solids. After cracking, the model describes the reversible part of the material's response using oriented damaged elasticity concepts and is designed for cases in which the concrete is subjected to monotonic straining at low confining pressure (Chaudhari and

Chakrabarti, 2012). On the other hand, the CDP approach defines the inelastic behaviour of concrete through isotropic tensile and compression plasticity in combination with isotropic damaged elasticity concepts and is designed for cases in which the concrete is subjected to cyclic, monotonic and or dynamic loading under low confining pressure (Sümer and Aktaş, 2015). Both the CDP and SC models can be used for plain and reinforced concrete. In the current simulation, the CDP model is adopted to simulate the concrete behaviour since it was shown to provide an accurate depiction of the behaviour in previous experimental studies (e.g. Al-Osta et al., 2017; Earij et al., 2017; Rabi et al., 2019).

The CDP model also required several other input parameters which are presented in Table 4.12.

Table 4.12: Material properties

Concrete			**CPD parameters**	
Compressive strength (N/mm^2)	30.6		Dilation angle (ψ)	30
Tensile strength (N/mm^2)	3.87		Low potential eccentricity (e)	0.1
Modulus of Elasticity (kN/mm^2)	33		Viscosity parameter (μ)	0.001
Poisson's ratio	0.2		f_{b0}/f_{c0}	1.16
Density (kg/m^3)	2500		K	0.667
Reinforcement	Ø8	Ø10		
Area (mm^2)	50.2	78.5		
Modulus of Elasticity (kN/mm^2)	205	205		
Yield strength (N/mm^2)	540	540		
Poisson's ratio	0.3	0.3		
Density (kg/m^3)	7850	7850		

The stress-strain relationship for unconfined concrete in compression is based on the relationship given in Equation 4.11:

$$d(\sigma_c)/d_\varepsilon = E_{it} \quad \text{(Eq. 4.11)}$$

where σ_c, d_ε and E_{it} are concrete stress, concrete strain and initial tangential modulus, respectively. Also, when the stress reaches the maximum value, $d(\sigma_c)/d_\varepsilon$ is equal to zero (Carreira and Chu, 1985). In the current work, the compressive stress-strain relationship is adopted from Carreira and Chu (1985), as given in Equation 4.12:

$$\sigma_c = \frac{\beta(\varepsilon_c/\varepsilon_c')f_c}{\beta - 1 + (\varepsilon_c/\varepsilon_c')^\beta} \quad \text{(Eq. 4.12)}$$

where σ_c and ε_c are the stress and strain of the concrete, respectively, f_c is the concrete compressive strength (in N/mm^2) and ε_c' is the corresponding concrete strain. In this model, ε_c' has a value of 0.002. Also, β can be obtained from Figure 4.43 showing the curves in terms of f_c'.

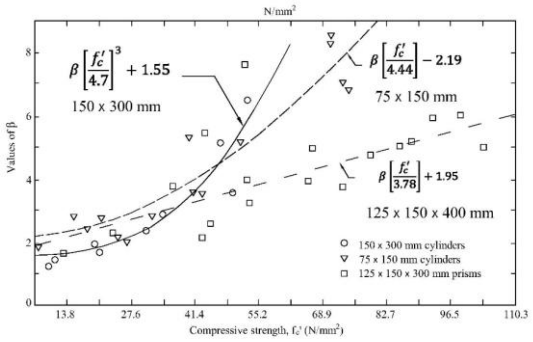

Figure 4.43: Relationship between β and f_c' (from Carreira and Chu (1985))

In terms of the steel reinforcement, this material is represented in the FE analysis using a bilinear isotropic hardening model with elastic-perfectly plastic behaviour (Figure 4.44), using the properties presented in Table 4.12.

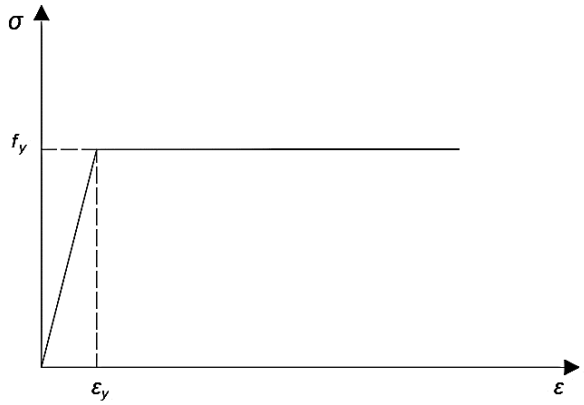

Figure 4.44: Stress-strain curve for steel reinforcement

- **Boundary conditions and loading**

In the experimental tests, the frames were subjected to axial vertical loading generated from the hydraulic actuator at the middle of the beams. However, in the simulations, the forces were defined as vertical displacement (U_1= 0 and U_2= 30 mm) to achieve the best results. Also, the boundary conditions in this analysis are illustrated in Figure 4.45, in which roller supports were used at the bottom of columns to restrain the displacement in one degree of freedom (U_2=0).

- **Model development and solution procedure**

The loading and boundary conditions of the experimental programme were replicated in the FE model, as shown in Figure 4.45. Therefore, a single point load was applied at the mid-span of the beam, and the base of the columns was on roller supports.

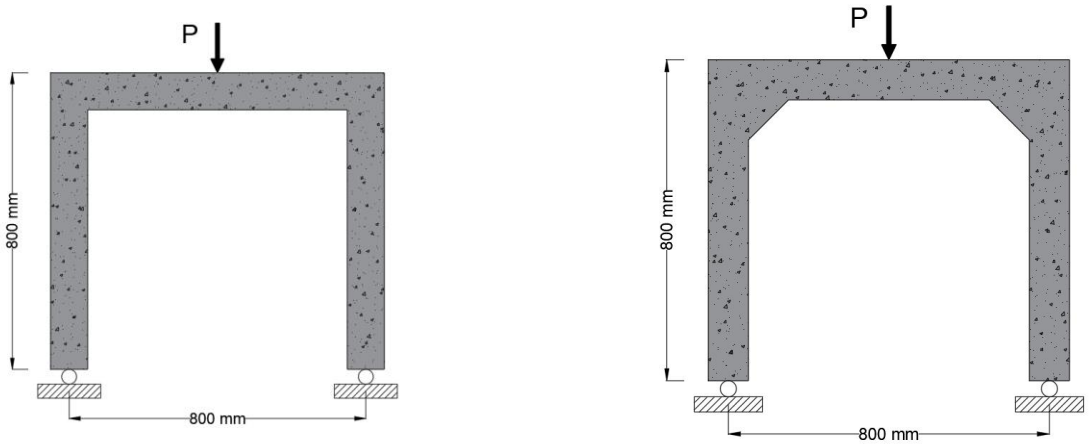

a) Standard connection b) Mini-Haunch connection

Figure 4.45: Schematic of the FE model arrangement with Boundary conditions and loading

- **Element type**

In this finite element simulation, the three-dimensional four-nodes linear tetrahedron element (C3D4) was adopted to model concrete (Figure 4.46a) with a 20 mm quadratic mesh size for the beam and columns elements (Figure 4.47). Also, the three-dimensional truss two-nodes element (T3D2) was used to model steel reinforcement (Figure 4.46b) with a 20 mm truss linear mesh size.

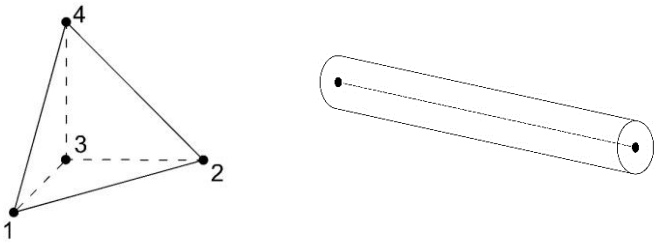

a) C3D4 b) T3D2

Figure 4.46: Concrete and reinforcement elements

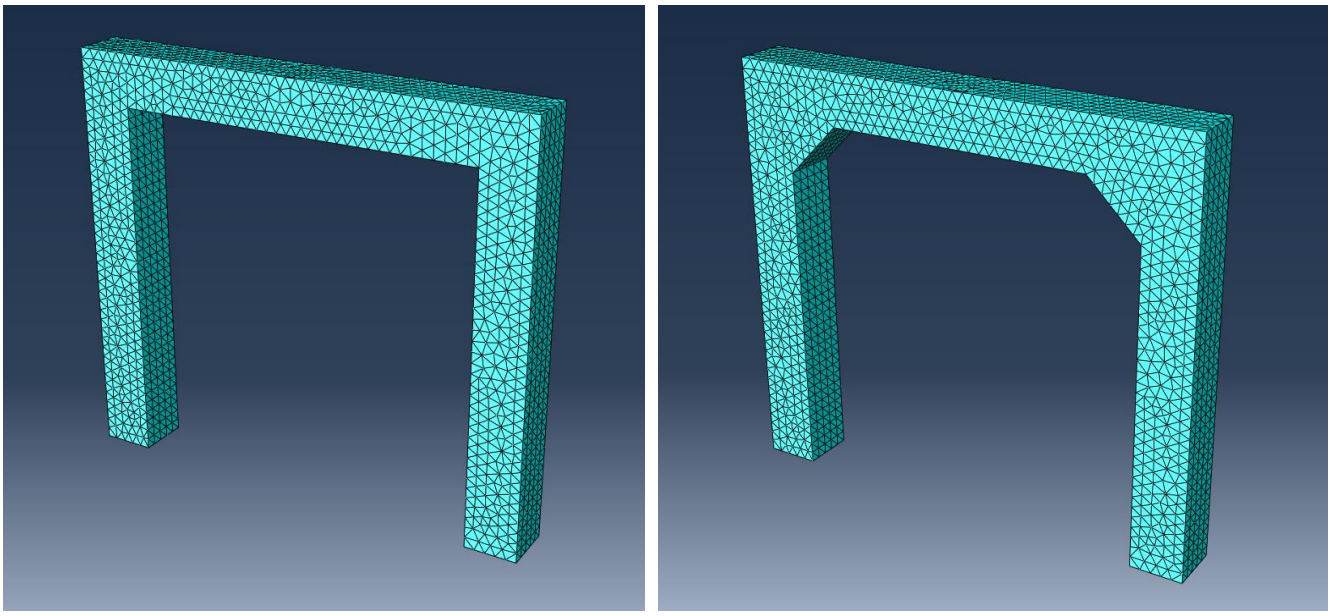

a) Standard connection b) Mini-Haunch connection

Figure 4.47: Frames element type

- **Analysis type**

Although the problem represented in the FE model was defined as static behaviour, due to the nonlinearity and complexity of the geometry and contact interactions, the model was analysed using the explicit dynamic solution procedure in ABAQUS to achieve convergence without compromising on accuracy. Furthermore, in order not to apply the loads as an impact load, the time was expanded up to 50 seconds divided into ten intervals. Then, to optimise the accuracy and computational efficiency, mass scaling was used for the whole model, and the target time increment is scaled to 0.001. This setup helps the FE model to achieve the required static response from a dynamic solution. One way to validate the static behaviour of the model is to compare the internal and kinetic energy outputs. If the kinetic energy is small friction of the internal energy (between 5 to 10%), the behaviour is considered to be static; otherwise, the FE model tends to provide a more dynamic response.

- **Mass scale**

In ABAQUS, the simulations tend to be time-consuming to complete their process; therefore, to achieve computational efficiency in either quasi-static or dynamic analyses, mass scaling can be used. This feature allows a simulation to be conducted with time efficiency without increasing the loading rate artificially.

In simulations involving rate-dependent damping or rate-dependent material, the loading rate cannot be increased since it simultaneously increases the material strain rates. At the point when the properties of the model change with the strain rate, artificially increasing the loading rate artificially changes the procedure.

In Equation 4.13 and 4.14, the relation between stability limit (the governing factor for the maximum time increment) and density of materials can be observed.

$$\Delta t = \frac{L^e}{c_d} \qquad \text{(Eq. 4.13)}$$

$$c_d = \sqrt{\frac{E}{\rho}} \quad \text{(Eq. 4.14)}$$

Where Δt, L^e, c_d, E and ρ are stability limit, characteristic element length, dilatational wave speed, modulus of elasticity and density, respectively. Based on Equation 4.14 and 4.15, increasing the density (ρ) of a material by a factor of β^2 reduces the wave speed by a factor of β and increases the stable time by a factor of β (ABAQUS/CAE User's Manual, 2013).

It is essential to mention that while increasing the loading rate, applying the loads should be gradual and smooth. In this regard, ABAQUS has a smooth built-in step amplitude graph (Figure 4.48) that can generate a smooth loading amplitude, and it is adopted in this analysis.

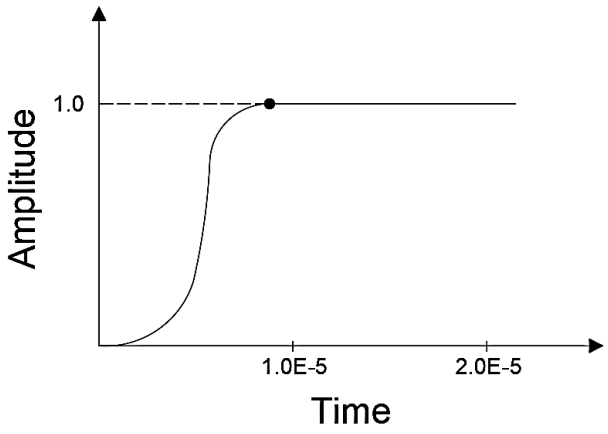

Figure 4.48: Abaqus amplitude curve

4.4 Sustainable Development of Medium Strength Concrete Using Polypropylene as Aggregate Replacement

In this section, the experimental method to investigate the effectiveness of Polypropylene as a fine aggregate replacement in the concrete mix design is described.

4.4.1 Concrete Mix Design to British Standards

A reference concrete mix was designed in compliance with British standards (BS EN 12620, 2002; BS 8500-1, 2015; BS 8500-2, 2015; BS EN 206, 2013) and the Concrete Society (Good

Concrete Guide 8, 2016) to attain the standard ST5 recommended concrete for general purposes and the S2 slump level (50 to 90 mm) to have the expected strength class of C20/25 (BS 8500-1, 2015). The reasoning behind the choice of this concrete strength class was to conform with the earlier studies and to ensure continuity in the concrete mix across the whole research whilst fulfilling the structural application requirement.

The design of the Reference Mix is seen in Table 4.13 per 1.0 m^3 of concrete, Table 4.14 per 150 mm^3 of concrete and Table 4.15 per mix of concrete.

Table 4.13: Reference mix design to British standards quantities per 1.0 m^3 of concrete

W/C	**Total weight**	**Water**		**Cement**		**Coarse Aggregate**		**Fine Aggregate**		**Plastic Aggregate**		
Ratio	kg	% of Mix	L	% of Mix	kg	% of Mix	kg	% of Mix	kg	% of Mix	% of Fine Agg	kg
0.56	2385.0	8.81	210.0	15.72	375.0	49.06	1170.0	26.42	630.0	0.0	0.0	0.0

Table 4.14: Reference mix design to British standards quantities per 150 mm^3 of concrete

W/C	**Total weigh t**	**Water**		**Cement**		**Coarse Aggregate**		**Fine Aggregate**		**Plastic Aggregate**		
Ratio	kg	% of Mix	L	% of Mix	kg	% of Mix	kg	% of Mix	kg	% of Mix	% of Fine Agg	kg
0.56	8.05	8.81	0.71	15.72	1.27	49.06	3.95	26.42	2.13	0.0	0.0	0.0

Table 4.15: Reference mix design to British standards quantities per mix of concrete

W/C	Total weight	Water		Cement		Coarse Aggregate		Fine Aggregate		Plastic Aggregate		
Ratio	kg	% of Mix	L	% of Mix	kg	% of Mix	kg	% of Mix	kg	% of Mix	% of Fine Agg	kg
0.56	72.44	8.81	6.38	15.72	11.39	49.06	35.54	26.42	19.14	0.0	0.0	0.0

4.4.2 Pilot Study

A pilot analysis was performed to determine the issues that could have arisen during the main experiments in the analysis. The adequacy of the experimental technique was tested together with the experimental concrete mixtures for both the reference mix and the first plastic-containing mixture (PP2.5), intended to decide if the optimal S2 slump level of workability can be attained.

4.4.3 Reference Mix

During the preparation of the reference mixture, all ingredients were mixed with water in increments of 0.5 L. It was established that at 5.50 L of water (0.88 L less than intended), the concrete mixture revealed that the concrete mix was too wet to be labelled as an S2 slump (based on slump test results), exhibiting three shear slumps in a row. At this stage, the engineering assessment was used to stiffen the reference mixture in order to attain the desired workability. Instead of only raising the volume of cement in the mixture, an average mixing ratio was taken from the Standard Mix Design for the combination of cement, coarse and fine aggregates while retaining a mixing of 5.50 L of water (reduced from 0.56 to 0.44 w/c). Despite not agreeing with the commonly accepted concrete mix ratio of 1:2:4 (Chudley and Greeno, 2016), Tables 4.13 to 4.15 display an average mix ratio of 1:2:3 (15.72%: 26.42%: 49.06%) for cement: fine aggregate: coarse aggregate. Therefore, the ingredients were used as cement 1 kg: fine aggregate 2 kg: coarse aggregate 3 kg, and subsequently combined with the current

reference mixture of concrete and also the slump test results indicated that the substance modification had hardened the reference mixture, providing a slump of 50 mm (S2 slump class).

4.4.4 Plastic-Containing Mixes

The reference mix concept was utilised as the basis for the design of the first plastic-containing mixture (PP2.5). The fine aggregate (sharp sand) was substituted by plastic aggregate at a rate of 2.50%. However, the measurement of the workability of the mixture using the slump test on two instances revealed that the mixture was a 20 mm slump and thus an S1 slump class. In order to assess the effectiveness of the findings of the PP2.5 mix and to validate the consistent mixing and delivery of mixed substances, 0.50% additional plastic aggregates were applied to create a concrete mix containing 3.0% plastic by fine aggregate mass (PP3.0). It was noted that the PP3.0 mix gives a stiffer mix and decreased slump assessment (below 20 mm) to that of the PP2.5 mix. A mass substituted the fine aggregate at a rate of 3.0% of the plastic aggregate. Slump test results revealed on two tests that the combination was operating in the S1 slump class (10 mm). These findings affirm the authenticity of the slump findings of the PP2.5 mix that the content distribution was adequate and consistent, and eventually, the added plastic aggregate stiffened the concrete mixture.

4.4.5 Experiment

- **Materials**

In this part of the research, concrete mixtures were prepared using Portland-Limestone Cement CEM II/A-L 32,5 R Tarmac, 'Blue Circle Portland-Composite Cement' (LaFarge, 2008)-as a cementitious binding agent, verified by Tarmac (Tarmac, 2017) to comply with the mechanical properties and chemical composition criteria set out in BS EN 197-1 (2011) and thus not to exceed 6-20% of the limestone content (BS EN 197-8) The key constituent properties of the cement used for this experiment are seen in Table 4.16. The fly ash used in this experiment was supplied by Omni-Cem (2011) of the Ratcliffe-on-Soar power station, Nottingham, England. Fly ash chemical constituent compounds included in this experiment are shown in Table 4.17.

Table 4.16: Main constituent properties of cement in this experiment (BS EN 197-1, 2011)

Property	**Cement (Quantity, %)**
Clinker (K)	80-94
Limestone (L)	6-20
Minor Additional Constituents	0-5

Table 4.17: Main chemical constituent properties of fly ash in this experiment (Omni-Cem, 2011)

Property	**Fly Ash (Quantity, %)**
Water-soluble chloride	<0.01
Acid soluble sulphates	0.72
Total sulphur	0.37
Calcium oxide	5.67
Magnesia	2.53
Silica	42.69
Ferric oxide	9.19
Alumina	23.09
Potassium oxide	2.27
Sodium oxide	0.72
Titanium dioxide	1.01
Others	11.73

The purpose of the use of these aggregate materials was to create a well-graded mix. Hence, Gravel Travis Perkins, including 'Gravel and Pea Shingle Trade Pack 10 mm' (Travis Perkins, 2019a), was used with a particle size varying from 4 mm to 10 mm, with no composite particle size exceeding 10 mm, and conforming to BS EN 12620 (2002). The fine aggregate used in the experiment was Quartz Sharp Sand Travis Perkins, 'Sharp/Grit Sand' (Travis Perkins, 2019b) with a particle size varying from 0 mm to 4 mm, with no aggregate particle size beyond 4 mm, in compliance with BS EN 12620 (2002), where the standard morphology of sharp sand particles was 'subangular to rounded' (Aggregate Industries, 2013). The coarse and fine aggregates were

used in their saturated condition shortly after collection and storage outside of the building site of the retailer. Plastic aggregate used for a fine aggregate (sharp sand) substitution in plastic-containing concrete mixtures was proprietary recycled polypropylene (PP) Axion Group Axypoly ABS52 (Group, 2018)-nominally manufactured in cylindrical particle size of 3 × 2 mm, smooth in surface texture. The material properties of the large, fine and plastic aggregates are shown in Table 4.18, with visual evidence of the particle size and morphology shown in Figures. 4.49 to 4.51.

Table 4.18: Material properties used in this experiment

Category	**Material**	**Particle Size (mm)**	**Bulk Density (kg/m^3)**	**Reference**
Cementitious Binding Agent	Portland-Limestone Cement	N/A	1440	Chudley and Greeno (2016)
Cementitious Binding Agent	Fly (Boiler) Ash	N/A	1300	(Good Concrete Guide 8, 2016)
Fine Aggregate	Sharp Sand	< 4mm	1250	Chudley and Greeno (2016)
Coarse Aggregate	Gravel	4-10mm	1200	Chudley and Greeno (2016)
Plastic Aggregate	PP	2x3mm	1075	Group (2018)

a) Cement packaging b) Cement particle size c) Fly ash packaging d) Fly ash particle size

Figure 4.49: Cementitious binding agent materials - product details and particle sizes

a) Coarse aggregate

b) Fine aggregate

Figure 4.50: Utilised aggregates

Figure 4.51: Plastic Aggregate Material

- **Concrete Mix Design Procedure**

In this experiment, six plastic-containing concrete mixtures were prepared with PP as a partial substitution of the fine aggregate mass in the mixture (sharp sand). Following the outcome of the pilot study, the PP amount of plastic-containing concrete mixtures rose at a rate of 0.50% and in doses between 0.50% to 3.00%, with coding for these mixtures from PP0.5 to PP3.0. Also, a 'control' concrete mix was developed as per the updated pilot study reference mix, offering a basis for evaluation of additional plastic-containing concrete mixtures. In order to solve the problem of decreased workability at larger PP doses shown in the pilot study, a further mixture (PP3.0FA) was introduced, including a 10.00% partial substitution of cement mass with fly ash. As Thomas has already said, M. (2007), the addition of 10% of fly ash could provide a water reduction of at least 3% of concrete mixtures. The water/cement ratio (w/c) was held at 0.44 for all mixtures in this experiment. The mixing ratios for all concrete mixtures are summarised in Table 4.19 per 1.0m^3 of concrete, Table 4.20 per 150 mm^3 of concrete and Table 4.21 per mix of concrete.

Note: In order to simplify the discussion hereafter, a reference to the usage of plastic aggregates in this experiment is shown simply as a percentage, e.g. PP1.0 = 1.00% plastic aggregate and represents only the use of plastic particles as the fine aggregate mass substitution in the mixture and not the use of plastic aggregates as a substitute for the total nature of the concrete mixture

Table 4.19: Main mix design, all mixes quantities per 1.0 m^3 of concrete

Mix No.	Mix code	W/C	Total weight	Water		Cement		Coarse Aggregate		Fine Aggregate		Plastic Aggregate			Fly Ash		
		Ratio	kg	% of Mix	L	% of Mix	kg	% of Mix	kg	% of Mix	kg	% of Mix	% Fine Agg	kg	% of Mix	% of Cement	kg
1	Control	0.44	2551.44	7.10	181.07	16.00	408.2	49.68	1267.49	27.23	694.65	0.00	0.00	0.00	0.00	0.00	0.00
2	PP0.5	0.44	2551.44	7.10	181.07	16.00	408.2	49.68	1267.49	27.09	691.18	0.14	0.50	3.47	0.00	0.00	0.00
3	PP1.0	0.44	2551.44	7.10	181.07	16.00	408.2	49.68	1267.49	26.95	687.70	0.27	1.00	6.95	0.00	0.00	0.00
4	PP1.5	0.44	2551.44	7.10	181.07	16.00	408.2	49.68	1267.49	26.82	684.23	0.41	1.50	10.42	0.00	0.00	0.00
5	PP2.0	0.44	2551.44	7.10	181.07	16.00	408.2	49.68	1267.49	26.68	680.76	0.54	2.00	13.89	0.00	0.00	0.00
6	PP2.5	0.44	2551.44	7.10	181.07	16.00	408.2	49.68	1267.49	26.55	677.28	0.68	2.50	17.37	0.00	0.00	0.00
7	PP3.0	0.44	2551.44	7.10	181.07	16.00	408.2	49.68	1267.49	26.41	673.81	0.82	3.00	20.84	0.00	0.00	0.00
8	PP3.0FA	0.44	2551.44	7.10	181.07	14.40	367.41	49.68	367.41	26.41	673.81	0.82	3.00	20.84	1.60	10.00	40.82

Table 4.20: Main mix design, all mixes quantities per 150mm^3 of concrete

Mix No.	Mix code	W/C	Total weight	Water		Cement		Coarse Aggregate		Fine Aggregate		Plastic Aggregate			Fly Ash		
		Ratio	kg	% of Mix	L	% of Mix	kg	% of Mix	kg	% of Mix	kg	% of Mix	%Fine Agg	kg	% of Mix	% of Cement	kg
1	Control	0.44	8.61	7.10	0.61	16.00	1.38	49.68	4.28	27.23	2.34	0.00	0.00	0.00	0.00	0.00	0.00
2	PP0.5	0.44	8.61	7.10	0.61	16.00	1.38	49.68	4.28	27.09	2.33	0.14	0.00	0.01	0.00	0.00	0.00
3	PP1.0	0.44	8.61	7.10	0.61	16.00	1.38	49.68	4.28	26.95	2.32	0.27	0.00	0.02	0.00	0.00	0.00
4	PP1.5	0.44	8.61	7.10	0.61	16.00	1.38	49.68	4.28	26.82	2.31	0.41	0.01	0.04	0.00	0.00	0.00
5	PP2.0	0.44	8.61	7.10	0.61	16.00	1.38	49.68	4.28	26.68	2.30	0.54	0.01	0.05	0.00	0.00	0.00
6	PP2.5	0.44	8.61	7.10	0.61	16.00	1.38	49.68	4.28	26.55	2.29	0.68	0.01	0.06	0.00	0.00	0.00
7	PP3.0	0.44	8.61	7.10	0.61	16.00	1.38	49.68	4.28	26.41	2.27	0.82	0.01	0.07	0.00	0.00	0.00
8	PP3.0FA	0.44	8.61	7.10	0.61	14.40	1.24	49.68	4.28	26.41	2.27	0.82	0.01	0.07	1.60	10.00	0.14

Table 4.21: Main mix design, all mixes quantities per mix of concrete

Mix No.	Mix code	W/C	Total weight	Water		Cement		Coarse Aggregate		Fine Aggregate		Plastic Aggregate			Fly Ash		
		Ratio	kg	% of Mix	L	% of Mix	kg	% of Mix	kg	% of Mix	kg	% of Mix	%Fine Agg	kg	% of Mix	% of Cement	kg
1	Control	0.44	77.50	7.10	5.50	16.00	12.40	38.50	12.40	27.23	21.10	0.00	0.00	0.00	0.00	0.00	0.00
2	PP0.5	0.44	77.50	7.10	5.50	16.00	12.40	38.50	12.40	27.09	20.99	0.01	0.50	0.11	0.00	0.00	0.00
3	PP1.0	0.44	77.50	7.10	5.50	16.00	12.40	38.50	12.40	26.95	20.89	0.27	1.00	0.21	0.00	0.00	0.00
4	PP1.5	0.44	77.50	7.10	5.50	16.00	12.40	38.50	12.40	26.82	20.78	0.41	1.50	0.32	0.00	0.00	0.00
5	PP2.0	0.44	77.50	7.10	5.50	16.00	12.40	38.50	12.40	26.68	20.68	0.54	2.00	0.42	0.00	0.00	0.00
6	PP2.5	0.44	77.50	7.10	5.50	16.00	12.40	38.50	12.40	26.55	20.57	0.68	2.50	0.53	0.00	0.00	0.00
7	PP3.0	0.44	77.50	7.10	5.50	16.00	12.40	38.50	12.40	26.41	20.47	0.82	3.00	0.63	0.00	0.00	0.00
8	PP3.0FA	0.44	77.50	7.10	5.50	14.40	11.16	38.50	11.16	26.41	20.47	0.82	3.00	0.63	1.60	10.00	1.24

Following the preparation of the concrete combination, the 'Slump Test' was carried out to determine the workability of the concrete 'the ease to position and compact concrete' (Gorse, Johnston and Pritchard, 2012) in compliance with BS EN 12350-2:2009c using the 'ELE International Slump Test Package BS and ASTM 34-0192' (ELE International, 2019b). Afterwards, the samples were cast into 150 × 150 × 150 mm steel casting moulds ELE International '34-4670 150 mm Cube Mould 2-Part Clamp Form, Cast Iron Construction' (ELE International, 2019a)-as typically displayed using the Control Mix in Figure 4.52. Concrete was poured and put in three average layers of 50 mm in each cube mould, tamped for 40 times per layer, then eventually vibrated on the vibrating table Controls System 'Vibrating Table 55-C0161/LCZ' until the air bubbles raised to the surface of the moulds.

Figure 4.52: Steel Cube Moulds used to Cast Concrete Specimens

Specimens were placed in two large curing tanks from ELE International (Large Curing Tank 34-6575 Series ELE International, 2017) and maintained at a constant 22.0°C water temperature for their respective curing period (7 or 28 days) and were cured immediately until further testing.

- **Testing**

At both of the corresponding curing days, 7 and 28 days, and after the cube density measurement, the specimens were tested for compressive strength using the ELE International 'ADR-Auto V2.0' Compression Testing Machine (ELE International, 2011) as illustrated in BS

EN 12390-4 (2000) and as displayed in Figure 4.53 Set to a loading rate of 13.50 kN/s. Both techniques for compressive strength testing have been carried out in compliance with BS EN 12390-3 (2009).

Figure 4.53: Compressive Strength Testing Machine

5 The Significance of Removing Shear Walls in Existing Low-Rise RC Frame Buildings

5.1 Introduction

In the UK, shear walls have been widely used to resist lateral forces in almost every concrete frame buildings. However, as indicated by The Concrete Centre, the construction industry has questioned the efficiency of utilising such components. Removing shear walls can affect the performance of a structure; however, it may increase its cost-effectiveness and improve sustainability.

In this analysis, the feasibility of removing shear walls in an existing residential concrete frame building was investigated by considering the following criteria:

- Serviceability of the design is an essential criterion in the performance of a building subjected to wind-induced forces for the occupants. In general, human response to building motion which is a complex psychological and physiological phenomenon, is more effectively measured by acceleration than other factors (Banks et al., 2014).
- Also, under SLS criteria, the design checks for slab sections (deflection and punching shear) should be calculated.
- Interstorey drift as a damage limitation requirement is another factor that should be considered in the performance of a building. According to Eurocode 8 Part 1, high values of interstorey drift may lead to severe damage and eventually collapse of a structure. Furthermore, for buildings having non-structural elements, the limitation of interstorey drift is vital to control the serviceability cracks, connections between blocks or stud partition walls and slabs.
- The cost and construction duration are essential criteria to be taken into account. Providing approaches to reduce the overall construction expenses and the programme

times will lead to more sustainable construction as such approach has a direct effect on two pillars of sustainability, namely environment (less environmental impact by reducing the required volume of concrete) and economy (reducing the construction cost).

- Since the wind force is directly dependant on the regional location, the response of a building to the subjected loads could be different in various areas in the UK. Furthermore, climate change will lead to higher wind speed in the coming years.

Furthermore, the evaluation of the structural criteria will be performed using global analyses by ETABS v16.2.1 and the other criteria, including the cost and time estimation, will be performed using Concept v3.

5.2 Results and discussion

5.2.1 First Stage

- **Structural Results**

Displacements

The following approach is developed to verify the obtained results from the first stage (the comparative study of the two structures with and without shear walls):

The comparative analysis of maximum displacement in both structures with shear walls (Case 1) and without shear walls (Case 2) is shown in Table 5.1 and demonstrated in Figure 5.1.

Table 5.1: Maximum storey displacement case 1 and 2

Storey	Height (m)	Case 1		Case 2	
		X-Axis (mm)	Y-Axis (mm)	X-Axis (mm)	Y-Axis (mm)
Roof	2.96	0.616	3.49	10.1	5.49
Storey 5	3.15	0.507	3.34	9.71	5.27
Storey 4	3.08	0.386	2.99	8.65	4.72
Storey 3	3.08	0.269	2.48	7.02	3.88
Storey 2	3.08	0.159	1.79	4.89	2.75
Storey 1	4.13	0.0682	0.977	2.51	1.43

From maximum storey displacement in Table 5.1, it could be observed that considering the location and orientation of shear walls and columns in both axes, the lateral displacements in case 1 for the X and Y axes were lower than the results from case 2, showing higher stiffness in the structural performance of the building with shear walls. Also, comparing the results for the X and Y axes in case 1 showed that since the shear walls were placed in line with the X-axis, the lateral displacements in the X-axis were much lesser than the results in the Y-axis. On the other hand, the results from case 2 were different since the lateral displacements in the X-axis were nearly twice that of the Y-axis due to the orientation and number of columns in each axis.

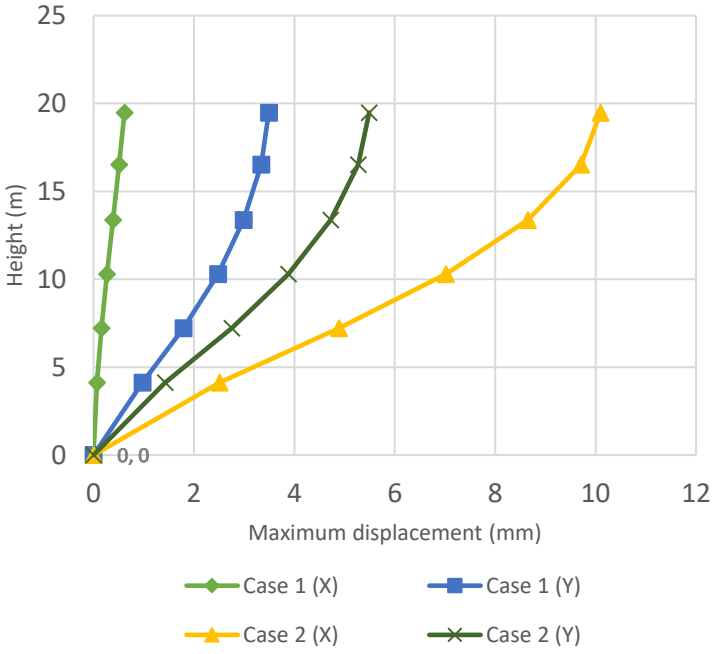

Figure 5.1: Comparison of maximum displacement in Case 1 and 2

Moreover, the results shown in Figure 5.1 support the previous results in which the lateral displacements in case 2 were higher than case 1, which illustrated the influence of shear walls as the lateral resisting elements in RC frame buildings.

Interstorey Drift

Based on the results in ETABS, the maximum interstorey drift values for wind actions in X and Y directions are shown in Table 5.2 along with the defined limitations (H/500) in BS 8110: Part 2 Cl 3.2.2.2 for RC frame buildings subjected to wind actions.

Table 5.2: Maximum storey drift

Storey	Height (m)	Case 1		Case 2		
		Drift X d_r (mm)	Drift Y d_r (mm)	Drift X d_r (mm)	Drift Y d_r (mm)	Limitation (mm)
Roof	2.96	0.111	0.152	0.444	0.221	5.92
Storey 5	3.15	0.122	0.345	1.06	0.548	6.31
Storey 4	3.08	0.119	0.521	1.63	0.846	6.15
Storey 3	3.08	0.111	0.688	2.13	1.13	6.15
Storey 2	3.08	0.092	0.814	2.38	1.32	6.15
Storey 1	4.13	0.068	0.977	2.51	1.43	8.25

In Table 5.2, it was noted that even though the interstorey drift values in case 2 were higher than case 1 in both axes, the values did not exceed the limits defined by the BS 8110 for each storey, and both buildings were within the safe range.

Moreover, Figure 5.2 was produced compare the interstorey drifts values in each axis.

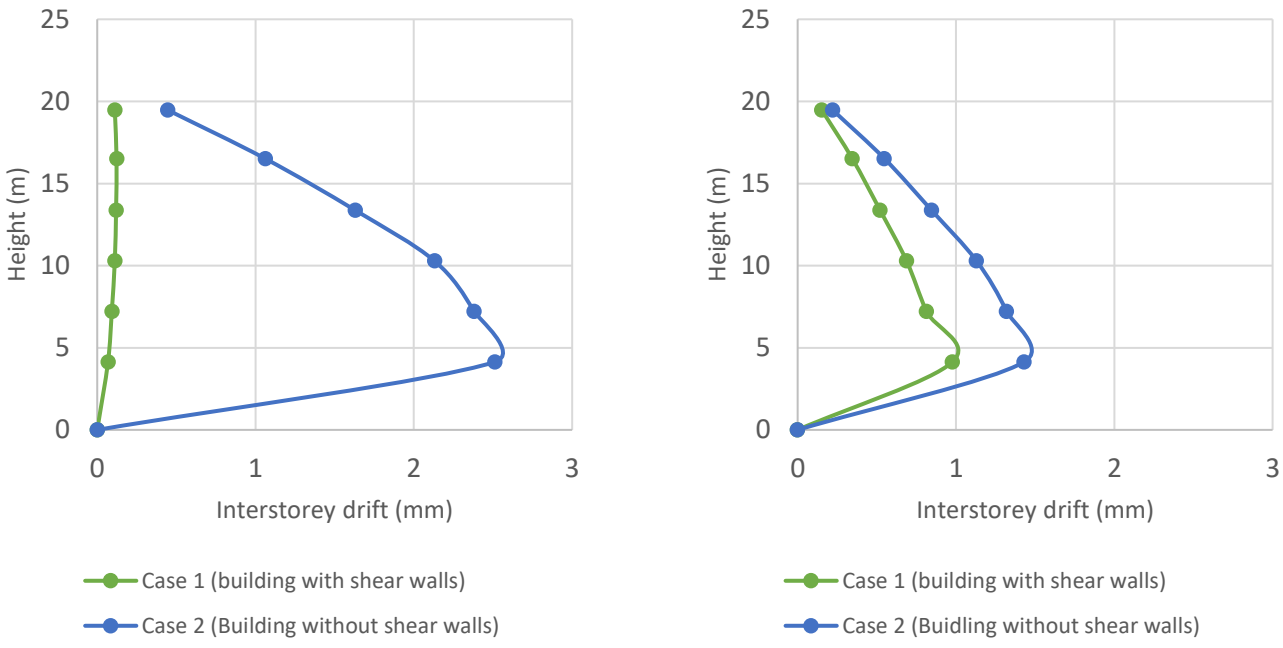

a) X-axis

b) Y-axis

Figure 5.2: Interstorey drifts

The values of interstorey drift also show that the drift in the building without shear walls (case 2) appear to be higher than the building with shear walls (case 1). Also, it is worth mentioning that the fluctuation at 5 m for both cases was due to the difference in the height between the ground storey and the other storeys.

Accelerations

There are ranges of standards for occupant comfort requirements in buildings, such as the NBCC: Section 4 and The Concrete Centre (Banks et al., 2014). Based on The Concrete Centre, the standard value for a 10-year wind-generated return period are as follows:

- 10 to 15 milli-g for residential occupancy
- 20 to 30 milli-g for office occupancy

The findings of the acceleration of buildings and human perception are shown in Table 5.3.

To calculate the acceleration based on the frequency and the maximum displacement, Equation 5.1 from SpaceAge Control (2001) can be used:

$$a = \frac{2\pi^2 \times f^2 \times d}{g} \quad \text{(Eq. 5.1)}$$

Where a, f, d and g represent acceleration (m/s^2), frequency (Hz), maximum displacement (m) and acceleration (m/s^2), respectively.

Table 5.3: Acceleration values for case 1 and 2

Mode of vibration	Frequency (cyc/sec)		Maximum displacement (mm)		Acceleration (m/s^2)		Acceleration (milli-g)	
	Case 1	Case 2	Case 1	Case 2	Case 1	Case 2	Case 1	Case 2
1	2.39	0.617	0.616	5.61	0.069	0.042	7.03	4.28
2	0.731	0.586	3.49	10.3	0.036	0.071	3.67	7.24

It was noted that for the first two principal modes of vibration, the acceleration values in both cases were lower than the threshold, and both buildings were within the safe range for the occupants' comfort criteria.

Shear Force

The storey shear represents the total lateral load applied to the base of a structure, and if the vertical elements in the building are not designed appropriately, it could result in shear failure.

In this analysis, the applied storey shear generated from wind actions are presented and compared to the hand calculated design wind loads:

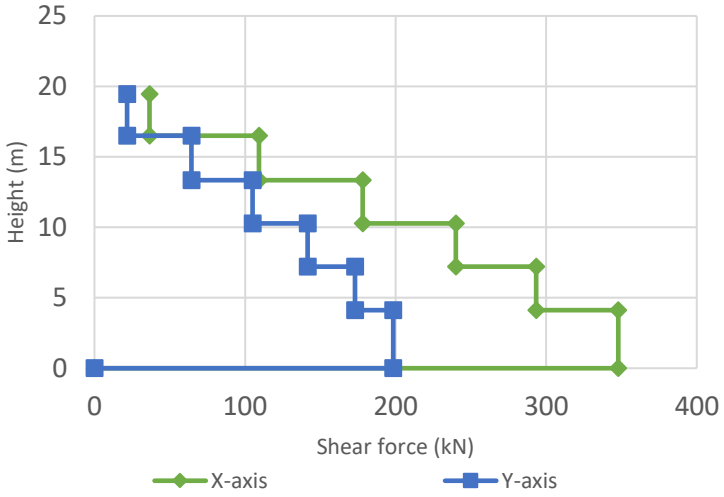

Figure 5.3: Shear force comparison case 2 (X and Y axis)

Table 5.4: Comparison of calculations

Method	**Base Shear Force X-axis (kN)**	**Base Shear Force Y-axis (kN)**
Hand Calculations	346.1	201.1
ETABS results	344.5	198.4
Percent Error (%)	0.46	1.3

Based on the values of shear forces in Figure 5.3, it can be noted that the shear forces from the hand calculations were in good agreement with ETABS results. The results are summarised in Table 4.4.

Overturning Moment

In a structure, the applied lateral loads will be multiplied by the height of the structure and create a moment at the base of the structure, which in high magnitudes can result in overturning failure mechanism. The following calculations check the overturning moment for the building:

Based on the cumulative mass in both X and Y directions (49.15 MN) obtained from ETABS, the resisting moment could be calculated:

Mass (calculated by ETABS) = 49.15 MN

$$M_o x = M_y + V_x h_f = 4.487 + 0.345 \times 1 = \mathbf{4.832\ MN.m} \text{ (Critical scenario)} \quad \text{(Eq. 5.2)}$$

$$M_o y = M_x + V_y h_f = 2.545 + 0.198 \times 1 = 2.743\ MN.m \quad \text{(Eq. 5.3)}$$

$$M_R = Mass \times Minimum\ lever\ arm\ (9.01\ m\ or\ 8.69\ m) \quad \text{(Eq. 5.4)}$$

$M_R x = 49.15 \times 8.69 =$ ***427.1 MN.m*** *(Critical scenario)*

$M_R y = 49.15 \times 9.01 = 442.8\ MN.m$

The critical resisting moment is 427.1 ≥ 4.832 MN.m

These calculations demonstrated that the overall overturning moment was much lower than the resisting moment of the building.

Flat Slab Deflection

Eurocode 2 Part 1-1 (BS EN 1992-1-1, 2014) deals with a design for deflection in flat slabs by several approaches in which limiting span to depth ratio was used in this analysis.

In Table 4.5, the results for flat slab deflection are illustrated, and the procedure to calculate the span to depth ratio is provided by Goodchild (2009), which is presented here.

In case 1 (building with shear walls), the slab between EF-3 to EF-5 due to its wide span was chosen.

The combination of actions was taken from EN 1990-2002 Expression 6.10b (shown here as Equation 5.5):

$$\sum_{j\geq 1} \xi_j \gamma_{G,j} G_{k,j} + \gamma_P P + \gamma_{Q,1} Q_{k,1} + \sum_{i>1} \gamma_{Q,i} \psi_{0,1} Q_{k,i} \quad \text{(Eq. 5.5)}$$

$n = 1.25 \times 8.125 + 1.5 \times 4 + 0.7 \times 0.73 = 16.7\ KN/m^2$

Design moment in a span:

$M_{Ed} = (1.25 \times 8.125 \times 0.09 + 1.5 \times 4 \times 0.1 + 0.7 \times 1 \times 0.73) \times 9.4^2 \times 5.65 = 1010\ kN.m$

Design moment in support:

$M_{Ed} = 16.7 \times 0.106 \times 9.4^2 \times 5.65 = 883\ kN.m$

Table 5.5: Apportionment of moments between column strips and middle strips

	M_{Ed}	
	Column strip	**Middle strip**
-ve (hogging)	0.7 x 883/2.35 = 263 kN.m/m	0.3 x 883/2.35 = 113 kN.m/m
+ve (sagging)	0.5 x 1010/2.35 = 215 kN.m/m	0.5 x 1010/2.35 = 215 kN.m/m

$$K = \frac{M_{Ed}}{bd^2} f_{ck} = 215 \times 10^6/(1000 \times 287^2 \times \frac{30}{1.5}) = 0.13 \quad \text{(Eq. 5.6)}$$

Z/d = 0.856 (Obtained from table 5 in Bond et al. (2006))

Z= 0.856 x 287 = 249 mm

$$A_s = M_{Ed}/f_{yd} Z = 215 \times 10^6/(500/1.15 \times 249) = 1985\ mm^2 \quad \text{(Eq. 5.7)}$$

Provided 7 B500B @ 142 mm = 2198 mm^2

$$\rho = A_s/bd = 1985 \times 100/1000 \times 285 = \%0.67 \quad \text{(Eq. 5.8)}$$

Deflection middle strip:

$$\textit{Allowable l/d} = N \times K \times F_1 \times F_2 \times F_3 \quad \text{(Eq. 5.9)}$$

N = 21.2 (taken from table C10 in Goodchild (2009))

K = 1.2 (for flat slab)

$F_1 = F_2 = 1$

$F_3 = 310/\sigma_s$ (Exp. 7.17 Eurocode 2 Part 1-1 (BS EN 1992-1-1, 2014)) (Eq. 5.10)

$$\sigma_s = \sigma_{su}(A_{s,req}/A_{s,prov})/\delta \quad \text{(Eq. 5.11)}$$

$\sigma_{su} = 250\ MPa$ (taken from Figure C3 in Goodchild (2009))

$\delta = 1.03$ (taken from Table C14 in Goodchild (2009))

$\sigma_s = 250 \times (1985/2198)/1.03 = 219$

$F_3 = 310/219 = 1.41$

Allowable l/d = 21.2 x 1.2 x 1 x 1 x 1.41 =35.9

Actual l/d = 9400/287 = 32.7

Allowable l/d = 35.9 ≥ Actual l/d = 32.7 → OK

Based on the calculations, it was confirmed that deflection in the flat slabs is not an issue, and the values are within the safe range defined by Eurocode 2 Part 1-1 (BS EN 1992-1-1, 2014).

In case 2, the deflection check values (building without shear walls) are:

Actual l/d = 9400/287 = 32.7

Allowable l/d = 33.4 ≥ Actual l/d = 32.7 → OK

Table 5.6: Flat slab deflection check (worst scenario)

Location	Allowable L/d	Actual L/d	Status
Case 1 (Building with shear walls)	35.9 (Storey 5- EF-1 to EF-3)	32.7	Passed
Case 2 (Building without shear walls)	33.4 (Storey 5- EF-1 to EF-3)	32.7	Passed

From Table 4.5, it can be observed that in the worst scenarios for both cases, flat slab defection ratios were within the allowable L/d.

Punching Shear (Case 1)

The results for the punching shear ratio are presented in Table 4.6, and the detailed procedure to calculate the punching shear is presented here.

In case 1, column F3 on the roof (the worst scenario) was chosen. The procedure was given by Goodchild (2009):

The following values were taken from ETABS design results:

Effective punching perimeter = *3095 mm*

Shear force = *439.4 kN*

Design shear stress = *0.75 MPa*

Concrete shear stress capacity = *0.48 MPa*

Punching shear ratio = *1.57*

u_1 = *2677.5 mm²*

According to Eurocode 2 Part 1-1 (BS EN 1992-1-1, 2014) CL 6.4.3 (2), the following checks should be carried out:

$V_{Ed} \leq V_{Rd,max} \rightarrow$ *0.75 MPa ≤ 3.6 MPa* *Pass*

$$V_{Rd,max} = 0.4\, \upsilon f_{cd} = 0.4 \times 0.53 \times 17 = 3.6\ MPa \qquad \text{(Eq. 5.12)}$$

$\upsilon = 0.6(1-f_{ck}/250) = 0.6 \times (1-30/250) = 0.53\ MPa$

$V_{Ed} \leq V_{Rd,c} \rightarrow 0.75\ MPa \geq 0.48$ Punching shear reinforcement is required

Also, the UK NA recommends $V_{Ed} \leq 2V_{Rd,c}$ which in this case *0.75 MPa ≤ 0.96 MPa*

Perimeter at which punching shear links are no longer required:

$$u_{out} = V_{Ed} \times \beta/(d \times V_{Rd,c}) = 621.8 \times 10^3 \times 1.4/287 \times 0.56 = 5416\, mm \quad \text{(Eq. 5.13)}$$

Length attribute to column face = *600 + 2 x 275 = 1150 mm*

Radius to u_{out} from face of column: $(5608 - 1150)/\pi = 1358\, mm$

Perimeter of shear reinforcement may stop at: *1414-1.5 × 275 = 1002* mm from face of column

S_r *= 275 x 0.75 = 207 say = 200 mm* (According to cl. 9.4.3(1) Eurocode 2 Part 1-1 (BS EN 1992-1-1, 2014))

S_t *= 275 x 1.5 = 415 say = 400 mm* (According to cl. 9.4.3(1) Eurocode 2 Part 1-1 (BS EN 1992-1-1, 2014))

$$F_{ywd.ef} = (250 + 0.25d) = 250 + 0.25 \times 287 = 322\ MPa \leq f_{yd} \quad \text{(Eq. 5.14)}$$

f_{yd} *= 500/1.15 = 434 MPa → OK*

$$A_{sw} \geq \frac{(V_{Ed} - 0.75V_{Rd,c})S_r u_1}{1.5 f_{ywd,ef}} \quad \text{(Eq. 5.15)}$$

$= (1.46 - 0.75 \times 0.54) \times 200 \times 2677.5/(1.5 \times 322) = 1023\, mm^2$ Per perimeter

$$A_{sw,min} \geq 0.08 \times \frac{f_{ck}^{0.5}(S_r S_t)}{1.5 f_{yk}} \quad \text{(Eq. 5.16)}$$

$= 0.08 \times 30^{0.5}(200 \times 400)/(1.5 \times 500) = 46 mm^2$

$$A_{sw}/u_1 = 1023/2677.5 = 0.38 mm^2 \quad \text{(Eq. 5.17)}$$

Using H8 (50 mm^2) maximum spacing = *50/0.38 = 132 mm*

H8 shear reinforcement at 132 mm is provided to prevent punching shear failure.

Punching shear values for case 2 (building without shear walls) are:

Punching shear ratio = 1.76, and the ratio is less than 2 according to $V_{Ed} \leq 2V_{Rd,c}$

To prevent punching shear failure, H8 at 124 mm shear reinforcement will be provided.

Table 5.7: Punching shear reinforcement ratio (worst scenario)

Location	Ratio	Status
Case 1 (Building with shear walls)	0.75 (Storey5- Column F1)	Passed
Case 2 (Building without shear walls)	1.76 (Storey5- Column F1)	Passed

The ratios in Table 4.6 demonstrate that the flat slabs in case 1 can provide adequate resistance to prevent shear failure, but in case 2, shear reinforcement was required.

- **Cost Estimation**

One of the objectives of this chapter was to estimate the cost difference between case 1 and 2. The cost estimates for construction in both cases are calculated by Concept software which uses the rates obtained from Goodchild, Webster and Elliott (2009) publication to estimate the construction cost.

Table 5.8: Cost estimation case 1

Component	Quantity	Rate	Quantity		Rate		Subtotal £K
Slabs	609 m³@	£95.00 +	15	T @	£750.00		69.1
Shear Walls	136 m³@	£110.00+	13.6	T @	£750.00		25.2
Columns	42 m³ @	£110.00+	12.6	T @	£750.00		14.1
Formwork (Vertical)			730	m² @	£32.00		23.4
Formwork (Horizontal - plain)			3043	m² @	£29.00		88.2
Formwork (Horizontal -ribbed)			0	m² @	£52.50		0.0
Hollow-core units			0	m² @	see "Rates"		0.0
						Total "superstructure"	220.0
					72.3	*£/m²*	
Stairs as %age of superstructure cost						14%	30.8
Foundations			50772	kN @	£1.89		95.7
Ground floor slab			507	m² @	£30.00		15.2
Cladding			1816	m² @	£330.00		599.2
						Structure and cladding total	960.9
Prelims and external works						10%	293.1
Finishes and walls						21%	615.5
Mechanical and Electrical						35%	1025.9
						Total construction	2895.5
					951.6	*£/m²*	
						TOTAL	2895.5

Table 5.9: Cost estimation case 2

Component	Quantity	Rate	Quantity		Rate		Subtotal £K
Slabs	609 m³@	£95.00 +	15	T @	£750.00		69.1
Columns	71 m³ @	£110.00+	12.6	T @	£750.00		17.3
Formwork (Vertical)			630	m² @	£32.00		20.2
Formwork (Horizontal - plain)			3043	m² @	£29.00		88.2
Formwork (Horizontal -ribbed)			0	m² @	£52.50		0.0
Hollow-core units			0	m² @	see "Rates"		0.0
						Total "superstructure"	194.8
					64.0	*£/m²*	
Stairs as %age of superstructure cost						14%	35.2
Sprayed fibre coating (two hours) fire protection*	86 m² @	£11.79					1.0
Foundations			50772	kN @	£1.89		95.7
Ground floor slab			507	m² @	£30.00		15.2
Cladding			1816	m² @	£330.00		599.2
						Structure and cladding total	941.1
Prelims and external works						10%	293.1
Finishes and walls						21%	615.5
Mechanical and Electrical						35%	1025.9
						Total construction	2875.7
					945.0	*£/m²*	
						TOTAL	2875.7

* It is required by the UK's Building Regulations that stair cores must be fire-resistant. By eliminating shear walls around the staircase, fire-resisting plasterboards were added to the cost estimation.

Based on Table 4.8 and 4.9, since the shear walls were excluded from the building, the quantity of concrete and rebar were decreased, but the number of columns increased in the construction process.

Moreover, the overall saving in case 2 was 0.67% of the estimated total cost (£2.89 million), which validates the cost-effectiveness of removing shear walls (even by replacing them with extra columns).

Concrete is an essential construction material but has negative impacts on the environment, e.g. CO_2 emissions, and in this analysis, it was illustrated the quantity of concrete in case 2 reduced. This has a positive impact on the sustainability of concrete construction. Reducing the volume of concrete reduces the negative environmental impact.

- **Time Estimation**

The existing RC frame building had been designed as a cast-in-situ concrete frame. It has been suggested that cutting out shear walls might cut out a day in a 14-day cycle, and this amount of time could be saved in the construction process.

5.2.2 Second Stage

- **Maximum Displacement**

In this section, the structural analyses results obtained from the various UK locations are presented and discussed. These include the comparison of the maximum storey displacement for Birmingham (Case 3), Edinburgh (Case 4), Belfast (Case 5) and Shetland (Case 6), as demonstrated in Table 4.10 and Figure 5.4.

Table 5.10: Maximum displacement case 3 to 6

Storey	Height (m)	Case 3 (Birmingham)		Case 4 (Edinburgh)		Case 5 (Belfast)		Case 6 (Shetland)	
		X-Axis (mm)	Y-Axis (mm)	X-Axis (mm)	Y-Axis (mm)	X-Axis (mm)	Y-Axis (mm)	X-Axis (mm)	Y-Axis (mm)
Roof	2.96	7.78	4.25	9.93	5.37	10.8	5.91	31.2	17.2
Storey5	3.15	7.45	4.08	9.49	5.15	10.4	5.68	29.9	16.4
Storey 4	3.08	6.65	3.67	8.46	4.62	9.26	5.11	26.7	14.8
Storey 3	3.08	5.44	3.04	6.89	3.81	7.57	4.23	21.7	12.2
Storey 2	3.08	3.84	2.19	4.84	2.72	5.35	3.06	15.1	8.69
Storey 1	4.13	2.03	1.18	2.51	1.43	2.82	1.65	7.62	4.53

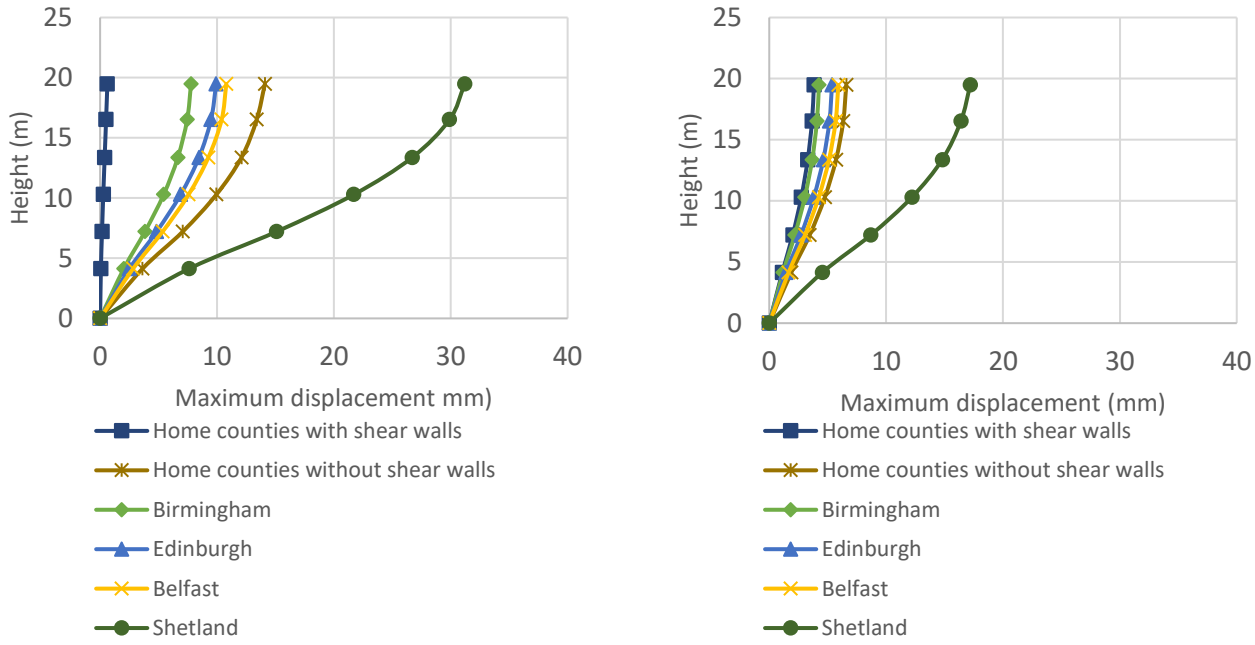

a) X-axis

b) Y-axis

Figure 5.4: Comparison of maximum displacements in all locations

The maximum displacements in cases 3 to 6 are illustrated in Table 4.10. Based on the acquired results in Figure 5.4a for all of the six cases, it was observed that the lateral displacement in the X direction for case 1 had the lowest value, which was the result of utilising the shear walls as expected. The highest lateral displacement was for case 6 (Shetland), which was corresponding to the value of wind pressure calculated in Table 4.3. Furthermore, as illustrated in Figure 5.4b,

the lowest lateral displacement in the Y direction was for case 1 (building with shear walls), which seems reasonable considering the presence of shear walls, and the highest value was for case 6 (Shetland) as expected.

- **Interstorey Drift**

The comparison of interstorey drift in Case3-6 is presented in Table 4.11:

Table 5.11: Maximum storey drift in cases3-6

Storey	Case 3(Birmingham)		Case 4 (Edinburgh)		Case 5 (Belfast)		Case 6 (Shetland)		Limitation (mm)
	Drift X d_r (mm)	Drift Y d_r(mm)	Drift X d_r(mm)	Drift Y d_r(mm)	Drift X d_r(mm)	Drift Y d_r(mm)	Drift X d_r(mm)	Drift Y d_r(mm)	
Roof	0.336	0.166	0.434	0.215	0.467	0.231	1.34	0.661	5.92
Storey5	0.799	0.412	1.03	0.533	1.11	0.573	3.23	1.66	6.31
Storey4	1.22	0.631	1.57	0.817	1.69	0.879	4.99	2.59	6.15
Storey3	1.59	0.847	2.06	1.09	2.22	1.18	6.63	3.53	6.15
Storey2	1.82	1.01	2.33	1.29	2.53	1.41	7.46	4.17	6.15
Storey1	2.03	1.18	2.51	1.43	2.82	1.65	7.62	4.53	8.25

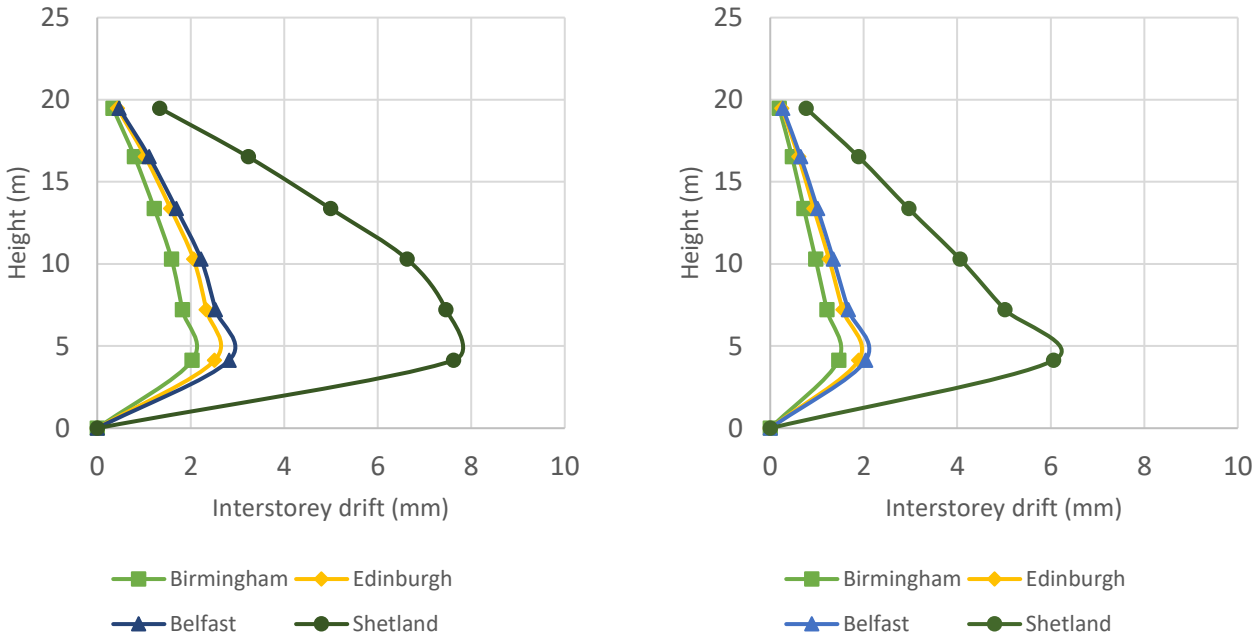

a) X-axis

b) Y-axis

Figure 5.5: Comparison of interstorey drift

From the values of interstorey drift for cases 3 to 6, as it is shown in Table 4.11, it can be concluded that except for case 6 (Shetland), the other cases were within the safe range defined by BS 8110: Part 2 Cl 3.2.2.2. Additionally, Figure 5.5 demonstrates the results based on the height of the buildings, which highlights that in all the cases, the interstorey drift values decreased as the height of the structure increased. This is expected as usually the value of interstorey drifts in structures drop with the increment of the height.

- **Acceleration**

The assessment of building response regarding human response for cases 3, 4, 5 and 6 are illustrated in Table 4.12:

Table 5.12: Acceleration in case 3 to 6

Mode	Frequency (Hz)				Acceleration (milli-g)			
	Case 3	Case 4	Case 5	Case 6	Case 3	Case 4	Case 5	Case 6
1	0.586	0.591	0.586	0.595	5.37	6.97	7.48	22.2
2	0.617	0.623	0.617	0.626	3.25	4.18	4.54	13.5

It was evident that the calculated accelerations for other locations (Birmingham, Edinburgh, Belfast) were within the defined safe range. However, this is not the case for Shetland because the acceleration has exceeded the safe range, and it failed to provide occupants comfort.

Since the beginning of this analysis, it was pointed out that the Shetland case was chosen only as of the worst possible case.

- **Shear Force**

Figure 5.6 demonstrates that the shear forces in the X direction in cases 3, 4, 5 and 6 tend to be higher than shear forces in the Y direction. It could be because of smaller dimensions and subsequently lower resistance in the X direction comparing to the Y direction.

a) X-axis

b) Y-axis

Figure 5.6: Shear force comparison in case 3 to 6 (Birmingham, Edinburgh, Belfast and Shetland)

It is also important to mention that based on the results, as the shear forces in a building increase, the stability of the structure in global analysis increases accordingly. However, this needs further investigation since, from a certain level, the individual elements (especially columns) cannot resist the applied shear forces and will fail.

- **Flat Slab Deflection**

The calculations to check deflection in the flat slab were provided earlier. In Table 4.13, only the values are presented. These calculations are based on exp. 6.10b in Eurocode 2 Part 1-1 (BS EN 1992-1-1, 2014) in which wind actions take place in the design calculations.

Table 5.13: Flat slab deflection check (worst scenario)

Location	Allowable L/d	Actual L/d	Status
Case 3 (Birmingham)	36.6 (Storey 5- EF-1 to EF-3)	32.7	Passed
Case 4 (Edinburgh)	34.9 (Storey 5- EF-1 to EF-3)	32.7	Passed
Case 5 (Belfast)	34.5 (Storey 5- EF-1 to EF-3)	32.7	Passed
Case 6 (Shetland)	24.1 (Storey 5- EF-1 to EF-3)	32.7	Failed

It was evident that deflection values in flat slabs for Birmingham, Edinburgh and Belfast were within the safe range defined by Eurocode 2 Part 1-1 (BS EN 1992-1-1, 2014); however, Shetland failed to fulfil the criteria.

- **Punching Shear**

The calculation to design the punching shear reinforcement was provided earlier. In Table 4.14, the results are presented:

Table 5.14: Punching shear reinforcement ratio (worst scenario)

Location	Ratio	Status
Case 3 (Birmingham)	1.84 (Storey5- Column F1)	Passed
Case 4 (Edinburgh)	1.84 (Storey5- Column F1)	Passed
Case 5 (Belfast)	1.87 (Storey5- Column F1)	Passed
Case 6 (Shetland)	2.34 (Storey2- Column F1)	Failed

In Table 4.14, the shear reinforcement ratio is calculated. Except for Shetland which failed to provide enough resistance, all the other cases passed the criteria with shear reinforcement to prevent punching shear failure.

5.3 Summary

In this chapter, the significance of utilising shear walls in RC frame buildings was assessed in two stages. In the first stage, the feasibility of removing shear walls in an existing UK residential building is investigated when the building is subjected to wind-induced actions, and building performance, cost-effectiveness and sustainability of construction were reviewed by using ETABS and Concept software. In the second stage, after validating the effectiveness of removing shear walls, the application of constructing the same building in various locations in the UK subjected to different wind loads was investigated, and the global performance of the buildings was discussed.

Based on the acquired results from the first and second stage of this analysis, the following summary can be drawn:

- The comparison of maximum lateral displacements in case 1 and 2 demonstrates that although case 1 (with shear walls) performed a stiffer behaviour, case 2 still can provide adequate serviceability and strength within the safe range defined by Eurocode 2 Part 1-1.
- The results from interstorey drift in Table 4.2 and 4.10 show that in all cases except for case 6 (Shetland), the values were within the safe range defined by BS 8110.
- The calculations section (Table 4.3 and 4.12) show the accelerations generated by the buildings with and without shear walls (in cases 1 and 2) and locations 3, 4 and 5 (Birmingham, Edinburgh and Belfast) were within the allowable range, and the comfort of the occupants will not be compromised. However, Shetland failed to provide occupants comfort by its high acceleration values.
- According to the acquired values from the overturning moment, it can be concluded that wind actions in low-rise buildings in the UK do not have a substantial impact to cause overturning failure mechanism.
- Deflection in flat slabs, as an essential check in Eurocode 2 Part 1-1, was checked in this analysis, and the results obtained that, except for Shetland, all the other 5 cases (Buildings with and without shear walls, Birmingham, Edinburgh, and Belfast) provided enough safety in accordance to Eurocode 2 Part 1-1.
- It was evident that flat slabs were vulnerable to punching shear and require shear reinforcement to prevent failure.
- By eliminating shear walls in the building, around 0.67% of the overall construction cost was saved, even when extra columns substituted it.
- Eliminating the shear walls also resulted in a reduction of construction time by one day in a 14-day cycle.

- This analysis illustrated that low-rise buildings in the UK could be constructed safely without shear walls and provide adequate serviceability and strength within the safe range defined by Eurocode 2 Part 1-1.
- Constructing RC frame buildings in the UK without shear walls reduces the construction cost and time without affecting the buildings' structural performance.

6 The Influence of Different Factors on Buildings' Height in the Absence of Shear Walls in Low Seismic Regions

6.1 Introduction

Shear walls are components typically included in reinforced concrete framed structures to resist lateral actions (Taleb et al., 2012). They are employed almost exclusively in the UK, especially in so-called low-rise buildings, which are up to five storeys (Emporis Standards, 2008 & 2009; Banks et al., 2014; NFPA, 2016). In recent years, experts at the Concrete Centre in the UK have questioned the extensive usage of shear walls, which is very costly to the construction industry, and the current work has been conducted as a direct consequence. Such elements, if used based on the design necessities, can provide stiffness to a structure that enables it to resist the applied lateral loads. On the other hand, if shear walls are employed regardless of the design requirements, this has a negative effect on the sustainability credentials of the final design, as well as the economic and structural efficiency. Accordingly, there is significant interest amongst the reinforced concrete construction sector in an investigation of the requirement for shear walls whilst maintaining and not compromising the occupants' safety.

In earlier studies in chapter 4, the significance of removing shear walls in an existing five-storey RC building near London in the UK was investigated. The results demonstrate that the frame itself, with rigid connections between the elements, can withstand the applied loads after the shear walls are removed, and the structural performance remains within the safe range, as defined by Eurocode 2 Part 1-1 (BS EN 1992-1-1, 2014). Furthermore, it was shown that the same building could be safely constructed in various locations in the UK with different latitude and wind pressure values. The current part of the research aims to build on this work and investigate the possibilities and limitations of increasing the height of a five-storey RC frame residential building without shear walls and to develop a deep understanding of the influential

parameters. In this analysis, the investigated parameters are concrete strength, column size, column shape and slab thickness.

6.2 Results and Discussion

6.2.1 Concrete Grade

The results for the influence of concrete grade were obtained using 750 × 250 mm column size (Figure 6.1) and 275 mm slab thickness on a building's lateral displacements in each storey subjected to wind action in the X and Y directions. The results are presented in Figure 6.2.

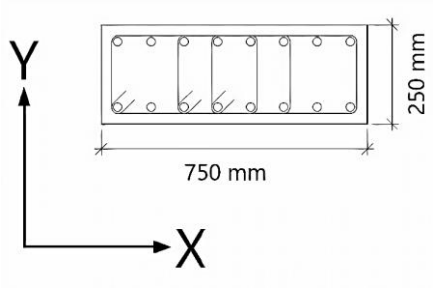

Figure 6.1: Column cross-section

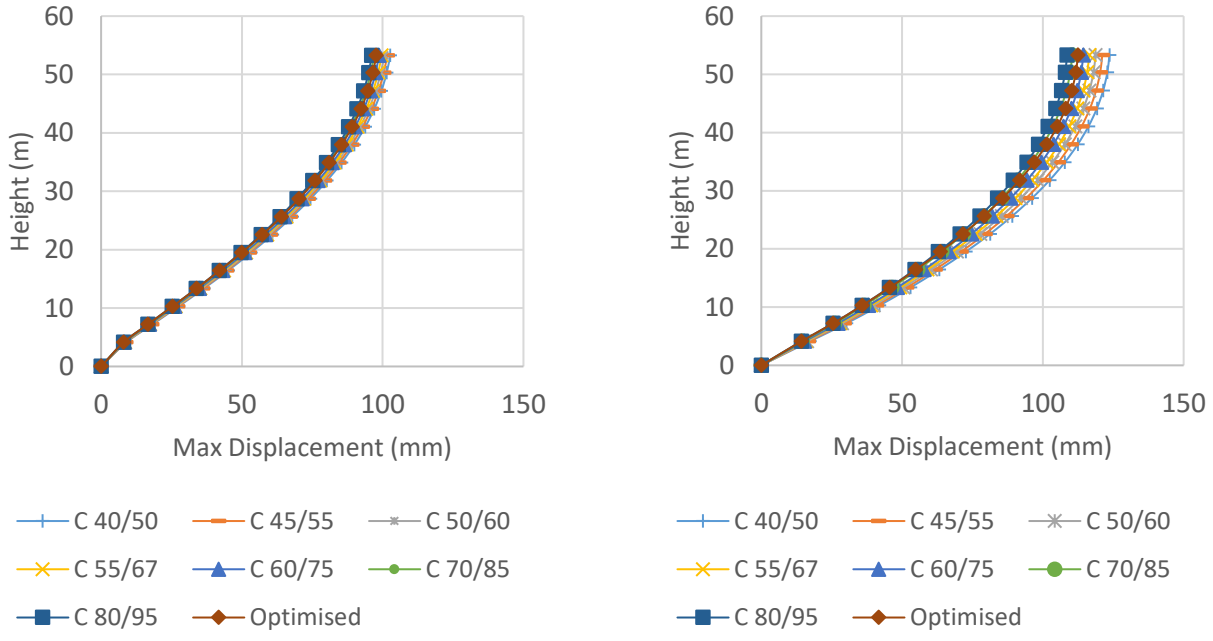

(a) X-direction (b) Y-direction

Figure 6.2: Influence of concrete strength on the maximum displacement of RC framed buildings

It can be observed that the building stiffness was gradually enhanced as the concrete grade increased, and the maximum displacement in both directions was reduced accordingly. It also was evident that the optimised concrete grade (shown in Table 6.1) performance was quite close to C80/95 in both directions, which was more favourable in terms of the economy by utilising a variation of concrete strength classes instead of using a high-strength concrete such as C80/95 for the whole structure.

6.2.2 Column Size

The results for the maximum displacements in buildings with different column sizes and another one with shear walls (200 mm thickness) were obtained using concrete-grade C40/50 and 275 mm slab thickness subjected to the wind load in X and Y directions and are illustrated in Figure 6.3.

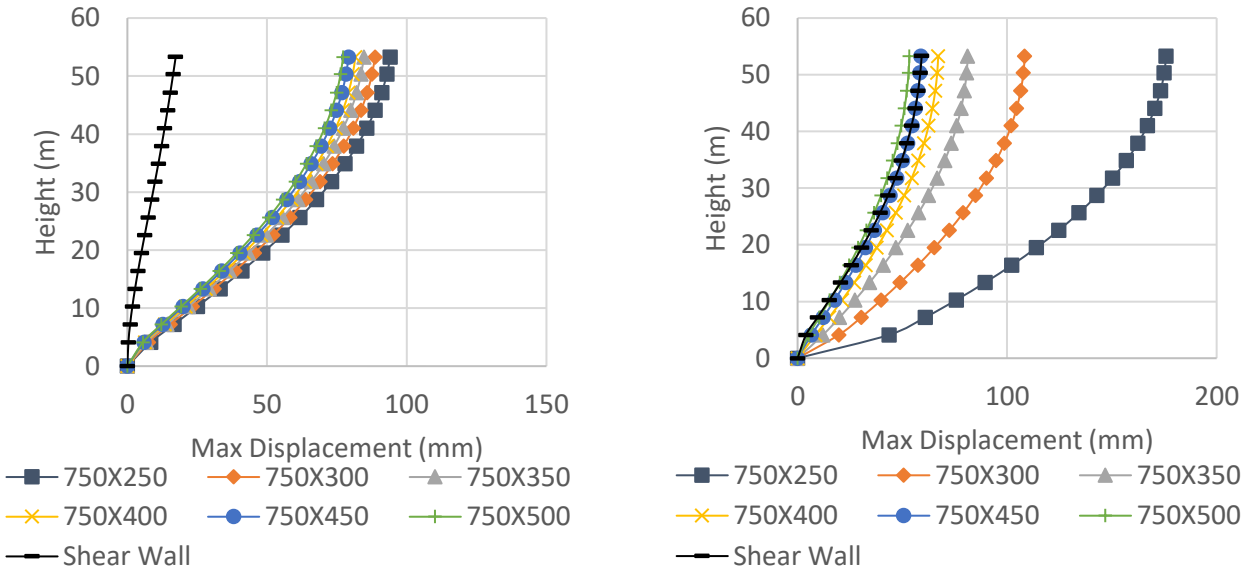

a) X-direction b) Y-direction

Figure 6.3: Influence of column size on the maximum displacement of RC framed buildings

It was evident that by increasing the column size, the maximum displacement was reduced; however, the trend was not the same in both directions. Due to the similarities in the columns' dimensions in the X direction, the range of displacements was lower than that of the Y direction. In both directions, the maximum displacement decreased with the increment of column size

from 750 × 250 mm to 750 × 500 mm. Furthermore, the shear walls showed quite stiff behaviour in the X direction with the least displacement, and in the Y direction, it had the second-least displacement. The difference between shear walls in the X and Y directions was due to their orientation in the building's design (Figure 6.3).

6.2.3 Column Shape

- **Maximum displacement**

Figure 6.4 provides a summary of the column's shapes effect using concrete grade C40/50 and 275 mm slab thickness on the building's lateral movements subjected to the wind load in the X and Y directions. The selected column section sizes were the most-used shapes for columns in the construction, and all of the three shapes had the same cross-sectional area.

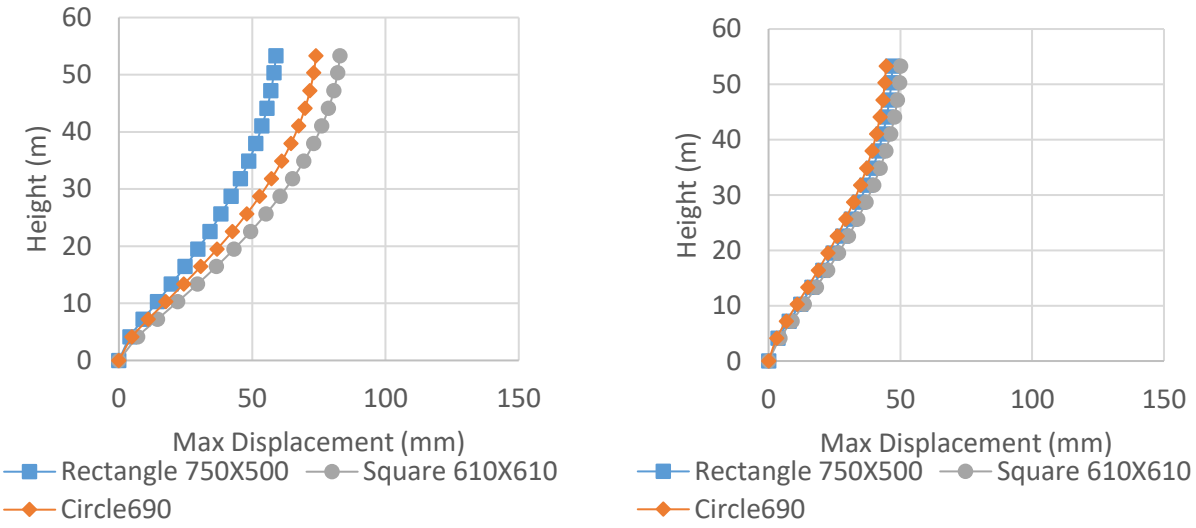

a) X-direction b) Y-direction

Figure 6.4: Influence of column shape on the maximum displacement of RC framed buildings

It was evident that, in both directions, the shape with the larger dimension resulted in stiffer behaviour and lowered lateral movements compared to the other shapes. In the X-direction, the rectangular shape had the lowest displacements, while the square cross-section had the highest one. On the other hand, the lateral displacements in the Y-direction were different, in which the circle had the lowest lateral movements and the square had the highest movements.

- **Punching shear**

There are several thresholds for punching shear ratio ($V_{Ed}/V_{Rd,c}$) in design guides, by defining limiting ratio for shear force over allowable shear without reinforcement, and two of them are utilised in this analysis. The UK National Annex suggests limiting the punching shear ratio to 2.5, while this value for Eurocodes is 2. The results for the influence of column shape on the punching shear in internal and corner columns are presented in Figure 6.5.

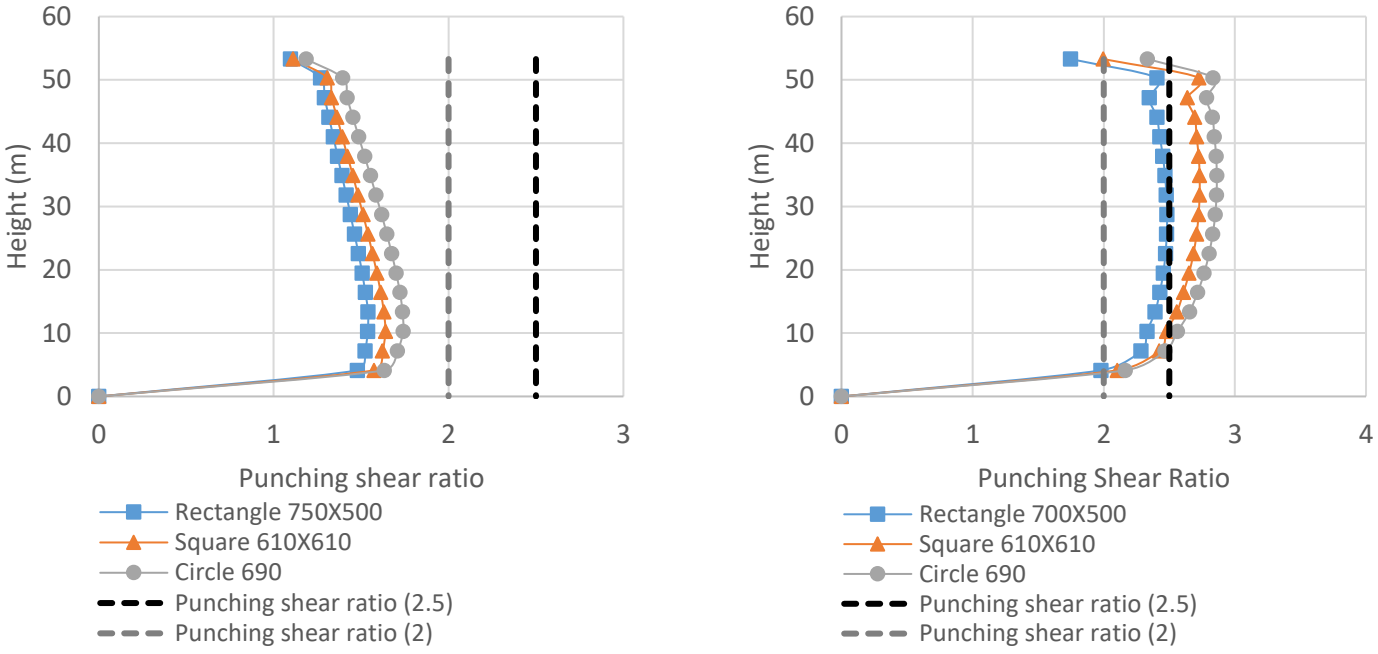

a) Internal column b) Corner column

Figure 6.5: Influence of column shape on the punching shear ratio of RC framed buildings

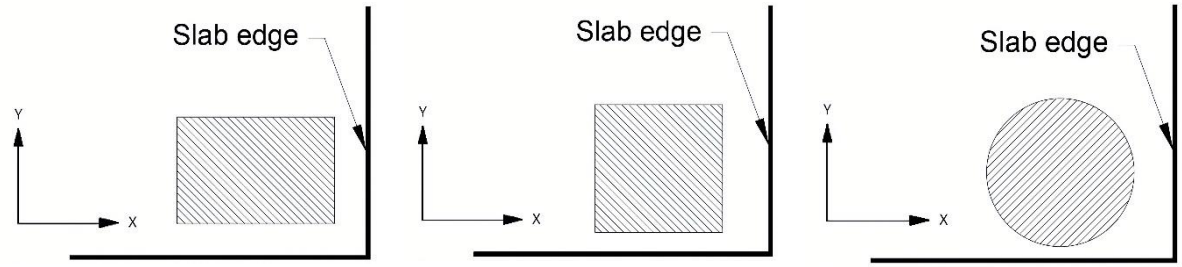

a) Rectangle column b) Square column c) Circle column

Figure 6.6: Corner columns with different shapes

As it was demonstrated in Figure 6.5, punching shear failure, as a significant issue in flat slabs, is more likely to happen in corner columns than edge or internal columns (Sacramento et al., 2012; Aalto and Neuman, 2017). Moreover, Figure 6.5a demonstrated in the internal columns

the punching shear ratios were within the safe range, both with 2 and 2.5 punching shear ratio limits, while, for the corner columns (Figure 6.5b), only the rectangular shape was lower than the threshold of 2.5 punching shear ratio, and none of them passed the 2 punching shear ratio. Besides, the shape of the columns' impact was more evident in the corner columns. Figure 6.6 shows where the control perimeter around the loaded area in the rectangular shape was more than the others, providing more space to distribute the applied loads.

It is possible to overcome the punching shear failure for corner columns with circular or square cross-sections by introducing Shear rails (Punching shear reinforcement), but this option was not considered here, as the implementation of the Shear rails leads to increase the overall construction cost (Max Frank, 2020).

6.2.4 Slab Thickness

- **Maximum displacement**

Figure 6.7 illustrates the results for the impact of flat slabs' thickness using 750 × 250 mm column size and C40/50 concrete grade on the building's lateral movements subjected to the wind actions in the X and Y directions.

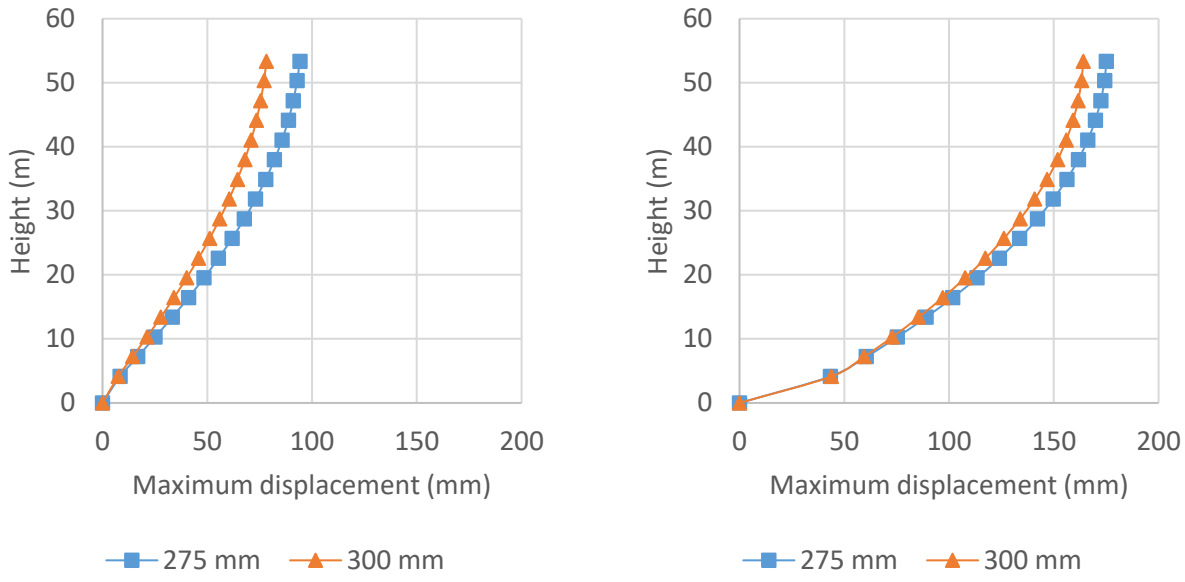

a) X-direction b) Y-direction

Figure 6.7: Influence of slab thickness on the maximum displacement of RC buildings5.5.

By increasing the slab's thickness by 25 mm, the building became stiffer, and the lateral displacements in the X and Y directions reduced accordingly. In both directions, the building with a 300 mm flat slab thickness resulted in lower lateral movements (14 mm displacement) compared to the building with a 275 mm flat slab thickness.

- **Punching Shear and slab thickness**

The results for the influence of increasing the slab thickness on punching shear are presented in Figure 6.8.

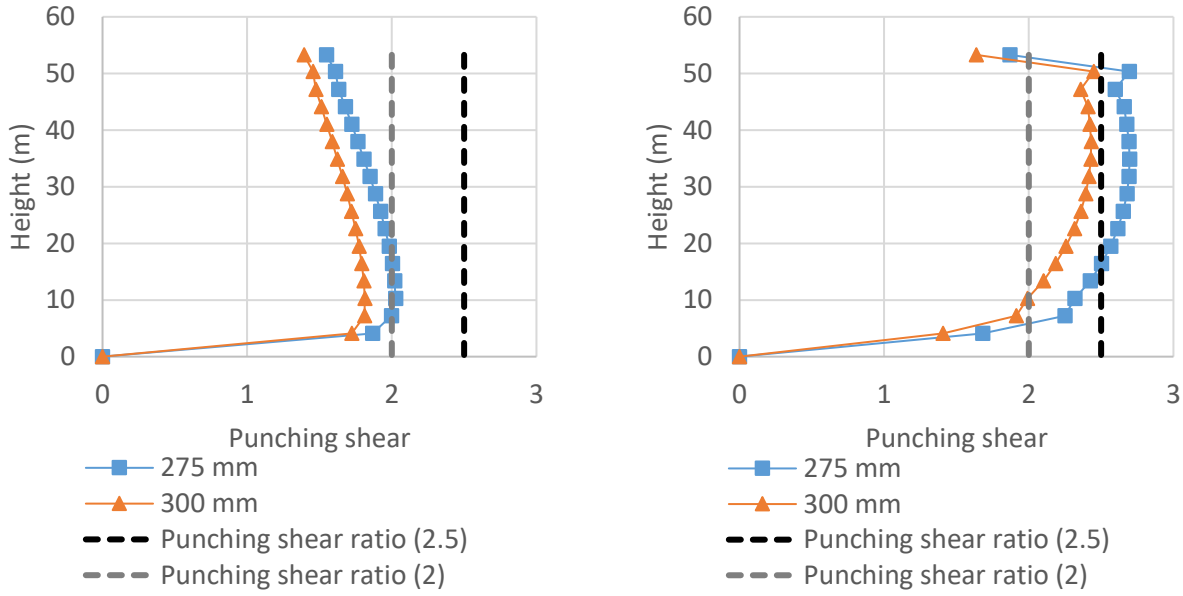

a) Internal column

b) Corner column

Figure 6.8: Influence of slab thickness on the punching shear ratio of RC framed buildings

As shown in Figure 6.8, the punching shear ratios in the internal columns were lower than the corner columns. Furthermore, increasing the slab thickness by 25 mm could lead to lower punching shear ratios within the safe range defined by the Eurocodes. However, compared to the internal columns, the corner columns failed to pass the 2 punching shear ratio limits, showing the vulnerability of flat slabs in punching shear failure.

6.2.5 Maximum Overall Height

In the previous section, the impacts of individual factors were assessed concerning the maximum overall height. In this section, the optimised concrete grade with different column sizes

(the details are shown in Table 6.1), slab thicknesses and punching shear ratios ($V_{Ed}/V_{Rd,c}$) was investigated to achieve the maximum overall height.

Table 6.1: Concrete strength grade variation for each column size

Concrete grade	**750 × 250**	**750 × 300**	**750 × 350**	**750 × 400**	**750 × 450**	**750 × 500**
C80/95	Storey 1-3	Storey 1-3	Storey 1-3	Storey 1-3	Storey 1-3	Storey 1-3
C70/85	Storey 4-6	Storey 4-6	Storey 4-6	Storey 4-6	Storey 4-6	Storey 4-6
C60/75	Storey 7-10	Storey 7-9	Storey 7-9	Storey 7-9	Storey 7-9	Storey 7-9
C55/67	-	Storey 10-11	Storey 10-11	Storey 10-12	Storey 10-12	Storey 10-13
C50/60	-	-	-	-	-	-
C45/55	-	-	-	-	-	-
C40/50	-	-	-	-	-	-

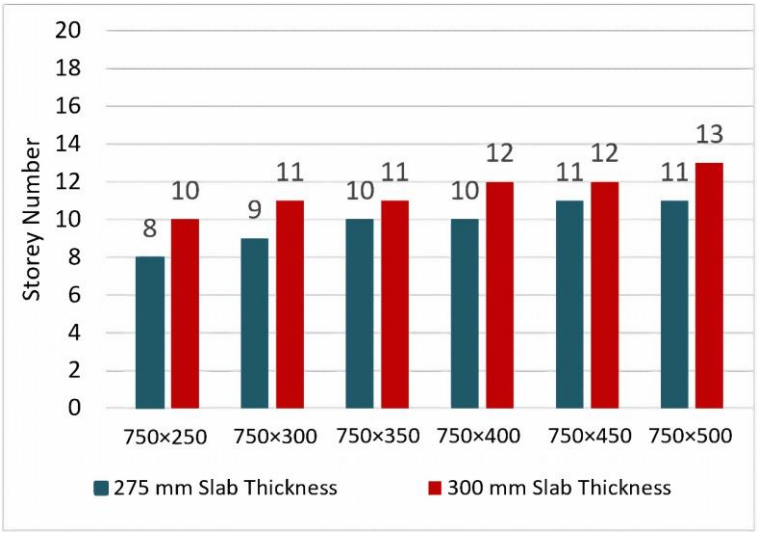

a) $V_{Ed}/V_{Rd,c}$ = 2

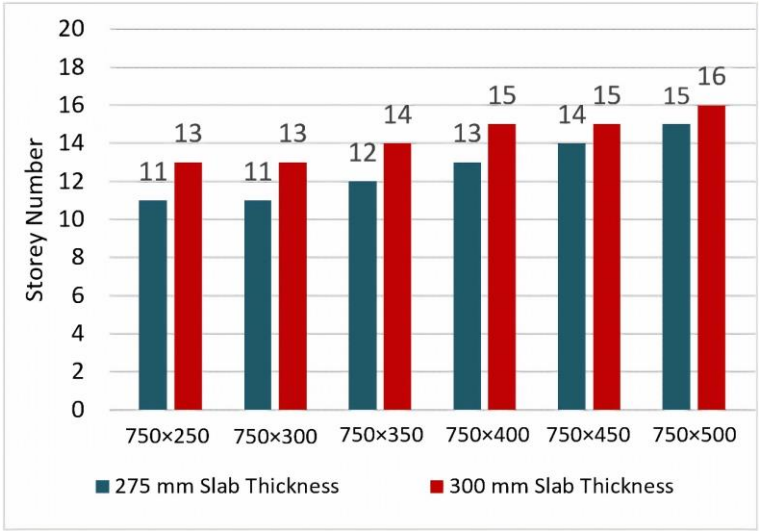

b) $V_{Ed}/V_{Rd,c}$ = 2.5

Figure 6.9: Maximum overall height with various sections

Figure 6.9 presents the results for the maximum overall height in an RC moment-resisting frame. The results demonstrated the maximum overall height for each column section; by increasing the slab thickness, the buildings could be built up to 2 more storeys. Furthermore, a comparison of the two graphs showed that increasing the punching shear ratio (between 2 and 2.5 punching shear ratios) directly increased the maximum overall height up to 3 storeys. Therefore, for the

investigated building with the optimised concrete grade (Table 6.1), 750 × 500 mm column section size and flat slab with a thickness of 300 mm could reach up to 16 storeys with 2.5 punching shear ratio, and up to 13 storeys with 2 punching shear ratio. These were the maximum overall heights for the proposed architectural plan.

- **Design check**

Interstorey drift

The comparison for the interstorey drift in the designed buildings with different column sizes and 300 mm slab thickness and 2 and 2.5 punching shear ratio limits are illustrated in Figures. 6.10 and 6.11.

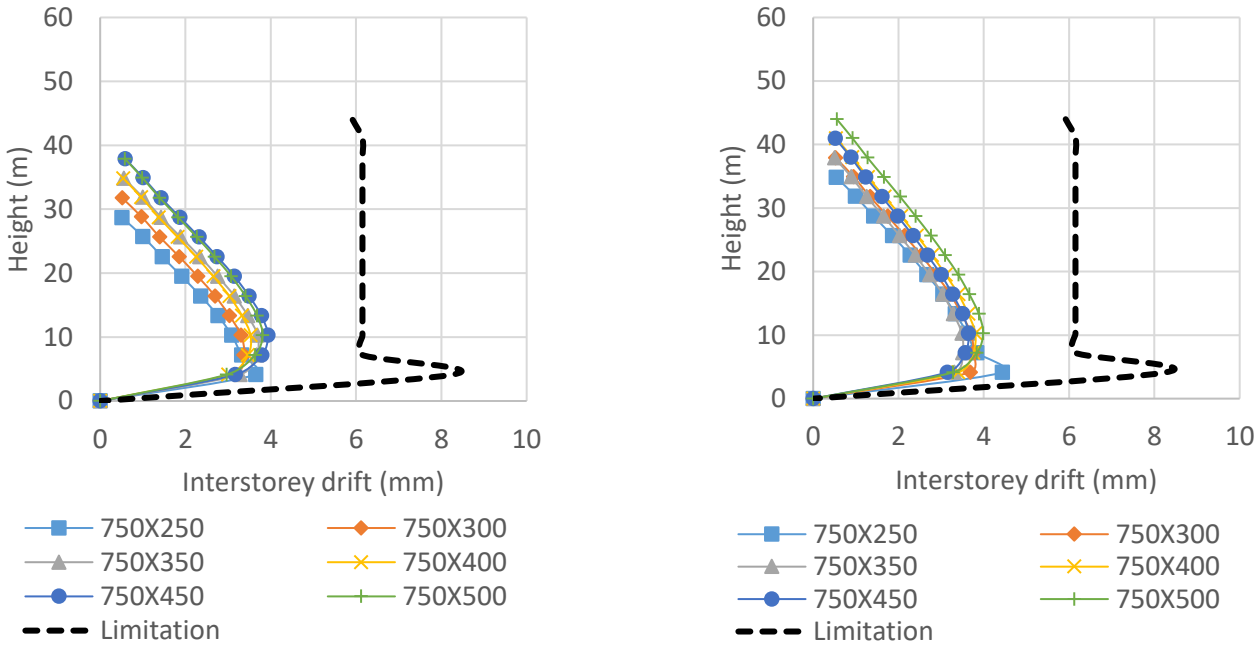

a) X-direction b) Y-direction

Figure 6.10: Influence of column size on the interstorey drift of RC framed buildings (punching shear ratio 2)

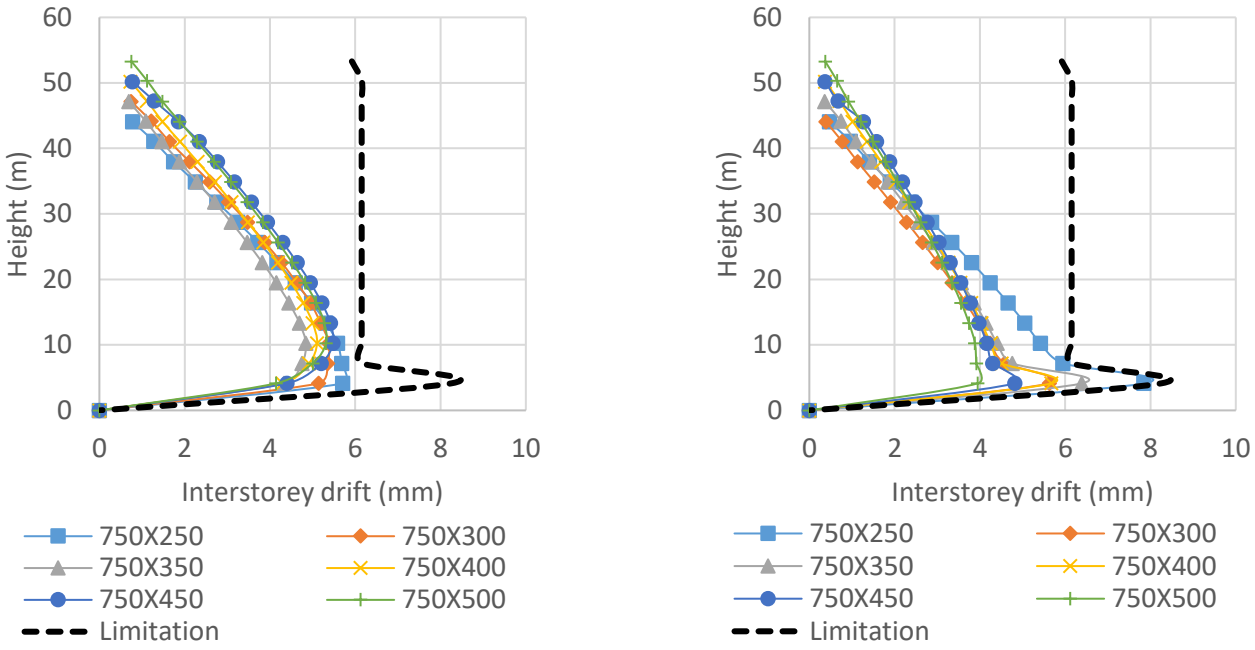

a) X-direction b) Y-direction

Figure 6.11: Influence of column size on the interstorey drift of RC framed buildings (punching shear ratio 2.5)

As presented in Figures 6.10 and 6.11, these designs were still within the safe range defined by Eurocode 2 Part 1-1 (BS EN 1992-1-1, 2014) in both X and Y directions. The fluctuation in interstorey drift's limit was due to the change in storey height between the first storey and other storeys (from 4.125 m to 3.075 m).

Punching shear ratio

The results for punching shear ratios in each case with 275 mm and 300 mm slab thickness are presented in Figs. 5.12 and 5.13.

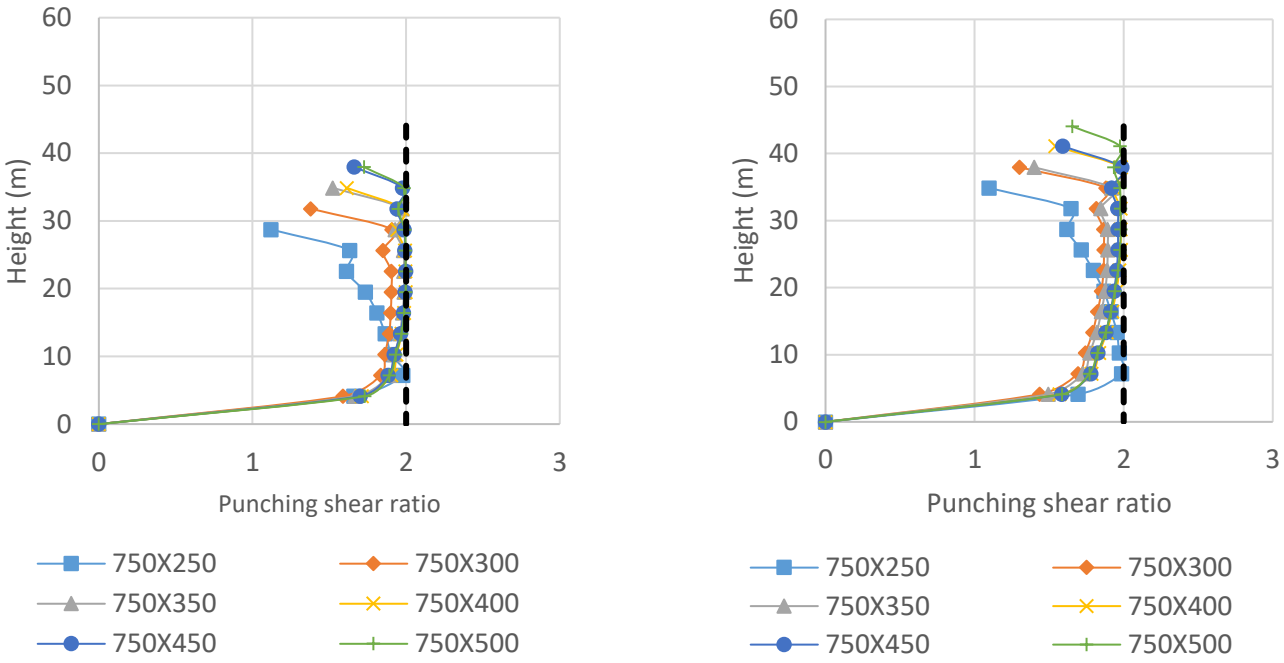

a) 275 mm slab thickness b) 300 mm slab thickness

Figure 6.12: Influence of column size on the punching shear ratio of RC framed buildings (punching shear ratio 2)

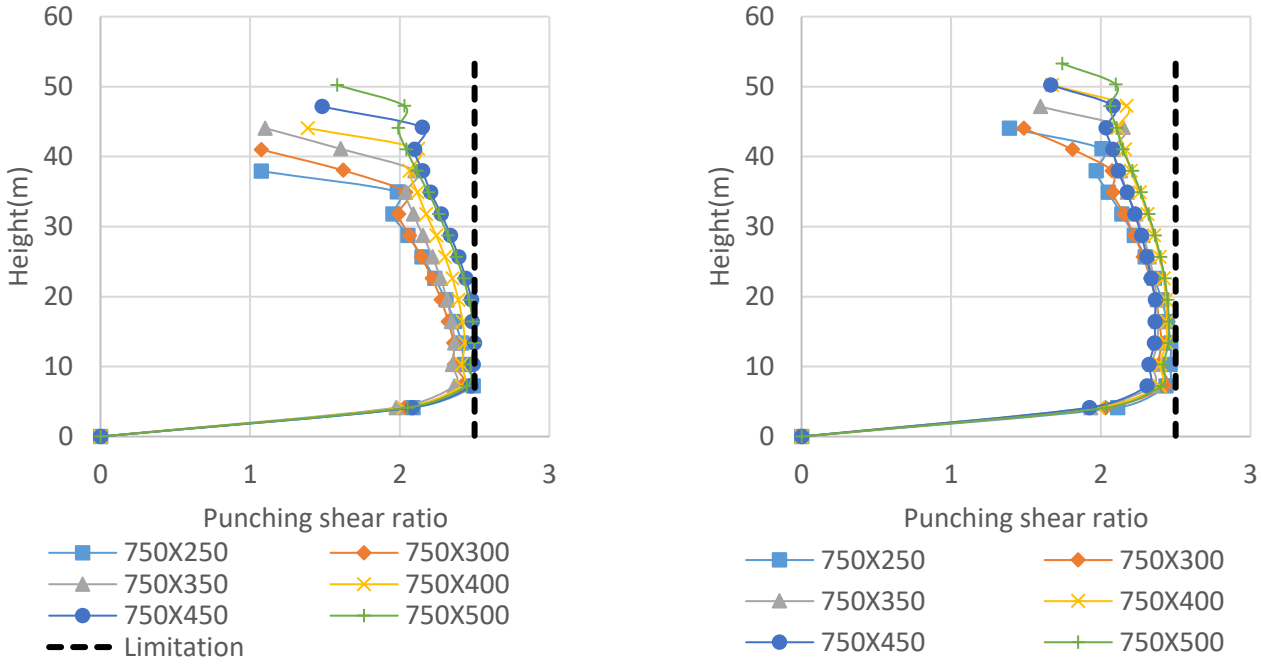

a) 275 mm slab thickness b) 300 mm slab thickness

Figure 6.13: Influence of column size on the punching shear ratio of RC framed buildings (punching shear ratio 2.5)

Changing the slab thickness can have an impact on the punching shear ratio. Punching shear ratios are given in Figures 6.12 and 6.13 for the buildings with slab thicknesses of 275 mm and 300 mm, and it can be observed that the punching shear ratios were within the safe range (2 and 2.5 punching shear ratio limits) for 13 (39 m)- and 16 (48 m) -storey buildings.

Acceleration

Since the maximum overall height for the building was achieved with 300 mm flat slab thickness, the results for the occupants' comfort measured in the top floors of each building are according to the following:

- *NBCC Part 4 limitations:*

The horizontal acceleration threshold for residential occupancy with a 10-year return period is 15 milli-g, which is shown in Figures 6.14 and 6.15. In this part, only the buildings with 300 mm flat slab thicknesses were chosen.

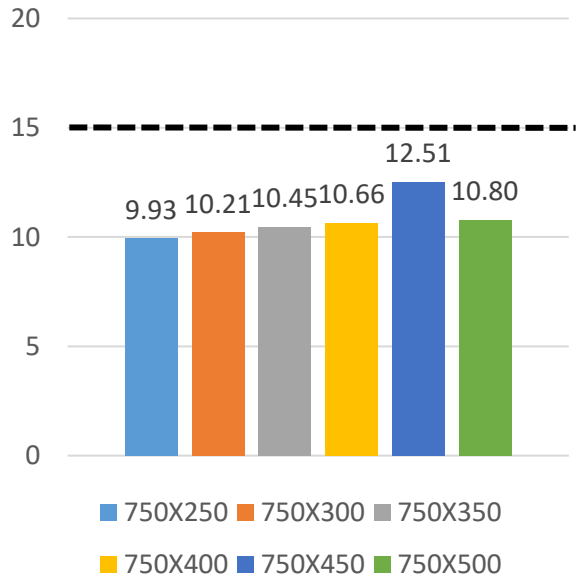

a) X-direction

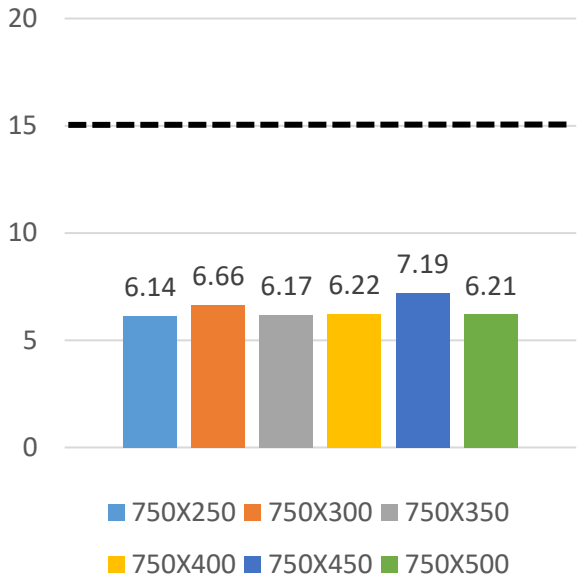

b) Y-direction

Figure 6.14: Influence of column size on horizontal acceleration (NBCC) of RC framed buildings (punching shear ratio 2)

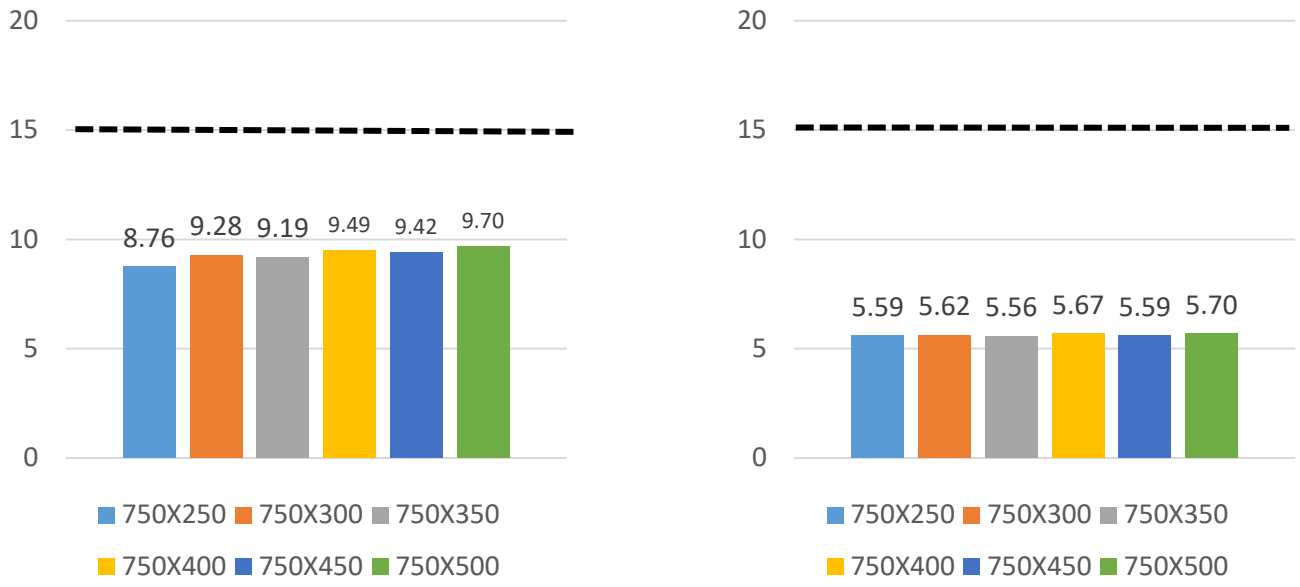

a) X-direction

b) Y-direction

Figure 6.15: Influence of column size on the horizontal acceleration (NBCC) of RC framed buildings (punching shear ratio 2.5)

In Figures 6.14 and 6.15, the horizontal accelerations in all buildings were within the acceptable limit, ranging from 9.93 to 12.51 milli-g in X-direction and 6.14 to 7.19 milli-g in Y-direction for 2 punching shear limit and 8.76 to 9.70 milli-g in X-direction and 5.56 to 5.70 milli-g in Y-direction for 2.5 punching shear limit. The difference between the accelerations in X and Y directions was due to the difference between the dimensions of columns in each direction being 750 mm in X-direction and ranging from 250 mm to 500 mm for Y-direction.

- *Melbourne Criteria:*

The horizontal acceleration threshold for residential occupancy with a 10-year return period of exceedance in Melbourne criteria is represented in Figures 6.16 and 6.17, and the results were based on the natural frequencies taken from the simulations and equations. In this part, only the buildings with 300 mm flat slab thicknesses were chosen.

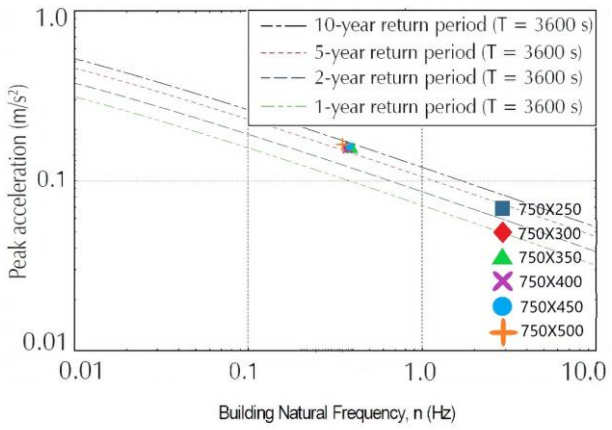

a) X-direction

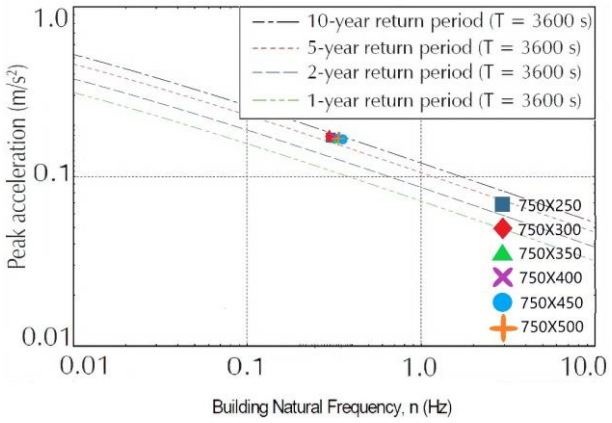

b) Y-direction

Figure 6.16: Influence of column size on horizontal acceleration (Melbourne) in RC buildings (punching shear ratio 2)

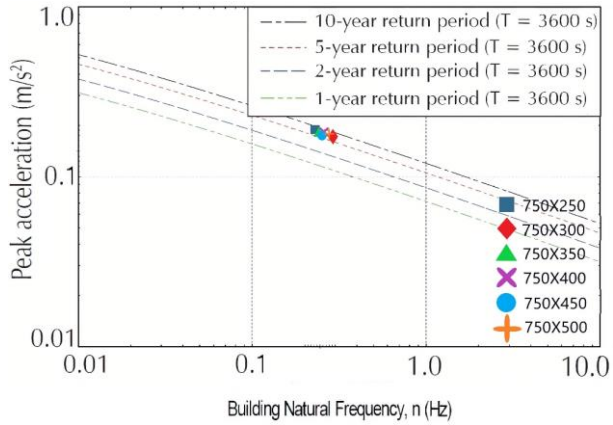

a) X-direction

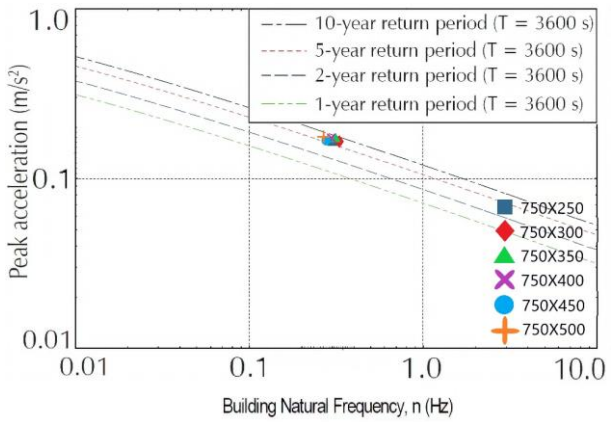

b) Y-direction

Figure 6.17: Influence of column size on horizontal acceleration (Melbourne) in RC buildings (punching shear ratio 2.5)

It can be observed that in both directions for 2 and 2.5 punching shear ratio limits, the buildings with a maximum overall height ranging from 13 to 16 storeys were acceptable for the residential occupancy with a 10-year return period in both criteria, and the residents' comfort was not compromised.

6.3 Summary

In this part of the research, the feasibility of the maximum overall height for an existing UK residential building, which is designed and constructed with shear walls, is investigated without shear walls when the building is subjected to wind-induced forces. To achieve the maximum overall height, contributory factors including concrete grade, column size, column shape and slab thickness are taken into account, and their impact on the building's structural performance is assessed according to Eurocode 2 Part 1-1 (BS EN 1992-1-1, 2014), using ETABS software. Based on the acquired results of this research, the following summary can be drawn:

- Increasing the concrete grade results in stiffer behaviour in a building and reduces the lateral displacements.
- Optimising the concrete grade in the building is a more practical approach and can result in acceptable structural behaviour.
- It was evident that there is a direct relationship between a column section size and the lateral displacements, in which the increase of column size reduces the lateral displacements.
- Different column shapes can change the buildings' lateral movements and influence the punching shear ratio, in which the rectangular shape achieved the lowest ratio.
- The change in flat slab thickness can directly affect the lateral stiffness of a building, which means by increasing the thickness, the lateral displacements, and the punching shear ratio reduces.
- Increasing the slab thickness can add up to 2 more storeys to the maximum overall height in the reinforced concrete frame building.
- In this analysis, the governing limitation was punching shear ratio, and if the simulations were based on $V_{Ed}/V_{Rd,c} = 2$, the maximum overall height would have been reduced to 13 storeys to comply with Eurocodes limits.

- The reference building was designed and constructed as a five-storey RC frame building with shear walls, and the achievements of this analysis demonstrated a practical potential to increase buildings' height only by removing the shear walls and optimising the key factors.
- This analysis demonstrated that depending on the architectural plan and the influencing factors, it is feasible to achieve the buildings' full potential in structural performance.

7 Enhance the Practical Design of Reinforced Concrete Moment-Resisting Frames

7.1 Introduction

In the UK, shear walls have been extensively used as vertical resisting elements to withstand the wind forces in almost every reinforced concrete frame building above three storeys. Recently the construction industry has questioned the need for shear walls in low-to-medium-rise RC frame buildings and the possibility of replacing them with moment-resisting frames. The main benefits of moment-resisting frames are reduced cost and increased environmental sustainability due to the reduction in the consumed volume of concrete during the construction process.

This chapter covers the different parts in the analysis and design of reinforced concrete moment-resisting frames with flat slabs compared to the normal design in the Eurocodes. This includes residential and office buildings up to 13 storeys high (44 m) and the height limitation, which is based on chapters 4 and 5.

This chapter covers the following questions:

- Is there any economic benefit in removing shear walls?
- Can shear walls be removed from UK reinforced concrete frame structures?
- What should be considered after removing the shear walls?
- How can we improve a building's ability to resist lateral load?

7.2 Limit States Criteria

Limit state design aims to provide adequate serviceability and safety at service and ultimate loads, as shown in Equation 7.1 (from EN 1990 expression 6.8):

$$E_d \leq R_d \qquad \text{(Eq. 7.1)}$$

In which E_d and R_d are the applied actions and the resistance of the member, respectively.

The design of RC moment-resisting frames requires verification that the following serviceability and ultimate limit state thresholds are not exceeded (Table 7.1):

Table 7.1: Limit state criteria

Serviceability Limit State (SLS)	**Ultimate Limit State (ULS)**
Horizontal displacement	Punching shear
Interstorey drift	Bending moment capacity of connections
Horizontal acceleration	Column slenderness
Flat slab deflection	

7.3 Application

Generally, RC moment-resisting frames provide flexibility to architectural designs and have less stiffness as opposed to RC frames with shear walls. Due to this behaviour, the application of adopting moment-resisting frames is limited to low-medium rise reinforced concrete frame buildings performing with moderate, horizontal displacements, shear forces and second-order (P-Δ) effects.

7.4 Design Procedure

Since RC moment-resisting frames have similar design procedure for loads, analysis, design of slabs, columns, walls and foundations to normal design, they are covered in The Concrete Centre How to publications (Figure 7.1). Here, only the differences are discussed:

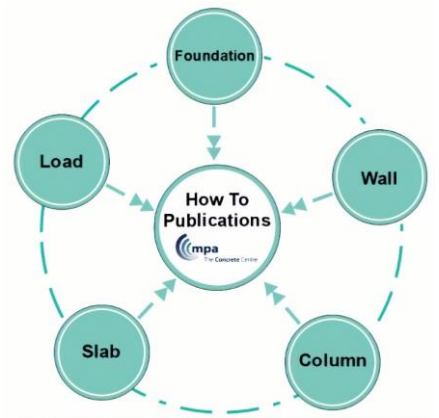

Figure 7.1: How to publications

7.4.1 Wind Load

Wind loading can be calculated according to EN1991-1-4 and depends on several factors, including the site location, building geometry and fundamental wind velocity. Here, the focus will be only on the structural factor and dynamic factor due to their impact on moment-resisting frames.

7.4.2 Structural Factor

The structural factor is essential in the calculation of wind load design to identify the behaviour of buildings subjected to wind actions, and it consists of two parts: a size factor (C_s) and a dynamic factor (C_d).

The size factor (C_s) can be calculated using Equation 7.2 from BS EN 1991-1-4:2010:

$$C_s = \frac{1+7\times I_v(Z_s)\times\sqrt{B^2}}{1+7\times I_v(Z_s)} \qquad \text{(Eq. 7.2)}$$

where:

I_v: Turbulence intensity

Z_s: Reference height

B^2: Background factor

Dynamic factor (C_d) represents a comparison between the maximum displacements due to the dynamic response of buildings with the static movement generated by a fixed force with the identical peak magnitude of the actual force.

In order to calculate the dynamic factor for RC frame buildings, the value for logarithmic decrement of structural damping (δ_s) could be taken as 0.1 according to BS EN 1991-1-4: Table F.2. Then, the dynamic factor could be calculated in Figure NA.9 in NA to BS EN 1991-1-4:2010.

Note: For RC frame buildings with shear walls around the stairs/lifts and under 20 m height, the dynamic factor could be taken as 1. Otherwise, for moment-resisting frames and buildings with larger heights, this value has to be calculated according to BS EN 1991-1-4, which is likely to be more than 1. This could lead to an increment in the applied lateral loads.

7.4.3 Connections

The design of RC moment resisting-frames with flat slabs depends on the moment capacity of the flat slab-column connections for stability and requires attention to the design and detailing. The connection between a flat slab and column is generally considered to be unsuitable to withstand large bending moments, especially at edge columns. However, in practice, many moment-resisting frames have performed efficiently in service. In Figure 7.2, the detailing of two flat slab-column connections is provided by Cresswell Riol (2007) and Calavera (2012).

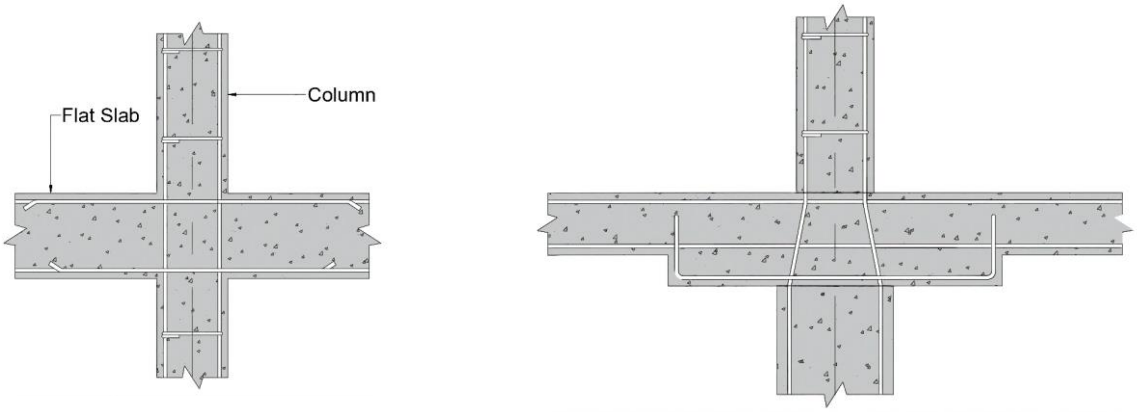

a) Flat slab-column b) Flat slab-column with drop panel

Figure 7.2: Connections detail

Moreover, edge and corner columns are more critical at their connections.

For edge columns, flexural and torsional cracks of the flat slab reduce the transfer bending moment capacity. In this case, before reaching the working load, initial cracks appear close to the face of the columns while plastic rotation forms with the increment of load. This behaviour is illustrated in Figure 7.3, where M_t and M_f are the torsions at the side of the column and the moments at the face of the column, and C_x and C_y are the column's dimension.

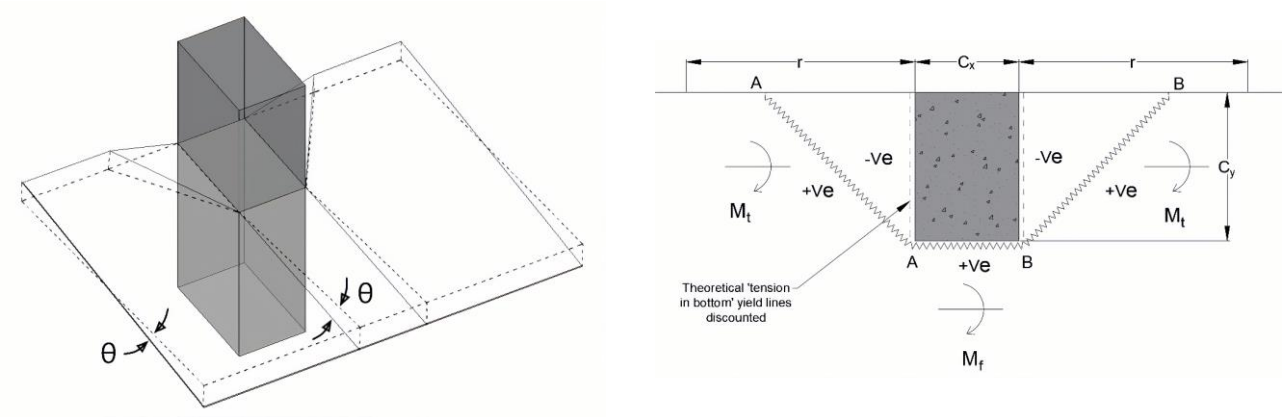

Figure 7.3: The yield-line mechanism at the edge column (Whittle, 1994)

7.4.4 Boundary Conditions

The boundary conditions are sets of additional constraints applied to structural elements (such as supports in frames and the connection between elements) in order to impose a particular type of behaviour on that element and, depending on the design assumptions, can vary from one structure to another. In RC moment-resisting frames, the connections between columns and slabs are considered to be fixed to transfer the moments. Otherwise, with pinned connections between flat slabs and columns, a mechanism could occur, and the whole building would fail.

7.5 Is There any Economical Benefit in Removing Shear Walls?

In chapter 4, the feasibility of removing shear walls in a typical UK five-storey RC frame residential building (19.5 m) located in Home Counties (Figure 7.4) was investigated to look at programme savings and reduction in the reinforced concrete package. The reference building was designed and constructed with shear walls (Figure 7.4).

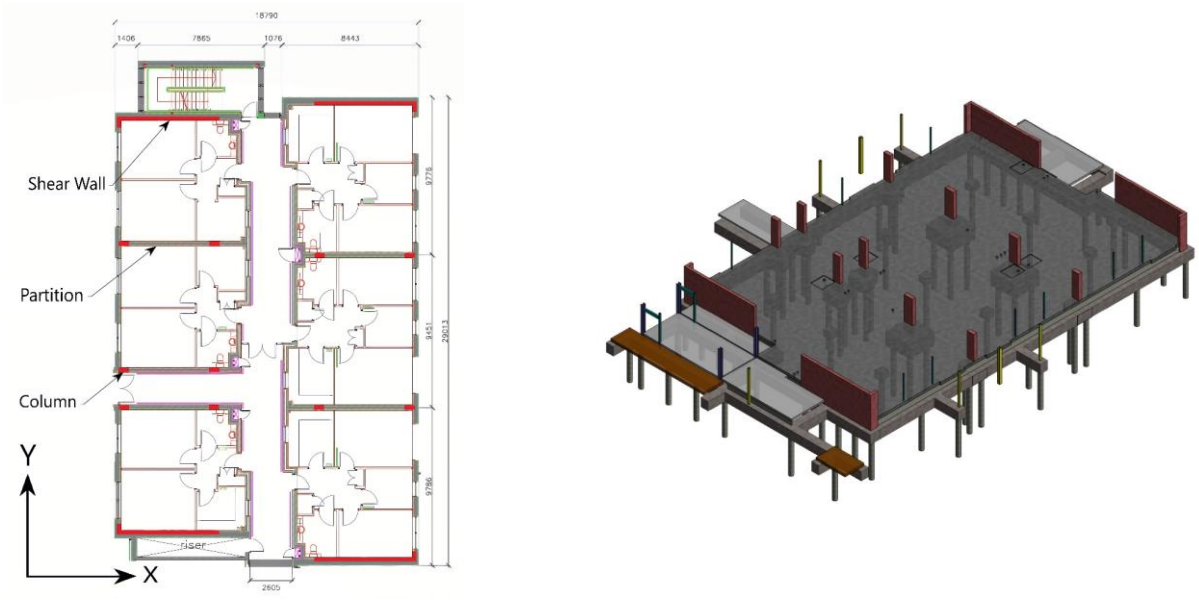

a) Architectural plan (values in mm) b) Column and shear walls layout

Figure 7.4: Reference design

This building was designed with 750 × 250 mm column sections (concrete grade C40), 275 mm flat slabs (concrete grade C30) and 200 mm shear walls (concrete grade C30). During the analysis, each shear wall was replaced with two similar column sections (750 ×250 mm) at both ends (Figure 7.5).

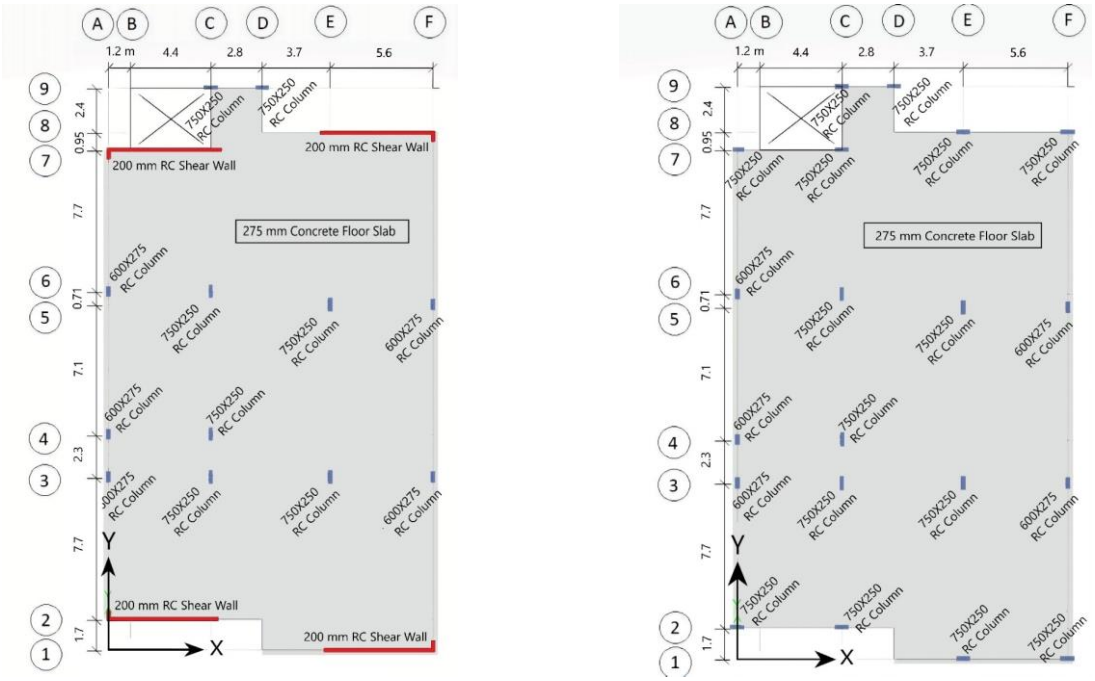

a) Building with shear walls b) Building without shear walls

Figure 7.5: Column and shear walls layout

7.5.1 Cost

Table 7.2 and 7.3 present the results to compare the construction cost in the residential RC frame buildings with and without shear walls (case 1 and 2):

Table 7.2: Total superstructure

Component	**With shear walls (Case 1) £K**	**Without shear walls (case 2) £K**
Slabs	69.1	69.1
Shear Walls	25.2	0
Columns	14.1	17.3
Formwork (Vertical)	23.4	20.2
Formwork (Horizontal - plain)	88.2	88.2
Total "superstructure."	**220**	**194.8**

Table 7.3: Total construction

Component	**With shear walls (Case 1) £K**	**Without shear walls (Case 2) £K**
Superstructure	220	194.8
Stairs as %age of superstructure cost	30.8	35.2
Gypsum plasterboard fire panel (30 min)	0	0.45
Foundations	95.7	95.7
Ground floor slab	15.2	15.2
Cladding	599.2	599.2
Structure & cladding total	**960.9**	**940.5**
Prelims & external works	293.1	293.1
Finishes & walls	615.5	615.5
Mechanical & Electrical	1025.9	1025.9
Total construction	**2895.4**	**2875**

According to Table 7.2, removing shear walls in this structure saves about 11% (approx £25k) on the superstructure's cost. Savings on shear walls and formwork are offset to a degree by the cost of additional columns. Considering the total construction costs in Table 7.3, the savings in shear walls are also offset by additional works to the stair enclosures. Nonetheless, the overall cost is some 0.67% (£20k in £2.89m) lower than for a building with shear walls.

Besides, in this case study, 165 m^3 of concrete was saved by removing the shear walls during the construction process.

7.5.2 Time

In terms of the construction time, it has been suggested that cutting out shear walls might cut out a day in a 14-day cycle, and this amount of time could be saved in the construction process. The saved time can also indirectly reduce the construction cost by reducing contract preliminaries and financial charges.

7.6 Can Shear Walls Be Removed From the UK Concrete Frame Structures?

Based on the results from finite element simulations in chapter 4, a comparative analysis was conducted between case 1 (buildings with shear walls) and case 2 (building without shear walls) to assess the impact of removing the shear walls on lateral movements of the buildings considering the bending moment capacity of connections and punching shear. Figures 7.6a and b demonstrate maximum displacements and interstorey drifts in case 1 and case 2 in the X and Y directions.

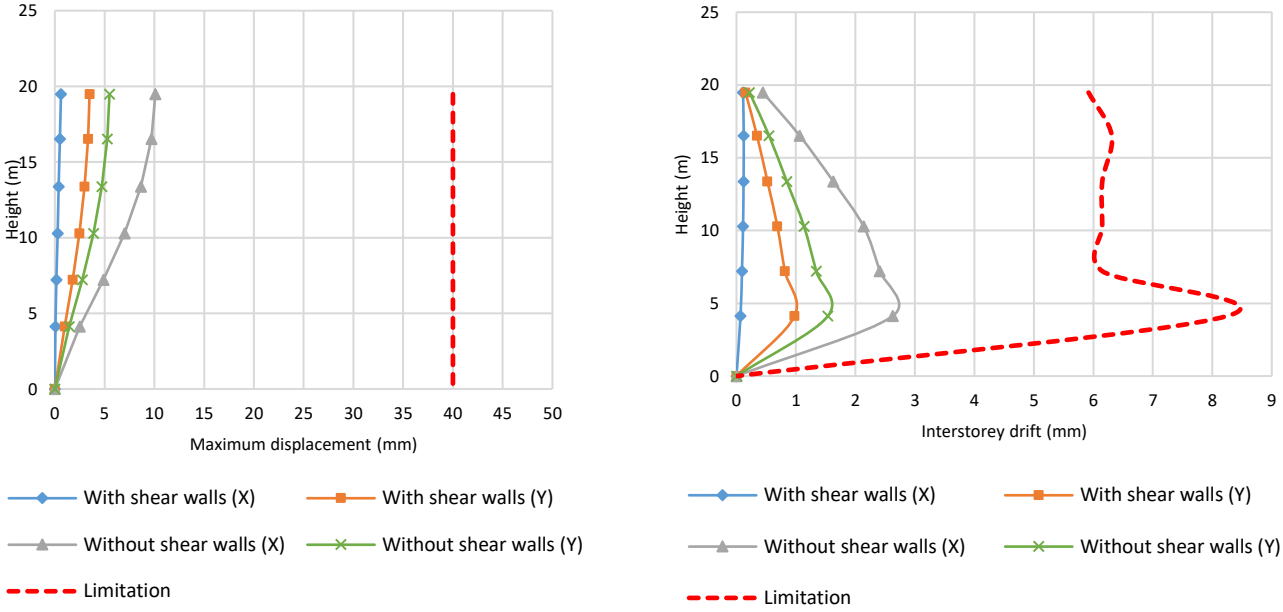

a) Maximum displacement in Case 1 and 2 b) Interstorey drifts in case 1 and 2

Figure 7.6: Structural analysis results

As shown in Figures 7.6a and b, the displacement and interstorey values in the building without shear walls are higher than the building with shear walls demonstrating the influence of shear walls as the lateral resisting elements to withstand the horizontal displacements. Nevertheless, both buildings were within the safe range in the design of building structures to Eurocode 2 and the basis of structural design (2010). The analysis showed that the shear walls could be removed from the typical UK RC frame building without compromising the safety of it.

7.7 What Should Be Considered After Removing the Shear Walls?

In the design of RC moment-resisting frames, several criteria should be checked to make sure the building provides adequate serviceability and strength.

7.7.1 Horizontal Movement

- **Displacement**

Limiting horizontal displacement under lateral load is essential for structural stability, potential damage to non-structural elements, architectural integrity and occupant comfort. For the lateral

distributed loads in Figure 7.7, the horizontal displacement (Δ) in first-order analysis can be calculated in Equation 7.3 to 7.8 (Tuken, 2009; Hwang and Moehle, 2000; BS EN 1998-1):

Uniform lateral load:

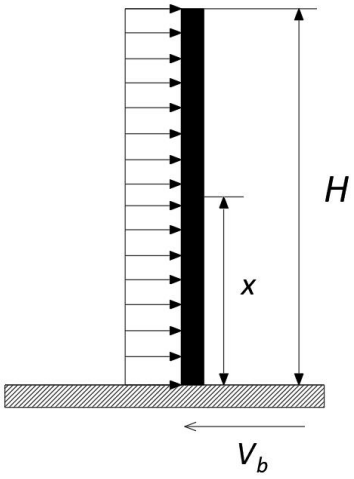

Figure 7.7: Uniform lateral load

$$\Delta = \frac{V_b}{K}\left[x - \frac{x^2}{2h}\right] \quad \text{(Eq. 7.3)}$$

$$K = \frac{12EI_c}{h^2} \times \frac{1}{1 + \frac{2I_c/h}{I_{s1}/L_1 + I_{s2}/L_2}} \quad \text{(Eq. 7.4)}$$

$$I_{s1} = \frac{B_{eff}h^3}{12} \quad \text{(Eq. 7.5)}$$

$$B_{eff} = \alpha\beta_{cr}B \quad \text{(Eq.7.6)}$$

$$\alpha = 2c_1 + \frac{1}{3}l_1 \quad \text{(Eq. 7.7)}$$

$$\beta_{cr} = 0.5\, I_g \quad \text{(Eq. 7.8)}$$

where:

V_b: Base shear

H: Storey height

K: Lateral stiffness

x: Height at level x

Δ: Horizontal displacement

E: Modulus of elasticity of concrete

I_c: Moment of inertia of column

$I_{s1} = I_{s2}$: Moment of inertia of slab

I_g: Gross moment of inertia

$l_1 = l_2$: Slab length

c_1: Column's dimension in the direction of the applied lateral load

B: Slab width

B_{eff}: Effective beam width

h: Slab thickness

α: Effective width factor

β_{cr}: Cracked stiffness factor

The fundamental period for an RC moment-resisting frame under wind actions can be approximately calculated using Equation 7.9 (Jacobs, 2008) and Figure 7.8:

$$T = C_t h_n^x \quad \text{(Eq. 7.9)}$$

In which h_n is the overall height of the building (in meters), and the coefficients x and C_t are 0.9 and 0.023 for RC moment-resisting frames, respectively.

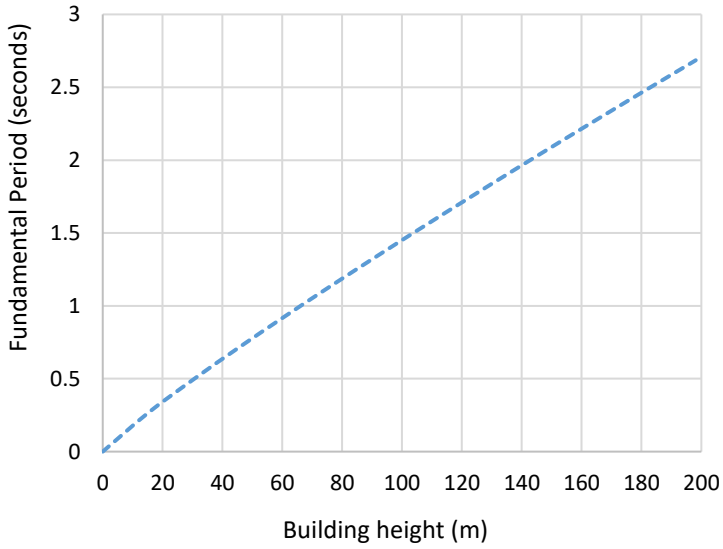

Figure 7.8: Approximate Fundamental Period vs height in RC moment-resisting frames

(Jacobs, 2008)

- **Interstorey Drift**

The interstorey drift can be calculated using Equation 7.10:

$$\delta = \frac{(\Delta_2 - \Delta_1)}{H} \quad \text{(Eq. 7.10)}$$

where

Δ_1: Displacement of the bottom of a storey

Δ_2: Displacement of the top of a storey

H: Storey height

- **Second-Order (P-Δ) Effect**

The lateral displacements due to the P-Δ effect can be calculated from Equation 7.11 (Naeim, 2001) using the iterative P-delta method. In this method, the first-order analysis is corrected by iteratively applying the P-Δ shears to the applied storey shear until the convergence is achieved when $\sum V_i \approx \sum V_{i-1}$ or $\Delta_i \approx \Delta_{i-1}$.

Note: For buildings with reasonable stiffness, the convergence is usually achieved within the first two cycles of iteration.

$$\sum V_i = \sum V_1 + \frac{(\sum P)_{\delta_{i-1}}}{h} \quad \text{(Eq. 7.11)}$$

where:

$\sum V_i$: Modified storey shear at the ith cycle

$\sum V_1$: First-order storey shear

$\sum P$: Sum of all Vertical loads acting on the floor

δ_{i-1}: Interstorey drift from the first-order analysis

h: Storey height

- In SLS, the serviceability cracks, connections between blocks or stud partition walls and slabs should be checked with the limitations defined by the Eurocodes. This criterion is particularly essential for moment-resisting frames due to their sway movements. According to the Manual for the design of building structures to Eurocode 1 Part 1-1 (BS

EN 1991-1-1, 2009) and basis of structural design (2010), the serviceability requirements to limit horizontal displacement and interstorey drift generated by wind are presented in Table 7.4.

Table 7.4: Indicative limiting values of horizontal deflections due to variable actions (Manual for the design of building structures to Eurocode 1 Part 1-1 (BS EN 1991-1-1, 2009) and basis of structural design, 2010)

Serviceability Requirement	**Serviceability Limit States Horizontal deflections**		
	Irreversible effects of Actions	**Reversible effects of Action**	
	Characteristic Combination (Expression 6.14b in EC0)	**Frequent Combination (Expression 6.15b in EC0)**	**Quasi-permanent Combination (Expression 6.16b in EC0)**
Function and damage to structural and non-structural elements • Single storey buildings Top of column • Each storey in a multi-storey building • The structure as a whole for a multi-storey building	$u \leq H/300$ $u_i \leq H_i/500$ to $H_i/300$ $u \leq H/500$	-	-
For crane gantry girders – horizontal deflections due to crane surge[a]	-	$\leq L/500$	-
Appearance	-	-	$u_i \leq H_i/250$
Note H Building's height H_i Storey height a Advice should be sought from the crane manufacturer			

In order to reduce the lateral movement of RC moment-resisting buildings, the following are suggested:

1. Use higher strength concrete
2. Increase the column cross-section size
3. Increase the stiffness of connections at the connections
4. Change column orientation (for rectangular columns)
5. Increase slab thickness

7.7.2 Flat Slab Deflection

In flat slabs, the deflection is usually maximum in the centre of the panel; therefore, it requires to be checked to prevent excessive deformations.

The following recommendations are provided to improve the flat slabs' deflection (Figure 7.15):

1. Increase the flat slab thickness
2. Reduce span to depth (l/d) ratio
3. Use compression reinforcement
4. Increase the number of columns
5. Use pre or post-tension slabs
6. Revise the deflection threshold for conservative limitations.
7. Use hidden beam

7.7.3 Horizontal Acceleration

There are no defined limitations in the Eurocodes or British standards for horizontal accelerations generated by wind actions. The alternative is to rely on Melbourne's criteria (Melbourne and Palmer, 1992), which is now the most commonly used criteria in the UK. This approach originates from Irwin's comfort criteria (Irwin, 1984), in which a survey of people in two buildings in the USA was conducted to establish 2% and 12% objection level criteria. Equation

7.12 taken from Melbourne and Palmer (1992) to calculate the peak horizontal acceleration for residential and office occupancy.

$$a = \sqrt{2 \ln n\, t}\ (0.68 + \ln R/5) \exp(-3.65 - 0.41 \ln n) \qquad \text{(Eq. 7.12)}$$

where

a: Acceleration [m/s^2]

n: Natural frequency [Hz]

t: Time duration of load [Sec]

R: Return period [Year]

The natural frequency n_1 for RC frame buildings taller than 50 m height could be estimated using Equation 7.13 taken from BS EN 1991-1-4:2010:

$$n_1 = \frac{46}{h}\ [Hz] \qquad \text{(Eq. 7.13)}$$

where h is the overall height of the building.

For buildings below 50 m height, Equation 7.9 could be used through $n_1(f) = \frac{1}{T}$.

The time duration (t) can be determined based on the nature of the event. In countries such as the United States, time is assumed to be 600 seconds due to the dominant storm activities. On the other hand, in the UK, since the storms happen in a more extended period, t is assumed to be 3600 seconds (Breeze, 2011). This relates to the load appropriate to the natural frequency and calculation of horizontal accelerations of buildings.

Moreover, the nominal return period, according to BS EN 1990, is 50 years equivalent to 0.02, the annual probability of exceedance. However, this value could be changed depending on the design assumptions. For exposure periods different from 50 years, Equations 7.14 and 7.15 could be used.

$$c_{prob} = 0.75\sqrt{1 - 0.2 \ln[-\ln(1-p)]} \qquad \text{(Eq. 7.14)}$$

$$p = \frac{1}{R} \qquad \text{(Eq. 7.15)}$$

In which:

c_{prob}: Probability factor

p: Annual probability of exceedance

R: Return period

In order to check the criteria for horizontal acceleration, the following threshold is provided:

The peak threshold level of acceleration relates to an objection level of 2% of the people present in the building. The horizontal peak acceleration criteria curves shown in Figure 7.9 were obtained using Equation 7.12.

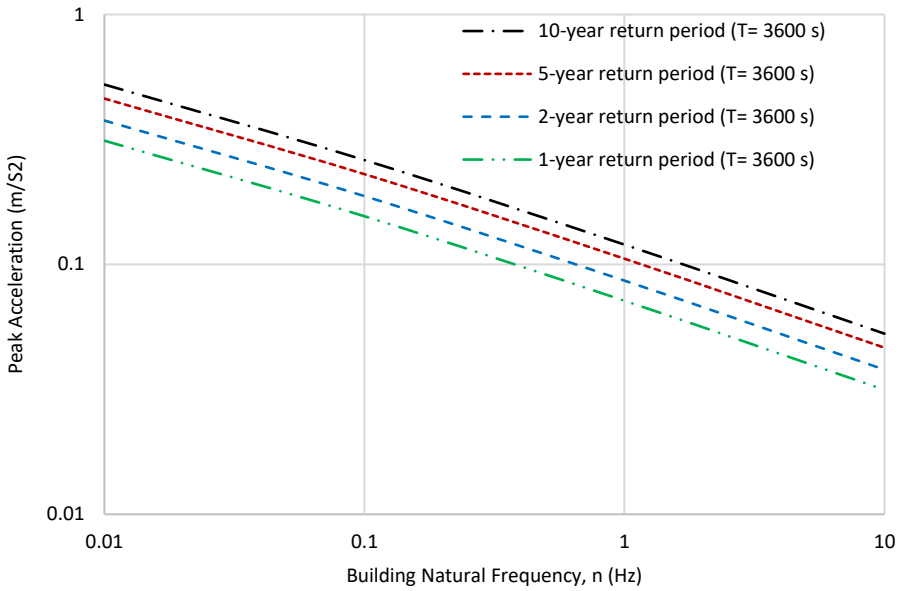

Figure 7.9: Limits for horizontal peak acceleration based on Melbourne and Palmer (1992)

The followings can improve the structural performance of buildings in horizontal accelerations (Figure 7.15):

1. Increase the column cross-section size
2. Increase the stiffness of connections at the connections
3. Increase slab thickness
4. Use passive, active and semi-active vibration control methods

7.7.4 Bending Moment Capacity of Connections

Due to the concentration of bending moments and shear stresses at the perimeter of columns and the weakness of flat slabs to transfer such loads without failure, it is essential to limit the transferrable loads at the column-slab connections, particularly at the edge and corner columns. In order to check the criteria for the bending moment capacity, the following guideline is given: According to BS EN 1992-1-1, perpendicular reinforcement to a free edge should be placed within the effective width of columns (b_e) to transmit bending moments from slabs to corner or edge columns (shown in Figure 7.10).

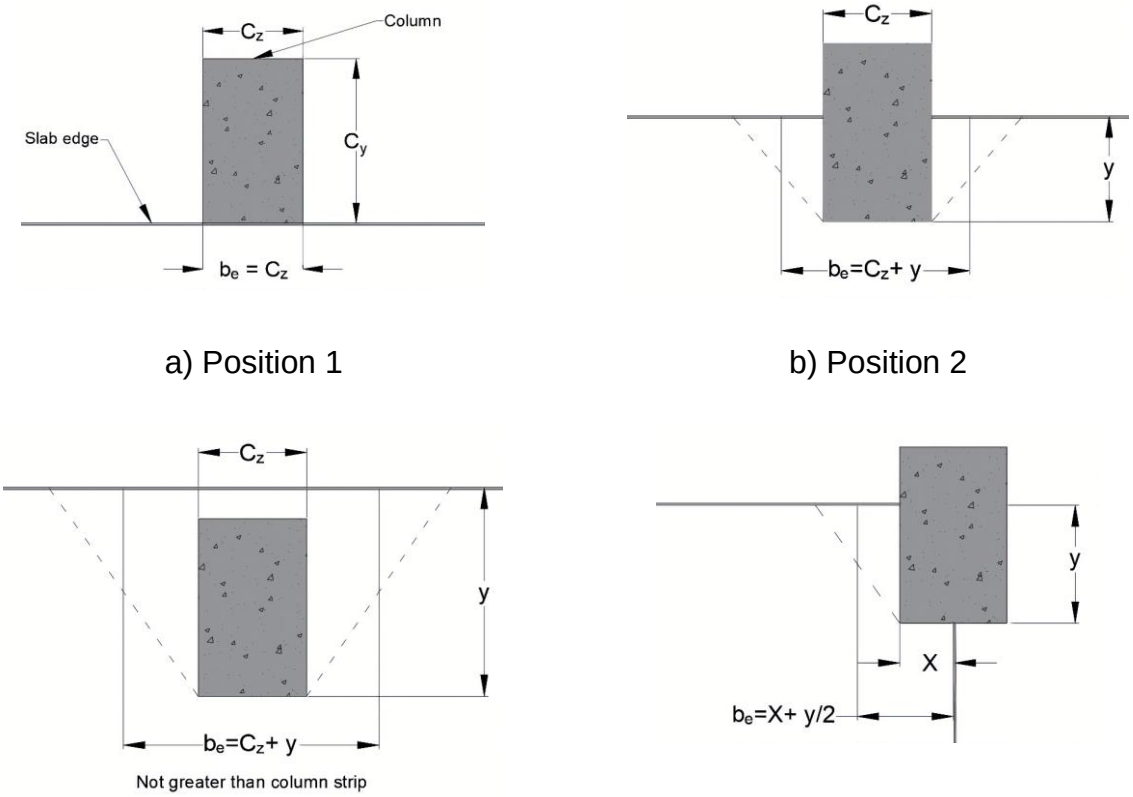

a) Position 1 b) Position 2

c) Position 3 d) Position 4

Figure 7.10: Effective width (b_e) of a flat slab for maximum transfer based on BS EN 1992-1-1 and Whittle (1994)

A further limit on the transferred bending moments is provided by BS EN 1992-1-1 to make sure over reinforcement does not happen to the section. Therefore, transferred bending moments

should be restricted to the moment of resistance of a rectangular column section (as shown in Equation 7.16) and the end span; the positive moment should be adapted accordingly.

$$M_{t,max} = 0.17 b_e d^2 f_{ck} \quad \text{(Eq. 7.16)}$$

In which:

b_e: Active breadth of a slab

d: The effective depth

f_{ck}: Characteristic compressive strength of concrete

The following recommendations can increase the capacity of connections to transfer the applied loads (Figure 7.15):

1. Increase column cross-section size
2. Increase slab thickness
3. Use higher strength concrete
4. Reduce the span of the slab
5. Relocate the column relative to the edge of the slab
6. Reduce the design load on the slab
7. Use hidden beam

7.7.5 Column Slenderness

Column slenderness is more critical in RC moment-resisting frames (unbraced) than RC frames with shear walls (braced). This is because in RC braced frames the shear walls are vertical elements that provide a relatively stiff resistance to horizontal and vertical loads resulting in lower horizontal and vertical forces applied to the columns. Therefore, the columns can be designed with relatively smaller dimensions.

While in RC unbraced frames, the applied loads are subjected only to the columns (as the vertical resisting elements). To resist and transfer this amount of load requires the columns to be designed with larger dimensions.

The slenderness of columns is given in Equation 7.17 by BS EN 1992.1.1:

$$\lambda = \frac{l_0}{i} \qquad \text{(Eq. 7.17)}$$

For unbraced members, l_0 could be calculated in Equation 7.18:

$$l_0 = l \times max \begin{cases} \sqrt{1 + 10 \times \frac{k_1 \times k_2}{1+k_1}} \\ \left(1 + \frac{k_1}{1+k_1}\right) \times \left(1 + \frac{k_2}{1+k_2}\right) \end{cases} \qquad \text{(Eq. 7.18)}$$

where:

i: the minimum radius of gyration of the uncracked section

l_0: the effective length of the member calculate

k_1, k_2: Relative stiffness at ends 1 and 2, respectively (k=0.1 recommended by BS EN 1992.1.1 for fixed ends)

l: Clear height

The followings are some suggestions to increase the capacity of columns (Figure 7.15):

1. Tie the columns in the middle
2. Increase the columns' tributary areas
3. Design columns with maximum area in the middle and least area at the ends like bulged columns
4. Use of BRBF (Buckling-restrained braced frames) to prevent buckling
5. Change the type of end connection for columns

7.7.6 Robustness

According to EN 1991-1-7:2006, a building should be designed in a way to provide robustness (withstand events like accidental explosions, fire, impact or the consequences of human error) without being damaged to an extent disproportionate to the original cause.

To enhance the robustness of flat slabs, the following detailing for bottom rebars are suggested (Figure 7.15):

1. Extend the bottom rebars within the clear cover distance of the slabs' free edge.
2. Increase the area of the bottom rebars anchored to the edge and corner columns.
3. Every second rebar has to be lap spliced with the adjacent panel's bottom rebar.

7.7.7 Punching Shear

When flat slabs are subjected to lateral loading, the shear stresses in the slab increase due to an unbalanced moment, and the flat slab-column connection is likely to fail by punching shear.

The sequence of failure tends to start from flexural cracks at the top surface of the flat slab when the cracking moment is reached the loading zone. Once the ultimate capacity reaches 60-70%, an inclined shear crack starts to develop, causing the shear force to be carried by friction in the compression zone and aggregate interlock beside the surface of the crack.

By increasing the applied load, the longitudinal reinforcement begins to yield (depending on the reinforcement ratio) at the face of the connection propagating towards the span. When the inclined crack's width expands further, the aggregate interlock loses its efficiency to resist the applied load resulting in more load resisted through dowel action. At the collapse load, the inclined crack penetrates the compression zone causing the brittle failure, as shown in Figure 7.11 (Reineck et al., 2001).

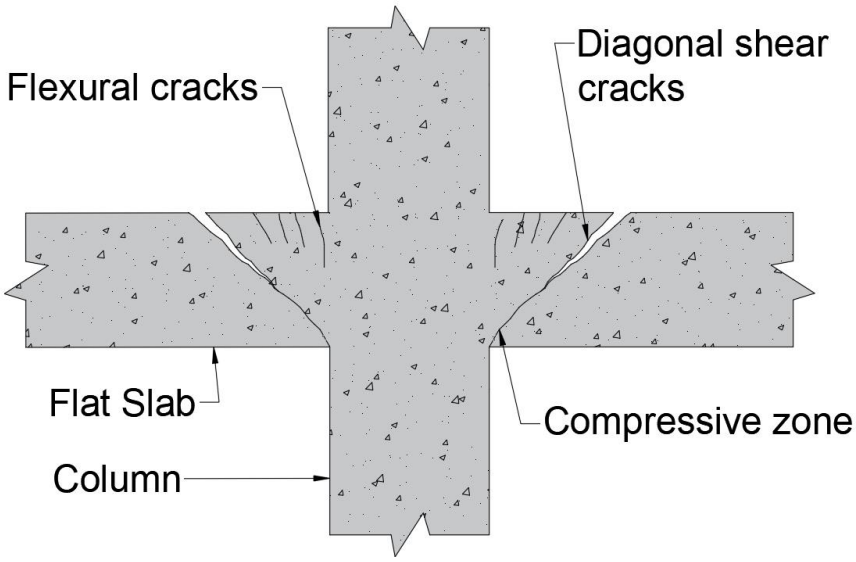

Figure 7.11: Punching shear failure mechanism

There is a potential issue with punching shear and rectangular edge columns and orientation (perpendicular or parallel to the edge), and the following considerations are required:

1. The control perimeter should be designed according to the orientation of the columns.
2. In rectangular columns, those parallel to the edge of slabs have relatively lower punching shear values compared to the perpendicular columns.
3. For columns with a width to depth ratio between 0.25-0.5, the punching shear ratio of perpendicular columns to the edge of the slab is up to 17% higher than parallel columns, while this value for columns having a ratio between 0.5-1 is reduced to 11%.

In order to decrease the punching shear ratios, these recommendations can be followed (Figure 7.15):

1. Increase the flat slab thickness
2. Use drop panel
3. Increase critical shear perimeter
4. Provide shear reinforcement
5. Use hidden beams
6. Increase column cross-section size

7.8 How Can We Improve a Building's Ability to Resist Lateral Load?

In chapter 5 a thorough investigation was conducted of several key factors, including concrete grade, column size, column shape and slab thickness on a five-storey RC frame building as a case study (Figure 7.4) to observe their influence on the building's structural performance. The investigated factors include seven concrete grades ranging from C40/50 to C80/95, three different column shapes using a square (610×610 mm), rectangle (700×500 mm) and circle (690 mm diameter) with around the same cross-section area of 385000 mm^2. Also, six-column sizes ranging from 750×250 mm with 50 mm increase in one dimension to 750×500 mm and two slab thicknesses of 275 mm and 300 mm.

Furthermore, an optimisation in the arrangement of the concrete grade was made using C55/67 to C80/95 for columns. In this optimisation, the concrete grades were distributed over the building's height using the higher strength at the lower storeys and lower strength at the higher storeys. The optimised concrete grade was achieved over various structural analyses using finite element simulations and monitoring the results.

7.8.1 Column Shape

A vital aspect of column shape is its impact on punching shear. In Figure 7.12, the punching shear results for different column shapes using optimised concrete grade with higher strength in the lower storeys and lower strength in the higher storeys for the columns (Table 6.3) and 275 mm slab thickness are provided:

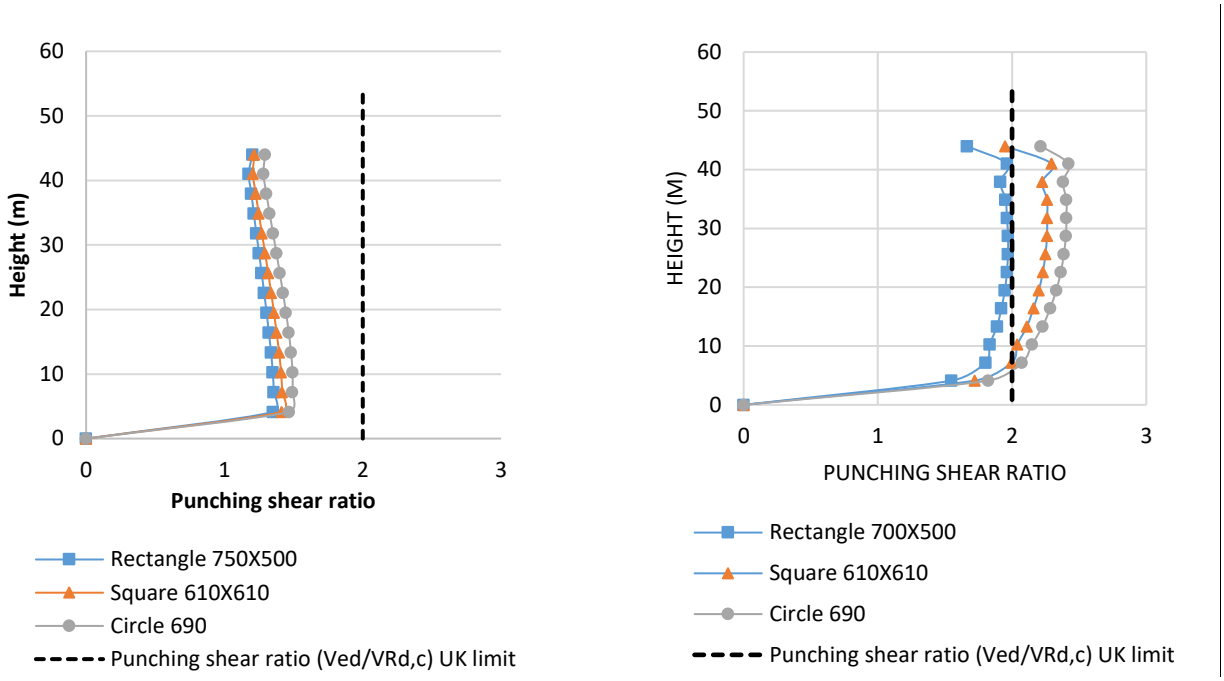

a) Internal column

b) Corner column

Figure 7.12: Punching shear ratio ($V_{Ed}/V_{Rd,c}$) at internal and corner columns in different shapes

As it can be seen in Figure 7.12, the punching shear ratio ($V_{Ed}/V_{Rd,c}$) was within the acceptable range only for the rectangular shape at the internal and corner columns since the internal columns represent the best case and the corner columns represent the worst-case scenario. Furthermore, the square and circle shapes failed to pass the criteria. Adequate perimeter area around a column has a direct impact on the punching shear as it can provide enough strength for the flat slab to transfer the loads without shear failure.

7.8.2 Column Size and Slab Thickness

The influence of column size and slab thickness on the maximum overall height of a building using the optimised concrete grade is shown in Figure 7.13:

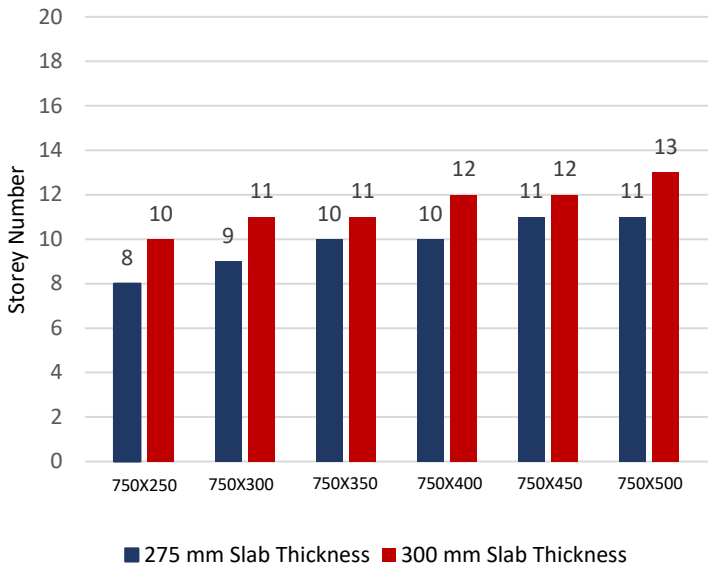

Figure 7.13: Maximum overall height in a different column and slab sections

The results demonstrate that increasing the width to depth ratio of column cross-sections can increase the building's overall height. It was also evident that increasing the slab thickness by 25mm results in an increase of building height by two storeys. However, the governing factor in this analysis was the punching shear ratio limiting the buildings' height. An approach to decide between the options is to conduct a cost-benefit analysis (CBA).

This approach is a systematic process where the decisions for applications are analysed to decide whether or not benefits outweigh the costs and by what margin. Here, the difference in the construction cost is presented in Figure 7.14 for three types of 13 storey buildings with various element sections.

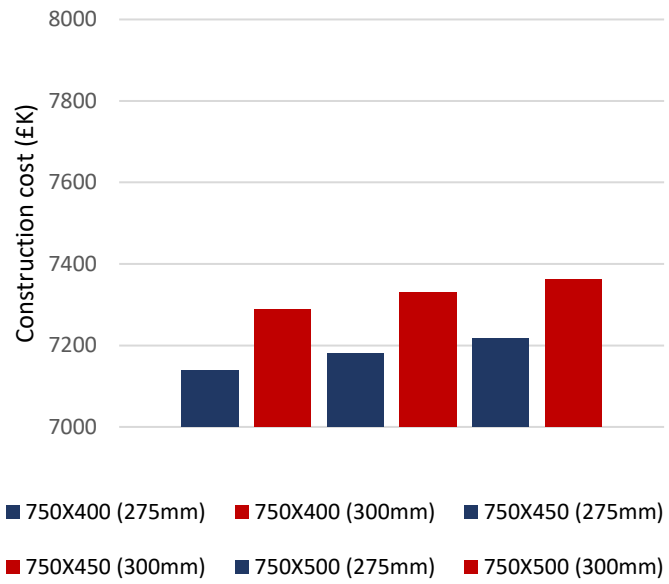

Figure 7.14: Cost estimation for various element sections

The building with 750×500 column section and 300mm slab thickness provides 13 storey RC moment-resisting frame buildings constructed in the UK.

Note: Considering the practical side of the design, it is advisable to design the buildings up to 12 storeys, since by increasing the height to 13 storeys the structural performance of the buildings is pushed to the defined limitations in the Eurocodes. In this situation, another factor such as human errors, could lead the structural performance of the building to fail.

7.9 Summary

In this guideline, the possibility of constructing RC frame buildings without shear walls in the UK adopting moment-resisting frames and flat slabs considering Eurocode 2 Part 1-1 (BS EN 1992-1-1, 2014) regulations was investigated. Furthermore, for typical reinforced concrete frame buildings in the UK, several key factors were optimised to obtain the maximum overall height in moment-resisting frames. This guideline is particularly important because it gives in-depth practical and technical advice based on thorough research.

The following is a summary of this chapter:

- By eliminating shear walls in the building, around 0.67% (£20k out of £2.8m) of the overall construction cost can be saved even when two rectangular columns in all storeys replace single shear walls.
- Eliminating the shear walls can result in a reduction of one day in the 14-day cycle of flat slab construction, and this amount of time could, in theory, be saved in the construction process.
- RC frame buildings in the UK can be constructed safely without shear walls and provide adequate serviceability and strength within the safe range defined by the Eurocodes.
- Adopting an optimisation of concrete grades in RC frame buildings can result in acceptable stiffness and strength.
- Rectangular column shapes can enhance the buildings' lateral movements and positively influence the punching shear ratio.
- Increasing the slab thickness by %10 can add up to 2 more storeys to the maximum overall height in RC frame buildings.
- The potential for reducing cost in low-to-medium-rise RC frame structures by at least 0.67% using flat slabs in moment frames has been demonstrated.

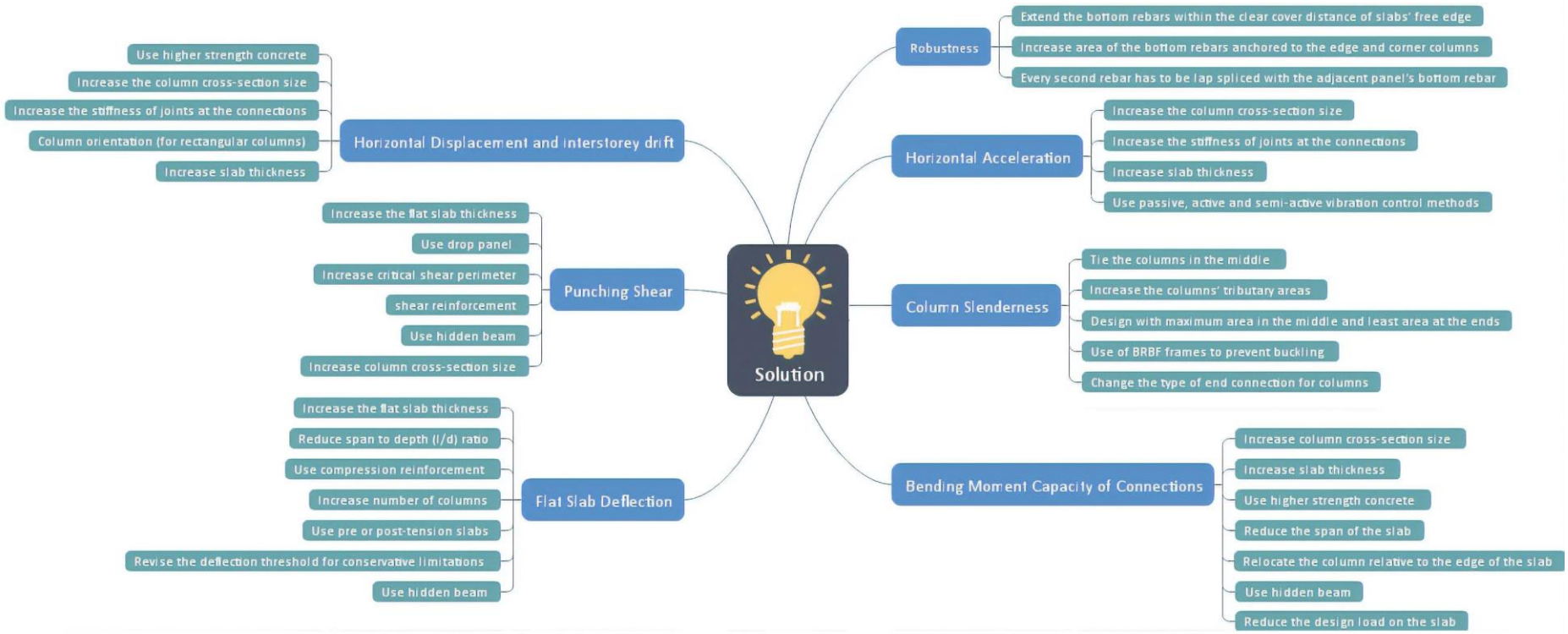

Figure 7.15: Solutions to enhance buildings' structural performance

8 Design a Mini-haunch connection

8.1 Introduction

This chapter is concerned with the behaviour of moment-resisting RC frames in regions with low levels of seismic activities, and it proposes a new connection design, the Mini-Haunch (MH), for improved structural efficiency. In the construction industry, various approaches have been developed to enhance the structural performance of concrete framed buildings, including moment-resisting frames as well as the use of shear walls to provide lateral stability. Currently, traditional structural materials, including concrete, are experiencing significant levels of scrutiny from the scientific and practising engineering communities for their environmental impact and economic credentials. The development of new materials has also increased the pressure, and therefore the need for new, improved and more efficient design methods and procedures is imperative (Dhir, Hewlett and Csetenyi, 2002).

Applications for moment-resisting frames are generally confined to low- to medium-rise buildings owing to having relatively low lateral stiffness compared with frames with shear walls (Gardner, 2015). This is significant when the structure is subjected to lateral loadings, such as during seismic events or strong winds. In order to achieve the most appropriate design, several criteria must be considered, including the structural performance, the construction method and also sustainability. Regarding the structural performance, it has been suggested that in the capacity design concept, in order to dissipate the absorbed energy, frames should be allowed to sway using their full potential (BS EN 1998-1, 2004), which can also provide sustainability in the economy of construction. This behaviour is unlikely to occur with the use of shear walls within frames as they significantly increase the lateral stiffness of buildings and do not allow the frames to sway, leading the designs to be more conservative and less structurally and materially efficient.

The connections between beams and columns have a direct impact on the structural performance in terms of the ultimate load-carrying capacity of the frame as well as the load transfer between elements in moment-resisting frames. However, most failures in moment-resisting frames occur in this area (Wight, Richart and MacGregor, 2012; Unanwa et al., 2000; Kaliluthin et al., 2014).

In this context, the current work aims to explore the performance of the proposed Mini-Haunch connection in RC moment-resisting frames and investigate its performance. This work is motivated by feedback received from members of the Concrete Centre in the UK, who felt a more efficient solution was both needed and possible. Globally, various design codes provide rules for the design and detailing of RC structures for the governing lateral loads (seismic or wind). In the UK design codes, since there are no considerable seismic activities, the governing source of lateral load is wind.

Based on the information available in the literature, it is concluded that there is a need for more research on the performance of RC frames with moment-resisting connections subjected to wind action as most of the previous studies have focused on the seismic response. This shortcoming is particularly crucial for countries such as the UK, in which the dominant lateral force in the design of buildings is from the wind. Since the fundamental behaviour of seismic activities and wind action are different, especially in terms of the load application area, the involvement of mass and base shear, and the cyclical nature of earthquakes, a different analysis and design approach is required. Furthermore, as depicted earlier, more research into cast-in-situ connections is also required, and there is vast potential within these details to improve both structural performance and efficiency. It is in this context that the current part of the research is undertaken, including the development of a new Mini-Haunch connection for RC frames. An experimental study was conducted on two RC frames with moment-resisting connections,

designed in accordance with the similitude approach, as described in the literature review. This is followed by a description of the complementary numerical analysis.

8.2 Experimental Results and Discussion

8.2.1 Strain Gauge

While performing the experimental tests under the hydraulic actuator, the four strain gauges attached to the longitudinal reinforcement were simultaneously logging the strain data through the quarter-bridge circuits to the PicoLog 6 software. It was observed that the strain data contained many noises in the readings, which could be the result of strain gauges being in contact with the concrete.

Moreover, it was noticed that one of the strain gauges (SG3) stopped working during the test, and there was no correlation between strain gauge readings and the compression test. Also, this issue was already encountered in the previous studies with strain gauges, including the experimental study conducted by Zaki and Rasheed (2020), who suddenly lost their strain data, and it was not recorded. Therefore, due to the insufficiency of strain gauges in this PhD research, it was decided to discard the application strain gauge.

8.2.2 Tests under Hydraulic Actuator

Based on the acquired results for the compressive strength, the values of the standard samples (S1, S2 and S3) were 29.1 N/mm^2, 32.9 N/mm^2 and 29.8 N/mm^2, respectively and for the Mini-Haunch samples (MH1 and MH2) were 24.6 N/mm^2 and 30.8 N/mm^2, respectively. Figure 8.1 presents an image of specimens S1 and MH1 following testing, which comprised a standard and Mini-Haunch connection, respectively.

a) S1

b) MH1

Figure 8.1: Images from the test programme after testing including specimens

The load versus vertical deflection responses from the tests are presented in Figure 8.2. It is clear that, in general, the five test specimens behaved similarly. The stiffness of the standard frames was marginally more significant in the early stages compared with the frames with mini-haunches, and they also reached the ultimate load at lower levels of deflection. Compared to the frames with standard connections, those with Mini-Haunch connections achieved lower ultimate loads. In terms of the failure mode, it was observed during testing that when the loads were applied, both flexural and shear cracks appeared from the bottom side of the beam and propagated to the top side of the section through crack patterns. When the scaled frames reached their ultimate capacity, the cracks had opened through the middle of the beam sections, and the frames failed under the mid-span of the beam with a combination of shear and tension stresses.

Furthermore, it was evident during the tests that the frames with Mini-Haunch connections behaved in a more ductile manner compared with the standard connection frames. This was further evident by more distributed flexural shear cracks in the beams of the Mini-Haunch connections in comparison to the standard connections, where more concentrated flexural cracks were observed in the middle of the beams. Also, it was observed that the standard connections achieved ultimate loads of 55.9 kN, 55.7 kN and 56.8 kN for S1, S2 and S3, respectively. The corresponding deflections at the ultimate loads were 6.4 mm, 7.1 mm and

13.9 mm, respectively. It is shown in Figure 8.2 that S3 had less initial stiffness compared with S1 and S2 and therefore reached its ultimate load at a greater deflection. There are several possible reasons for this, such as localised cracking, experimental inaccuracy with concrete preparation, etc. On the other hand, the ultimate loads for the frames with the Mini-Haunch connections were 49.3 kN and 54.4 kN for MH1 and MH2, respectively, and the corresponding deflections 8.6 mm and 11.3 mm, respectively.

Note: It is worth mentioning that despite the higher workability (S2), the Mini-Haunch connection performed almost the same as the standard connection when subjected to vertical loading.

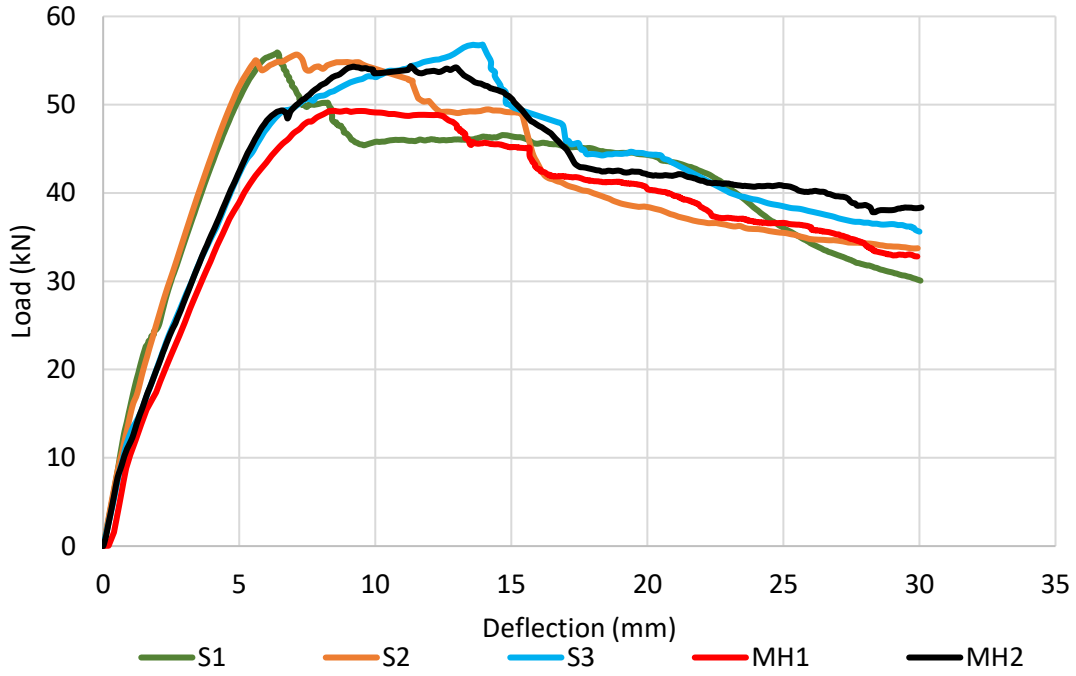

Figure 8.2: Compression test results for the scaled frames

8.3 Finite Element Analysis Results and Discussion

8.3.1 Results of Numerical Analysis with ANSYS

After performing numerous finite element analyses with ANSYS software, it was concluded that ANSYS was unable to provide the ideal nonlinear behaviour of the modelled frames and only could demonstrate the findings in the elastic zone. Further efforts to reach the plastic failure of the modelled frames in ANSYS ultimately ended in rigid body errors that could not be fixed

partly due to the inconvenient bond between the reinforcement and the concrete. Therefore, it was decided to change the finite element software to Abaqus that has already shown efficient results in reinforced concrete sections in various studies (Dai et al., 2014; Earij et al., 2017; Elchalakani et al., 2018; Rahman et al., 2019; Zhou et al., 2020).

8.3.2 Validation of the Numerical Analysis with Abaqus

The results obtained from the previously discussed experimental tests are used herein to validate the FE model in terms of the load-deflection response and also failure mode. Table 8.1 and Figure 8.3 present the load-deflection responses from the RC frames with (a) standard connections (S) and (b) Mini-Haunch connections (MH).

Table 8.1: The experimental and the FE model results for frames with standard and Mini-Haunch connections

Tests	Ultimate load (kN)		Deflection (mm)	
	Experiment	FE model	Experiment	FE model
S1	55.9	51.9	6.4	11.8
S2	55.7		7.1	
S3	56.8		13.9	
MH1	49.3	52.2	8.9	9.9
MH2	54.4		11.3	

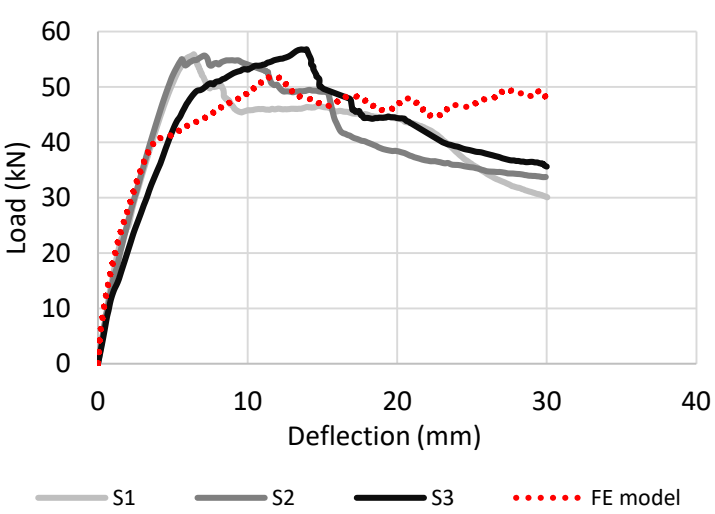

a) Standard connections

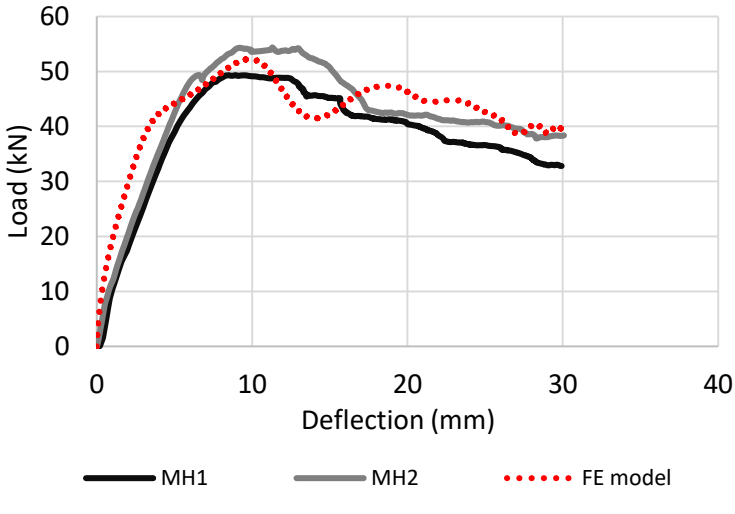

b) Mini-Haunch connections

Figure 8.3: Comparison between the experimental results and the FE models

For the standard connection, the experimental results show that the ultimate load for S1, S2 and S3 was 55.9 kN, 55.7 kN and 56.8 kN, respectively, with corresponding deflections at the centre of the beam of 6.4 mm, 7.1 mm and 13.9 mm, respectively. The FE model predicts an ultimate capacity of 51.9 kN and a corresponding ultimate deflection of 11.8 mm. On the other hand, for the Mini-Haunch connection (MH), the experimental results demonstrate ultimate loads of 49.3 kN and 54.4 kN were achieved for MH1 and MH2, respectively, with corresponding deflections of 8.9 mm and 11.3 mm. For this arrangement, the FE model predicts an ultimate load and deflection of 52.2 kN and 9.9 mm, respectively. Therefore, for both the frames with standard and Mini-Haunch connection types, the FE model can provide a realistic depiction of both the overall and ultimate behaviour.

Figure 8.4 presents a comparison between (a) the crack pattern and distribution of stresses and (b) the corresponding experimental image for the S1 frame. Similar images for MH1 are given in Figure 8.5. In these images, the simulated stress patterns show the location of the plastic strain due to tension (indicated as “PE, Maximum Principal”) in the frames, which is likely to be the location of crack initiation. Both Figure 8.4 and Fig 7.5 demonstrate almost identical crack initiations between the experimental and simulated frames, beginning at the bottom centre of the beams and spreading upwards with flexural and shear cracks. Furthermore, in Figure 8.4 and Figure 8.5, the crushing of concrete is shown at the top centre of the beams towards the left for the Mini-Haunch and the standard frames. Therefore, it can be concluded that the experimental and FE results are in good agreement.

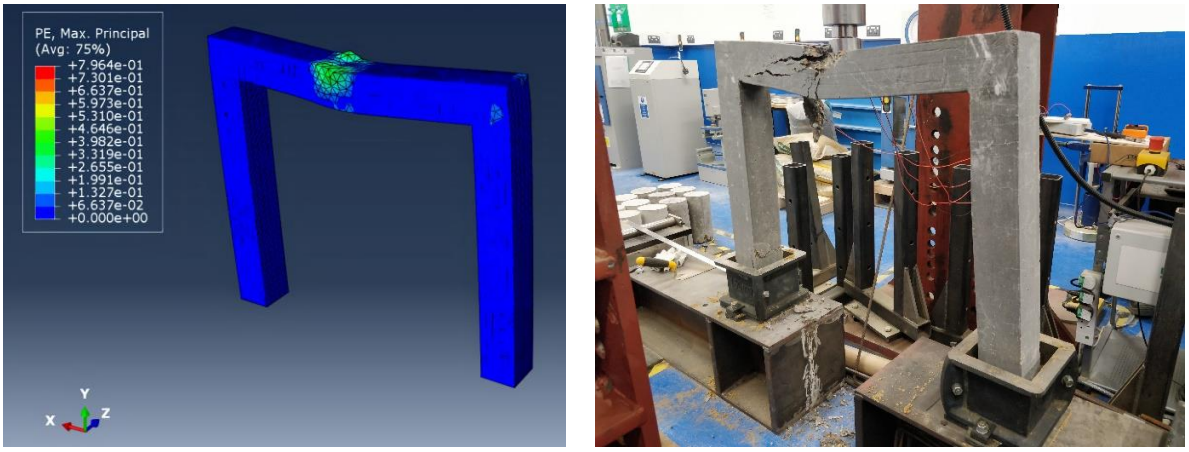

a) The FE model b) The experiments

Figure 8.4: Crack development for the S1 connection

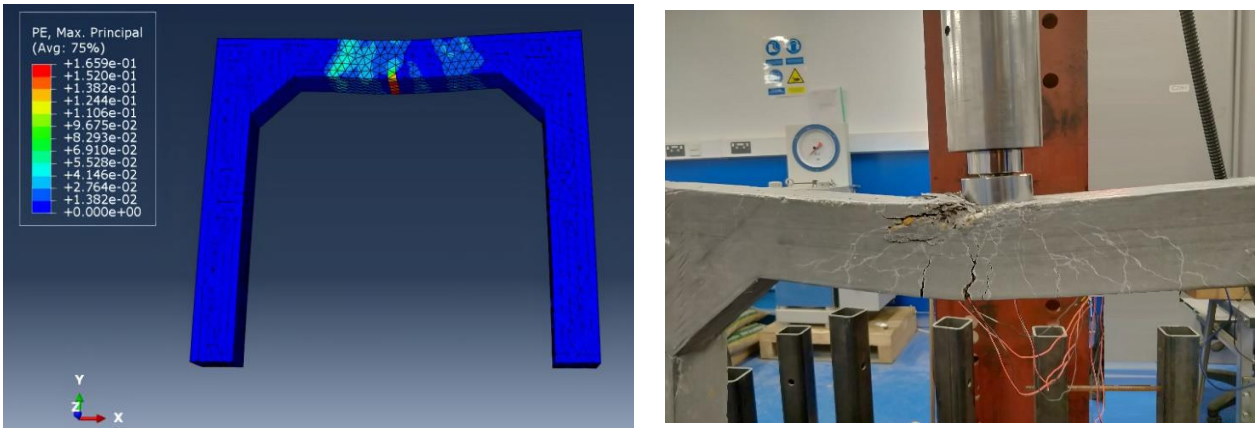

a) The FE model b) The experiments

Figure 8.5: Crack development for the MH1 connection

8.3.3 Influence of Horizontal Loading on the Connections

The overarching motivation for this work is to investigate the necessity of shear walls for lateral stability in the design of low- to medium-rise RC framed structures in non-seismic areas. Therefore, in the current section, the influence of horizontal loading on RC frames with Mini-Haunch connections is studied using the validated ABAQUS models. In these FE models, the applied loads are defined as horizontal displacements (U_1=16 mm) at the top left corner of the frames (Figure 8.6), and the bottom of the columns are fixed in order to restrain the displacement and rotation in six degrees of freedom (i.e. $U_1 = U_2 = U_3 = UR_1 = UR_2 = UR_3 = 0$, where U_1, U_2 and U_3 are the translational degrees of freedom and UR_1, UR_2 and UR_3 are the rotational degrees

of freedom). The results of the frames' FE models, subjected to the horizontal loading, are presented in Figures 8.7 and 8.8 in terms of load-displacement responses and failure modes.

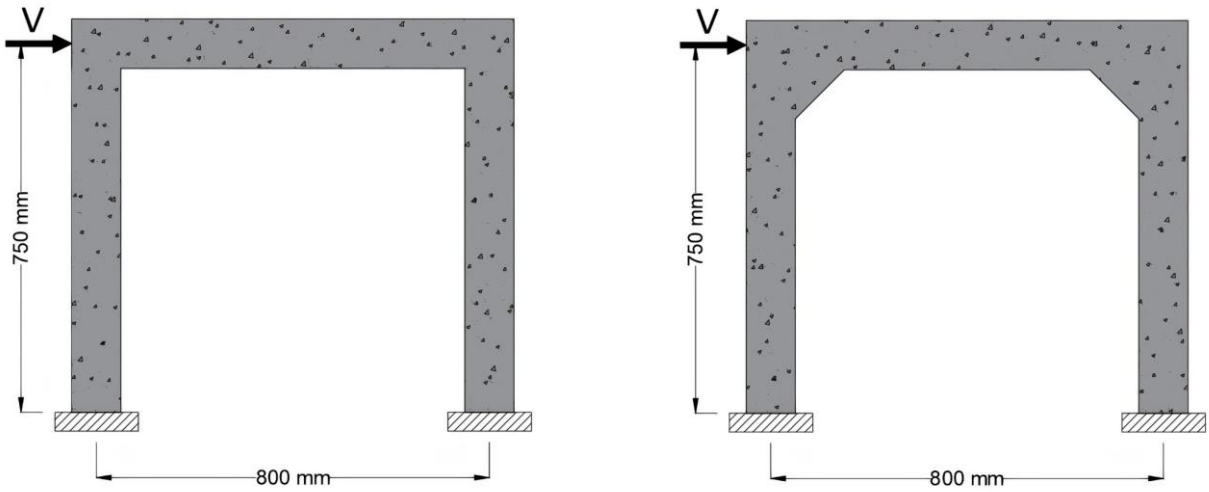

Figure 8.6: Boundary conditions and loading for the frames

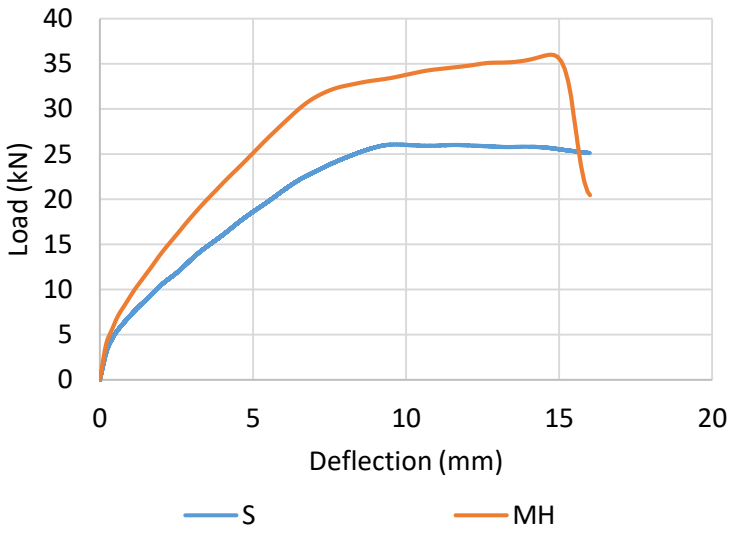

Figure 8.7: Simulations of the frames with Standard (S) and Mini-Haunch (MH) connections subjected to horizontal loading

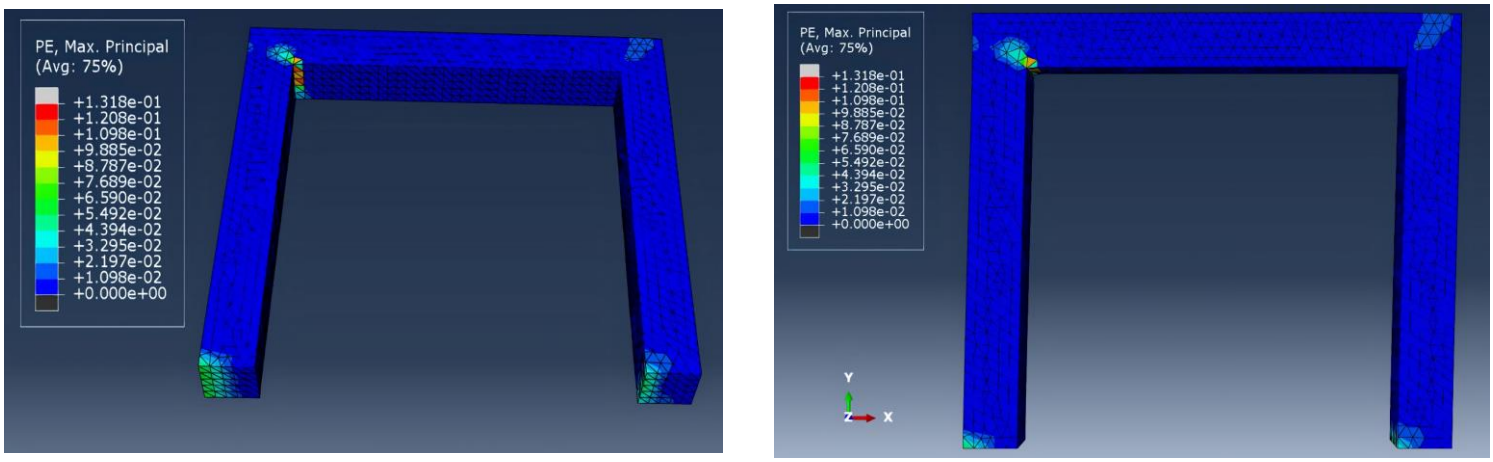

a) S connection

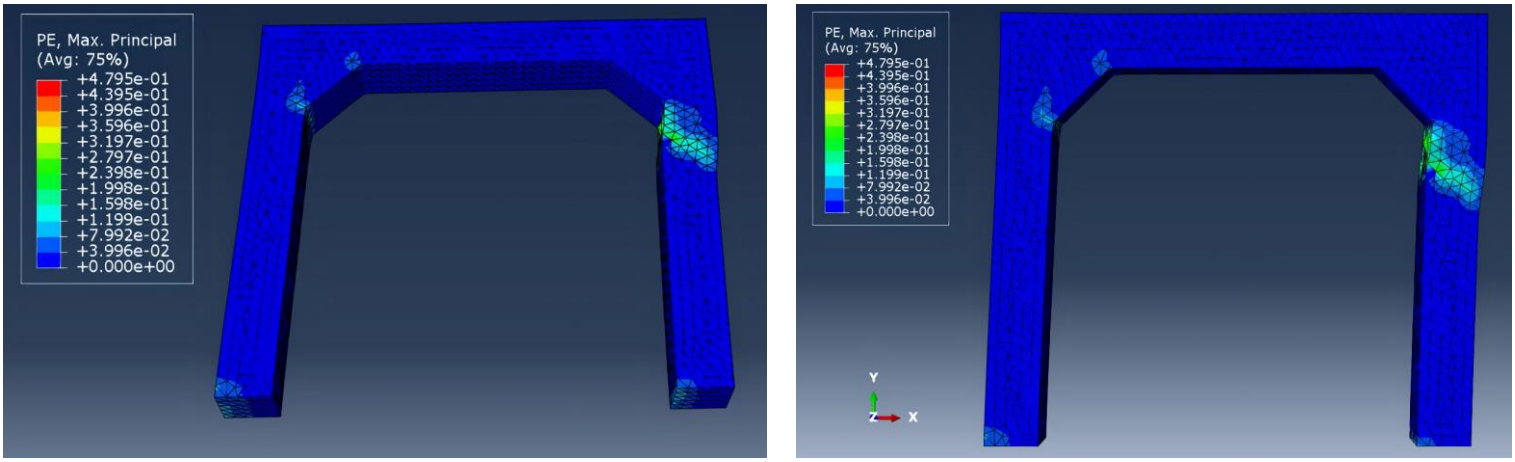

b) MH connection

Figure 8.8: Comparison between the connections subjected to horizontal loading

From Figure 8.7, it is observed that the frame with a standard connection (S) achieves an ultimate horizontal load of 26.1 kN with a corresponding displacement of 9.7 mm. On the other hand, under a similar loading arrangement, the frame with a Mini-Haunch connection achieves an ultimate strength of 36 kN and ultimate displacement of 14.7 mm. Comparing the load-displacement results show that the ultimate strength increased by 38% by designing a frame with a Mini-Haunch connection. Also, the Mini-Haunch connection demonstrates 52% higher lateral displacements and therefore is capable of providing a more ductile response compared with the standard connection.

Figure 8.8 shows the failure modes for standard and Mini-Haunch connections. It is shown that the crack initiation and propagation for the standard connection are located at the top left and top right of the beam-column connections, which highlight the vulnerability of the frame in this zone. On the other hand, for the Mini-Haunch connection, the crack initiation and propagation are more focused on the column regions, which demonstrates the enhanced capability of the Mini-Haunch connections for transferring the horizontal loads. It is noteworthy that failure in the columns is not favourable in design and, following the strong column-weak beam concept, it is preferable for beams to fail before columns in order to avoid a sudden building collapse. However, in this simulation, if the columns are designed to perform stronger than beams, the Mini-Haunch connection could significantly improve the structural performance of RC frame buildings.

In light of this, another finite element analysis is performed on a frame with relatively larger column cross-sections, subjected to lateral loading, to investigate the compatibility of the Mini-Haunch connection with the strong column-weak beam concept. In this regard, the column cross-section is increased to 150 × 100 mm as a typical cross-section size (Shakir-Khali and Mouli, 1990; Wang et al., 2020; Thirumurugan et al., 2020). Also, the beam cross-section remained as 100 × 100 mm (Figure 8.9) with the same horizontal loading and fixed supports (i.e. $U_1 = U_2 = U_3 = UR_1 = UR_2 = UR_3 = 0$) at the base of the columns.

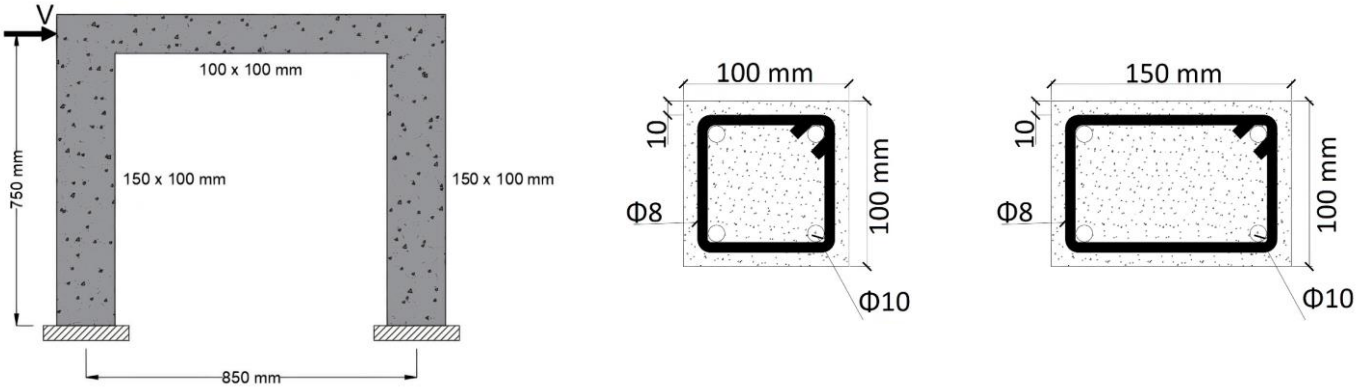

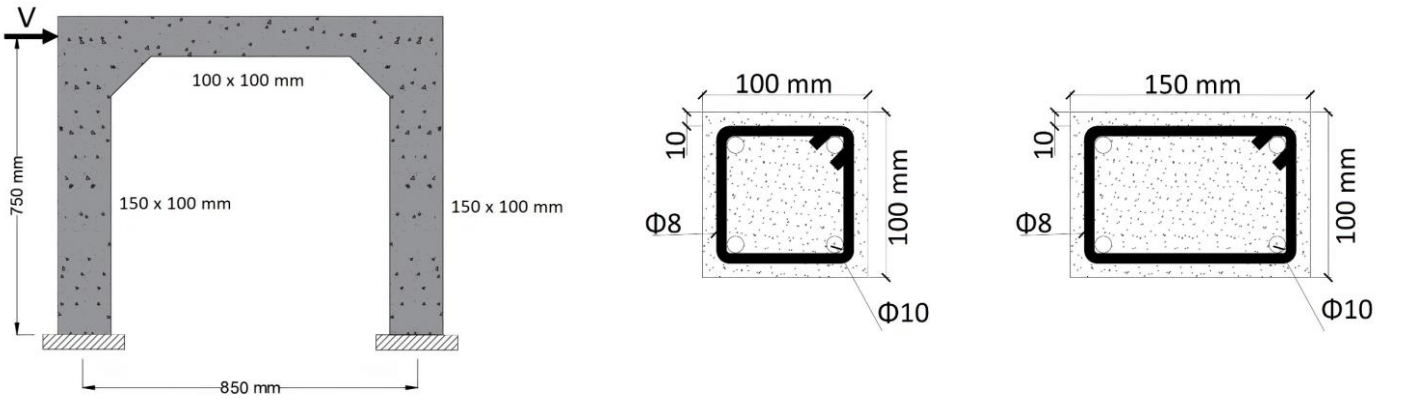

a) Frames b) Beam cross-section c) Column cross-section

Figure 8.9: Boundary and loading conditions for the frame

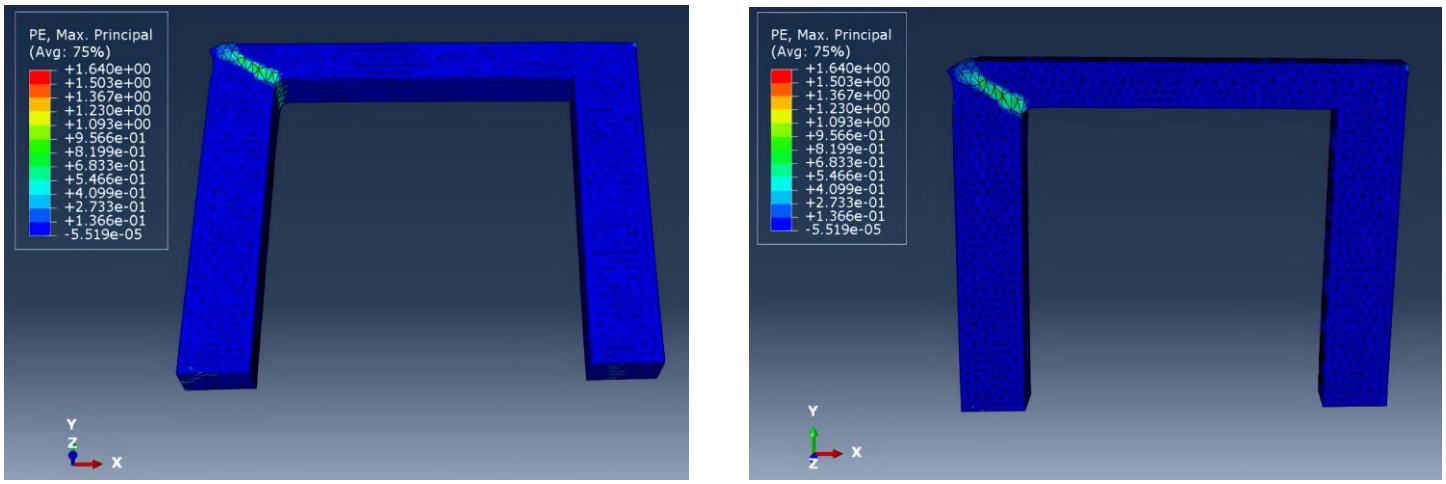

a) S connection

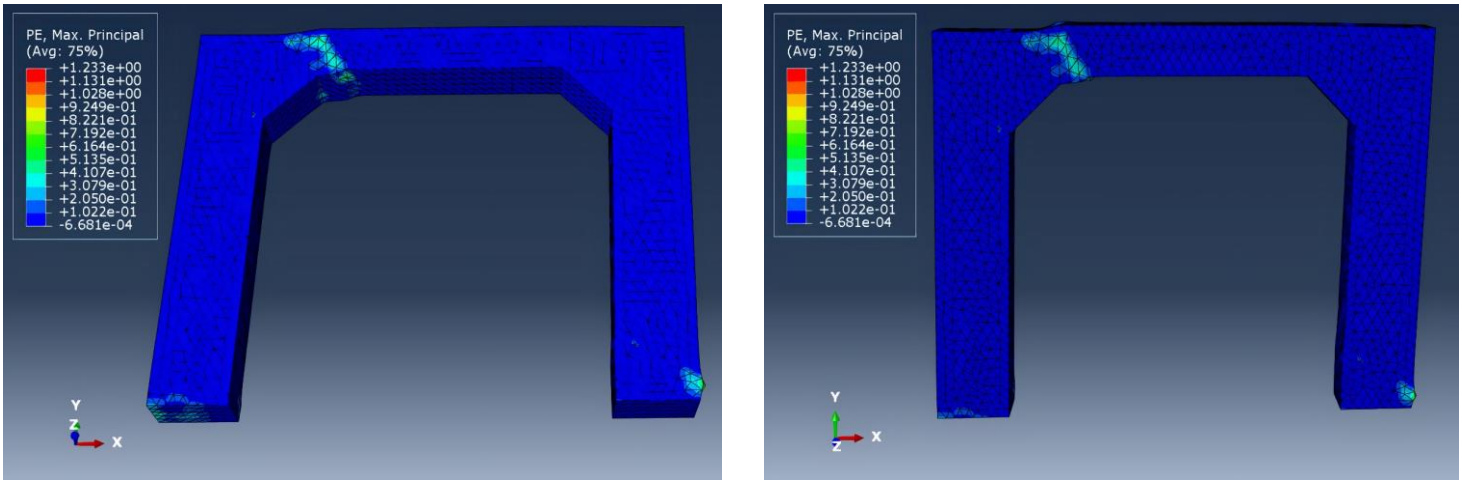

b) MH connection

Figure 8.10: The failure mechanism subjected to horizontal loading

It is observed in Figure 8.10 that for the frame with standard connections, failure occurs at the beam-column connection. While for the frame with Mini-Haunch connections, failure happens at the beam (i.e. the weakest part) rather than at the connections or columns, illustrating that the Mini-Haunch connection complies with the strong column-weak beam concept and can assist in designing to avoid a disproportionate or sudden collapse.

8.4 Summary

This chapter proposes and investigates a new type of connection, known as the Mini-Haunch connection, for RC moment-resisting frames to enhance the lateral stability and structural performance when shear walls are not provided. This new Mini-Haunch connection is an efficient method in terms of the innovation in the design and is compared to standard connections in order to investigate its effectiveness through experimental tests in the laboratory. Besides, the development of a FE model is presented and validated and then employed to analyse the behaviour further. The key observations from this part of the research are summarised as follows:

- According to the experimental results, the overall behaviour of the frames with standard connections or Mini-Haunch connections is quite similar in terms of capacity even though the Mini-Haunch connection was constructed with a lower strength concrete.
- The experimental results of the Mini-Haunch connection demonstrated a more ductile behaviour compared to the standard connection under vertical loading.
- Under horizontal loading, the Mini-Haunch connection demonstrated a significant enhancement in comparison to the standard connection, giving 138% greater capacity. Also, the ductility of the Mini-Haunch frames was improved compared to that of the frames with standard connections.

- In the standard connection, cracks initiated from the corner of beam-column connections highlighting the vulnerability of such designs. However, for the Mini-Haunch connection, the cracks were more focused on the columns rather than the connections.
- Increasing the column cross-section results in shifting the failure mechanism to the beam, rather than the columns, for the frames with Mini-Haunch connections.

9 Sustainable Development of Medium Strength Concrete Using Polypropylene as Aggregate Replacement

9.1 Introduction

Plastic is a polymer-based material, which, due to its durability, strength to weight ratio, corrosion resistance and versatility, can be used in a wide range of applications, and it has several benefits in sustainability. However, this material, due to its characteristics, has a few drawbacks, including high embodied energy, low modulus of elasticity and high thermal expansion, which require further detailing to be utilised in construction.

In terms of sustainability, plastic materials are recyclable, which makes them more flexible to the requirements, and the production of plastic materials consumes less water. Moreover, the environmental cost to utilise alternative materials over plastic would be nearly four times greater due to the plastic's greater efficiency (Wagner, 2016).

In the construction industry, it can be said that with the level of experienced plastic consumption, an ongoing responsibility is shown for this sector to innovate alternatives for the application of recycled plastic waste continually. In 2017, Great Britain alone utilised 60,321 tonnes of natural aggregate for use in construction, with 24,038 tonnes of gravel and 24,632 tonnes of sand used in concrete, comparable to 6,309 tonnes of sand used for general building (Department for Business, Energy and Industrial Strategy, 2018). The mining of natural aggregate for use in concrete presents a significant environmental concern, not only for the energy and emission cost offered to the atmosphere in the extraction and transportation of said material but simply through long-term availability and damage of a natural resource. Babafemi et al. (2018) stated the need for further research into the structural application of plastic in an effort "to grow confidence in the use of plastic aggregates in concrete" and begin the development of industry-

recognised guidelines for use in the construction industry. With the consumption of sand for concreting (typically used as fine aggregate) exceeding that of gravel (typically the coarse aggregate in the concrete mix), along with plastic already being utilised at present in non-structural applications, the implementation of plastic as a fine aggregate replacement in the development of structural concrete, is a topic highlighted for consideration as a viable solution for recycling waste plastic at the landfill.

9.2 Results and Discussion

9.2.1 Workability

Workability of control and plastic-containing concrete specimens (including PP3.0FA) are shown quantitatively in Table 9.1, visually as concrete slumps in Figure 9.1. With the recommended workability for the ST5 Standardised Concrete Mix design in the British Standards, in this part of the research, the slump test is considered as an S2 slump class (slump between 50 mm and 90 mm). The control mix was thus established to achieve workability within the S2 slump class, being 50 mm as a base of comparison for plastic containing mixes.

The workability of fresh concrete typically decreased with the addition of plastic to the concrete mix. Workability of plastic-containing mixes (excluding PP3.0FA) offered a slump range of 10-50 mm and an average slump of 32 mm. A reduction in workability, therefore, was experienced, ranging from 0-40 mm and offering an average slump reduction of 18 mm across these mixes. All plastic containing mixes (excluding PP3.0FA) therefore demonstrated an S1 slump class (between 10 and 40 mm) according to British Standards Institution BS EN 206:2013+A1:2016c with mix PP0.5 the only mix offering an S2 slump class at 50 mm, matching that of the control mix.

Increasing plastic aggregate in the concrete mix coincided with a linear decline in workability. As seen in Figure 9.2, as the level of replacement plastic aggregate was applied in 0.50% increments from 0.50%-3.00% in mixes PP0.5-PP3.0, respectively, workability declined in

increments of 10 mm from the previous mix. It is generally found that increasing plastic in the concrete mix causes a gradual decline in workability (Poonyakanet al., 2018; Smarzewski, 2018; Rubio-de Hita, 2018; Sosoi et al., 2018; Zaleska et al., 2018a).

Implementation of fly ash offered a mitigating effect on reductions experienced using plastic in the concrete mix. Moreover, concrete mix PP3.0, containing 100% cement, demonstrated workability of a 10 mm slump, the addition of fly ash as 10% replacement of cement in mix PP3.0FA demonstrated a 200% increase in workability to that of PP3.0 at 30 mm, and 20 mm reduction on the control mix (compared to a 40 mm reduction from control to mix PP3.0). With this, using fly ash allowed an additional 1.00% of plastic aggregate to be applied to the plastic-containing concrete mix of equivalent workability being mix PP2.0. Workability improvement is generally found in concrete mixes without plastic aggregate (Yao, 2015; Hemalatha and Ramaswamy, 2017; Xu and Shi, 2018).

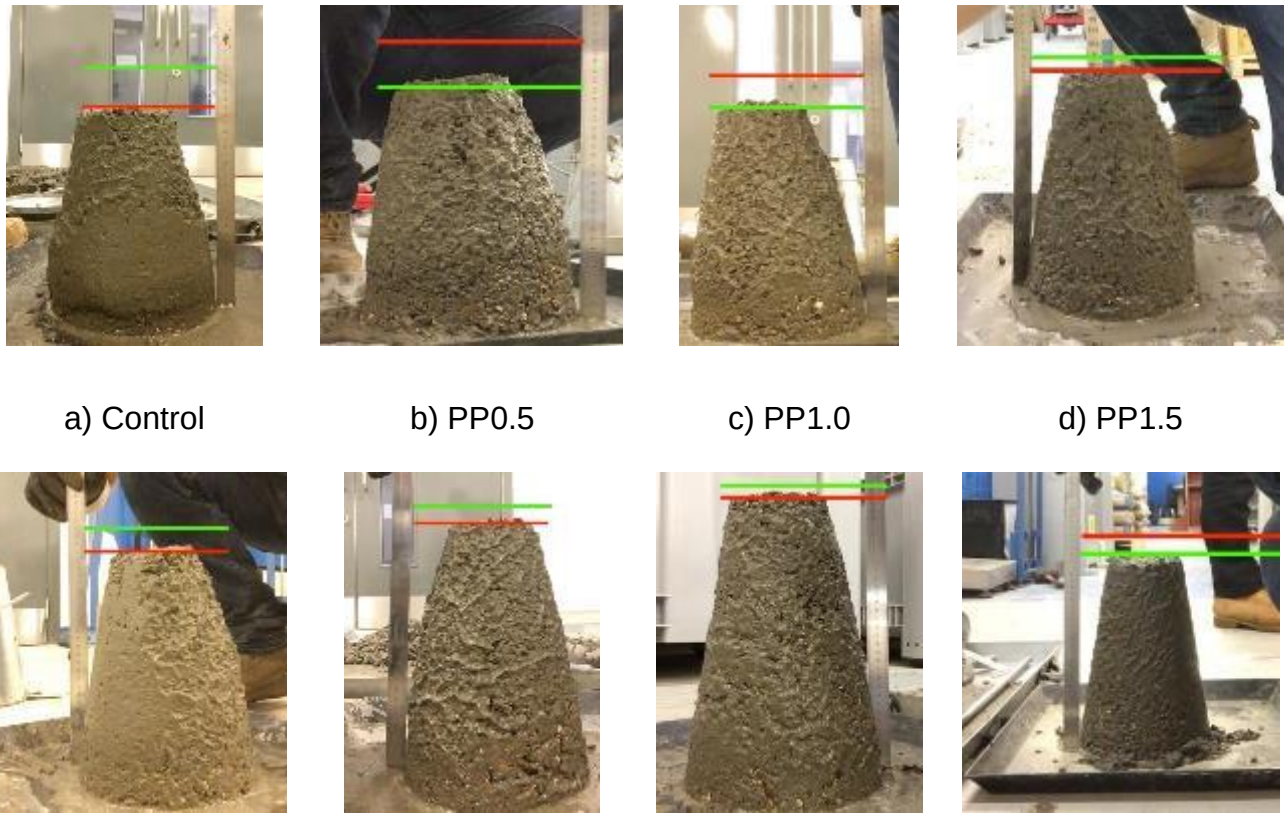

a) Control b) PP0.5 c) PP1.0 d) PP1.5

e) PP2.0 f) PP2.5 g) PP3.0 h) PP3.0FA

Figure 9.1: Workability of concrete mixes slump test

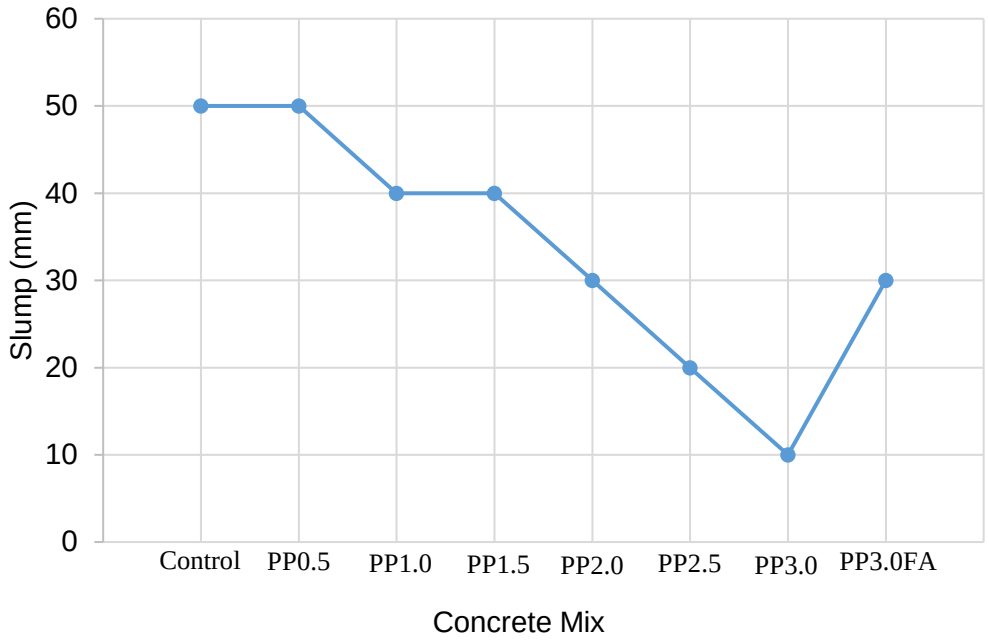

Figure 9.2: Workability results of all concrete mixes

9.2.2 Compressive Strength

Compressive strength results of control and plastic-containing concrete specimens (including PP3.0FA) are shown in Table 9.1 and Figure 9.3. Compressive strength findings for the three control mix specimens tested at 7 days curing ranged from 21.00 to 21.54 N/mm^2 and offered a mean compressive strength of 21.22 N/mm^2. The 28-day curing condition offered a range from 30.12 to 31.04 N/mm^2 and a mean value of 30.50 N/mm^2. It was presented that from 7 to 28 days curing, compressive strength developed and increased by a further 9.28 N/mm^2 (or 44% from 7 days). It should be noted that 25 N/mm^2 is the British Standards BS 8500-1:2015+A1:2016a requirement for the ST5 concrete mix design compressive strength, and therefore, it was apparent that at 7 days curing, the control mix nearly achieved the compressive strength requirement set out in the British Standards, and at 28 days curing, exceeded this requirement.

The compressive strength of concrete specimens decreased with the addition of plastic at both 7 and 28 days of curing. As shown in Figure 9.3, compressive strength testing was undertaken on plastic-containing concrete specimens (excluding PP3.0FA) demonstrated an average

reduction of 4.55 and 5.77 N/mm^2 at 7 and 28 days curing in comparison to the control mix. At 7 days of curing, compressive strength values ranged from 15.03 to 18.06 N/mm^2 and hosted a collective mean compressive strength of 16.67 N/mm^2. At 28 days of curing, compressive strength ranged from 23.62 to 26.44 N/mm^2, offering a collective mean value of 24.73 N/mm^2. Therefore, it was evident that as curing time increased, the compressive strength increased significantly, with an average increase of 48.59% from 7 to 28 days, respectively, presented as an increase of 8.06 N/mm^2.

The declining compressive strength experienced in this experiment when plastic aggregate was added to the concrete mix, as well as the development of this mechanical property of concrete from 7 to 28 days curing, is a trend consistent with the majority of previous research assessed (Saxena et al., 2018; Sosoi et al., 2018; Thorneycroft et al., 2018; Zaleska et al., 2018a; Smarzewski, 2018; Jacob-Vaillancourt and Sorelli, 2018; Poonyakan et al., 2018; Rubio-de Hita, 2018; Zaleska et al., 2018b; Ejiogu et al., 2018; Zaleska et al., 2018c). It can be said that from the current experiment, at the type, shape and morphology of the plastic used along with the hydrophobic nature of plastic generally, the addition of plastic aggregate to the concrete mix interrupted the interfacial matrix within the concrete, offering an inevitable reduction in the bonding of plastic and hydrated-cementitious material, leading to an enhancement of micro-cracks to failure under compressive loading (Saxena et al., 2018; Sosoi et al., 2018; Thorneycroft et al., 2018; Zaleska et al., 2018b; Ejiogu et al., 2018).

Compressive strength generally increased with the increasing levels of plastic aggregate in plastic-concrete mixes (excluding PP3.0FA), irrelevant of curing timeframe. At 7 days curing, compressive strength increased from 16.02 N/mm^2 for mix PP0.5 (containing 0.50% plastic) to 16.73 N/ mm^2 for mix PP3.0 (containing 3.00% plastic), peaking at 18.06 N/mm^2 for mix PP2.5 (containing 2.50% plastic). At 28 days curing, values increased from 23.62 N/mm^2 for mix PP0.5 to 24.50 N/mm^2 for mix PP3.0, again peaking for mix PP2.5 at 26.44 N/mm^2.

With the overall increase in compressive strength experienced as plastic increased in the concrete mix, shown in Figure 9.3, only 2 of the 5 plastic-containing concrete mixes (excluding PP3.0FA) demonstrated an increase from the previous mix at 7 days curing, however at 28 days curing, the opposite was apparent in which 3 out of the 5 mixes increased in compressive strength. This rise in the compressive strength that was achieved by increasing the level of plastic aggregate in the concrete mix is a finding contrary to the previous studies (Babafemi et al., 2018; Saxena et al., 2018; Sosoi et al., 2018; Zaleska et al., 2018a; Smarzewski, 2018; Poonyakan et al., 2018; Rubio-de Hita, 2018; Ejiogu et al., 2018). Based on previous research, increasing levels of plastic in the concrete mix, along with the hydrophobic nature of plastic and characteristics of the plastic aggregate used as previously mentioned, should have further progressed the development of porous concrete and production of air voids within the concrete mix (Saxena et al., 2018; Thorneycroft et al., 2018; Smarzewski, 2018; Zaleska et al., 2018b; Ejiogu et al., 2018); however, it can be said that since tension propagates failure in concrete (Thorneycroft et al., 2018), the increasing levels of plastic used in this experiment despite being small increments of 0.50% offered an increasingly elastic enhancement of the concrete mix during maximal compressive loading (Sosoi et al., 2018; Thorneycroft et al., 2018).

Table 9.1: experiment results (mean values per concrete mix for 7 and 28 days)

Mix code	Workability	7 day curing period		28 day curing period	
	Slump	Density	Compressive strength	Density	Compressive strength
	(mm)	(kg/m^3)	(N/mm^2)	(kg/m^3)	(N/mm^2)
Control	50	2245.13	21.22	2251.25	30.50
Pp0.5	50	2229.75	16.02	2230.78	23.62
Pp1.0	40	2223.55	17.43	2226.70	24.80
Pp1.5	40	2204.71	16.74	2211.62	25.23
Pp2.0	30	2203.92	15.03	2215.82	23.78
Pp2.5	20	2219.26	18.06	2144.60	26.44
Pp3.0	10	2218.60	16.73	2223.58	24.50
Pp3.0fa	30	2212.34	14.17	2234.62	20.85

The enhanced elasticity of the mix may be due to the foldability of the plastic (Saxena et al., 2018) combined with the columnar shape of the aggregate to offer absorption of additional compressive strength. It is also possible that the 2 mm × 3 mm particle size of plastic aggregate used, rather than developing further air voids as previously mentioned, actually minimised air voids during the initial compaction of concrete into cube moulds and offered a positive contribution to the overall grading of the aggregates in the concrete mix, shown in previous research (Thorneycroft et al., 2018; Zaleska et al., 2018b; Ejiogu et al., 2018), and the current experiment, to increase compressive strength.

In general, plastic-containing concrete mixes (excluding mix PP3.0FA) marginally failed to achieve the ST5 standardised prescribed concrete mix compressive strength requirement. At 28 days curing, the compressive strength of 25 N/mm^2 required for classification of plastic-containing concrete mixes (excluding mix PP3.0FA) as hosting sufficient strength for an ST5 standardised prescribed concrete mix failed to be achieved by an average of 0.27 N/mm^2 (or 1.1%). It was experienced, however, that 2 out of the 5 mixes (excluding PP3.0FA) exceeded

the 25 N/mm^2 requirements, with mix PP1.5 and PP2.5 achieving 25.23 and 26.44 N/mm^2, respectively. It can be said that when considering the partial factors of safety applied to the structural application of concrete, with the use of the plastic aggregate applied, and the compressive strength findings in the current experiment, replacing fine aggregate in the concrete mix by mass can be applied up to a maximum of 3.0%, without a significant reduction in compressive strength of the concrete mix.

The use of fly ash as a 10% partial replacement by mass of cement further reduced compressive strength. As seen in Figure 9.3, at 7 days curing, mix PP3.0FA offered a compressive strength of 14.17 N/mm^2, being a 7.05 N/mm^2 (or 33.2%) reduction on the control mix, and a 2.56 N/mm^2 (or 15.3%) reduction on the concrete mix hosting the equivalent level of plastic and 100% cement mix PP3.0. This trend continued at 28 days curing when compared to the control mix, a 9.65 N/mm^2 (or 31.6%) reduction in compressive strength was experienced to 20.85 N/mm^2; interestingly, fly ash caused a similar reduction at 28 days curing to that of 7 days curing of 14.9% (or 3.65 N/mm^2) when compared to mix PP3.0. At both curing dates, the addition of fly ash caused the most significant reduction in compressive strength of all mixes assessed in the current experiment. It was finally apparent that the early development of compressive strength was not significantly influenced with the addition of fly ash to the mix, and when compared to mix PP3.0, mix PP3.0FA slowed the development of compressive strength at 7 days by 0.32% with mix PP3.0 achieving 68.28% of the final 28-day compressive strength at 7 days curing, and mix PP3.0FA 67.96%, respectively.

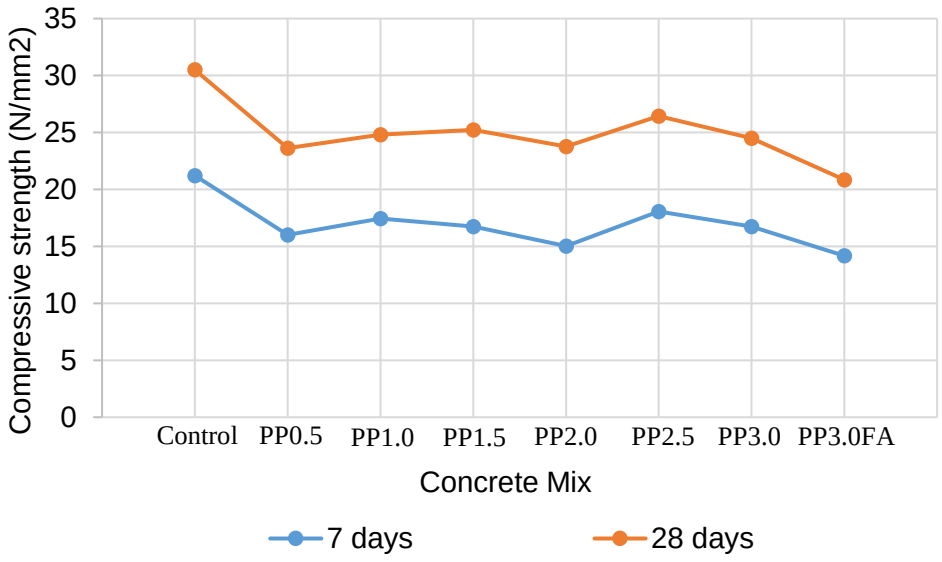

Figure 9.3: Compressive strength results of all concrete mixes at 7 and 28 days curing

9.2.3 Plastic Particles Distribution

Concrete specimens cast in this experiment, broken in half following compressive strength testing at respective 7 and 28 days curing, can be seen typically in Figure 9.4 at 28 days curing. Breaking of concrete specimens following compressive strength testing at both 7 and 28 days curing demonstrated plastic aggregate used in this experiment were evenly distributed throughout each respective 150mm^3 concrete cube. This finding suggests that the plastic aggregate used in this experiment was not affected by hand compaction, vibration, or curing conditions and was evenly sampled for each mix.

a) Control

b) PP0.5

c) PP1.0

d) PP1.5

e) PP2.0 f) PP2.5

g) PP3.0 h) PP3.0FA

Figure 9.4: Breaking of concrete cubes per mix at 28 days curing

9.3 Summary

In this part of the research, the influence of recycled PP plastic aggregate on the compressive strength and workability of concrete was assessed. Based on the results, the following summary is drawn:

- It is typically seen that workability is negatively affected by the addition of plastic aggregate, worsening further as additional plastic is incorporated into the concrete mix.
- The increased surface area of columnar-shaped, smooth textured plastic aggregate used in this experiment appeared to increase frictional resistance and viscosity within the mixing matrix, thus limiting free movement between particles contained within the concrete mix and reducing workability.
- The current experimental work demonstrated a typical decline in compressive strength with the addition of plastic aggregate, despite this reduction generally mitigated as the level of plastic in the concrete mix increased.
- Two of the seven plastic-containing concrete mixes tested in the current experimental work exceeded the ST5 standardised prescribed concrete mix compressive strength requirement at 28 days curing of 25 N/mm^2, being mix PP1.5 and PP2.5 (containing

1.50% and 2.50% plastic aggregate, respectively), whereby the remaining plastic-containing concrete mixes failed to achieve this requirement by an average of 0.27 N/mm^2.

- For all concrete mixes tested in the current experimental work, breaking of hardened concrete cube specimens at both 7 and 28 days curing demonstrated no bias distribution of concrete mix materials, including plastic aggregate.
- Whilst not the direct focus of the current experimental work, it appears the incorporation of fly ash as a partial replacement of cement in the concrete mix positively influences workability, however, unless incorporation of fly ash is managed carefully, as with traditional concrete containing only cement, the physical and chemical characteristics of fly ash can significantly, and negatively, influence the compressive strength of the concrete mix.

10 Conclusion and Suggestions for Future Research

10.1 Conclusion

This PhD research focused on enhancing structural performance and financial and environmental sustainability of construction through modifications in the design and developing an innovative beam-column connection to reduce the consumed cement and aggregate in the construction industry. The research findings are provided in more details in the following:

- This research showed that shear walls in low to medium-rise reinforced concrete frame buildings in the UK could be removed while improving construction sustainability in the economy and environment. This was achieved by reducing the amount of concrete used in the construction while providing adequate serviceability and strength for the case study.
- The proposed case study was located in various areas in the UK, e.g. Birmingham, Edinburgh, Belfast and Shetland Island, with different latitude and wind pressure to investigate the climate influence on the structural performance of buildings. It was shown that all the buildings (except for Shetland Island) could provide safe structural performance within the safe range defined by Eurocodes.
- The investigation on key factors including optimised concrete grade, column size, column shape and slab thickness was carried out on the case study. The results showed that increasing the slab thickness by ten percent can directly add up to two more storeys to the maximum overall height in RC frame buildings. Also, it was noticed that the governing limitation was punching shear ratio, and with a value of 2, the maximum overall height could reach up to 13 storeys to comply with Eurocodes limits.
- The Mini-Haunch connection was designed and experimentally compared with a standard connection. This design was developed to promote the use of moment-resisting

frames in UK construction instead of shear walls and reduce the amount of consumed concrete. According to the results, the frames' behaviour opposed to vertical loading for standard and Mini-Haunch connections were quite similar in terms of capacity even though the Mini-Haunch connection was constructed with lower concrete strength. Moreover, the results for horizontal loading demonstrated that the Mini-Haunch connection provided a significant enhancement in capacity, ductility and higher energy absorption in the elastic region (resilience) to withstand and absorb the applied lateral forces in comparison to the standard connection.

- The results proved the effectiveness of the Mini-Haunch connection to comply with the strong column-weak beam concept. In this regard, it was demonstrated that the failure in the frame with Mini-Haunch connection occurred in beams rather than columns or connections, while for the standard connection, the failure initiated from the connection.
- The results on the application of partially substituting fine aggregate with Polypropylene showed that two of seven Polypropylene containing concrete mixes tested in the experimental work exceeded the ST5 standardised prescribed concrete mix compressive strength requirement. This result illustrated the potential of plastic polymers in concrete mix designs to reduce the amount of consumed natural resources in the construction industry.

10.2 Recommendations for further research

This PhD research covered the identified gaps in knowledge by investigating the application of reinforced concrete moment-resisting frames and addressing the identified issues in the construction industry with regard to development in the design of moment-resisting frames in high-wind regions. These advances include the prospect of eliminating shear walls in UK typical buildings, examining the effect of various factors on structural performance and the overall height constraint of reinforced concrete (RC) moment-resisting frames and producing a

guideline for the design and construction of moment-resisting frames in the UK. Also, an innovative and efficient connection was designed in RC moment-resisting frames to effectively improve the limitations of this system further.

There are also other areas of reinforced concrete structures that need additional research and improvement, including the following criteria:

- Since the lateral loading of the scaled frames in this research was conducted using finite element simulations, it is advised that the lateral performance of the Mini-Haunch connection to be studied by experimental studies.
- The findings of this research have shown a satisfactory outcome for the use of polypropylene in the design of the concrete mix. It is proposed that the effect of polypropylene as a fine aggregate substitute on the mechanical and thermal properties of the concrete mixture be studied in order to understand further the characteristics of this plastic polymer in the design of the concrete mixture.
- As an advancement to the use of Polypropylene in the concrete mix design, it is proposed to carry out experimental studies on the performance of scaled reinforced concrete frames using polypropylene-containing concrete mixtures in order to observe the effect of this mixture design on scaled prototypes.
- As shown in this research, the Mini-Haunch connection can improve the structural performance of RC frames subjected to vertical and horizontal loading. It is proposed to investigate further the performance of this connection in seismic regions through experimental and finite element simulation studies.

References

3ds.com. 2007. Abaqus Unified FEA - SIMULIA™ By Dassault Systèmes®. [online] Available at: <https://www.3ds.com/products-services/simulia/products/abaqus/> [Accessed 13 September 2020].

Aainawala, M. and Pajgade, P. (2014). Design of Multistoried R.C.C. Buildings with and without Shear Walls. International Journal Of Engineering Sciences & Research Technology, 7(3), pp.498-510.

Aalto, J. & Neuman, E. (2017), Comparison of punching shear design provisions for flat slabs, Master Thesis, Royal Institute of Technology (KTH), Stockholm, Sweden.

ABAQUS/CAE User's Manual (2013). 6th ed. Providence, RI, USA: Dassault Systèmes Simulia.

Adam, M., Said, M., Mahmoud, A. and Shanour, A., 2015. Analytical and experimental flexural behavior of concrete beams reinforced with glass fiber reinforced polymers bars. Construction and Building Materials, 84, pp.354-366.

Adheem, A., 2013. Nonlinear analysis of reinforced concrete beams strengthened in shear with NSM FRP rods. Journal of University of Babylon for Engineering Sciences, 21(1), pp.160-173.

Akhil Ahamad, S. and Pratap, K., 2020. Dynamic analysis of G + 20 multi storied building by using shear walls in various locations for different seismic zones by using Etabs. Materials Today: Proceedings.

Alkarani & Ravindra, R. (2013), Evaluation of punching shear in flat slabs, International Journal of Research in Engineering and Technology, Bangalore, India, November.

Al-Rousan, R., 2020. Behavior of Circular Reinforced Concrete Columns Confined with CFRP Composites. Procedia Manufacturing, 44, pp.623-630.

Al-Tamimi, A., Ibrahim, A. and Al-Sughaiyer, N., 2014. Evaluation of Sustainability of Multistory Reinforced Concrete Structure. Physics Procedia, 55, pp.445-450.

Aly, A. & Abburu, S. (2015), on the design of high-rise buildings for multi-hazard: fundamental differences between wind and earthquake demand, Shock and Vibration, 2015(1), 1-22. https://doi.org/10.1155/2015/148681.

Ambrose, J. & Vergun, D. (1995), Simplified Building Design For Wind And Earthquake Forces, Wiley, New York, NY, USA.

Archer, C. and Jacobson, M. (2005). Evaluation of global wind power. Journal of Geophysical Research, 110(D12).

Asha, P. and Sundararajan, R., 2011. Seismic Behaviour Of Exterior Beam-Column Joints With Square Spiral Confinement. Asian Journal Of Civil Engineering (Building And Housing), 12(3).

Avşar, Ö., Bayhan, B. & Yakut, A. (2012), Effective flexural rigidities for ordinary reinforced concrete columns and beams, The Structural Design of Tall and Special Buildings, 23(6), 463-482. https://doi.org/10.1002/tal.1056.

Babafemi, A.J., Savija, B., Paul, S.C. and Anggraini, V. (2018) Engineering Properties of Concrete with Waste Recyled Plastic: A Review. Sustainability, 10(11), p.1-26. (Available at: https://www.mdpi.com/2071-1050/10/11/3875).

Balineni, H., Jagarapu, D. and Eluru, A., 2020. Analysis of dry and wet connections in precast beam-column joint using ABAQUS software. Materials Today: Proceedings.

Banks, C., Burridge, J., Cammelli, S. & Chiorino, M. (2014), Tall Buildings - Structural Design Of Concrete Buildings Up To 300 M Tall, MPA The Concrete Centre and Fédération internationale du béton (fib), London, UK.

Barr, J., 2017. Regression Results For Skyscraper And Height Happiness. Rutgers University-Newark.

Bathe, K., 2016. Finite Element Procedures. 2nd ed. New Jersey: Prentice Hall, Pearson Education, Inc.

Belletti, B., Walraven, J. and Trapani, F., 2015. Evaluation of compressive membrane action effects on punching shear resistance of reinforced concrete slabs. Engineering Structures, 95, pp.25-39.

Bernal, D. (1987), Amplification factors for inelastic dynamic p–Δ effects in earthquake analysis, Earthquake Engineering & Structural Dynamics, 15(5), 635-651. https://doi.org/10.1002/eqe.4290150508.

Bond, A. (2011), How To Design Concrete Structures Using Eurocode 2, MPA - The Concrete Centre, Camberley, Surrey, UK.

Bond, A., Brooker, O., Harris, A., Harrison, T., Moss, R., Narayanan, R. and Webster, R. (2006). How to Design Concrete Structures using Eurocode 2. London: The Concrete Centre.

Breccolotti, M., Gentile, S., Tommasini, M., Materazzi, A., Bonfigli, M., Pasqualini, B., Colone, V. and Gianesini, M., 2016. Beam-column joints in continuous RC frames: Comparison between cast-in-situ and precast solutions. Engineering Structures, 127, pp.129-144. https://doi.org/10.1016/j.engstruct.2016.08.018.

Breeze, G. (2011), Dynamic Comfort Criteria for Structures, BRE Trust, Watford, UK.

British Standards Institution (2000) BS EN 12390-4:2000: Testing Hardened Concrete Part 4– Compressive Strength – Specification for Testing Machines. London: British Standards Institute.

British Standards Institution (2008) BS EN 12620:2002+A1:2008 (Incorporating Corrigendum May 2004): Aggregates for Concrete. London: British Standards Institute.

British Standards Institution (2009c) BS EN 12350-2:2009: Testing Fresh Concrete Part 2 – Slump Test. London: British Standards Institute.

British Standards Institution (2011) BS EN 12390-3:2009 (Incorporating Corrigendum August 2011): Testing Hardened Concrete Part 3 – Compressive Strength of Test Specimens. London: British Standards Institute.

British Standards Institution (2015) BS EN 197-1:2011 (Incorporating Corrigenda November 2011 and October 2015): Cement Part 1: Composition, Specifications and Conformity Criteria for Common Cements. London: British Standards Institute.

British Standards Institution (2016a) BS 8500-1:2015+A1:2016 (Incorporating Corrigendum No. 1): Concrete – Complementary British Standard to BS EN 206 Part 1: Method of Specifying and Guidance for the Specifier. London: British Standards Institute.

British Standards Institution (2016b) BS 8500 2:2015+A1:2016: Concrete – Complementary British Standard to BS EN 206 Part 2: Specification for Constituent Materials and Concrete. London: British Standards Institute.

British Standards Institution (2016c) BS EN 206:2013+A1:2016 (Incorporating corrigendum May 2014): Concrete — Specification, Performance, Production and Conformity. London: British Standards Institute.

Broth, Z. and Hoult, N., 2020. Dynamic distributed strain sensing to assess reinforced concrete behaviour. Engineering Structures, 204, p.110036.

Bryman, A., 2012. Social Research Methods. Johanneshov: TPB.

BS EN 1990. (2017), Eurocode 0: Basis of Structural Design, British Standards, London, UK.

BS EN 1991-1-1. (2002), Eurocode 1: Actions on Structures - Part 1-1: General Actions - Densities, Self-Weight, Imposed Loads for Buildings, British Standards, London, UK.

BS EN 1991-1-4. (2010), Eurocode 1: Actions on Structures - Part 1-4: General Actions - Wind Actions, British Standards, London, UK.

BS EN 1992-1-1. (2014), Eurocode 2: Design of Concrete Structures - Part 1-1: General Rules and Rules for Buildings, British Standards, London, UK.

BS EN 1998-1. (2004), Eurocode 8: Design of structures for earthquake resistance - Part 1: General rules, seismic actions and rules for buildings, British Standards, London, UK. https://doi.org/10.3403/03244372.

BS EN 206-1. (2013), concrete. Specification, Performance, Production and Conformity, British Standards, London, UK. https://doi.org/10.3403/02248618U.

Building Materials, 161(1), p.63-69. (Available at: https://www-sciencedirectcom.ezproxy.uwl.ac.uk/science / article/pii/S0950061817323474).

Building a Low-Carbon Economy, 2008. 1st ed. London: The Stationery Office.

Calavera, J., 2012. Manual For Detailing Reinforced Concrete Structures To EC2. Spon Press.

Cao, X., Wu, L. and Li, Z., 2020. Behaviour of steel-reinforced concrete columns under combined torsion based on ABAQUS FEA. Engineering Structures, 209, p.109980.

Carreira, D. and Chu, K., 1985. Stress-Strain Relationship for Plain Concrete in Compression. ACI Journal Proceedings, 82(6). https://doi.org/10.14359/10390.

Casaburo, A., Petrone, G., Franco, F. and De Rosa, S., 2019. A Review of Similitude Methods for Structural Engineering. Applied Mechanics Reviews, 71(3).

Ceanet.com.au. (2018). ETABS. [Online] Available at: http://www.ceanet.com.au/Products/ETABS.aspx [Accessed 13 Aug. 2018].

Chandurkar, P. and Pajgade, P. (2013). Seismic Analysis of RCC Building with and Without Shear Wall. International Journal of Modern Engineering Research (IJMER), 3(3), pp.1805-1810.

Chen, C. and Lin, K., 2009. Behavior and strength of steel reinforced concrete beam–column joints with two-side force inputs. Journal of Constructional Steel Research, 65(3), pp.641-649. https://doi.org/10.1016/j.jcsr.2008.03.010.

Chen, C., Suswanto, B. and Lin, Y., 2009. Behavior and strength of steel reinforced concrete beam–column joints with single-side force inputs. Journal of Constructional Steel Research, 65(8-9), pp.1569-1581. https://doi.org/10.1016/j.jcsr.2009.04.003.

Choi, H., Choi, Y. and Choi, C., 2013. Development and testing of precast Concrete beam-to-column connections. Engineering Structures, 56, pp.1820-1835. https://doi.org/10.1016/j.engstruct.2013.07.021.

Chudley, R. and Greeno, R. (2016) Building Construction Handbook. 11th Ed. Oxon: Routledge.

Ciarlet, P. and Lions, J., 1991. Finite Element Methods (Part 1). Amsterdam: North Holland.

Cismasiu, C., Ramos, A., Moldovan, I., Ferreira, D. and Filho, J. (2017). Applied element method simulation of experimental failure modes in RC shear walls. Computers and Concrete, 19(4), pp.365-374.

Cohen, L., Manion, L. and Morrison, K., 2009. Research Methods In Education. London: Routledge.

Coutinho, C., Baptista, A. and Dias Rodrigues, J., 2016. Reduced scale models based on similitude theory: A review up to 2015. Engineering Structures, 119, pp.81-94.

Cresswell Riol, B., 2007. Standard Method Of Detailing Structural Concrete. London: Institution of Structural Engineers.

Creswell, J., 2003. Research Design. Thousand Oaks: Sage Publications, p.7.

Croke, B. (2017) Developing a Polypropylene Recycling Infrastructure [Online]. (Available at: https://search-proquestcom.ezproxy.uwl.ac.uk/docview/1907238538?pqorigsite=summon)

Dai, X., Lam, D., Jamaluddin, N. and Ye, J., 2014. Numerical analysis of slender elliptical concrete filled columns under axial compression. Thin-Walled Structures, 77, pp.26-35.

Darwin, D., Nilson, A. and Dolan, C., 2016. Design Of Concrete Structures. New York: McGraw-Hill Education.

Davies, A., 2018. Modern Methods Of Construction. London: Royal Institution of Chartered Surveyors (RICS), pp.6-7.

Dassault Systèmes, 2018. Abaqus FEA. ABAQUS Inc.

Department for Business, Energy and Industrial Strategy (2018) Monthly Statistics of Building Materials and Components: August 2018, No. 522 [Online] (Available at:https://assets.publishing.service.gov.uk/government/uploads/system/uploads/attachment_data/file/737942/18-cs9__Construction_Building_Materials__Bulletin_August_2018.pdf).

Dhir, R., Hewlett, P. and Csetenyi, L., 2002. Innovations and Developments in Concrete Materials and Construction. In: Proceedings of the International Conference held at the University of Dundee. Dundee: Thomas Telford Publishing, p.iii. https://doi.org/10.1680/iadicmac.31791.

Dok, G., Caglar, N., Ilki, A. and Yilmaz, C., 2020. Effect of impact loading on residual flexural capacity of high-strength reinforced concrete beams. Structures, 27, pp.2466-2480.

Earij, A., Alfano, G., Cashell, K. and Zhou, X., 2017. Nonlinear three-dimensional finite-element modelling of reinforced concrete beams: Computational challenges and experimental validation. Engineering Failure Analysis, 82, pp.92-115. https://doi.org/10.4203/ccp.108.3.

Ejiogu, I. K., Ejiogu. P. A. P., Nkeonye, P. O. and Yaro, S. A. (2018) The Effect of ElevatedTemperature on the Mechanical Properties of Waste Plastics Polyethylene Trephthalate (PET) and Low Density Polyethylene (LDPE) Filled Normal Concrete Blocks. International Journal for Research in Applied Science & Engineering Technology, 6(5), p.1510-1520.(Available at: http://www.ijraset.com/fileserve.php?FID=16084)

Elchalakani, M., Karrech, A., Dong, M., Mohamed Ali, M. and Yang, B., 2018. Experiments and Finite Element Analysis of GFRP Reinforced Geopolymer Concrete Rectangular Columns Subjected to Concentric and Eccentric Axial Loading. Structures, 14, pp.273-289.

Ele International (2011) ADR-Auto V2.0 Range Accurate and Consistent Testing [Online] (Available at: http://www.testele.fi/pdf/ADR_Auto_V2_Brochure_Datasheet_09_11.pdf)

Ele International (2017) Operating Instructions: Large Curing Tank - 34-6575 Series[Online] (Available at: https://www.ele.com/Product/large-curing-tank-c-w-with-circulatingpump-heater-thermostat-unit-and-lower-rack/79)

Ele International (2019a) 150mm Cube Mould 2-Part Clamp Type, Cast Iron Construction,BS EN Compliant (34-4670)

Ele International (2019b) Slump Test Set BS & ASTM. C/W Slump Cone Base Plate SteelRule Tamping Rod & Funnel (34-0192) [Online]. (Available at:https://www.ele.com/Product/slump-test-set-bs-astm-c-w-slump-cone-base-plate-steel-ruletamping-rod-funnel-/66).

Emporis (2008), Low-rise building (ESN 49213); Emporis GMBH, Hamburg, Germany. www.emporis.com/building/standard/15/low-rise-building.

Emporis (2009), High-rise building (ESN 18727); Emporis GMBH, Hamburg, Germany. www.emporis.com/building/standard/3/high-rise-building.

ETABS. (2018), ETABS software; Computers and Structures Inc, New York, USA. www.csiamerica.com/products/etabs

Eurocode 8: Design of structures for earthquake resistance. (2013). London: BSI Standards Limited.

European Commission, 2016. The European Construction Sector. Internal Market, Industry, Entrepreneurship and SMEs Directorate General.

Farmer, M., 2016. The Farmer Review Of The UK Construction Labour Model. London: Construction Leadership Council (CLC), p.8.

G. S. Saisaran, V. Yogendra Durga Prasad & T. Venkat Das (2016), Pushover analysis for concrete structures at seismic zone-3 using ETABS software, International Journal of Engineering Research & Technology (IJERT), 5(3), 739-746.

Gan, V., Chan, C., Tse, K., Lo, I. and Cheng, J., 2017. A comparative analysis of embodied carbon in high-rise buildings regarding different design parameters. Journal of Cleaner Production, 161, pp.663-675.

Gardner, D., Lark, R., Jefferson, T. and Davies, R., 2018. A survey on problems encountered in current concrete construction and the potential benefits of self-healing cementitious materials. Case Studies in Construction Materials, 8, pp.238-247.

Gardner, A., 2015. Stability of Buildings Part 4: Moment Frames. London: Institution of Structural Engineers.

Genikomsou, A. and Polak, M., 2015. Finite element analysis of punching shear of concrete slabs using damaged plasticity model in ABAQUS. Engineering Structures, 98, pp.38-48.

Ghayeb, H., Razak, H. and Sulong, N., 2017. Development and testing of hybrid precast concrete beam-to-column connections under cyclic loading. Construction and Building Materials, 151, pp.258-278. https://doi.org/10.1016/j.conbuildmat.2017.06.073.

Ghorpade, A. and Swamy, B. (2018). Study on the Performance of Flat Slab Structure Using Pushover Analysis With and Without Shear Wall. International Research Journal of Engineering and Technology (IRJET), 5(7), pp.660-665.

González, M. and García Navarro, J., 2006. Assessment of the decrease of CO2 emissions in the construction field through the selection of materials: Practical case study of three houses of low environmental impact. Building and Environment, 41(7), pp.902-909.

Goodchild, C. (2009), Worked Examples To Eurocode 2, The Concrete Centre, Camberley, Surrey, UK.

Goodchild, C., Webster, R. and Elliott, K. (2009). Economic concrete frame elements to Eurocode 2. Surrey: The Concrete Center.

Gorse, C., Johnston, D. and Pritchard, M. (2012) A Dictionary of Construction, Surveying and Civil Engineering. Oxford: Oxford University Press.

Group (2018) Axpoly ABS52 1007 – Product Information Sheet: Black ABS ResinGrade [Online] (Available at:https://axiongroup.co.uk/wp/wpcontent /uploads/2019/01/axpoly-abs52-1007-product-info-sheet.pdf).

Hassan, N., Sherif, A. and Zamarawy, A., 2017. Finite element analysis of reinforced concrete beams with opening strengthened using FRP. Ain Shams Engineering Journal, 8(4), pp.531-537.

Hemalatha, T. and Ramaswamy, A. (2017) A review on fly ash characteristics e Towards promoting high volume utilization in developing sustainable concrete. Journal of Cleaner Production, 147, p.546-559. (Available at: https://www-sciencedirectcom.ezproxy.uwl.ac.uk/science/article/pii/S0959652617301294)

Hobbs, D., 2001. Concrete deterioration: causes, diagnosis, and minimising risk. International Materials Reviews, 46(3), pp.117-144.

Holmes, J. (2004). Wind loading of structures. London: Spon Press.

Homes England (2018) Housing Statistics: 1 April 2018 – 30 September 2018 [Online] (Available at: https://assets.publishing.service.gov.uk/government/uploads/system/uploads/attachment_data/file/760193/Housing_Statistics_November_2018.pdf).

Hosseini, M., Hosseini, H. and Hosseini, A. (2014). Study Effective of Wind Load on Behavior of ShearWall in Frame Structure. Journal of Engineering Research and Applications, 4(11), pp.23-33.

Höweler, E. (2003), Skyscraper, Thames & Hudson, London, UK.

Huang, B., Li, Q., Xu, S. and Zhang, L., 2019. Static and fatigue performance of reinforced concrete beam strengthened with strain-hardening fiber-reinforced cementitious composite. Engineering Structures, 199, p.109576.

Huang, M., Li, Q., Chan, C., Lou, W., Kwok, K. and Li, G., 2015. Performance-based design optimization of tall concrete framed structures subject to wind excitations. Journal of Wind Engineering and Industrial Aerodynamics, 139, pp.70-81.

Huang, Y., Mazzarolo, E., Briseghella, B., Zordan, T. and Chen, A., 2017. Experimental and numerical investigation of the cyclic behaviour of an innovative prefabricated beam-to-column joint. Engineering Structures, 150, pp.373-389. https://doi.org/10.1016/j.engstruct.2017.07.056.

Hueste, M., Lepage, A., Wallace, J. and Browning, J. (2007). Seismic Design Criteria for Slab-Column Connections. ACI Structural Journal, 104(4), pp.448-458.

Hughes, A. (2014). Wind actions to BS EN 1991-1-4. Ascot: Steel construction Institute.

Hutt, C., 2017. Risk-Based Seismic Performance Assessmentof Existing Tall Steel Framed Buildings. Ph.D. University College London.

Hyeon-Jong, H., Gao, M. and Chang-Soo, K. (2019), Minimum thickness of flat plates considering construction load effect, Techno-Press, 69(1), 1-10. https://doi.org/10.12989/sem.2019.69.1.001.

Ibañez, C., Hernández-Figueirido, D. & Piquer, A. (2018), Shape effect on axially loaded high strength CFST stub columns, Journal of Constructional Steel Research, 147(1), 247-256. https://doi.org/10.1016/j.jcsr.2018.04.005.

Ingrid Cloud. (2018), Wind Simulations; Stockholm, Sweden. www.ingridcloud.com/product-tour/get-started/

Jacob-Vaillancourt, C. and Sorelli, L. (2018) Characterization of Concrete Composites with Recycled Plastic Aggregates from Postconsumer Material Streams. Construction and Building Materials, 182(1), p.561-575 (Available at:https://www.sciencedirectcom.ezproxy.uwl.ac.uk/science/article/pii/S0950061818314752).

Jayalekshmi, B. and Chinmayi, H. (2015). Seismic behavior of RC framed shear wall buildings as per IS 1893 and IBC provisions. Geomechanics and Engineering, 9(1), pp.39-55.

Jayasundara, H., Koliyabandara, S. and Wijesundara, K. (2017). Comparative Study of Diagrid System and Shear Wall System for Resisting Wind Loads Using Different Design Approaches. Sri Lanka: SOCIETY OF STRUCTURAL ENGINEERS, pp.1-9.

Jirawattanasomkul, T., Likitlersuang, S., Wuttiwannasak, N., Ueda, T., Zhang, D. and Shono, M., 2020. Structural behaviour of pre-damaged reinforced concrete beams strengthened with natural fibre reinforced polymer composites. Composite Structures, 244, p.112309.

Johann, F., Carlos, M. and Ricardo, F. (2015). Wind-induced motion on tall buildings: A comfort criteria overview. Journal of Wind Engineering and Industrial Aerodynamics, 142, pp.26-42.

Jolly, A. & Vijayan, V. (2016), Structural Behaviour of Reinforced Concrete Haunched Beam A Study on ANSYS and ETABS, International Journal of Innovative Science, Engineering & Technology, 3(8), 495-500.

Kaliluthin, A., Kothandaraman, S. and Suhail Ahamed, T., 2014. A Review on Behavior of Reinforced Concrete Beam-Column Joint. International Journal of Innovative Research in Science, Engineering and Technology, 3(4), pp.11299-11310.

Kaung, J. and Wong, H., 2011. Effectiveness of Horizontal Stirrups in Joint Core for Exterior Beam-Column Joints with Nonseismic Design. Procedia Engineering, 14, pp.3301-3307. https://doi.org/10.1016/j.proeng.2011.07.417.

Kazaz, İ., Yakut, A. and Gülkan, P., 2006. Numerical simulation of dynamic shear wall tests: A benchmark study. Computers & Structures, 84(8-9), pp.549-562.

Kent, D. and Park, R., 1971. Flexural Members with Confined Concrete. Journal of the Structural Division, 97(7), pp.1969-1990.

Khanh, B., 2012. Developing A Framework For Assessing Sustainability Of Tall-Building Projects. Ph.D. University of Sheffield.

Kim, N., Kwak, Y. and Chang, S., 2003. Modified Similitude Law for Pseudodynamic Test on Small-scale Steel Models. Journal of the Earthquake Engineering Society of Korea, 7(6), pp.49-57. https://doi.org/10.5000/EESK.2003.7.6.049.

Kim, N., Lee, J. and Chang, S., 2009. Equivalent multi-phase similitude law for pseudodynamic test on small scale reinforced concrete models. Engineering Structures, 31(4), pp.834-846. https://doi.org/10.1016/j.engstruct.2008.06.008.

Kline, S., 1986. Similitude and Approximation Theory, Springer, New York, USA. https://doi.org/10.1007/978-3-642-61638-9.

Kwok, K., Hitchcock, P. and Burton, M. (2009). Perception of vibration and occupant comfort in wind-excited tall buildings. Journal of Wind Engineering and Industrial Aerodynamics, 97(7-8), pp.368-380.

LaFarge (2008) Blue Circle Cement: Data Sheet [Online] (Available at: http://www.beersltd.co.uk/downloads/ coshh/blue_circle_cement_CEMII.pdf).

Lapi, M., Ramos, A. & Orlando, M. (2019), Flat slab strengthening techniques against punching-shear, Engineering Structures, 180(1), 160-180. https://doi.org/10.1016/j.engstruct.2018.11.033.

Lee, S., Abolmaali, A., Shin, K. and Lee, H., 2020. ABAQUS modeling for post-tensioned reinforced concrete beams. Journal of Building Engineering, 30, p.101273.

Li, Q., Wu, J., Fu, J., Li, Z. & Xiao, Y. (2010), Wind effects on the world's tallest reinforced concrete building, Proceedings of the Institution of Civil Engineers - Structures and Buildings, 163(2), 97-110. https://doi.org/10.1680/stbu.2010.163.2.97.

Li, Y., Zhang, J. and Li, Q. (2014), Experimental investigation of characteristics of torsional wind loads on rectangular tall buildings, Structural Engineering and Mechanics, 49(1), 129-145. https://doi.org/10.12989/sem.2014.49.1.129.

Lu, W., Chen, T. and Lin, I., 2015. Shear strength of reinforced concrete dapped-end beams with shear span-to-depth ratios larger than unity. Journal of Marine Science and Technology (Taiwan), 23(4). https://doi.org/10.6119/JMST-015-0511-1.

Lu, X., Urukap, T., Li, S. and Lin, F., 2012. Seismic behavior of interior RC beam-column joints with additional bars under cyclic loading. Earthquakes and Structures, 3(1), pp.37-57.

Malhotra, V., 2010. Global warming and role of supplementary cementing materials and superplasticisers in reducing greenhouse gas emissions from the manufacturing of Portland cement. International Journal of Structural Engineering, 1(2), p.116.

Mander, J., Priestley, M. and Park, R. (1988), Theoretical Stress-Strain Model for Confined Concrete, Journal of Structural Engineering, 114(8), 1804-1826.

Masi, A., Santarsiero, G., Lignola, G. and Verderame, G., 2013. Study of the seismic behavior of external RC beam–column joints through experimental tests and numerical simulations. Engineering Structures, 52, pp.207-219.

MayField, B., Kong, K. and Bennison, A., 1971. Corner joint details in structural light weight concrete. ACI Proceedings, 68(5), pp.366-372. https://doi.org/10.14359/11336.

Melbourne, W. & Palmer, T. (1992), Accelerations and comfort criteria for buildings undergoing complex motions. Journal of Wind Engineering and Industrial Aerodynamics, 41(1-3), 105-116. https://doi.org/10.1016/0167-6105(92)90398-T.

Mendis, P., Ngo, T., Haritos, N. and Hira, A., 2007. Wind Loading on Tall Buildings. Electronic Journal of Structural Engineering, 7(1).

Met Office. (2018). UK snow and facts. [Online] Available at: https://www.metoffice.gov.uk/learning/precipitation/snow/snow-in-the-uk [Accessed 20 Jul. 2018].

Moreno, C. & Sarmento, A. (2011), Punching shear analysis of slab-column connections, International Conference on Recent Advances in Nonlinear Models – Structural Concrete Applications, Coimbra, Portugal, November.

Monserrat López, A., Miguel Sosa, P., Bonet Senach, J. and Fernández Prada, M., 2020. Experimental study of shear strength in continuous reinforced concrete beams with and without shear reinforcement. Engineering Structures, 220, p.110967.

MPA - The Concrete Centre, Camberley, Surrey, UK.

Murty, C., Goswami, R., Vijayanarayanan, A. & Mehta, V. (2012), Some Concepts in Earthquake Behaviour of Buildings, Gujarat State Disaster Management Authority, Gujarat, India.

Musson, R. and Sargeant, S. (2007). Eurocode 8 seismic hazard zoning maps for the UK. Seismology and Geomagnetism Programme. British Geological Survey, pp.42-43.

National building code of Canada. (2010), Canadian Commission on Building and Fire Codes (CCBFC), National Research Council Canada, Institute Ottawa, Canada.

Naveen E, S., Abraham, N. and S D, A., 2019. Analysis of Irregular Structures under Earthquake Loads. Procedia Structural Integrity, 14, pp.806-819.

Nie, X., Fu, B., Teng, J., Bank, L. and Tian, Y., 2020. Shear behavior of reinforced concrete beams with GFRP needles. Construction and Building Materials, 257, p.119430.

Nikishkov, G., 2004. Introduction To The Finite Element Method.

Omni-Cem (2011) Report for EON-UK: Ratcliffe PFA and FBA Samples. Internal Omni-Cem report. Unpublished.

Ortiz, O., Castells, F. and Sonnemann, G., 2009. Sustainability in the construction industry: A review of recent developments based on LCA. Construction and Building Materials, 23(1), pp.28-39.

Parastesh, H., Hajirasouliha, I. and Ramezani, R., 2014. A new ductile moment-resisting connection for precast concrete frames in seismic regions: An experimental investigation. Engineering Structures, 70, pp.144-157. https://doi.org/10.1016/j.engstruct.2014.04.001.

Paulay, R. and Scarpas, A., 1981. The behavior of exterior beam column joint. Bulletin of the New Zealand National Society for Earthquake Engineering, 14(3).

Paulay, T. & Priestley, M. (1992). Seismic Design of Reinforced Concrete and Masonry Buildings, J. Wiley & Sons, New York, NY, USA.

Peake, S., 2004. Delivering the Kyoto baby. Refocus, 5(1), pp.52-53.

Pettinga, D. & Priestley, N. (2008), Accounting for P-delta effects in structures when using direct displacement-based design, The 14th World Conference on Earthquake Engineering, Beijing, China, October.

Plastics Europe (2017) Plastics – the Facts 2017: An Analysis of European Plastics Production, Demand and Waste Data [Online]. (Available at: https://www.plasticseurope.org /application/files/1715/2111/1527/Plastics_the_facts_2017_FINAL_for_website.pdf).

Poonyakan, A., Rachakornkij, M., Wecharatana, M. and Smittakorn, W. (2018) Potential Useof Plastic Wastes for Low Thermal Conductivity Concrete. Materials, 11(10), p.2-17.(Available at: https://www.mdpi.com/1996-1944/11/10/1938).

Punch, K., 2005. Introduction To Social Research. London: Sage.

Punching shear reinforcement Shearail (2020), Max Frank article for Punching shear reinforcement Shearail; Bavaria, Germany. www.maxfrank.com/intl-en/products/reinforcement-technologies/06-punching-shear-reinforcement-shearail/

R. Wagner, "Plastics and Sustainability A valuation of Environmental Benefits, Costs and Opportunities for Continuous Improvements", Memphis, Tennessee, 2016.

Rabi, M., Cashell, K. and Shamass, R., 2019. Flexural analysis and design of stainless steel reinforced concrete beams. Engineering Structures, 198, p.109432. https://doi.org/10.1016/j.engstruct.2019.109432.

Rahman, A., Goh, W., Mohamad, N., Kamarudin, M. and Jhatial, A., 2019. Numerical analysis and experimental validation of reinforced foamed concrete beam containing partial cement replacement. Case Studies in Construction Materials, 11, p.e00297.

Ramu, M., Prabhu Raja, V. and Thyla, P., 2013. Establishment of structural similitude for elastic models and validation of scaling laws. KSCE Journal of Civil Engineering, 17(1), pp.139-144. https://doi.org/10.1007/s12205-013-1216-x.

Rasikan, A. and Rajendran, M. (2013). Wind Behavior of Buildings with and without Shear Wall. International Journal of Engineering Research and Applications (IJERA), 3(2), pp.480-485.

Rubio-de Hita (2018) Reuse of Plastic Waste of Mixed Polypropylene as Aggregate inMortars for the Manufacture of Pieces for Restoring Jack Arch Floors with Timber Beams. Journal of Cleaner Production, 198(1), p.1515-1525.

Sacramento, P., Ferreira, M., Oliveira, D. & Melo, G. (2012), Punching strength of reinforced concrete flat slabs without shear reinforcement, IBRACON Structures and Materials, 5(5), 659-691. https://doi.org/10.1590/S1983-41952012000500005.

Sato, J., Vecchio, F. and Andre, H., 1989. Scale-Model Testing of Reinforced Concrete Under Impact Loading Conditions. Canadian journal of civil engineering, 16(4), pp.459-466. https://doi.org/10.1139/l89-075.

Saxena, R., Siddique, S., Gupta, T., Sharma, R.K. Chaudhary, S. (2018) Impact Resistance and Energy Absorption Capacity of Concrete Containing Plastic Waste. Construction and Building Materials, 176(1), p.415-421. (Available at: https://www-sciencedirectcom. ezproxy.uwl.ac.uk/science/article/pii/S0950061818310948).

Schueller, W. (1977), High-Rise Building Structures, J. Wiley & Sons, New York, NY, USA.

Scott, A. (1998), Dimensions of Sustainability, E. & F.N. Spon, London, UK.

Sekaran, U., 1992. Research Methods For Business. New York: Wiley.

Sev, A., 2009. How can the construction industry contribute to sustainable development? A conceptual framework. Sustainable Development, 17(3), pp.161-173.

Shakir-Khali, H. and Mouli, M., 1990. Further tests on concrete-filled rectangular hollow-section columns. The Structural Engineer, 68(20), pp.405-413.

Shufeng, L., Qingning, L., Hao, Z., Haotian, J., Lei, Y. and Weishan, J., 2018. Experimental study of a fabricated confined concrete beam-to-column connection with end plates. Construction and Building Materials, 158, pp.208-216. https://doi.org/10.1016/j.conbuildmat.2017.10.025.

Simitses, G., Starnes, Jr., J. and Rezaeepazhand, J., 2000. Structural similitude and scaling laws for plates and shells - A review. 41st Structures, Structural Dynamics, and Materials Conference and Exhibit. https://doi.org/10.2514/6.2000-1383.

Singh, S., Nagar, R. & Agrawal, V. (2016), A review on properties of sustainable concrete using granite dust as replacement for river sand, Journal of Cleaner Production, 126(1), 74-87. https://doi.org/10.1016/j.jclepro.2016.03.114.

Smarzewski, P. (2018) Flexural Toughness of High-Performance Concrete with Basalt and Polypropylene Short Fibres. (Available at:https://www.sciencedirectcom.ezproxy.uwl.ac.uk/science/article/pii/S0263822318304227).

Smith, R. (2011). Deflection Limits in Tall Buildings—Are They Useful?. Structures Congress 2011.

Sosoi, G., Barbuta, M., Serbanoiu, A.A., Babor, D. and Burlacu, A. (2018) Waste as Aggregate Substitution in Polymer Concrete. Procedia Manufacturing, 22(1), p.347-351. (Available at:https://www.sciencedirect.com/science/article/ pii/S2351978918303469).

Spaceagecontrol.com. (2001). Relationship Among Displacement, Velocity, Frequency, and Acceleration During Sinusoidal Motion. [online] Available at: https://www.spaceagecontrol.com/calcsinm.htm [Accessed 14 Sep. 2018].

Sridhar, R. and Prasad, R., 2019. Vibration Based Damaged Detection of Steel Fiber Reinforced concrete. Materials Today: Proceedings, 18, pp.3321-3329.

Structural use of concrete - part 2. (2005). London: British Standards Institution.

Sümer, Y. and Aktaş, M., 2015. Defining parameters for concrete damage plasticity model. Challenge Journal of Structural Mechanics. https://doi.org/10.20528/cjsmec.2015.07.023.

Taleb, R., Bechtoula, H., Sakashita, M., Bourahla, N. and Kono, S. (2012), Investigation of the shear behaviour of multi-story reinforced concrete walls with eccentric openings, Computers & concrete, 10(4), 361-377. https://doi.org/10.12989/cac.2012.10.4.361.

Tarmac (2017) Cement Declaration of Performance Sheet [Online] (Available at:https://dop.asp-bd.co.uk/DOP_FILES/562355_Dunbar_mastercrete.pdf)

Thakur, A. and Singh, A. (2014). Comparative Analysis of a Multistoried Residential Building with and Without Shear Wall using STAAD Pro. International Journal of Recent Research Aspects, 1(1), pp.54-57.

The Concrete Society (2016) Good Concrete Guide 8: Concrete Practice – Guide on the Practical Aspects of Concreting. 2nd Ed. Camberley, Surrey: The Concrete Society.

The National Fire Protection Association (NFPA). (2016), High-Rise Building Fires, NFPA fire analysis & research, Quincy, MA, USA.

Thirumurugan, V., Ganesan, T., Satyanarayanan, K., Parthasarathi, N. and Prakash, M., 2020. Experimental behaviour on seven storeyed infilled frame with pneumatic interface pressure. Materials Today: Proceedings. https://doi.org/10.1016/j.matpr.2020.03.491.

Thomas, M. (2007) Concrete: Optimizing the Use of Fly Ash in Concrete. Portland CementAssociation. [Online] (Available at:https://www.cement.org/docs/defaultsource /Fc_concrete_technology/is548-optimizing-the-use-of-fly-ash-concrete.pdf).

Thorneycroft, J., Orr, J., Savoikar, P. and Ball, R.J. (2018) Performance of Structural Concrete with Recycled Plastic Waste as a Partial Replacement for Sand. Construction and

Travis Perkins (2019a) Travis Perkins Gravel and Shingle Trade Pack 10mm [Online] (Available at: https://www.travisperkins.co.uk/Travis-Perkins-Gravel-and-Shingle-Trade-Pack-10mm/p/996244)

Travis Perkins (2019b) Travis Perkins Grit/Sharp Sand Trade Pack [Online] (Available at: https://www.travisperkins.co.uk/Travis-Perkins-Grit-Sharp-Sand-Trade-Pack/p/996242)

Tsay, R. (2019), A study of BIM combined with ETABS in reinforced concrete structure analysis, IOP Conference Series: Earth and Environmental Science, 233(2), 1-6. https://doi.org/10.1088/1755-1315/233/2/022024.

Uher, T. and Lawson, W., 1998. Sustainable development in construction. In: Proceedings CIB World Building Congress. Rotterdam, Netherlands: in-house publishing.

Uma, S. and Jain, S., 2006. Seismic design of beam-column joints in RC moment resisting frames – Review of codes. Structural Engineering and Mechanics, 23(5), pp.579-597. https://doi.org/10.12989/sem.2006.23.5.579.

Unanwa, C., McDonald, J., Mehta, K. and Smith, D., 2000. The development of wind damage bands for buildings. Journal of Wind Engineering and Industrial Aerodynamics, 84(1), pp.119-149. https://doi.org/10.1016/s0167-6105(99)00047-1.

V.Chaudhari, S. and A. Chakrabarti, M., 2012. Modeling of Concrete for Nonlinear Analysis using Finite Element Code ABAQUS. International Journal of Computer Applications, 44(7), pp.14-18. https://doi.org/10.5120/6274-8437.

Vasudevan, G. and Kothandaraman, S., 2013. Vasudevan, G., Kothandaraman, S. (2011). Parametric study on Nonlinear Finite Element Analysis on Flexural Behavior of RC beams using

ANSYS, International Journal of Civil and Structural Engineering, Volume 2, No 1. International Journal of Civil & Structural Engineering, 2(1), pp.98-111.

Wang, F., Yang, J., Nyunn, S. and Azim, I., 2020. Effect of concrete infill walls on the progressive collapse performance of precast concrete framed substructures. Journal of Building Engineering, p.101461. https://doi.org/10.1016/j.jobe.2020.101461.

Wight, J., Richart, F. and MacGregor, J., 2012. Reinforced Concrete: Mechanics and Design. Upper Saddle River, N.J.: Pearson.

Wiki.csiamerica.com. (2018). Product Descriptions - Technical Knowledge Base - Computers and Structures, Inc. - Technical Knowledge Base. [Online] Available at: https://wiki.csiamerica.com/display/kb/Product+Descriptions [Accessed 7 Aug. 2018].

Xingyu, G., Yiqing, D. and Jiwang, J., 2020. Flexural behavior investigation of steel-GFRP hybrid-reinforced concrete beams based on experimental and numerical methods. Engineering Structures, 206, p.110117.

Xu, G. and Shi, X. (2018) Characteristics and Applications of Fly Ash as a Sustainable Construction Material: a State-of-the-Art Review. Resources, Conservation & Recycling, 136, p.95-109. (Available at: https://www-sciencedirect-com.ezproxy.uwl.ac.uk/science/article/pii/S092134491830140X)

Yao, Z.T., Ji, X.S., Sarker, P.K., Tang, J.H., Ge, L.Q., Xia, M.S. and Xi, Y.Q. (2015) AComprehensive Review on the Applications of Coal Fly Ash. Earth-Science Reviews, 141(1):p.105-121. (Available at:https://espace.curtin.edu.au/bitstream/handle/20.500.11937/17671/212814_139843_Paper_published_Earth_Sciences_Review_V_141_2015_pp_105-121.pdf?sequence=2)

Yılmaz, M. and Bakış, A., 2015. Sustainability in Construction Sector. Procedia - Social and Behavioral Sciences, 195, pp.2253-2262.

Zaki, M. and Rasheed, H., 2020. Behavior of reinforced concrete beams strengthened using CFRP sheets with innovative anchorage devices. Engineering Structures, 215, p.110689.

Zaleska, M., Pavlikova, M., Jankovsky, O., Lojka, M., Pivak, A. and Pavlik, Z. (2018c)Experimental Analysis of MOC Composite with a Waste-Expanded Polypropylene-Based Aggregate. Materials, 11(6), p.1-15. (Available at: https://www.mdpi.com/1996-1944/11/6/931)

Zaleska, M., Pavlikova, M., Studnicka, J. and Pavlik, Z. (2018a) Effect of Waste Expanded Polypropylene-Based Aggregate on Mechanical and Thermal Properties of Lightweight Concrete. IOP Conference Series: Materials Science and Engineering, 371(1), p.1-6. (Available at: http://iopscience.iop.org/article/10.1088/1757899X/371/1/012002/pdf).

Zaleska, M., Pavlikova, M., Studnicka, J. and Pavlik, Z. (2018b) Effect of Waste Expanded Polypropylene-Based Aggregate on Mechanical and Thermal Properties of Lightweight Concrete. IOP Conference Series: Materials Science and Engineering, 371(1), p.1-6.

Zhi, L., Chen, B. and Fang, M. (2015), Wind load estimation of super-tall buildings based on response data. Structural Engineering and Mechanics, **56**(4), 625-648. https://doi.org/10.12989/sem.2015.56.4.625.

Zhou, Y., Hu, X., Pei, Y., Hwang, H., Chen, T., Yi, W. and Deng, L., 2020. Dynamic load test on progressive collapse resistance of fully assembled precast concrete frame structures. Engineering Structures, 214, p.110675.